F.W. Klaiber, T.J. Wipf, F.M. Russo
R.R. Paradis, R.E. Mateega

# Field/Laboratory Testing of Damaged Prestressed Concrete Girder Bridges

December 1999

Sponsored by the
Iowa Department of Transportation
Project Development Division and the
Iowa Highway Research Board

Iowa Department of Transportation

Iowa DOT Project HR-397

## Final

# REPORT

IOWA STATE UNIVERSITY
OF SCIENCE AND TECHNOLOGY

Department of Civil and Construction Engineering

F.W. Klaiber, T.J. Wipf, F.M. Russo
R.R. Paradis, R.E. Mateega

# Field/Laboratory Testing of Damaged Prestressed Concrete Girder Bridges

December 1999

Sponsored by the
Iowa Department of Transportation
Project Development Division and
the Iowa Highway Research Board

Iowa DOT Project HR-397

**Final**

# REPORT

IOWA STATE UNIVERSITY
OF SCIENCE AND TECHNOLOGY

Iowa Department of Transportation

Department of Civil and Construction Engineering

# *ABSTRACT*

Due to frequent accidental damage to prestressed concrete (P/C) bridges caused by impact from overheight vehicles, a project was initiated to evaluate the strength and load distribution characteristics of damaged P/C bridges. A comprehensive literature review was conducted. It was concluded that only a few references pertain to the assessment and repair of damaged P/C beams. No reference was found that involves testing of a damaged bridge(s) as well as the damaged beams following their removal.

Structural testing of two bridges was conducted in the field. The first bridge tested, damaged by accidental impact, was the westbound (WB) I-680 bridge in Beebeetown, Iowa. This bridge had significant damage to the first and second beams consisting of extensive loss of section and the exposure of numerous strands. The second bridge, the adjacent eastbound (EB) structure, was used as a baseline of the behavior of an undamaged bridge. Load testing concluded that a redistribution of load away from the damaged beams of the WB bridge was occurring. Subsequent to these tests, the damaged beams in the WB bridge were replaced and the bridge retested. The repaired WB bridge behaved, for the most part, like the undamaged EB bridge indicating that the beam replacement restored the original live load distribution patterns.

A large-scale bridge model constructed for a previous project was tested to study the changes in behavior due to incrementally applied damage consisting initially of only concrete removal and then concrete removal and strand damage. A total of 180 tests were conducted with the general conclusion that for exterior beam damage, the bridge load distribution characteristics were relatively unchanged until significant portions of the bottom flange were removed along with several strands. A large amount of the total applied moment to the exterior beam was redistributed to the interior beam of the model.

Four isolated P/C beams were tested, two removed from the Beebeetown bridge and two from the aforementioned bridge model. For the Beebeetown beams, the first beam, Beam 1W, was tested in an "as-removed" condition to obtain the baseline characteristics of a damaged beam. The second beam, Beam 2W, was retrofit with carbon fiber reinforced polymer (CFRP) longitudinal plates and transverse stirrups to strengthen the section. The strengthened Beam was 12% stronger than Beam 1W. Beams 1 and 2 from the bridge model were also tested. Beam 1 was not damaged and served as the baseline behavior of a "new" beam while Beam 2 was damaged and repaired again using CFRP plates. Prior to debonding of the plates from the beam, the behavior of both Beams 1 and 2 was similar. The retrofit beam attained a capacity greater than a theoretically undamaged beam prior to plate debonding.

Analytical models were created for the undamaged and damaged center spans of the WB bridge; stiffened plate and refined grillage models were used. Both models were accurate at predicting the deflections in the tested bridge and should be similarly accurate in modeling other P/C bridges. The moment fractions per beam were computed using both models for the undamaged and damaged bridges. The damaged model indicates a significant decrease in moment in the damaged beams and a redistribution of load to the adjacent curb and rail as well as to the undamaged beam lines.

# *TABLE OF CONTENTS*

**LIST OF FIGURES** ..... ix

**LIST OF TABLES** ..... xv

**CHAPTER 1 INTRODUCTION** ..... 1

1.1. Background ..... 1
1.2. Research Objectives ..... 2
1.3. Research Tasks ..... 2

**CHAPTER 2 LITERATURE REVIEW** ..... 5

2.1. Bridge Testing ..... 5
2.2. Beam Testing and Repair ..... 10

**CHAPTER 3 I-680 FIELD TEST RESULTS** ..... 23

3.1. Test Objectives ..... 32
3.2. Test Procedures and Instrumentation Description ..... 32
3.3. Baseline: 1997 Test Results ..... 35
3.3.1. Single Truck Test Results ..... 37
3.3.1.1. Lane 1 Test Results ..... 37
3.3.1.2. Lane 2 Test Results ..... 47
3.3.1.3. Lane 3 and Lane 4 Test Results ..... 51
3.3.2. Multiple Truck Test Results and Validity of Superposition ..... 51
3.3.2.1. Lanes 1 and 2 Loaded Simultaneously ..... 52
3.3.2.2. Lane 1 Loaded with Two Test Trucks ..... 53
3.3.2.3. Lane 2 Loaded with Two Test Trucks ..... 59
3.3.3. Baseline Test Result Summary and Conclusions ..... 60
3.4. WB Bridge Retest (1998) Results ..... 62
3.4.1. Single Truck Test Results ..... 63
3.4.1.1. Lane 1 Test Results ..... 63
3.4.1.2. Lane 2 Test Results ..... 67
3.4.2. Multiple Truck Tests and Validity of Superposition ..... 67
3.4.2.1. Lanes 1 and 2 Loaded Simultaneously ..... 67
3.4.2.2. Lane 1 Loaded with Two Test Trucks ..... 68
3.4.2.3. Lane 2 Loaded with Multiple Trucks ..... 69

3.4.3. WB Bridge Retest Summary and Conclusions ..... 69

**CHAPTER 4 LABORATORY BRIDGE TEST RESULTS ..... 71**

4.1. Test Objectives ..... 74
4.2. Test Procedures and Instrumentation Description ..... 74
4.3. Experimental Results and Analysis ..... 87
4.3.1. Undamaged Bridge Tests ..... 87
4.3.1.1. Strains in the P/C Beams ..... 87
4.3.1.2. Deflections in the P/C Beams ..... 88
4.3.1.3. R/C Diaphragms ..... 92
4.3.1.4. R/C Bridge Deck ..... 92
4.3.2. Damage Level Comparison ..... 92
4.3.2.1. Influence of Damage on P/C Beam Strains ..... 94
4.3.2.2. Influence of Damage on P/C Beam Deflections ..... 98
4.3.2.3. Influence of Damage on R/C Bridge Deck Strains ..... 103
4.3.2.4. Influence of Damage on Prestressing Strands ..... 103
4.3.2.5. Influence of Damage on Transverse Load Distribution ..... 104
4.4. Conclusions ..... 109

**CHAPTER 5 ISOLATED BEAM TESTS ..... 111**

5.1. Beebeetown Beam Tests ..... 111
5.1.1. Beam 1W ..... 113
5.1.1.1. Beam 1W Test Results ..... 119
5.1.1.1.1. Service Load Test ..... 119
5.1.1.1.2. Ultimate Load Test ..... 123
5.1.1.2. Beam 1W Test Summary ..... 129
5.1.2. Beam 2W ..... 129
5.1.2.1. Service Load Tests on Damaged Specimen ..... 130
5.1.2.2. Repair of Beam 2W ..... 137
5.1.2.2.1. Service Load Test ..... 140
5.1.2.2.2. Ultimate Load Test ..... 142
5.2. Summary of Beebeetown Beam Tests ..... 147
5.3. ISU Model Bridge Beams ..... 148
5.3.1. Beam 1 – Control Specimen ..... 149
5.3.2. Beam 2 – FRP Repaired Specimen ..... 169
5.3.2.1. Repair Details ..... 169
5.3.2.2. Service Load Tests ..... 173

5.3.2.3. Ultimate Load Test ..... 179
5.4. ISU Model Bridge Beam Test Summary ..... 185
5.5. P/C Beam Strengthening Conclusions ..... 190

**CHAPTER 6 STRUCTURAL ANALYSIS AND MODELING ..... 191**

6.1. Mechanics of Live Load Distribution ..... 191
6.2. Computer Modeling ..... 198
6.3. Validation of Modeling Techniques ..... 209
6.3.1. Grillage Model Validation ..... 209
6.3.2. Stiffened Plate Model Validation ..... 213
6.3.2.1. Comparison of STAAD and ADINA Models ..... 213
6.3.3. Model Validation Summary ..... 218
6.4. Analytical Results for the Beebeetown Bridges ..... 218
6.4.1. Undamaged and Repaired Bridge Results ..... 218
6.4.1.1. Stiffened Plate Model of the Undamaged/Repaired Bridges ..... 219
6.4.1.2. Grillage Model of the Undamaged and Repaired Bridges ..... 228
6.4.2. Analysis of the Damaged Center Span ..... 233
6.4.3. Center Span Analytical Modeling Summary ..... 238

**CHAPTER 7 SUMMARY, CONCLUSIONS AND RECOMMENDATIONS ..... 241**

7.1. Summary ..... 241
7.2. Conclusions and Recommendations ..... 244

**CHAPTER 8 NEEDS FOR FURTHER INVESTIGATION ..... 247**

**CHAPTER 9 ACKNOWLEDGEMENTS ..... 249**

**APPENDIX A SAMPLE COMPUTER MODELS ..... 251**

A.1. Barker and Puckett Example Grillage (Section 6.3.1 and Figure 6.6) ..... 252
A.2. Barker and Puckett Downstand Grillage (Section 6.3.1 and Figure 6.7) ..... 253
A.3. I-680 Stiffened Plate Model SP-3 (Section 6.4.1 and Figure 6.11) ..... 254

**REFERENCES ..... 257**

# *LIST OF FIGURES*

Figure 3.1. Overview of WB (Foreground) and EB Bridges ..... 24
Figure 3.2. Elevation View of WB Bridge, Looking West (Damaged Beam 1W in Center Span) ..... 24
Figure 3.3. Iowa DOT B Beam Cross-Section ..... 25
Figure 3.4. I-680 over County Road L34, Plan View of Beams and Deflection Transducer Layout ..... 26
Figure 3.5. I-680 over County Road L-34: Location of Diaphragm and Beam End Strain Gage ..... 27
Figure 3.6. I-680 over County Road L-34: Truck Positions, Load Lanes, and Location of Deflection Transducers ..... 28
Figure 3.7. Underside of Damaged WB Bridge, Beam 1W at Left ..... 30
Figure 3.8. Elevation View of Beam 1W, Exterior (North) Face Shown ..... 30
Figure 3.9. Underside of Beam 1W Damaged Bottom Flange ..... 31
Figure 3.10. South Face of Damaged Beam 2W ..... 31
Figure 3.11. Strain Gages on Beam End Web and Flange Adjacent to the Pier Diaphragm ..... 36
Figure 3.12. Tripod Mounted Deflection Transducers Under an End Span ..... 36
Figure 3.13. Test Truck Positioned in Lane 1 ..... 38
Figure 3.14. Comparison of Deflections at Transverse Sections W1 and E1: Truck in First Span ..... 38
Figure 3.15. Comparison of Deflections at Transverse Section W2 and E2: Truck in Center Span ..... 39
Figure 3.16. Comparison of Deflections at Transverse Section W3 and E3: Truck in Center Span ..... 39
Figure 3.17. Longitudinal Deflected Shape, Beams 1W - 5W: Truck 1 at L1W-P5 ..... 41
Figure 3.18. Longitudinal Deflected Shape, Beams 1E – 3E: Truck 1 at L1E-P5 ..... 41
Figure 3.19. Behavioral Models for Diaphragms Under Load ..... 42
Figure 3.20. WB Bridge Diaphragm Strains: Lane 1W Loaded ..... 43
Figure 3.21. EB Bridge Diaphragm Strains: Lane 1E Loaded ..... 44
Figure 3.22. Midspan Intermediate Diaphragm Detail from the Original Design Plans ..... 45
Figure 3.23. Exposed Strand Strains: Lane 1W Loaded ..... 48
Figure 3.24. Deflections at Transverse Section W3: Lane 2W Loaded ..... 48
Figure 3.25. Deflections at Transverse Section E3: Lane 2E Loaded ..... 49
Figure 3.26. Diaphragm Strains, EB Bridge: Lane 2E Loaded ..... 50
Figure 3.27. Exposed Strand Strains: Lane 2W Loaded ..... 50
Figure 3.28. Photograph of Test Trucks 1 and 2 in Adjacent Lanes on the EB Bridge, WB Similar ..... 52
Figure 3.29. Deflections at Transverse Section W3: Lanes 1W and 2W Loaded ..... 53
Figure 3.30. Deflections at Transverse Section E3: Lanes 1E and 2E Loaded ..... 54
Figure 3.31. Trucks 1 and 2 at P4 and P6 on the EB Bridge, WB Similar ..... 55
Figure 3.32. Deflections at Transverse Section W3: Lane 1W Loaded with Trucks 1 and 2 ..... 55
Figure 3.33. Deflections at Transverse Section E3: Lane 1E Loaded with Trucks 1 and 2 ..... 56
Figure 3.34. Longitudinal Deflected Shape, Beam 1W: Trucks 1 and 2 in Lane 1W ..... 57

Figure 3.35. Longitudinal Deflected Shape, Beam 1E: Trucks 1 and 2 in Lane 1E ..... 57
Figure 3.36. Deflections at Transverse Section W3: Lane 2W Loaded with Trucks 1 and 2 ..... 59
Figure 3.37. Deflections at Transverse Section E3: Lane 2E Loaded with Trucks 1 and 2 ..... 60
Figure 3.38. Deflection Comparisons at Transverse Section W/E1: Lane 1W/1E Loaded ..... 64
Figure 3.39. Deflection Comparisons at Transverse Section W/E3: Lane 1W/1E Loaded ..... 64
Figure 3.40. Deflection Comparisons at Transverse Section W/E4: Lane 1W/1E Loaded ..... 65
Figure 3.41. Longitudinal Deflected Shapes, Beams 1W - 3W: Lane 1W Loaded ..... 66
Figure 3.42. Deflection Comparisons, Transverse Section W/E3: Lanes 1 and 2 Loaded ..... 68
Figure 3.43. Deflection Comparisons, Transverse Section W/E3: Lane 1 Loaded with Trucks 1 and 2 ..... 69
Figure 3.44. Comparative Deflected Shape, Lane 2 Loaded with Multiple Trucks ..... 70
Figure 4.1. Overall Dimensions of the Bridge Model ..... 72
Figure 4.2. Prestressed Beam Cross Sections ..... 73
Figure 4.3. Loading Frame for Applying Loads to the Bridge Model ..... 75
Figure 4.4. Load Positions Used to Test the Bridge Model ..... 75
Figure 4.5. Location of Strain Gages on Prestressed Concrete Beams ..... 77
Figure 4.6. Location of Bridge Deck Strain Gages ..... 78
Figure 4.7. Location of Diaphragm Strain Gages ..... 78
Figure 4.8. Layout of Prestressing Strand Strain Gages ..... 79
Figure 4.9. Damage Levels Consisting of Concrete Removal Only ..... 82
Figure 4.10. Severed Prestressing Strand Exhibiting Necking Down Behavior ..... 84
Figure 4.11. Profile View of the Damaged Region of Beam 3 ..... 84
Figure 4.12. Strand Removal in Prestressed Concrete Beam 3 ..... 85
Figure 4.13. Beam Strains: Load at the 1/4 Point, Midspan and 3/4 Point of Each Individual Beam, Undamaged Condition ..... 89
Figure 4.14. Beam 1 Deflections at the 1/4 Point, Midspan and 3/4 Point, Undamaged Condition ..... 90
Figure 4.15. Beam Deflections: Load at Midspan of Each Individual Beam, Undamaged Condition ..... 91
Figure 4.16. Bridge Deck Longitudinal Strains: Load at Midspan of Each Beam, Undamaged Condition ..... 93
Figure 4.17. Maximum Bottom Beam Strains: Load at Position 5 ..... 95
Figure 4.18. Maximum Bottom Beam Strains: Load at Position 3 ..... 96
Figure 4.19. Maximum Bottom Beam Strains: Load at Position 6 ..... 97
Figure 4.20. Influence of Damage on Longitudinal Beam 1 Deflections: Load on Beam 1 ..... 100
Figure 4.21. Influence of Damage on Longitudinal Beam 2 Deflections: Load on Beam 2 ..... 101
Figure 4.22. Influence of Damage on Longitudinal Beam 3 Deflections: Load on Beam 3 ..... 102
Figure 5.1. Beams 2W and 1W Isolated in Preparation for Removal from the WB Bridge ..... 112
Figure 5.2. Beam 1W During Removal from the WB Bridge ..... 112
Figure 5.3. Overall View of Test Setup; Beam 1W in Position for Testing ..... 114

Figure 5.4. Close Up View of Damaged South Face of Beam 1W Prior to Testing ..... 114
Figure 5.5. Close Up View of Damaged North Face of Beam 1W Prior to Testing ..... 115
Figure 5.6. End View of Beam 1W Prior to Testing ..... 115
Figure 5.7. General View of Test Setup and Instrumentation Layout, Beam 1W ..... 118
Figure 5.8. Service Test of Beam 1W: Applied Moment vs. Deflection ..... 120
Figure 5.9. Service Test of Beam 1W: Applied Moment vs. Midspan Strains ..... 120
Figure 5.10. Service Test of Beam 1W: Location of Midspan Neutral Axis ..... 121
Figure 5.11. Service Load Test of Beam 1W: Variation in Strand Strains ..... 122
Figure 5.12. South Face of Beam 1W West of Midspan Following the Ultimate Load Test ..... 124
Figure 5.13. South Face of Beam 1W Looking East Following Ultimate Load Test ..... 124
Figure 5.14. North Face Damage in Beam 1W Following Ultimate Load Test ..... 125
Figure 5.15. Cracks on South Face of Beam 1W East of Midspan Following Ultimate Load Test ..... 125
Figure 5.16 Ultimate Load Test of Beam 1W: Applied Moment vs. Deflection ..... 126
Figure 5.17 Ultimate Load Test of Beam 1W: Applied Moment vs. Curvature at W Quarter Point ..... 127
Figure 5.18 Ultimate Load Test of Beam 1W: Applied Moment vs. EI at Quarter Points ..... 127
Figure 5.19 Ultimate Load Test of Beam 1W: Applied Moment vs. Midspan NA Location ..... 128
Figure 5.20 Ultimate Load Test of Beam 1W: Applied Moment vs. Midspan Curvature ..... 128
Figure 5.21. Exposed Strand Strains: Ultimate Load Test of Beam 1W ..... 129
Figure 5.22. South Face of Damaged Beam 2W Prior to Repair ..... 131
Figure 5.23. End Elevation of Beam 2W Prior to Repair (Looking East) ..... 131
Figure 5.24. North Face Damage West of Midspan Diaphragm, Beam 2W ..... 132
Figure 5.25. Underside of Damaged Flange, Beam 2W, Strain Gages on Strands 5 and 6 ..... 132
Figure 5.26. Pre and Post Strengthening Instrumentation on Beam 2W ..... 133
Figure 5.27. Service Test 3 of Beam 2W: Applied Moment vs. Displacement ..... 134
Figure 5.28. Service Test 5 of Beam 2W: Applied Moment vs. Displacement ..... 134
Figure 5.29. Service Test 5 of Beam 2W: Applied Moment vs. NA Location at E 1/4 Point ..... 135
Figure 5.30. Service Test 5 of Beam 2W: Applied Moment vs. NA Location in Damaged Region ..... 136
Figure 5.31. Variation in Beam 2W NA Location with Service Tests ..... 136
Figure 5.32. Service Tests of Beam 2W: Variation in EI ..... 137
Figure 5.33. Trowel, Spatula and Roller Used for Application of Epoxy and CFRP Plates ..... 138
Figure 5.34. Installation of CFRP Reinforcing Plates to Repaired Bottom Flange of Beam 2W ..... 138
Figure 5.35. Completed Installation of CFRP Reinforcing Plates on Beam 2W ..... 139
Figure 5.36. Placement of CFRP Fabric External Stirrups on Beam 2W ..... 139
Figure 5.37. Service Test 2 of Repaired Beam vs. Pre-Repair Service Test 5: Moment vs. Deflection ..... 141
Figure 5.38. Service Test 2 of Repaired Beam 2W: Applied Moments vs. NA Location ..... 141
Figure 5.39. Vertical / Inclined Cracks in FRP Stirrups in Previously Damaged Region of Beam 2W ..... 143

Figure 5.40. Debonded Overlay in Constant Moment Region of Beam 2W Near Ultimate Load ..... 143
Figure 5.41. South Face of Beam 2W West of the Midspan Diaphragm ..... 144
Figure 5.42. Fractured CFRP Stirrups and Debonded Plates Near Midspan of Repaired Beam 2W ..... 144
Figure 5.43. Ultimate Load Test of Beam 2W: Applied Moment vs. Deflection ..... 145
Figure 5.44. Ultimate Load Test of Beam 2W: Response of Midspan Strain Gages ..... 145
Figure 5.45. Ultimate Load Test of Repaired Beam 2W: Moment vs. Strains in Damaged Region ..... 147
Figure 5.46. Ultimate Load Test of Repaired Beam 2W: Change in EI, West Quarter Point ..... 147
Figure 5.47. Actuator Placement for Beam 1 Load Test ..... 150
Figure 5.48. Self Contained Reaction Frame Under Beam 1 ..... 150
Figure 5.49. Bearing of Self-Contained Frame on the Bottom of Beam 1 ..... 151
Figure 5.50. Schematic and Boundary Conditions for Beam 1 Loading ..... 151
Figure 5.51. Beam 1 Cracking Test: Load per Actuator vs. Live Load Displacement ..... 152
Figure 5.52. Crack Patterns at 100 kip Total Load Following the Beam 1 Cracking Test ..... 152
Figure 5.53. Analytical and Measured Deflections Along Beam 1, 60 Kips per Actuator ..... 154
Figure 5.54. Measured vs. Predicted Deflections Along Beam 1 Using Experimental EI Value ..... 155
Figure 5.55. Actuator Load vs. Measured Curvature, Beam 1 ..... 155
Figure 5.56. Beam 1 Crack Patterns Following the Unsuccessful Ultimate Load Test ..... 156
Figure 5.57. Ultimate Load vs. Cracking Test, Beam 1: Applied Load vs. Deflection ..... 157
Figure 5.58. Ultimate Load Test of Beam 1: Applied Load vs. NA Locations ..... 157
Figure 5.59. Service Test of Cracked Beam 1: Applied Moments vs. Deflection ..... 159
Figure 5.60. Service Test of Cracked Beam 1: Applied Moment vs. Midspan NA Location ..... 159
Figure 5.61. Service Test of Cracked Beam 1: Midspan Strain Profiles ..... 160
Figure 5.62. Service Test of Cracked Beam 1: Midspan Moment vs. Curvature ..... 160
Figure 5.63. Service Test of Cracked Beam 1: Moment vs. NA Location at Quarter Points ..... 161
Figure 5.64. Service Test of Cracked Beam 1: Applied Moment vs. Quarter Point Curvature ..... 161
Figure 5.65. Service Test of Cracked Beam 1: Moment vs. EI ..... 162
Figure 5.66. Applied Moment at Midspan vs. Crack Opening Displacement, Ultimate Test of Beam 1 ... 164
Figure 5.67. Ultimate Load Test of Beam 1: Applied Moment vs. Deflection ..... 164
Figure 5.68. Ultimate Load Test of Beam 1: Applied Quarter Point Moment vs. NA Location ..... 166
Figure 5.69. Ultimate Load Test of Beam 1: Moment vs. Computed EI ..... 166
Figure 5.70. Overview of Beam 1 Crack Patterns Following the Ultimate Load Test ..... 167
Figure 5.71. Extensive Vertical Cracking in the Constant Moment Region of Beam 1 ..... 167
Figure 5.72. Diagonal Tension Cracks in High Moment/Shear Region of Beam 1 ..... 168
Figure 5.73. Web Shear Cracks in Beam 1 Adjacent to the Support ..... 168
Figure 5.74. Damaged Bottom Flange of Beam 2, Removed Strands in Foreground ..... 170
Figure 5.75. Completed Concrete Repair on Beam 2 ..... 170

Figure 5.76. Installation of S1012 Reinforcing Plates on Beam 2 Bottom Flange ..... 172
Figure 5.77. Installation of GFRP Wrap on Bottom and Sides of the Bottom Flange of Beam 2 ..... 172
Figure 5.78. Instrumentation Layout, Repaired Beam 2 ..... 174
Figure 5.79. Beam 2 Prior to Testing; CFRP Plates and GFRP Wrap Visible on Bottom Flange ..... 175
Figure 5.80. Strain Gages on CFRP Plates at Midspan of Beam 2 ..... 175
Figure 5.81. Service Test of Undamaged/Unstrenghened Beam 2: East Quarter Point Data ..... 177
Figure 5.82. Service Test of Beam 2: Response of Midspan Region ..... 178
Figure 5.83. Beam 2 Service Load Response: Repaired West Quarter Point ..... 180
Figure 5.84. Applied Midspan Moment vs. Crack Opening, Beam 2 ..... 181
Figure 5.85. Beam 2 Ultimate Load vs. Baseline (Beam 1) Results: Applied Moment vs. Deflection ..... 181
Figure 5.86. Partial Debonding of the Beam 2 Bottom Plates Between the GFRP Confining Wraps ..... 183
Figure 5.87. Failure of the Beam 2 Bottom Plates as well as the North Face Plate ..... 183
Figure 5.88. Failure of the Original P/C Beam 2 Substrate Near Midspan ..... 185
Figure 5.89. Fracture of GFRP Wrap and Voided Flange in Beam 2 Following Plate Debonding ..... 185
Figure 5.90. Ultimate Load Test of Beam 2: Undamaged East Quarter Point ..... 186
Figure 5.91. Ultimate Load Test of Beam 2: Midspan Region ..... 187
Figure 5.92. Ultimate Load Test of Beam 2: Repaired West Quarter Point ..... 188
Figure 6.1. Schematic of 5-Beam Bridge Studied by Tamberg (1968) ..... 194
Figure 6.2. Prestressed Beam Idealization, Eby et al. (1973) ..... 195
Figure 6.3. Torsional Constant for Rectangular Sections ..... 197
Figure 6.4. Grillage Idealizations of a Typical Beam and Slab Bridge ..... 199
Figure 6.5. Stiffened Plate Model for Load Distribution ..... 208
Figure 6.6. Applied Loads and Resulting Bending Moment Diagrams, Grillage Model ..... 211
Figure 6.7. Downstand Grillage Model of Barker and Puckett's Example Bridge ..... 212
Figure 6.8. STAAD Stiffened Plate Model of the Aswad and Chen Test Bridge ..... 214
Figure 6.9. Moments Resisted by Each Beam of the Aswad and Chen Test Bridge ..... 216
Figure 6.10. Stiffened Plate Model of the Barker and Puckett Example Bridge ..... 216
Figure 6.11. Isometric View, Center Span with Load at L1-P4 ..... 219
Figure 6.12. Analytical vs. Experimental Deflection, Stiffened Plate Models SP-1 to SP-4 ..... 222
Figure 6.13. Analytical vs. Experimental Deflection, Stiffened Plate Models SP-5 to SP-8 ..... 223
Figure 6.14. Analytical vs. Experimental Deflection, Stiffened Plate Models SP-9 to SP-12 ..... 224
Figure 6.15. Analytical vs. Experimental Deflection, Stiffened Plate Models SP-13 to SP-16 ..... 225
Figure 6.16. Plan and Isometric View of Downstand Grillage of the I-680 Center Span ..... 229
Figure 6.17. Idealization of Equivalent Member Loads for Wheel Loads Between Beam Elements ..... 230
Figure 6.18. Moments in Longitudinal Beams as Predicted by the Stiffend Plate and Grillage Models ..... 231
Figure 6.19. Comparison of Experimental, Stiffened Plate and Grillage Model Deflected Shapes ..... 232

Figure 6.20. Stiffened Plate Model of Damaged WB Center Span, Load at L1-P4&P6 Shown ..... 234
Figure 6.21. Comparison of Experimental and Analytical Deflections for the Damaged WB Bridge..... 235
Figure 6.22. Load Distribution Comparisons, WB Bridge, Undamaged and Damaged Models ..... 237
Figure 6.23. Transverse Slab Bending, WB Bridge, Load Case L1-P4&P6..... 237

# *LIST OF TABLES*

Table 3.1. Description of Prestressed Beams in the Beebeetown Bridges ..... 25
Table 3.2. Test Truck Position Matrix for Field Testing of the Beebeetown Bridges ..... 34
Table 3.3. Comparison of Exposed Strand Strains, Lane 1W Loaded with Trucks 1 and 2 ..... 58
Table 3.4. Comparison of Beam End Strains, Lane 1W Loaded with Trucks 1 and 2 ..... 58
Table 4.1. Dimensions of the Damaged Region in Beam 3 ..... 86
Table 4.2. Influence of Damage on Midspan Bottom Beam Strains in Beam 2 ..... 98
Table 4.3. Influence of Damage on Beam 3 Midspan Deflections ..... 103
Table 4.4. Influence of Damage on Reinforced Concrete Deck Strains with Load at Position 6. ..... 105
Table 4.5. Influence of Damage on Average Strand Strains at Given Load Positions. ..... 105
Table 4.6. Influence of Damage on Moment Fractions: Load at Position 3. ..... 108
Table 4.7. Influence of Damage on Moment Fractions: Load at Position 6. ..... 108
Table 4.8. Influence of Damage on Moment Fractions: Load at Position 9. ..... 109
Table 5.1. Predicted Strengths of Beam 1W ..... 116
Table 5.2. Properties of CFRP Repair Materials Used for the Repair of Beam 2W ..... 140
Table 5.3 Cementitious Patch Material Properties Used on Beam 2 ..... 171
Table 5.4. FRP and Epoxy Properties Used in the Repair of Beam 2 ..... 173
Table 6.1. Torsional Constant, $K_t$, for Iowa DOT Standard P/C Beams ..... 197
Table 6.2. Comparison of STAAD Solution to Published Grillage Results ..... 211
Table 6.3. Comparison of Plane and Downstand Grillage Models ..... 213
Table 6.4. Comparison of STAAD Models Using Different Modeling Techniques. ..... 214
Table 6.5. Variable Parameters in Center Span Stiffened Plate Models ..... 220
Table 6.6. Computed Moments in Beams 1-3, 5 Due to Variations in Load Placement and Model Parameters ..... 226
Table 6.7. Grillage Properties for Longitudinal and Transverse Members, Undamaged Center Span ..... 230
Table 6.8. Member Properties of the Undamaged and Damaged Iowa DOT 55 ft Long P/C B Beams ..... 234

# *CHAPTER 1*
# *INTRODUCTION*

## *1.1. Background*

In the summer of 1996, an unknown overheight vehicle struck a 3-span prestressed concrete (P/C) bridge carrying I-680 over County Road L34 near Beebeetown, Iowa. Due to concerns about the remaining strength of the damaged beams, unknown effect of the damage on the load distribution patterns in the remaining structure, and concerns regarding the durability and effectiveness of any proposed repair, it was decided that the beams would be replaced.

The decision to replace the two damaged beams was made prior to the initiation of this research; it was in fact the impetus for the project. Frequently the decision to replace a damaged prestressed beam is made because of a lack of knowledge about the reserve strength of the bridge rather than from calculations that definitively indicate that the bridge has been compromised. The damaged P/C bridge previously described provided a unique opportunity to perform an in-place assessment of load distribution in damaged and undamaged bridges. The availability of the P/C laboratory bridge model also made it possible to investigate the strength of damaged beams and to determine the effectiveness of FRP repair techniques. To the authors' knowledge, no other research program has been conducted where a bridge was tested in various stages, damaged and repaired, and the beams from the same bridge subsequently tested for strength and repairability. Other research programs have addressed either the live load or beam strength aspects of this work but none have been as comprehensive as the work described herein. Refer to Chapter 2 for a review of work previously performed in the area of load distribution and damaged prestressed beam performance.

Although this research concentrates on the live load distribution of damaged bridges and the performance of damaged beams under load, satisfactory live load distribution and ultimate strength are not sufficient criteria for making decisions to repair or replace damaged prestressed concrete beams. Effective repair techniques must be used which allow for the restoration of strength and which promote long-term continued durability of the damaged member. Cracking under service loads may give rise to environmental damage of the prestressing strands and may also lead to premature fatigue failure of the strands. These effects should all be considered along with assessment of structural strength.

## *1.2. Research Objectives*

The objectives for this project were fairly comprehensive in that they attempted to answer a number of questions related to the complex behavior of bridge structures as well as isolated beams. The research had the following objectives:

- Determine the load distribution patterns in undamaged and damaged bridges.
- Ascertain whether the live load distribution in damaged bridges can be predicted with reasonable accuracy.
- Establish the effect of damage on the remaining strength of P/C beams.
- Determine whether damaged beams be economically and effectively repaired with strength as the controlling factor.

In order to provide answers for these various objectives, this research project was undertaken. The research consisted of static load testing of bridges in the field, static testing of a large-scale bridge model in the laboratory, testing of damaged beams removed from field service, and testing of intentionally damaged and control specimens from the laboratory model bridge. In addition to the experimental tasks, analytical work was conducted to help validate/corroborate the experimental data. These various tasks are described below.

## *1.3. Research Tasks*

This project had a series of tasks, all of which are associated with the collection of information regarding either load distribution or remaining strength properties of damaged P/C bridges and beams.

The first task was to review literature related to this project. The literature review was continually updated throughout the progression of the project so that even very recently published items are included. A short synopsis of some of the pertinent literature is presented in Chapter 2 of this report. Additional literature can be found in Mateega (1997) and Paradis (1998). On some of the research tasks, there is a significant amount of information concerning the general topic, i.e., load distribution, yet when specific searches were made for literature concerning the effects of damage on load distribution, little useful information was found. This is also the case for the topic of beam repair where a significant body of information exists concerning the repair of reinforced concrete (R/C) elements yet little information was found on the strengthening of P/C bridges.

Following the literature review, a number of parallel research tasks were started. The primary experimental work for the project concerned the field and laboratory testing of P/C bridges as well as the isolated P/C beams tested in various conditions.

In Chapter 3, results from the field tests conducted on the damaged I-680 bridge, the adjacent undamaged bridge, and the damaged bridge again following repair which consisted of complete beam replacement. The research was conducted using loaded trucks of known axle weight distribution and

configuration. This method of field testing, used extensively throughout the years, provided baseline experimental data through which assessments were made concerning the effect of the isolated damage on the load distribution in the damaged bridge. The experimental data were also used to help validate the performance of analytical models created to explain the load distribution.

Experimental results of a comprehensive investigation of load distribution on a model bridge constructed and tested in the laboratory facilities of Iowa State University (ISU) are presented in Chapter 4. The ISU bridge model, approximately 40 ft long and 18 ft wide, and consisting of three Iowa DOT standard "A" beams, was previously constructed for use in an investigation of the lateral load response of various diaphragms. However, the bridge, never being significantly loaded during the previous work, was suitable for experimentally determining live load distribution. The model was tested in the undamaged condition, damage consisting of various degrees of concrete removal, and again with damage consisting of concrete and strand removal. The model was tested a total of 180 times to determine the effects of various degrees of damage and load locations. Progressive damage was created to detect when "critical" levels of damage were inflicted such that a change in load distribution characteristics was evident.

The test results from the testing of four isolated P/C beams are presented in Chapter 5. In this chapter, two of the beams recovered from the damaged I-680 WB bridge are tested as well as two beams from the ISU bridge model which was dismantled following the laboratory bridge tests. For the I-680 beams, one beam was tested "as-is" to obtain the baseline performance, stiffness and strength, of a P/C beam damaged in service. The second beam was strengthened using carbon fiber reinforced polymer (CFRP) plates and fabric following additional intentional strand damage. The strengthening was intended to replicate the lost strength of the several severed strands. One beam from the ISU bridge model had not been damaged in prior work and thus served as the baseline behavior of a "new" beam. The second beam, intentionally damaged and subsequently repaired with CFRP materials, was used to assess the effectiveness of the strengthening system.

Analytical models of the I-680 bridge are presented in Chapter 6 along with a series of models of other bridges used to validate the performance of the analysis software. Following presentation of the results from other authors concerning the live load distribution in two different structures, the results from the I-680 bridges are presented. The intent of the analytical models was to first create a model that predicted the measured response of the undamaged bridges obtained during the field tests. Following calibration of the model to the undamaged bridges, simulated damage was applied to the model and evaluation of the load distribution characteristics of the damaged bridge was made. The analytical models described in Chapter 6 can be used to evaluate the load distribution characteristics of both undamaged and damaged P/C bridges.

Finally, the report concludes with a summary of results and recommendations for implementation in Chapter 7, and a description of the areas requiring additional study identified through the conduct of this work in Chapter 8.

# *CHAPTER 2*
# *LITERATURE REVIEW*

The purpose of this chapter is to briefly discuss some of the relevant literature reviewed during conduct of this research. Additional pertinent literature can be found in Mateega (1997) and Paradis (1998).

Literature from many sources was reviewed for this project. Because there are a variety of project tasks, there is a short discussion in this chapter of the literature pertaining to all of the tasks. To reiterate, this project involved the field testing of bridges, laboratory testing of a full-scale bridge model, predictions of live load distribution, testing of isolated prestressed concrete beams, repair assessment, and structural analyses of bridge systems. The literature pertaining to live load distribution and computer modeling is presented in Chapter 6, which deals with structural modeling.

## *2.1. Bridge Testing*

The load testing of bridges takes one of two forms, service level tests for purposes of confirming the performance of the structure under design loads and ultimate load tests on decommissioned or model bridges intended to assess ultimate strength characteristics. Literature pertaining to both types of tests is presented herein.

In recognition of the enhanced performance of bridge structures obtained through load testing as compared to theoretical predictions of capacity, the "Manual for Bridge Rating Through Load Testing" was published in 1998 as NCHRP Research Results Digest 234 (National, 1998; Lichtenstein, 1993). In the manual, recommendations on when and how to use diagnostic load testing were made and a number of successful diagnostic load tests were documented and discussed. The authors contend that diagnostic load testing is a powerful tool for assessing the strength characteristics of old bridges and bridges whose strength is low based on theoretical predictions. The low strength predictions are due to a number of factors typically neglected in conventional structural calculations. These additional sources of stiffness and strength can typically be attributed to enhanced live load distribution, unanticipated composite action, unintended end restraint and participation of curb and rail sections as edge stiffening elements. Deatherage (1987) confirms many of these sources of unanticipated stiffness and load distribution.

In "Evaluation and Repair of Impact-Damaged Prestressed Concrete Bridge Girders", Zobel, Jirsa, Fowler and Carrasquillo (1997) report on the load testing of a damaged prestressed concrete bridge in Texas. The bridge in question is a four span structure with 65 ft end spans and 95 ft interior spans on a 5°30' right ahead skew. There are four beams on 7 ft-4 in. centers with a 6.5 in. slab. A total of 26-1/2 in.$\phi$, 270 ksi strands were used in each beam.

Damage was located on Beams 1, 2 and 4. Damage to Beam 1 was severe and was centered near the prestressing steel hold down point. There were four completely severed strands, and the remaining

strands were completely exposed over a length of 16 ft. A significant portion of the web from Beam 1 was destroyed. Damage to Beams 2 and 4 was moderate to minor, essentially concrete damage and slight cracking.

Tests were conducted on the two interior spans, one of which was undamaged and the other was damaged as previously described. The tests used a vehicle similar in weight and size to the one described in Chapter 3 of this report. The total test vehicle weight was 53,460 lbs. with a distribution of 22% to the front axle and the remaining 78% distributed to the rear tandem; this is 1/3 heavier and 3 ft longer than the standard AASHTO H20-44 design vehicle.

Tests conducted on the damaged north span indicated symmetry in the response of the bridge even in the presence of severe asymmetric damage. With the test truck centered over the damaged region, the maximum deflection in the damaged north span Beam 1 was 0.22 in. Measured deflections in the undamaged south interior span were also symmetric, the maximum deflection being 0.16 in., approximately 1/16 in. less than in the damaged north span. The deflection of the damaged span is L/5,000, an indication of excellent performance even in the presence of extreme damage. After testing, this bridge was recommended for repair.

The Florida DOT has tested a number of bridges in the recent past with the general conclusion that the load limitations prescribed by theoretical analysis are unduly conservative. Shahawy (1995) describes the use of diagnostic load testing in Florida on a damaged prestressed concrete bridge that carries the Florida Turnpike over I-595. This bridge test is also described in NCHRP Research Results Digest 234 (National, 1998). Special load-testing trucks, each of which has a maximum loaded weight of 202 kips, were employed by the Florida DOT for the test.

The Turnpike bridge consists of five spans of simply supported AASHTO beams. The longest span of 151 ft had twelve AASHTO Type V beams spaced at 5 ft-11 in. The bridge deck is 7 in. thick and has typical crash barriers on each side. Because of the length of the span, shoring was used to support the beams during deck casting and curing. During removal of the shoring, a piece of the falsework assembly impacted the side of the bridge causing a 10 ft long crack in the bottom flange of Beam 2 with spalling of concrete near the impact area and exposure of several strands. The strands were found to be undamaged but seven were considered to be unbonded for moment strength calculations. This resulted in a 10% reduction in the moment strength of the beam, however the beam was still adequate for the design moments.

Because of the innovative nature of the design and the presence of accidental damage, this bridge was chosen for testing. Load testing consisted of two trucks placed in adjacent traffic lanes to maximize the midspan moments in the damaged span. Results of three different load tests at increasing load levels from 100 kips to 204 kips indicated a linear elastic response. The experimental results were compared to the theoretical results from a three-dimensional stiffened plate finite element model. The experimentally recorded deflections and stresses (via strain measurements) were approximately 65% of those obtained using the analytical model but the theoretical and experimental deflected shapes were of the same general

shape. This indicates accurate prediction of load distribution but inaccurate prediction of total structural stiffness.

Burdette and Goodpasture (1974) describe the ultimate load test of a decommissioned prestressed concrete highway bridge. The objective of the research was to observe the behavior of the bridge as it was progressively loaded to failure and to compare the load–deflection behavior with that obtained from analytical predictions based on the strain compatibility method.

The bridge consisted of four simply supported 66 ft spans on a 20 degree skew. The cross-section consisted of four AASHTO Type III precast beams, spaced 9 ft on center with a 7 in. composite cast-in-place deck. The bridge was originally designed for the 1963 AASHO HS20 loading. For the field test, the load points were configured to simulate the placement of the eight rear wheels of two HS20 trucks.

For purposes of comparing the measured and predicted deflections, deflections at midspan were averaged and plotted versus total load. The concrete was assumed to be a bilinear elastic–plastic material and the prestressing steel was modeled using a known stress-strain curve provided from the manufacturer. From the material property curves, moment-curvature diagrams were developed and from these, analytical predictions of deflection. The bridge was considered to act as a single, wide beam with uniform distribution of the point loads across the transverse width of the bridge. Composite behavior was assumed throughout. The measured response is slightly stiffer than predicted in the elastic range, while the analytical curve is "steeper" once composite action is lost. Overall, the load-deflection curve was a reasonable estimate of the bridge behavior with the predicted strength of 1,267 kips being some 11% higher than the 1,140 kips measured. This difference is due to the loss of composite action. The applied load at failure is roughly nine times the load of an HS20 trailer excluding impact.

Burdette and Goodpasture (1988) report the results of a number of in-situ bridge load tests in NCHRP 306. The study was intended to compile domestic and foreign data on bridge testing with the objective of identifying aspects of observed behavior that are not commonly considered in bridge analysis and rating. They concluded that there are several aspects that cause bridges to behave different than expected including unintended continuity, unintended composite action, skew effects, and variation in transverse load distribution. Edge stiffening was cited as the reason that exterior beams attract more load and thus relieve the interior beams. They, and other researchers, i.e. Buckle, Dickson and Phillips (1985), indicate that unless this curb and rail are designed to act integrally with the bridge to the ultimate state, the curb/rail may shear away from the deck and the stiffening effect will be lost as ultimate load is approached. This edge stiffening effect is a detriment for damaged exterior beams since additional load will be attracted to members less capable of supporting it.

Of particular interest in the NCHRP 306 report is the extensive bibliography of bridge test summaries presented. One of these references (Gosbell and Stevens, 1968) reports the results of a test conducted on a bridge with similar beam spacing to the two Beebeetown test bridges. The bridge was loaded eccentrically in one lane to approximately three times the anticipated cracking load. The authors

concluded, *"remarkably little variation occurs in the distribution coefficients even after extensive cracking had developed at loads several times the initial cracking load. The use of distribution coefficients derived for elastic action therefore appears to be reasonable for approximate estimation of post cracking behavior."* They concluded that a wide beam theory assuming all beams equally sharing the load near ultimate was not appropriate.

Abdel-Halim, McClure and West (1987) comment on the experimental and analytical results of an ultimate load test conducted on a horizontally curved, 121 ft long, precast segmental bridge constructed on the test track of the Pennsylvania State University. The experimental and finite element results were compared to the theoretical results obtained using classical flexural analysis methods.

An allowance for tension stiffening was provided by the specification of an unloading branch of the tensile stress – strain curve. A crack in the element was assumed to soften the element in all directions, i.e. isotropically, but some shear stiffness was included. The prestressing steel was modeled with a strain-hardening model and the mild steel was assumed distributed throughout the concrete with a corresponding change in modulus of elasticity of the concrete brick elements.

Testing of the prototype bridge took nine days. Each day a higher increment of load was applied, sustained, and then released. The following day, loads were increased past the prior level. Load was applied in increments of 100 kips per day. A maximum load of 955 kips was applied to the bridge which was greater than the capacity predicted by either the finite element or standard strain compatibility methods. The finite element analysis prediction was 920 kips while the strain compatibility prediction was 901 kips; the finite element analysis was closer to the experimental results in both load and deflection for all stages of loading. As a predictor of ultimate strength, the strain compatibility method is only 5.65% less than the experimental result but the deflection at ultimate, 43.5 in., is over twice that observed, 22.1 in. The conventional strain compatibility method was not accurate at predicting deflection, especially in the inelastic state. The measured strength of this beam results in a live load factor at failure of 5.15, much higher than the specified live load factor of 2.17 specified in the Load Factor provisions of the AASHTO Standard Specifications (AASHTO, 1996). This large reserve strength is typical of prestressed concrete members designed for crack control at service conditions.

Buckle, Dickson and Phillips (1985) report on the ultimate load behavior of three reinforced concrete T-beam bridges tested in-situ to failure in New Zealand. In their research, it was found that a significant under-prediction of ultimate moment (by approximately 1/3) occurred. Only a finite element analysis conducted using an eccentrically stiffened plate model was able to capture the membrane effects and nonlinear behavior of the structure. A special element type was employed for the reinforced concrete modeling known as a filament element. Filament elements can capture the biaxial stress state in the slab and can assume an uncracked, compression yield, crushed, and cracked (with or without tension stiffening) state with iteration during each load cycle to determine the element status and to adjust the stiffness matrix accordingly. The experimental results were compared to three different finite element analyses – no tensile

strength of concrete, tensile strength up to cracking, and tensile strength to cracking followed by tension stiffening. The analyses with some allowance for tension were significantly closer to the predicted load deflection curve than was the model that ignores concrete tensile strength. Even the models that were presumed uncracked generate larger deflections than the prototype structures, which were significantly cracked before testing. The authors attributed this to not being able to model the stiffness contribution of the barrier rail, the effects of load distribution, and the degree of end restraint.

It was recommended that because of the enhanced load capacity of these exterior beams due to the presence of the stiff rail system that permit loads not be centered on the bridge but be located in an exterior lane. In such a position, the large moment of inertia of the edge stiffened beam results in lower stresses than if the permit vehicle was centered over the interior of the bridge.

The conclusion of their research was that observed strengths far in excess of those predicted by ultimate strength theory were present. An eccentrically stiffened plate model using filament elements accurately predicted the strength. A finite element model of this complexity was recommended as a minimum for predicting the ultimate strength of concrete bridges.

Idriss and White (1991) discus the role that secondary load paths assume when a bridge is subjected to a localized damage. In their work, they have concentrated on the performance of damaged multiple stringer steel beam bridges. Idriss and White rightly contend that the assessment of redundant load paths is critical in evaluating damaged structures.

The analysis performed in the research was based on the plastic collapse theory involving the sequential formation of plastic hinges throughout a structure during incremental loading. To determine the suitability of their model, the authors compared the predicted load-deflection response of four bridges to the experimental results from full-scale tests of the structures during the AASHTO road test experiments of the 1960's. Excellent correlation was found up to the formation of permanent set after which the analytical model predicted deflections that were smaller than the measured deflections.

In order to study deterioration/damage effects, two bridges, a 50 ft non-composite rolled shape structure and a 180 ft composite plate girder structure were studied. Both bridges had four longitudinal beams, an 8 in. concrete slab and a 28 ft roadway width. Three levels of damage were studied, flange loss of 50%, 100%, and a full-depth crack extending up to the bottom of the top flange. The bridges were loaded with two lanes of live load with the trucks positioned at midspan to cause maximum positive moment.

Both bridges demonstrated the expected response, a local defect in the exterior beam caused a corresponding increase in load and deflection in adjacent beams with the beam closest to the damage receiving the majority of the redistributed load. The more severe a defect, the more significant the redistribution. Incremental collapse followed a predictable pattern, formation of plastic hinges in the damaged member, shedding of load to the slab and diaphragm nearest the defect, formation of failure mechanisms in the nearest beam, shedding of load, etc. The more severe the defect, the greater the distress

in the surrounding slab and adjacent diaphragms. The 50 ft span was able to sustain a live load of 5.0, 4.11, 3.1, and 3.0 times the AASHTO HS20 live load plus impact load for no defect, a 50% loss of flange, 100% loss of flange, and full depth crack, respectively. The 180 ft span had similar load factors of 6.6, 5.0, 3.4, and 2.0. It should be noted that first member failure was far below these load factors, lending support to the importance of load redistribution/shedding in determining the ultimate strength of a bridge.

## *2.2. Beam Testing and Repair*

In two NCHRP reports, NCHRP 226 and NCHRP 280, Shanafelt and Horn (1980, 1985) presented the first comprehensive examination of the problem of repairing impact damaged prestressed concrete bridge beams. Phase I of the report, NCHRP 226, concentrated on the state-of-the-art in the assessment and repair of impact damaged prestressed concrete bridge beams while NCHRP 280 presented a manual of recommended practice and the results from a number of repair technique experiments. Shanafelt and Horn found that accidental damage was the cause of over 80% of the damage reported to prestressed concrete bridge beams. Their two reports address the service, overload, and ultimate strength of damaged beams as well as cost, speed of repair and ease of application of a variety of repair techniques.

In Phase I of the investigation, it was determined that there was a great disparity in levels of damage considered acceptable/repairable. Some agencies analyze a bridge in its damaged condition for the loads the damaged beam is expected to carry while others choose to remove any beam whose capacity is less than that of the original design. Some agencies remove any beam with a loss of prestressing while others consider the amount of steel lost.

Phase I presented analytical calculations illustrating the strengthening of severely damaged beams. Severe damage was broadly defined as damage to the concrete and reinforcing of a prestressed concrete beam. This damage could include significant loss of section of the bottom flange or web, apparent damage to the prestressing steel, or appreciable misalignment of the bottom flange of the beam. Severe damage was reported in 15% of the bridges according to a survey conducted during the NCHRP 226 project. The types of repairs studied include repair with externally bonded rebar, external post-tensioning using strands or bars, the use of a mild steel external sleeve, and the use of internal strand splices. The external rebar and post-tensioning repairs all require the restoration of the original cross-section as well as the addition of external concrete corbels to house the new reinforcing.

Shanafelt and Horn advocate the use of preload when repairing damaged prestressed concrete beams. Preload consists of the application of a load to the damaged beam prior to repair. This preload may be applied via jacks or by a loaded vehicle. Once the beam is patched and the patch concrete reaches a minimum specified strength, the preload is removed, the beam rebounds, and the patch concrete effectively precompressed as if it had been prestressed. This preload will increase the durability of the patch material, as in most cases it will prevent cracking under live load. This uncracked section is analogous to an

undamaged beam for stress computations. At the time the NCHRP 226 report was written, nine transportation agencies reported the use of preload in the repair of damaged beams.

A concern for damaged beams is their remaining fatigue life. Engineers typically ignore the possibility of fatigue in prestressed concrete however Shanafelt and Horn report that strands stressed to a maximum stress range of 10% of their ultimate tensile strength have a fatigue life of approximately $2x10^6$ cycles. This is not usually a concern in uncracked beams since the fatigue stress range is relatively small in an uncracked specimen. However, in the presence of cracks, the stress range in a strand is significantly higher. Shanafelt and Horn reported in NCHRP 226 that *"There are no known fatigue tests of beams that suffered concrete fractures due to overheight vehicle impacts. There have been fatigue tests of girders that have been cracked by test loads."* (NCHRP 226 p. 34) The test results of intentionally cracked beams indicate fatigue failures in as little as 458,000 cycles for cyclic loads applied to a heavily cracked beam at high nominal stress levels, 48% to 54% of the ultimate strength of the beam. Failure occurred in approximately $3x10^6$ cycles when the nominal stresses, computed on the basis of an uncracked section, were kept below $6\sqrt{f'_c}$ . These stress computations based on an uncracked section are often cited in prestressed beam fatigue research though they are of little meaning since the beam is cracked and it is the stress range in the strands of the cracked section that influences the beam fatigue life.

Concurrent with the Iowa State University research, the University of Texas at Austin conducted a multi-part study on the state-of-the-art of prestressed concrete beam repair, the results of which are briefly described herein. Several companion papers are available in addition to the published reports. These papers include Jones (1996); Feldman, Jirsa and Kowal (1998); Zobel, Carrasquillo and Fowler (1997); and Civjan, Jirsa, Carrasquillo and Fowler (1998).

"Current Practice in the Repair of Prestressed Bridge Girders", Report FHWA/TX-96/1370-1, is a report written by Feldman, Jirsa, Fowler, and Carrasquillo (1996) at the University of Texas at Austin for the Texas DOT. Originally published in August 1993, and subsequently revised in June 1996, the report is essentially a revisiting of the issues originally explored in the NCHRP 226 and 280 reports with some additional information pertaining to nondestructive evaluation techniques for assessing the damage to prestressed concrete bridge beams. In this report, a survey of current practice related to the assessment and repair of damaged prestressed bridges in the various Texas DOT Districts as well in other states and the provinces of Canada was conducted. One of the interesting observations of the survey is that for beams which were judged to be severely damaged, (i.e., those where strands are exposed and damaged or severed, concrete is lost, and the beam is offset), in 54% of the cases in the United States and Canada, the beam was replaced while in 46% of the cases, the beam was repaired. This is an indication that a blanket characterization that when strands are damaged the beam should be replaced is unnecessary. This is consistent with the recommendations made by Shanafelt and Horn in their two NCHRP reports. The Texas DOT report also asserts that which the Iowa State research project will attempt to prove, *"Even if one or*

*more girders are damaged, the structural performance of the bridge may not be affected due to the possibility of load redistribution and safety factors used in the original design"*.

"Method to Evaluate Remaining Prestress in Damaged Prestressed Bridge Girders", is written by Civjan, Jirsa, Carrasquillo, and Fowler (1995) of the University of Texas at Austin for the Texas DOT. The work was also published in paper form as Civjan et al. (1998). Civjan et al. concluded during their research that many agencies are reluctant to repair beams with exposed strands or significant loss of section. Their research endeavored to provide a means for rationally assessing the effect of localized damage on remaining prestressing force.

Because there is always a degree of uncertainty when assessing the long-term losses in prestressed beams and henceforth a degree of uncertainty in computing the behavior of the beam as a whole, it was desired to develop a nondestructive technique whereby the effective prestress in a prestressing strand could be measured. The apparatus should not only be able to measure the remaining effective prestress in a strand but should also be small enough that it could be used on a damaged beam where the length of exposed strand may only be a few feet. The instrument developed uses the applied lateral load vs. deflection response to estimate the remaining force in the strand. The instrument can be installed on exposed strand lengths as small as 1 ft-6 in. which should encompass most exposed strands whose prestress is suspect following an impact.

The instrument consists of a load cell, dial gage, and a small jack that provides a lateral load against the exposed strand. The dial gage and load cell are used to measure the load vs. deflection response. From charts that correlate the load vs. deflection response of the exposed strand to the level of prestressing force, a fairly accurate estimate of strand force can be made.

For the final prototype instrument, a 12 in. gage length was used. A series of tests were conducted on exposed strand lengths of 1 ft-6 in. up to 3 ft-9 in. long. Length effects were determined to be insignificant. Simple curves were developed that relate the slope of the load-displacement response of the laterally loaded strand to the strand tension. From the calibration tests, a test manual was developed.

The instrument was used to measure the stress introduced into prestressing strands of a damaged beam that were spliced in the lab. It was concluded that the instrument is an accurate and easy to use method of evaluating the effective prestress in damaged beams and in assessing the tension introduced into spliced strands.

In "Evaluation and Repair of Impact-Damaged Prestressed Concrete Bridge Girders", Zobel, Jirsa, Fowler and Carrasquillo (1997) report on the repair of a damaged prestressed concrete beam removed from a railroad bridge in Austin, TX. Companion papers include Jones (1996), Feldman et al. (1998), Zobel, Carrasquillo and Fowler (1997), and Zobel and Jirsa (1998). The objective of the beam test program was to study a variety of nondestructive damage assessment techniques, investigate the effectiveness of internal strand splices and to evaluate various patching materials and methods. Their report is extensive and

contains valuable information that supplements and further validates much of the other research on prestressed concrete beam repairs.

"Reusability and Impact Damage Repair of Twenty-Year-Old AASHTO Type III Girders" is a report prepared by Olson, French, and Leon (1992) for the Minnesota DOT. A companion paper that also describes the research is Leon (1990). The objectives of the research were:

- Determine the effective prestress in a series of beams removed from service after 20 years
- Determine the influence of damage on beam performance
- Evaluate the worthiness of internal splicing and external post-tensioning techniques
- Develop a model to estimate strand stress ranges in damaged beams

Four beams were tested, one undamaged, one with severed strands, one with severed strands and internal splices, and the final one with severed strands and an externally post-tensioned splice. The splices were similar to those used by Shanafelt and Horn in NCHRP 226 and 280.

Beam 1 was used as a control specimen to determine the effective prestress in the strands and also to observe the fatigue performance of the beam. Following the fatigue loading, an ultimate load test was conducted. Measurements of the loads required to crack the beam as well to reopen the cracks indicated that the effective prestress in the beams was on the order of 130 ksi, a 45 ksi reduction from the initial jacking stress of 0.7 x 250 ksi = 175 ksi. During the fatigue tests, the beam was subjected to increasing loads so as to produce different magnitudes of bottom fiber tensile stresses. Loads were applied so that the nominal bottom fiber stress based on uncracked section properties was 0, 3, 6, or $12\sqrt{f'_c}$ . Results indicate that for an effective stress of 130 ksi and a nominal stress of $12\sqrt{f'_c}$ in the bottom flange, the stress range in the strands was 31.4 ksi and the fatigue life was 570,000 cycles. If the effective stress is reduced to 110 ksi, as was measured in subsequent beam tests where stress in the exposed strands was measured directly, the fatigue life drops to 130,000 cycles. This assumes that all strands are intact. The ultimate load test on this beam indicated that the beam had a capacity of 53,110 in-kips at a centerline deflection of 21.5 in. Failure was eventually by crushing of the slab at midspan and a secondary compression failure in the top flange of the beam. The measured strength was compared to the AASHTO equation prediction of 47,100 in-kips, the ACI/PCI equation prediction of 47,140 in-kips, and the assumption that all strands yield prediction of 48,800 in-kips. The measured strength was found to be higher than the predicted strength in all cases.

Beam 2 was used to study an incrementally damaged beam. First the beam was cracked similar to Beam 1. A pre-damage fatigue program of 500,000 cycles at a nominal tension of $3\sqrt{f'_c}$ and $1.5 \times 10^6$ cycles at nominal $6\sqrt{f'_c}$ were imposed. Following this portion of the test, concrete was removed from the bottom flange and an additional 500,000 cycles were imposed. Two strands were then severed; after 300,000 additional cycles, a third strand broke. Following 200,000 more cycles, a fourth strand was severed. When the loading was started again, the beam began to deflect in an unstable manner. Over the

next 17,600 cycles, the deflection increased by more than 18% under a constant cyclic load. The measured remaining effective prestress in this beam was approximately 110 ksi, indicating a loss of 65 ksi had taken place. Prior to any strands being damaged, the strands experienced a stress range of approximately 25 ksi, corresponding to a predicted fatigue life of 1.28 million cycles. After two strands were severed and the third strand broke, the stress range in the fourth exposed strand increased to 40 ksi corresponding to a predicted fatigue life of only 247,000 cycles. The severing of only 3 of the 30 strands in the beam resulted in a reduction in fatigue life of over 80%. A small reduction in the total prestress force corresponded to a drastic increase in stress range for a slightly damaged beam. The ultimate strength of this beam was only 71% of Beam 1 but had a larger ultimate deflection of approximately 26 in.

Beam 3 was used to study the behavior of an internally spliced damaged beam. Following a cracking load and pre-damage fatigue program similar to those described above, two strands were severed and spliced using a chuck and turnbuckle assembly similar to that shown in Shanafelt and Horn's NCHRP 226 and 280 reports. The severed strands are anchored in chucks which are connected by rigid pieces of threaded high strength rod to an opposite thread turnbuckle. One of the threaded rods was also a load cell used to measure the force in the spliced strand. As the turnbuckle is tightened, it draws the severed strand together and re-tensions the strand. Following installation of the first splice, the beam was preloaded and anchorage seating losses occurred; following re-tensioning of the first splice to the original design level, the second splice was installed and the beam preloaded. The second splice was not subsequently re-tightened. A patch was installed, and after three days, the preload removed. This method of internal repair, with the exception of the use of a load cell, is also described in Shanafelt and Horn (1980, 1985), Feldman, Jirsa, Fowler and Carrasquillo (1996) and Zobel, Jirsa, Fowler and Carrasquillo (1997), all mentioned previously in this chapter. During the post-repair fatigue testing of the damaged beam, one of the repaired strands suffered a fatigue fracture adjacent to the spliced region. Prior to fatigue failure, the stress in the adjacent undamaged strands was essentially the same as if no strands had been severed. The stress range in the spliced strands increased significantly because the repair is significantly axially stiffer than the original strands. Based on this stiffness difference, the measured stress ranges in the repaired strands were 1.5 - 2 times greater than those in the undamaged strands, thus the reason for the observed fatigue fracture in the spliced strand. During the ultimate load test, at a load of 55% of the ultimate load of Beam 1, and a midspan deflection of approximately 2.5 in., the patch concrete containing the repaired strands spalled and subsequently the spliced strands failed. This was due to the incompatibility of the deformation of the very flexurally rigid splice and the rotations at the midspan of the beam. This incompatibility of curvature forced the patch away from the beam and caused the strands to fracture. The beam attained a maximum capacity of approximately 82% of Beam 1 and an ultimate displacement of 21 in.

Halsey and Miller (1996) discuss the destructive testing of two prestressed concrete beams removed from service after forty years. The bridge from which the beams were removed consisted of inverted T-beams with a cast-in-place concrete fill that tied the units together and provided the riding

surface. The objectives of the research were to determine the effective prestressing force and ultimate load behavior. The authors made comparisons to results from specimens cast and tested at the time the bridge was constructed. This research is unique in that data from beams tested after being in service for forty years can be compared to the original baseline data.

A single point load test was conducted; deflections at the quarter points were measured and clip gages were used to measure concrete strains. Material properties were determined by core extraction following testing and indicated concrete compressive strengths of 11,790 psi for the beam concrete and 8,430 psi for the fill concrete. By contrast, the 1954 control beams had a strength of roughly 6,000 psi and 4,300 psi for the prestressed and fill concrete, respectively. This illustrates the sometimes dramatic increases in concrete strength with time.

Test results indicate that the specimens were both strong and ductile. A well-defined pre and post cracking stiffness were observed along with considerable deflection prior to failure. The concrete strain at the top of the beam prior to failure was measured to be –6,000 με, well in excess of the code-specified maximum usable strains of –3,000 με commonly considered in design. The computer program, Response, presented by Collins and Mitchell (1991) was used with the tension stiffening option employed. Measured material properties were input to the program. The results of the analysis yielded moment-deflection curves that were extremely accurate. Similar correlation of moments to concrete strain and strand strain was observed. This validates the moment-curvature method of analysis for predicting deflections and the ultimate capacity of prestressed concrete beams.

Effective prestress was studied in several ways. In one of the specimens, a strand was exposed over a short length, strain gaged and then cut; measured strains indicated a loss of 34%. Halsey and Miller question the accuracy of this result. Additional prestress loss computations were based on either the observed load at the formation of the first crack or the crack reopening load. Using these methods, loss values of between 21-27% were determined with the crack reopening method providing slightly smaller estimates of loss. The AASHTO method of predicting loss indicates an expected loss of 27% thus corroborating the crack formation/reopening methods of loss prediction. Examining the crack reopening load, one can conclude that cracks reopen at much lower loads than the load which corresponds to the knee in the load vs. deflection curve. Thus, the load-deflection curve knee should not be interpreted as the crack reopening load or unrealistically low estimates of prestress loss will be determined.

Results of the current research agree well with the original control specimen results and indicate no degradation of performance over the forty-year service life. Significant increases in concrete strength were observed. In general, the research concluded that losses and ultimate strength could be accurately determined, as could the load-displacement behavior of the beam up to the ultimate strength.

Pessiki, Kaczinski and Wescott (1996) discuss the laboratory testing of two Pennsylvania DOT type 24/60 prestressed concrete I-beams removed from service after approximately 28 years of service. The 89 ft long beams were 60 in. deep with 24 in. wide flanges. The beams were tested without a structural

slab, which had been removed during demolition of the bridge. Tests were conducted to determine the effective prestressing force and the ultimate load behavior of the beams which are undamaged and uncracked prior to testing. Beam testing was in three phases; cracking tests, crack reopening tests and ultimate load tests.

Three-point bending tests were conducted with a point load at midspan. Sixteen strain gages were mounted on the beam to determine the strain profile over the beam depth. Following initial crack observation, the load was slightly increased and all cracks marked. This process was repeated five more times to document additional cracks in the midspan region. The beams were also loaded and unloaded numerous times to determine the decompression load, i.e., the load at which the bottom fiber stress was zero. Decompression was established in three ways; visual observation of crack reopening, strain gage installation adjacent to known cracks and LVDT installation over known cracks. Strain gages mounted adjacent to a crack would read a linear tensile strain increase (reduction in precompression) until the crack opened at which point the strains remain constant with increasing load. LVDT measurements also produce a bilinear response with the crack width growing rapidly after the bottom flange is decompressed. The bilinear knee in the curve was used to establish a decompression load. Using the aforementioned methods, the crack reopening load was determined to be approximately 92 kips at midspan using the strain gage method, 103 kips using the LVDT method and 110-115 kips using visual observation. The strain gage method produced consistent readings through multiple load tests and was used to calculate prestress losses. It should be noted that the authors of this report, in examining the work of Pessiki, Kaczinski and Wescott, determined that simply examining the load-deflection plots is not sufficient to determine crack reopening. The bilinearity of the load-deflection curves occurs at a load much higher than the decompression load and should not be interpreted as the decompression load rather the onset of more severe structural cracking. This is confirmed by other researchers whose work has been reviewed herein (Halsey and Miller, 1996; Labia, Saiidi and Douglas, 1997).

Using the measured decompression load, Pessiki et al. determined a prestress loss of approximately 18% as compared to approximately 30% using three different empirical methods including the AASHTO equations. The measured losses were only 60% of that predicted.

The ultimate strength tests of these beams required an applied load of close to 250 kips corresponding to a total dead and live load moment of approximately 6,500 ft-kips and a shear of 166 kips. These values are in excess of the AASHTO predicted strengths by 7% for moment and 2% for shear. The beams ultimately failed in a combination of diagonal tension and concrete crushing near midspan. It is worth noting that these beams were not designed for this magnitude of shear near midspan.

Labia, Saiidi and Douglas (1997) discuss the testing of two 70 ft long pretensioned hollow box beams removed after 20 years of service from a bridge in Reno, NV. The research objective was to assess the behavior of the beams after service, in particular, the prestress loss and ultimate load behavior, and to compare the measured results with those predicted by code.

The specimens were tested in four-point bending with two equal point loads applied to create a constant moment region over the central 6 ft of the beam. The slab was purposely transversely sawcut between the point loads to eliminate composite action. The behavior of the beam was the only item of interest. A series of crack detection gages were mounted along the bottom of the beam over the central 10 ft in order to determine the first crack. An accelerometer was also mounted to the bottom flange to measure the cracking load. Several strands were exposed and instrumented near midspan.

Material properties were obtained from samples taken from the beams. The beam concrete had a compressive strength of 8,450 psi, and a modulus of elasticity of 5,500 ksi. This is in contrast to a specified strength of 4,000 psi. The steel strands had an ultimate tensile strength of 272 ksi and a modulus of elasticity of 30,020 ksi. These material properties were used in their theoretical calculations.

The first test conducted on each of the two beams was a cracking test. The accelograms provided the first indication of cracking followed by further accelogram spikes and visible cracking and lastly by rupturing of the crack detection gages. The change in slope of the load-deflection diagram occurs at a moment 18% higher than the moment that was applied when the crack was determined experimentally. This is further confirmation of the poor estimate of cracking when relying solely on the load-deflection response of a beam. The first cracks have essentially no effect on overall beam stiffness.

Estimates of prestress loss were based on several methods: crack reopening load, strand severing, use of suspended weights from the strands and measurement of the change in strain in the strands. The measured loss averaged 62 ksi as compared to the assumed lump-sum loss of 35 ksi used in the original design. Results from the ACI, AASHTO and PCI methods for computing losses whose values ranged from 43 to 50 ksi with a more refined time step approach yielding a loss of close to 55 ksi. Values from all of these methods, the value from the lump sum estimate in particular, are much less than measured losses. The authors attribute this to high shrinkage rates in higher strength concrete as well as increased creep losses due to Reno's temperature and humidity conditions.

The ultimate load test correlated very well with both the ACI/AASHTO method of calculating the ultimate moment and the strain compatibility method. The computed values were 91 and 97% of that measured for the ACI/AASHTO and strain compatibility methods when specified material properties were used and 95% and 101% respectively when measured material properties were used. The box failed in an explosive nonductile mode at a top fiber strain of –2,034 $\mu\varepsilon$ with vertical cracks at roughly the stirrup spacing in the constant moment region and inclined cracks in adjacent portions of the beams. The top slab, previously sawcut, delaminated from the beams as the ultimate load was approached. There was excellent agreement between the load-deflection curve for this beam and the one generated using the Collins and Mitchell (1991) computer program, Response, when measured material properties were used in the model. The correlation is highly dependent on the failure strain in the concrete. These beams had insufficient ductility due to the low failure strain in the concrete as well as the low amount of prestressing due to excessive prestress loss. The measured strand strain at failure was only slightly above yield.

Saiidi, Labia and Douglas (1997) comment on the repair and fatigue performance of a similar beam. Similar to the first two beams tested, this box beam was tested in four-point bending with the composite action in the maximum moment region purposely reduced by saw cutting of the cast-in-place slab. Four strands were exposed in the bottom of the box beam. Two of these strands were purposely severed and repaired with an internal strand splice mechanism similar to that used by Shanafelt and Horn as well as the University of Minnesota and University of Texas researchers. The research objective was to test the strand repair mechanism's sensitivity to fatigue including periodic static overloads.

Following installation of a concrete patch in the tension zone under a preload intended to precompress the patch concrete, a series of tests were conducted. A series of four static tests was conducted to check for splice slippage; no slip was detected. A cracking test followed by three crack reopening tests was then conducted. The maximum design load was applied for approximately 508,000 cycles to cause a bottom flange nominal tension stress (based on uncracked section properties) of $6\sqrt{f'_c}$ . Saiidi, Labia and Douglas cite work that indicates that a small number of overloads 20% above the normal design loads can cause significant increases in the strand stress range and thus lead to a diminished fatigue life. In order to test this theory, periodic overloads at 1.75 and 2 times the AASHTO HS20-44 design load level were applied during the fatigue testing.

In comparing results from the intact and repaired strands, a number of conclusions were drawn. The repaired strand strains were somewhat higher than the adjacent intact strands. This is consistent with what researchers at the University of Minnesota have found (Olson, French and Leon, 1992). The increased stress in the repaired strand is attributed to the axial stiffness and restraint of the repair assembly. From first cracking to the final overload test conducted nearly 500,000 cycles of full design load later (which included 11 overload tests) the range of stress in the intact and repaired strands increased 71% and 92%, respectively, even though the peak loads were kept constant. Deflections at a similar load were found to increase by 19% from the first cracking test to the final overload test. Cracks propagated from 12 in. in the cracking test to 17 in. from the bottom of the beam in the final overload test.

The ultimate load capacity of this beam was 87% of that of the two control specimens. Deflection was 65% of the other beams. Failure of this beam was through flexural-shear underneath one of the load points. The patch was still intact at this point and inspection of the beam following collapse did not reveal the existence of fatigue fractures in the stirrups or strands. The shear failure was attributed to a reduced concrete shear strength due to the formation of cracks during the fatigue testing. The cracks reduce the shear strength of concrete and also subject the stirrups to an increased stress range, which has been shown by other researchers to fracture the stirrups bridging the cracks. The authors concluded that fatigue in conjunction with periodic overloads cause sufficient cracking to render a beam particularly vulnerable to a shear failure. They cite work by Kreger, Bachman and Breen (1989) who similarly concluded that cracked beams are sensitive to fatigue failure in shear. Both the work by Saiidi, Labia and Douglas as well as that by Kreger, Bachman and Breen suggest that a significant reduction in concrete shear strength be made in

order to account for reduced strength once cracking begins. This guarantees an adequate number of stirrups so that fracture can be prevented.

Lane, Leeming, Darby and Fasholé-Luke (1997) discuss the testing of 18 m long post-tensioned concrete beams removed from service in the UK in 1993 due to corrosion of the post-tensioning tendons. Corrosion was due to improper grouting of the post-tensioning ducts and subsequent significant corrosion of the tendons in the anchorage zone. A total of ten beams were removed from the bridge and preserved for structural testing as part of the ROBUST (stRengthening Of Bridges Using polymeric compoSite maTerials) program in the UK. One of the main objectives of the ROBUST program was to develop design guidelines for the FRP strengthening of reinforced and prestressed concrete beams. An extensive experimental and analytical study on model beams 1.0 m, 2.3 m, and 4.5 m long, was conducted in addition to the full-scale tests described herein. One of the unique features of the CFRP strengthening work described in the following text is the use of prestressed plates as well as the more traditional unstressed plates.

The 18 m long post-tensioned concrete bridge beams were tested in four-point bending with loads 3 m on center applied symmetrically about midspan. A number of various strengthening techniques were studied including unstressed and 50% stressed plates, one to three layers of material, anchored or unanchored plate ends, and various strip lengths. The strip stress was monitored during severing of some of the tendons. Because the beams were tested without a composite slab, the five tendons in each beam represented an over-reinforced condition. To remedy this, three of the tendons were cut at 1.5 m on center in four locations near the center of the beams; CFRP plate stresses were monitored to detect stress transfer during severing. All beams were tested to 80% of ultimate prior to retrofitting and again following retrofitting. Displacements were monitored, as were strains in the concrete and composite material.

Numerical modeling using ANSYS was employed in this research. A model using 8 noded quadrilateral isoparametric 2D plane-strain elements was first used. This model gave acceptable results for the plated beams but unacceptable accuracy in the un-plated beams, which is attributed to the model's inability to include the effects of cracking. Additionally, the model required "tuning" for every test to give an acceptable degree of accuracy. For this reason it was a poor prediction model and its use was discontinued. A second model using the SOLID65 3D Reinforced Concrete Solid element in ANSYS was generated. This model was used to check the experimental values of the 1 m and 2.3 m long model beams tested in prior portions of the ROBUST program and gave excellent results for both plated and un-plated beams. This model was able to predict the response of beams prior to testing. For this reason, the SOLID65 model was used for the post-tensioned beam experiments. Further information on the ROBUST analytical program can be found in Lane, Fasholé-Luke and Leeming (1997).

Results of the testing indicate that for Beam 2 in which the retrofit consisted of two layers (three plates per layer) of unstressed 90 mm x 1 mm plates, with unanchored ends placed over a 15.8 m length, the effect of the retrofit was significant. The beam with three severed tendons out of five behaved like a

beam with only two severed tendons, the CFRP replacing the stiffness and strength of one post-tensioning tendon. The increase in strength was approximately 60% over the un-plated control specimen. The analytically predicted values and the experimental deflections and ultimate load were in excellent agreement.

A separate beam was monitored during the loading to 80% of ultimate. Strain gages placed directly under one of the core holes drilled to relieve the prestressing force were 46% to 64% higher than predicted while stresses in the center of the beam in the CFRP plate were only 16% of that predicted. The stresses were not symmetric about midspan though the loading was. The general conclusion of the authors was that at preexisting cracks (points of weakness) the stress in the plate is locally very high while in undisturbed regions between the cracks, the stress is low. The plates had locally debonded near the core holes during testing due to the locally high stresses around the radial cracks extending from the core holes. An estimate of plate stress using linear strain distributions results in a safe estimate of plate stress as compared to a somewhat lower estimate using finite element methods. Both approaches neglected the presence of holes however and thus underestimate the stress concentrations around previously cracked concrete.

Aboutaha et al. (1997) discuss the strengthening of a 30 ft long severely damaged AASHTO Type II prestressed concrete beam. Following a series of tests in which both ends of the beam were tested to failure as propped cantilevers to study the bond strength of pretensioned concrete beams, it was decided to strengthen the beams using CFRP composites. The strengthening was carried out following the initial bond tests in which the beams experienced major cracking, crushing of the concrete zone and loss of 80% of their initial stiffness. The cracking was primarily a series of major flexural cracks that extended into the top flange. The loss of stiffness is attributable to permanent deformation of the prestressing strands as well as slip of the strands. Although the damage was significant, it was thought that the beams were repairable.

Repair consisted of patching of the damaged compression zone with an epoxy mortar whose strength was comparable to the beam strength, 10,000 psi, as well as installation of two different configurations of the Mitsubishi Replark strengthening system. End “A” was retrofit with three layers of fabric on the bottom and sides of the tension flange and two on each side of the web. End “B” had six layers of material on the bottom of the flange, four on the sides of the flange and two on each side of the web. All fibers were oriented longitudinally. The tensile strength of the fabric is 160 ksi and the Modulus of Elasticity is 10,000 ksi.

The CFRP restored the stiffness of the repaired beam from 20% of the initial stiffness to 50% of the initial stiffness. CFRP or FRP’s in general are effective in strength restoration but not necessarily in stiffness restoration. By supplying enough material to restore the beam stiffness, the strength of the beam would have been triple that of the baseline undamaged specimen. Additionally, the application of a significant amount of tensile material to the beam just to restore stiffness will significantly change the ductility of the section, making it generally much more brittle.

The response of the repaired beam was excellent; it exhibited good ductility and had an ultimate strength much higher than the undamaged original beam. The failure load and deflection of the repaired beam were both higher than in the undamaged specimen. The externally bonded CFRP greatly increased the flexural capacity of the beam and subsequently the shear demand during experimental loading. The ultimate failure of the beam was a combination shear/bond failure at the termination of the CFRP with the concrete cover and strip peeling away from the beam. The ultimate load applied to the basic beam was 225 kips at End "A" and 250 kips at End "B". The repaired strengths are approximately 325 kips and 350 kips at the two ends, respectively.

Aboutaha et al. concluded that the CFRP application was an effective means of restoring elastic stiffness as well as providing additional strength to truck damaged bridge beams. They indicate that additional research is needed to develop design guidelines.

Nanni, Arduini and Boothby (1997) document the use of CFRP to strengthen a series of undamaged and precracked reinforced concrete laboratory specimens. Specimens representative of both slab and beam geometries were tested. Only the beam specimens are discussed herein.

The control beam, M1, failed as expected in a ductile fashion with the concrete crushing only after a long yield plateau. Specimens MM2 and MM3, retrofit with one layer of unidirectional material oriented along the beam, failed following debonding of the CFRP sheets from the beams. The debonding began in the constant moment region near one of the flexural cracks and progressed toward the end of the beam. Application of two more layers for specimen MM4 resulted in only slightly more strength since failure was still governed by shear and debonding failures. Beam MM5 was retrofit with two longitudinal and one transverse ply on the bottom face along with one ply in each direction on the vertical faces of the beams. This specimen failed at a load more than twice that of the control specimen and nearly twice that of the other retrofit specimens. Ultimate failure was by shear of the beam at the support point.

Nanni, Arduini and Boothby concluded that when debonding failure controls strengthening schemes, there is little benefit to providing excessive material. Testing of preimpregnated as well as wet lay-up material retrofits revealed very little difference in results. The performance of the precracked specimens was not much different than uncracked specimens with only a slight decrease in stiffness. Surface preparation by sand blasting was demonstrated to be only slightly better than sanding. The effectiveness of transverse plies was deemed to be very important in preventing premature peeling and delamination.

# *CHAPTER 3*
# *I-680 FIELD TEST RESULTS*

This Chapter describes the results of a field test conducted in June 1997, on two similar pretensioned concrete I-beam bridges located in Beebeetown, IA, as well as a follow-up test conducted in August 1998. The bridges carry I-680 over county road L34 northeast of Council Bluffs, IA. The bridges are asymmetric three-span structures designed by the Iowa DOT in August 1965. The spans measure 43 ft-1 1/2 in., 56 ft-3 in., and 47 ft-3 1/2 in. from east to west between the substructure centerlines. An overview and elevation view of the structures are presented in Figures 3.1 and 3.2.

There are eleven beam lines in each structure. The first seven beam lines adjacent to the median are on 5 ft centers. This spacing is typical of Iowa DOT practice at the time these bridges were designed and constructed. In order to account for a ramp taper on both the eastbound (EB) and westbound (WB) bridges, flared beam lines are present on both structures. The flared beams are spaced at 3 ft-6 in. centers as a minimum and flare out to 5 ft-0 in. on center at their widest point. Iowa DOT "B" beams are used in all spans, types B1, B4, and B2, for the east, center, and west spans, respectively. These beams all have the same cross section and are different only in the pattern and amount of prestressing. A typical "B" beam is presented in Figure 3.3. The original beams are composed of concrete having a specified 28-day strength of 5,000 psi and contain 7/16 in. $\phi$, 250 ksi stress-relieved strands. With the exception of Beams 1W and 2W in the center span of the WB bridge which will be described later in more detail, all beams are original to the bridge. The bridges were designed per the 1961 AASHO (now AASHTO) Standard Specification for Highway Bridges for H20-S16 loading. A 6 in. nominal slab was originally specified for both bridges with a subsequent 1 1/2 in. dense concrete overlay in 1985. However, the measured thickness of the slab-in-place including overlay exceeded 9 in. when the damaged beams were removed from the WB bridge. The overlay was approximately 3 in. thick. A description of the bridges as well as the instrumentation layout and position of test loads is presented in Figures 3.4 through 3.6.

Overheight vehicles have struck the WB bridge in Beebeetown numerous times. In 1985, a collision resulted in the replacement of two of the original B4 beams with an Iowa DOT standard beam known as a B55R. The B55R has a similar geometric cross-section as the original B4 but has a different strand configuration.

Table 3.1 describes the beam designation and strand configuration for all beams in both the WB and EB structures.

**Figure 3.1. Overview of WB (Foreground) and EB Bridges.**

**Figure 3.2. Elevation View of WB Bridge, Looking West (Damaged Beam 1W in Center Span).**

Note: Unless otherwise noted, all dimensions are in inches.

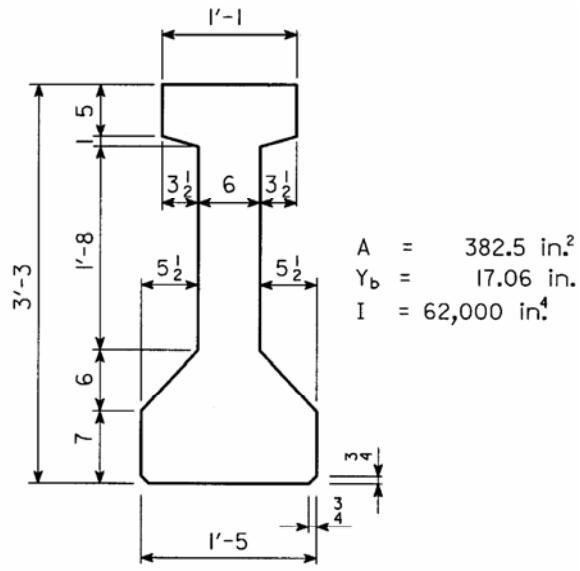


**Figure 3.3. Iowa DOT B Beam Cross-Section.**

**Table 3.1. Description of Prestressed Beams in the Beebeetown Bridges.**

| BRIDGE | SPAN | BEAM TYPE | STRAND PATTERN |
|---|---|---|---|
| Westbound | East | B1 | 17 straight, 7/16 in., 250 ksi stress-relieved strands |
| | Center | • B4, Beams 3-11<br>• B55R, Beams 1-2, 1997 Test<br>• LXB55, Beams 1-2, 1998 Test | • 16 straight, 6 harped, 7/16 in., 250 ksi stress-relieved strands<br>• 14 straight, 4 harped, 1/2 in., 250 ksi stress-relieved strands<br>• 12 straight, 4 harped, 1/2 in., 270 ksi low-relaxation strands |
| | West | B2 | 19 Straight, 7/16 in., 250 ksi stress-relieved strands |
| Eastbound | East | B1 | 17 straight, 7/16 in., 250 ksi stress-relieved strands |
| | Center | B4 | 16 straight, 6 harped, 7/16 in., 250 ksi stress-relieved strands |
| | West | B2 | 19 Straight, 7/16 in., 250 ksi stress-relieved strands |

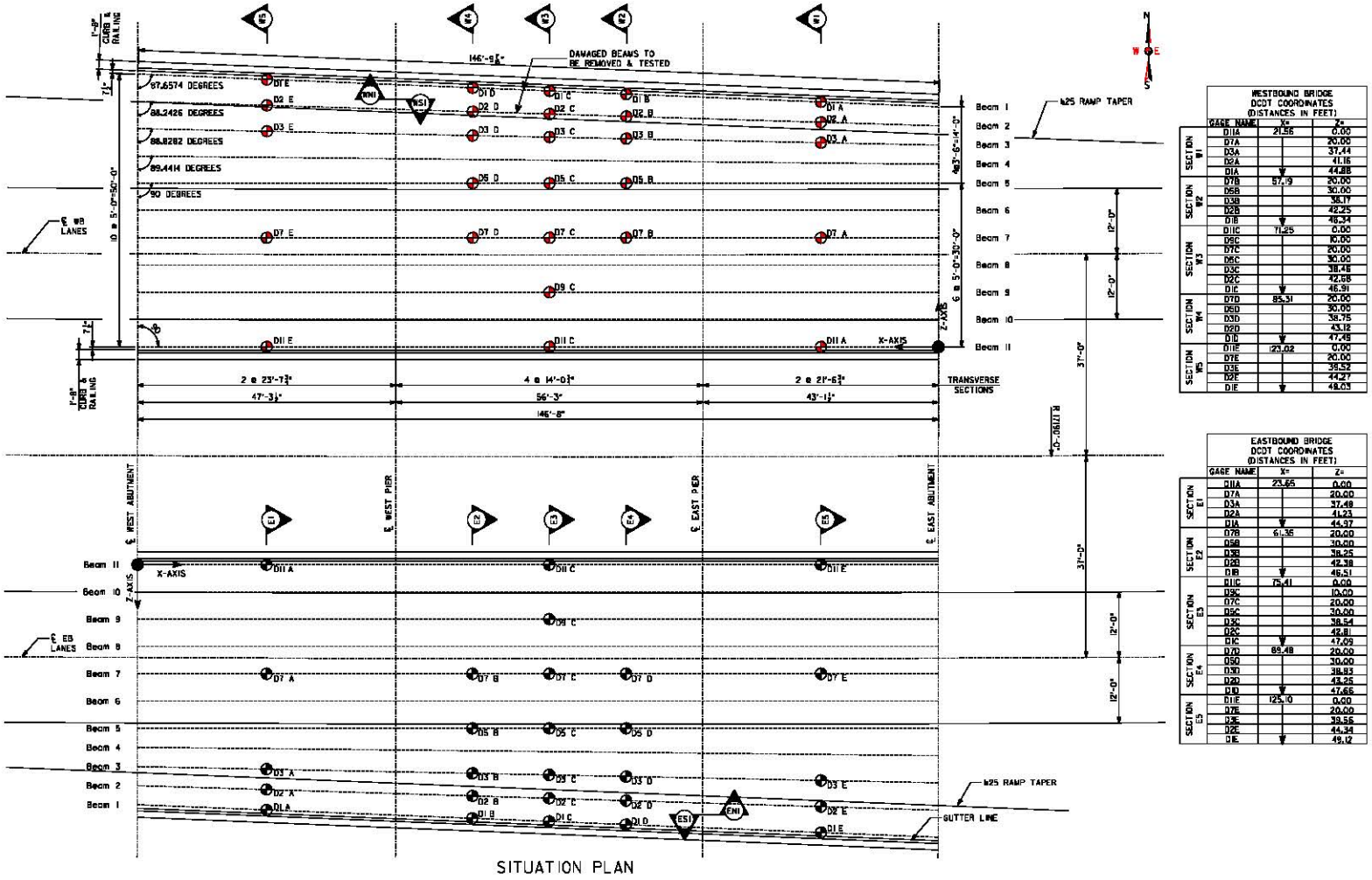


WESTBOUND BRIDGE DCDT COORDINATES (DISTANCES IN FEET)

| | GAGE NAME | X= | Z= |
|---|---|---|---|
| SECTION W1 | D11A | 21.56 | 0.00 |
| | D7A | | 20.00 |
| | D3A | | 37.44 |
| | D2A | | 41.16 |
| | D1A | | 44.88 |
| SECTION W2 | D7B | 57.19 | 20.00 |
| | D5B | | 30.00 |
| | D3B | | 38.17 |
| | D2B | | 42.25 |
| | D1B | | 46.34 |
| SECTION W3 | D11C | 71.25 | 0.00 |
| | D9C | | 10.00 |
| | D7C | | 20.00 |
| | D5C | | 30.00 |
| | D3C | | 38.48 |
| | D2C | | 42.68 |
| | D1C | | 46.91 |
| SECTION W4 | D7D | 85.31 | 20.00 |
| | D5D | | 30.00 |
| | D3D | | 38.75 |
| | D2D | | 43.12 |
| | D1D | | 47.48 |
| SECTION W5 | D11E | 123.02 | 0.00 |
| | D7E | | 20.00 |
| | D3E | | 39.52 |
| | D2E | | 44.27 |
| | D1E | | 49.03 |

EASTBOUND BRIDGE DCDT COORDINATES (DISTANCES IN FEET)

| | GAGE NAME | X= | Z= |
|---|---|---|---|
| SECTION E1 | D11A | 23.65 | 0.00 |
| | D7A | | 20.00 |
| | D3A | | 37.48 |
| | D2A | | 41.23 |
| | D1A | | 44.97 |
| SECTION E2 | D7B | 61.36 | 20.00 |
| | D5B | | 30.00 |
| | D3B | | 38.25 |
| | D2B | | 42.38 |
| | D1B | | 46.51 |
| SECTION E3 | D11C | 75.41 | 0.00 |
| | D9C | | 10.00 |
| | D7C | | 20.00 |
| | D5C | | 30.00 |
| | D3C | | 38.54 |
| | D2C | | 42.81 |
| | D1C | | 47.09 |
| SECTION E4 | D7D | 89.48 | 20.00 |
| | D5D | | 30.00 |
| | D3D | | 38.83 |
| | D2D | | 43.25 |
| | D1D | | 47.66 |
| SECTION E5 | D11E | 125.10 | 0.00 |
| | D7E | | 20.00 |
| | D3E | | 39.56 |
| | D2E | | 44.34 |
| | D1E | | 49.12 |

**Figure** Error! No text of specified style in document.**.1. I-680 over County Road L34: Plan View of Beams and Deflection Transducer Layout.**

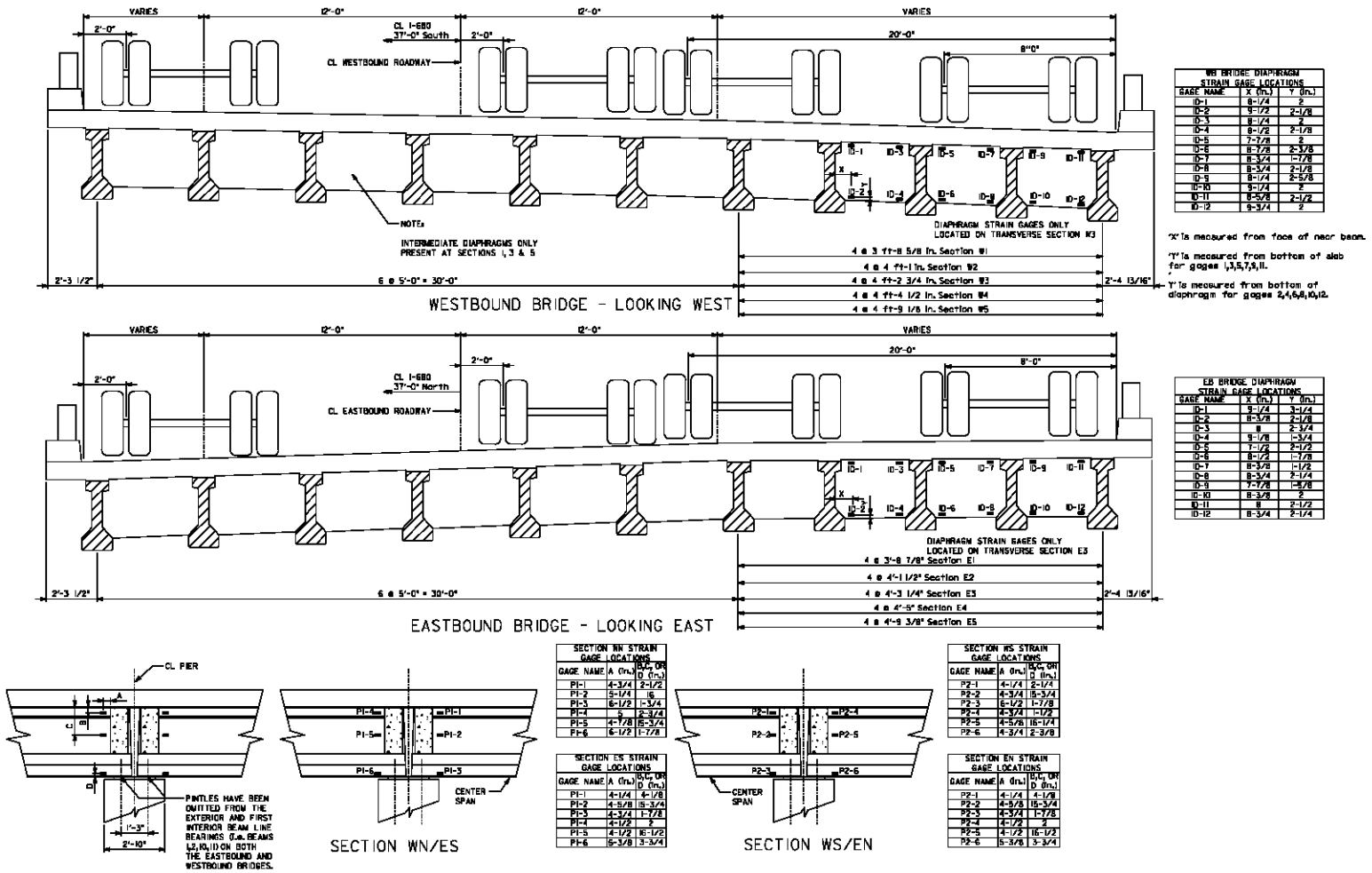


| WB BRIDGE DIAPHRAGM STRAIN GAGE LOCATIONS | | |
|---|---|---|
| GAGE NAME | X (in.) | Y (in.) |
| ID-1 | 8-1/4 | 2 |
| ID-2 | 9-1/2 | 2-1/8 |
| ID-3 | 8-1/4 | 2 |
| ID-4 | 8-1/2 | 2-1/8 |
| ID-5 | 7-7/8 | 2 |
| ID-6 | 8-7/8 | 2-3/8 |
| ID-7 | 8-3/4 | 1-7/8 |
| ID-8 | 8-3/4 | 2-1/8 |
| ID-9 | 8-1/4 | 2-5/8 |
| ID-10 | 9-1/4 | 2 |
| ID-11 | 8-5/8 | 2-1/2 |
| ID-12 | 9-3/4 | 2 |

| EB BRIDGE DIAPHRAGM STRAIN GAGE LOCATIONS | | |
|---|---|---|
| GAGE NAME | X (in.) | Y (in.) |
| ID-1 | 9-1/4 | 3-1/4 |
| ID-2 | 8-3/8 | 2-1/8 |
| ID-3 | 8 | 2-3/4 |
| ID-4 | 9-1/8 | 1-3/4 |
| ID-5 | 7-1/2 | 2-1/2 |
| ID-6 | 8-1/2 | 1-7/8 |
| ID-7 | 8-3/8 | 1-1/2 |
| ID-8 | 8-3/4 | 2-1/4 |
| ID-9 | 7-7/8 | 1-5/8 |
| ID-10 | 8-3/8 | 2 |
| ID-11 | 8 | 2-1/2 |
| ID-12 | 8-3/4 | 2-1/4 |

| SECTION WN STRAIN GAGE LOCATIONS | | |
|---|---|---|
| GAGE NAME | A (in.) | B,C, OR D (in.) |
| PI-1 | 4-3/4 | 2-1/2 |
| PI-2 | 5-1/4 | 16 |
| PI-3 | 6-1/2 | 1-3/4 |
| PI-4 | 5 | 2-3/4 |
| PI-5 | 4-7/8 | 15-3/4 |
| PI-6 | 6-1/2 | 1-7/8 |

| SECTION ES STRAIN GAGE LOCATIONS | | |
|---|---|---|
| GAGE NAME | A (in.) | B,C, OR D (in.) |
| PI-1 | 4-1/4 | 4-1/8 |
| PI-2 | 4-5/8 | 15-3/4 |
| PI-3 | 4-3/4 | 1-7/8 |
| PI-4 | 4-1/2 | 2 |
| PI-5 | 4-1/2 | 16-1/2 |
| PI-6 | 5-3/8 | 3-3/4 |

| SECTION WS STRAIN GAGE LOCATIONS | | |
|---|---|---|
| GAGE NAME | A (in.) | B,C, OR D (in.) |
| P2-1 | 4-1/4 | 2-1/4 |
| P2-2 | 4-3/4 | 15-3/4 |
| P2-3 | 6-1/2 | 1-7/8 |
| P2-4 | 4-3/4 | 1-1/2 |
| P2-5 | 4-5/8 | 16-1/4 |
| P2-6 | 4-3/4 | 2-3/8 |

| SECTION EN STRAIN GAGE LOCATIONS | | |
|---|---|---|
| GAGE NAME | A (in.) | B,C, OR D (in.) |
| P2-1 | 4-1/4 | 4-1/8 |
| P2-2 | 4-5/8 | 15-3/4 |
| P2-3 | 4-3/4 | 1-7/8 |
| P2-4 | 4-1/2 | 2 |
| P2-5 | 4-1/2 | 16-1/2 |
| P2-6 | 5-3/8 | 3-3/4 |

**Figure** Error! No text of specified style in document..**2. I-680 over County Road L-34: Location of Diaphragm and Beam End Strain Gages.**

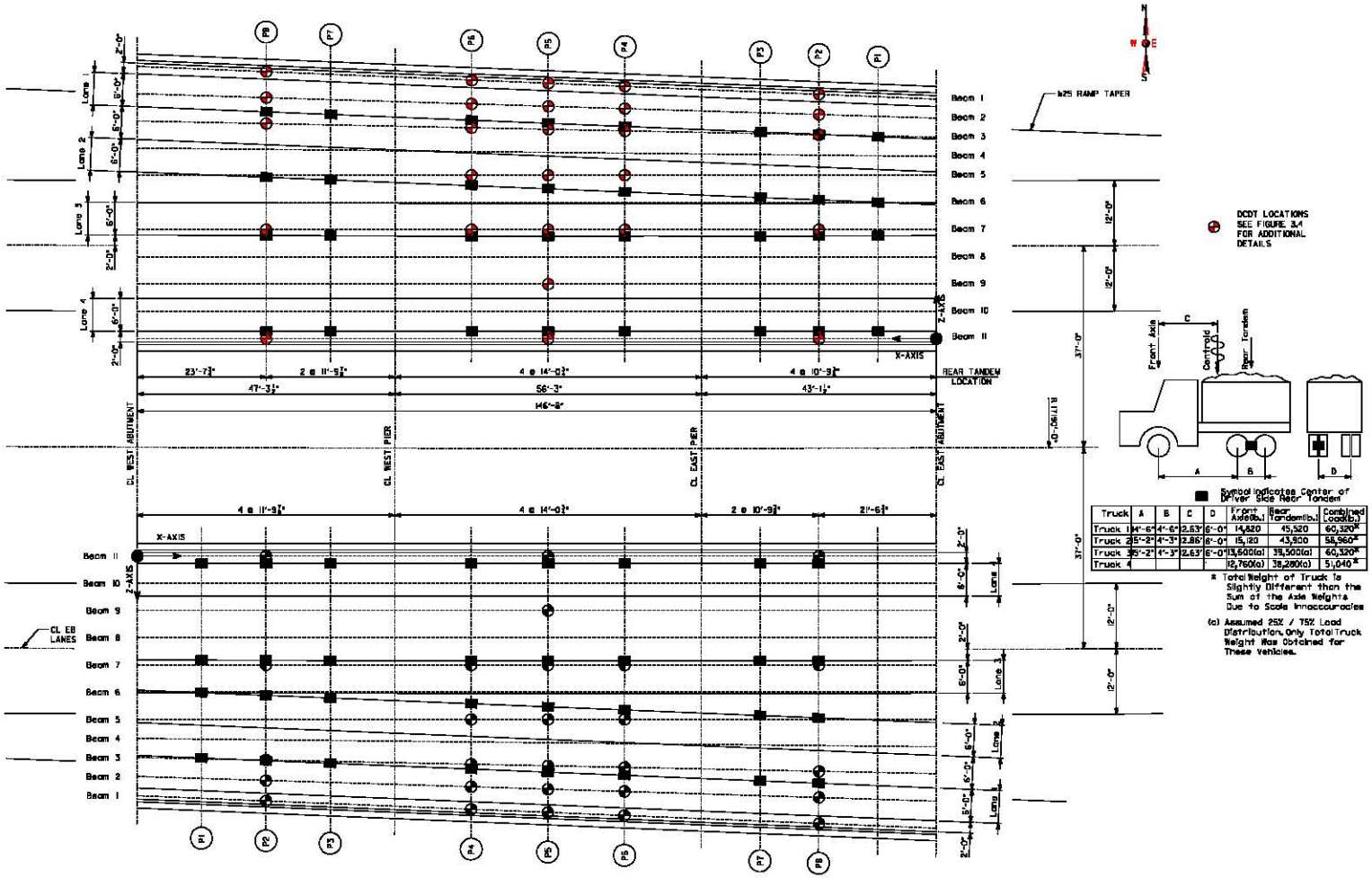


| Truck | A | B | C | D | Front Axle(lbs.) | Rear Tandem(lbs.) | Combined Load(lbs) |
|---|---|---|---|---|---|---|---|
| Truck 1 | 14'-6" | 4'-6" | 2.63' | 6'-0" | 14,620 | 45,520 | 60,320* |
| Truck 2 | 25'-2" | 4'-3" | 2.86' | 6'-0" | 15,120 | 43,920 | 58,960* |
| Truck 3 | 25'-2" | 4'-3" | 2.63' | 6'-0" | 13,600(a) | 39,500(a) | 60,320* |
| Truck 4 | | | | | 12,760(a) | 38,280(a) | 51,040* |

**Figure** Error! No text of specified style in document..**3. I-680 over County Road L-34: Truck Positions, Load Lanes, and Location of Deflection Transducers.**

The impetus for this research project was the collision of an unknown vehicle with the north three beams of the overhead WB structure in July 1996. Damage was centered ±5 ft west of the midspan diaphragm of the center span. The damage to the WB bridge was such that approximately 6 ft of the bottom flange was spalled or fractured from the north fascia beam, Beam 1W, exposing numerous prestressing strands. Several of the strands in Beam 1W seem to be lax; however, no strands were severed during this collision. There was a preexisting severed strand from a 1993 collision. There was less damage on the first interior beam, Beam 2W. Significant cracking of the bottom flange as well as fracturing of the core concrete was present in both beams, but to a lesser extent on Beam 2W. Web cracking spread over the west half of Beams 1W and 2W. Cracking seems to have been arrested by the midspan cast-in-place concrete diaphragm. The second interior beam, Beam 3W, was also damaged, but not as severely, with the damage consisting of the spalling of a patch installed following prior collisions with the bridge. Representative photographs of the damaged regions of the bridge are presented in Figures 3.7 through 3.10.

The Iowa DOT Office of Bridges and Structures decided that Beams 1W and 2W of the center span needed to be replaced while Beam 3W would simply be patched. While awaiting removal, Beams 1W and 2W were struck several additional times. The additional damage from these incidents was not documented. However, when removed in October 1997, the beams were reexamined and found to have sustained a significant amount of additional damage. Beams 1W and 2W were subsequently transported to the test facilities of Wilson Concrete in La Platte, Nebraska where they were tested as part of this project (see Chapter 5 for details). The replacement beams installed at that time have subsequently been hit several times, the most recent collision necessitating a future replacement project. The damaged WB bridge now has its third set of beams along the north side due to frequent impacts. Costs for the 1997 removal and replacement of Beams 1W and 2W, patching of Beam 3W, and replacement of the partially removed bridge deck and barrier rail were $70,920 in addition to $3,400 for field inspection, design, and detailing.

The clearance under the north beams of the WB bridge was measured to be ±13 ft-9 in.; the bridge is now posted for a clearance of 13 ft-7 in. Substandard vertical clearance is the main cause of bridge damage in Iowa. An internal study by the Iowa DOT in 1995 found that of all hit bridges, the most common cause of damage was impact from construction equipment (Phillips et al, 1995). The study also concluded that adequate clearance was not a safeguard against collision. Examining all bridges damaged by impact in the time period of 1990 to 1995, the study revealed that fifteen structures had clearance in excess of 15 ft and seven in excess of 16 ft. In many collisions, the offender is unknown and the Iowa DOT bears the financial responsibility of repairing the bridge.

**Figure 3.4. Underside of Damaged WB Bridge, Beam 1W at Left.**


**Figure 3.5. Elevation View of Beam 1W, Exterior (North) Face Shown.**

**Figure 3.6. Underside of Beam 1W Damaged Bottom Flange.**


**Figure 3.7. South Face of Damaged Beam 2W.**

## 3.1. Test Objectives

In-situ load testing has been used for a number of years to establish load carrying capacity of bridges whose load capacity is either difficult to determine using conventional rating methods, or whose rating is low based on simple analytical techniques. The tests are intended to provide a more detailed assessment of the true capacity of the structure. Load testing is a powerful and relatively inexpensive tool at the disposal of today's bridge engineers faced with an ever-deteriorating inventory. The focus of the load tests conducted as part of this project was to determine the flow of forces in a damaged and complementary undamaged bridge as well as in the repaired damaged bridge. The objectives of the testing were as follows:

- Evaluate whether redundant load paths were available for the redistribution of load in the damaged bridge, and if so, describe the load path.
- Determine the live load distribution characteristic of the various bridges tested.
- Ascertain whether the redistribution of load overloaded elements that were not originally damaged.

The answer to the first objective is somewhat evident. It is well known that typical multiple stringer bridges are highly redundant in that "failure" of an individual superstructure element does not constitute collapse of the structure. Even bridges considered to be non-redundant, such as steel thru-girder bridges, have been shown to have impressive reserve capacity even in the case where a main member is severely damaged (Daniels, 1989). Although bridges are generally designed as a series of discrete elements, there is a great deal of connectivity throughout the bridge. The interconnection of the adjacent stringers through a common slab is generally acknowledged as the primary means of transverse live load distribution with the intermediate diaphragms participating to a lesser degree. It was anticipated that the results of the load tests would indicate that the actual moments in the most heavily loaded beams would be less than those predicted using theoretical analysis. This reduction is obviously beneficial in keeping a damaged element in service.

## 3.2. Test Procedures and Instrumentation Description

In order to validate or disprove these initial assertions regarding the strength and load distribution characteristics of damaged prestressed concrete bridges, it was decided to extensively instrument the two I-680 bridges and conduct a series of load tests. The tests performed were as follows:

- Damaged WB Bridge, Static Load Tests, June 1997
- Undamaged EB Bridge, Static Load Tests, June 1997
- Repaired WB Bridge, Static Load Tests, August 1998

These tests were intended to help answer whether or not the damaged WB bridge behaved differently than the undamaged EB structure as determined by a series of baseline static load tests. The similarities and differences in the response would demonstrate the influence of main member damage on

the live load distribution patterns in a prestressed concrete bridge. However, because of potential behavioral differences in the bridges due to simple construction variations, a retest of the WB bridge was conducted in August 1998 following the installation of replacement beams. This retest permitted direct comparison of the before and after response of the bridge in which the damaged members were replaced. This before and after comparison eliminates the supposition that the WB and EB bridges should behave the same in the absence of damage and limits the discussion of damage effects to results obtained from testing the same structure multiple times.

The static tests used loads of known magnitude and configuration described in Figure 3.6. These trucks are well suited for bridge testing because their short wheelbase allows for concentration of load over a short length and because they are capable of being heavily loaded. However, as the data will later indicate, due to the close beam spacing, relatively large curb and rail section located adjacent to the exterior beam lines, short spans and thick slab plus overlay, the response of the bridge under even the most extreme load cases was small.

Most of the tests were conducted with a single truck at various longitudinal and transverse positions. In 1997, the baseline tests used Trucks 1 and 2 while the 1998 retest of the repaired WB bridge used Trucks 3 and 4. The vehicles were essentially the same with the exception that the 1998 trucks were somewhat lighter. The experimental data from these tests have been linearly scaled in the following discussions to correct for the differences in truck weights.

The tests were designed to place the truck at specified transverse locations on the bridge, i.e. a specified “Lane” location, and incrementally move the truck taking a reading at predetermined longitudinal positions. The lane locations, L1 through L4, and longitudinal positions, labeled P1-P8, are presented in Figure 3.6. It should be noted that the farthest west quarter point of the WB bridge and farthest east quarter point of the EB bridge were not included as test positions because at these locations, the front axle of the truck would have been off the bridge.

A matrix of test cases is presented in Table 3.2. The same matrix was used for testing of the WB and EB bridges with the exception that in the 1998 retest, load cases in Lane 4 were omitted. The table presents the test designation and indicates by shading the location of the center of the test vehicle(s) rear tandem. Tests in which a single block is shaded are tests in which only one test vehicle, Truck 1 in 1997 or Truck 3 in 1998 was employed. Tests with multiple shaded entries included multiple trucks in the same lane or side-by-side in adjacent lanes. As a truck was moved in the longitudinal direction through the various lanes, static deflections and strain readings were taken at numerous positions in the span.

**Table 3.2. Test Truck Position Matrix for Field Testing of the Beebeetown Bridges.**

| | Lane 1 | | | | | | | | Lane 2 | | | | | | | | Lane 3 | | | | | | | | Lane 4 | | | | | | | |
|---|---|---|---|---|---|---|---|---|---|---|---|---|---|---|---|---|---|---|---|---|---|---|---|---|---|---|---|---|---|---|---|---|
| Test # | 1 | 2 | 3 | 4 | 5 | 6 | 7 | 8 | 1 | 2 | 3 | 4 | 5 | 6 | 7 | 8 | 1 | 2 | 3 | 4 | 5 | 6 | 7 | 8 | 1 | 2 | 3 | 4 | 5 | 6 | 7 | 8 |
| L1-P1 | ■ | | | | | | | | | | | | | | | | | | | | | | | | | | | | | | | |
| L1-P2 | | ■ | | | | | | | | | | | | | | | | | | | | | | | | | | | | | | |
| L1-P3 | | | ■ | | | | | | | | | | | | | | | | | | | | | | | | | | | | | |
| L1-P4 | | | | ■ | | | | | | | | | | | | | | | | | | | | | | | | | | | | |
| L1-P5 | | | | | ■ | | | | | | | | | | | | | | | | | | | | | | | | | | | |
| L1-P6 | | | | | | ■ | | | | | | | | | | | | | | | | | | | | | | | | | | |
| L1-P7 | | | | | | | ■ | | | | | | | | | | | | | | | | | | | | | | | | | |
| L1-P8 | | | | | | | | ■ | | | | | | | | | | | | | | | | | | | | | | | | |
| L2-P1 | | | | | | | | | ■ | | | | | | | | | | | | | | | | | | | | | | | |
| L2-P2 | | | | | | | | | | ■ | | | | | | | | | | | | | | | | | | | | | | |
| L2-P3 | | | | | | | | | | | ■ | | | | | | | | | | | | | | | | | | | | | |
| L2-P4 | | | | | | | | | | | | ■ | | | | | | | | | | | | | | | | | | | | |
| L2-P5 | | | | | | | | | | | | | ■ | | | | | | | | | | | | | | | | | | | |
| L2-P6 | | | | | | | | | | | | | | ■ | | | | | | | | | | | | | | | | | | |
| L2-P7 | | | | | | | | | | | | | | | ■ | | | | | | | | | | | | | | | | | |
| L2-P8 | | | | | | | | | | | | | | | | ■ | | | | | | | | | | | | | | | | |
| L3-P1 | | | | | | | | | | | | | | | | | ■ | | | | | | | | | | | | | | | |
| L3-P2 | | | | | | | | | | | | | | | | | | ■ | | | | | | | | | | | | | | |
| L3-P3 | | | | | | | | | | | | | | | | | | | ■ | | | | | | | | | | | | | |
| L3-P4 | | | | | | | | | | | | | | | | | | | | ■ | | | | | | | | | | | | |
| L3-P5 | | | | | | | | | | | | | | | | | | | | | ■ | | | | | | | | | | | |
| L3-P6 | | | | | | | | | | | | | | | | | | | | | | ■ | | | | | | | | | | |
| L3-P7 | | | | | | | | | | | | | | | | | | | | | | | ■ | | | | | | | | | |
| L3-P8 | | | | | | | | | | | | | | | | | | | | | | | | ■ | | | | | | | | |
| L1&L2-P2 | | ■ | | | | | | | | ■ | | | | | | | | | | | | | | | | | | | | | | |
| L1&L2-P5 | | | | | ■ | | | | | | | | ■ | | | | | | | | | | | | | | | | | | | |
| L1&L2-P8 | | | | | | | | ■ | | | | | | | | ■ | | | | | | | | | | | | | | | | |
| L1-P2&P5 | | ■ | | | ■ | | | | | | | | | | | | | | | | | | | | | | | | | | | |
| L1-P2&P8 | | ■ | | | | | | ■ | | | | | | | | | | | | | | | | | | | | | | | | |
| L1-P5&P8 | | | | | ■ | | | ■ | | | | | | | | | | | | | | | | | | | | | | | | |
| L1-P4&P6 | | | | ■ | | ■ | | | | | | | | | | | | | | | | | | | | | | | | | | |
| L2-P2&P5 | | | | | | | | | | ■ | | | ■ | | | | | | | | | | | | | | | | | | | |
| L2-P2&P8 | | | | | | | | | | ■ | | | | | | ■ | | | | | | | | | | | | | | | | |
| L2-P5&P8 | | | | | | | | | | | | | ■ | | | ■ | | | | | | | | | | | | | | | | |
| L2-P4&P6 | | | | | | | | | | | | ■ | | ■ | | | | | | | | | | | | | | | | | | |
| L4-P1 | | | | | | | | | | | | | | | | | | | | | | | | | ■ | | | | | | | |
| L4-P2 | | | | | | | | | | | | | | | | | | | | | | | | | | ■ | | | | | | |
| L4-P3 | | | | | | | | | | | | | | | | | | | | | | | | | | | ■ | | | | | |
| L4-P4 | | | | | | | | | | | | | | | | | | | | | | | | | | | | ■ | | | | |
| L4-P5 | | | | | | | | | | | | | | | | | | | | | | | | | | | | | ■ | | | |
| L4-P6 | | | | | | | | | | | | | | | | | | | | | | | | | | | | | | ■ | | |
| L4-P7 | | | | | | | | | | | | | | | | | | | | | | | | | | | | | | | ■ | |
| L4-P8 | | | | | | | | | | | | | | | | | | | | | | | | | | | | | | | | ■ |

A schematic instrumentation plan is shown in Figure 3.5. Photos of typical instrumentation used in this portion of the project are presented in Figures 3.11 and 3.12. The instrumentation for the 1997 tests consists of deflection transducers mounted under the bridge, strain gages mounted on four of the exposed strands of the WB bridge, strain gages on the middle span intermediate diaphragms connecting Beams 1 through 4, and strain gages at the end regions of Beams 1 and 2 near the pier diaphragms. The transducer and exposed strand strain gage readings were recorded using a portable Megadac data acquisition system. Concrete strains were recorded using a Hewlett-Packard data acquisition system.

The diaphragm strain gages were installed to detect the participation of the diaphragms in live load distribution. It was initially hypothesized by the authors that the structural participation of a diaphragm may be more pronounced when there is a defect in an exterior beam and traffic is positioned to heavily load the exterior beam. In this scenario, there is more of a tendency for the damaged exterior member to deflect relative to the stiffer interior beam, thus inducing additional forces into the diaphragm and slab spanning between the beams. The beam end gages, installed on Beams 1W and 2W on both sides of the west pier of the WB bridge and on Beams 1E and 2E on both sides of the east pier of the EB bridge, were intended to measure the strain profile through the depth of the beam at the beam ends. Because of the unusual support conditions, the anticipated response of these gages was unknown. Instead of the beam ends being encased in a common pier diaphragm and the longitudinal slab bars used for negative moment continuity as is commonly done in continuous prestressed beam construction, the beams have a gap of several inches between their ends over the piers. The only continuous structural element at the pier is the slab, curb and rail. Further complicating the boundary conditions is the fact that pintles between the curved sole plate and masonry plate were purposely omitted from Beams 1, 2, 10 and 11 in the original design. A detail of this is presented in Figure 3.5.

## ***3.3. Baseline: 1997 Test Results***

Although a total of 43 tests were conducted on each bridge, only the results from selected tests are presented. The majority of the data presented involves loading the center spans of the two bridges to examine the difference in response attributable to the collision damage. However, tests remote from the damage are also significant in that the two bridges should respond somewhat similarly in these areas since the damage should only have a localized effect. For these reasons, the WB bridge was retested once the damaged beams were replaced so that the EB bridge could be isolated from the effects of damage discussion. The 1998 retest data will be presented later in Section 3.4.

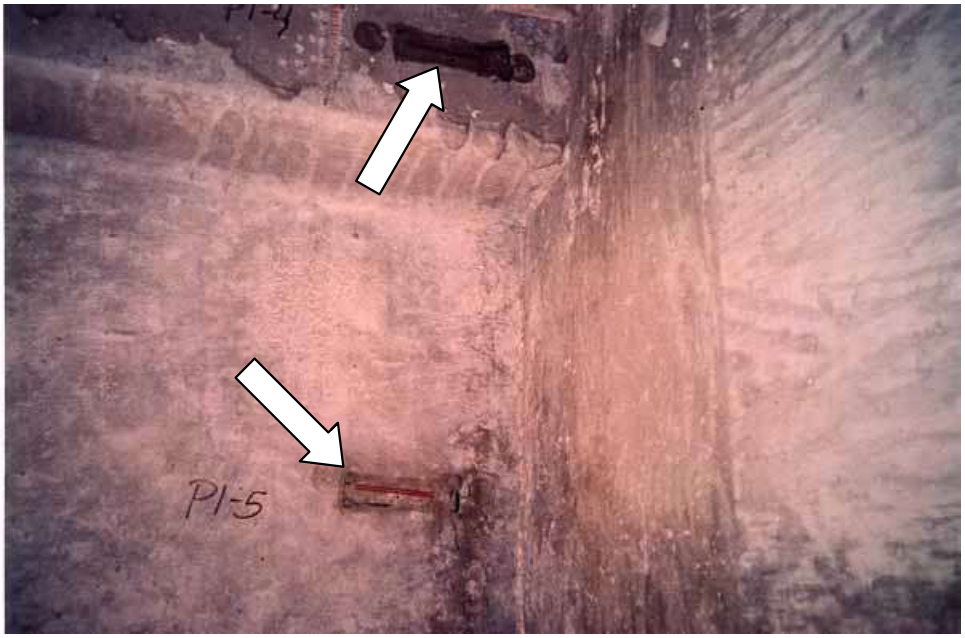


**Figure 3.8. Strain Gages on Beam End Web and Flange Adjacent to the Pier Diaphragm.**

**Figure 3.9. Tripod Mounted Deflection Transducers Under an End Span.**

Deflection data plotted at various transverse sections through the bridge will be used to illustrate the distribution of load amongst the various members. Diaphragm strain data will be discussed in conjunction with the transverse deflected shape data to delineate the influence of the diaphragms in distributing live load. The beam end strain gages are used to indicate apparent restraint/continuity. In addition to the beam end strain data, longitudinal deflected shapes will also be used to describe the boundary conditions and restraint. Finally, strain data from the exposed strands of the WB bridge will be used to quantify the effects of damage on the stress range in the damaged strands.

### *3.3.1. Single Truck Test Results*

The majority of the tests conducted on the dual bridges employed single trucks. Tests in which the rear tandem was located at midspan of one of the spans provided the most consistent data. Comparing the response of the bridge under the action of a single truck to that predicted by analytical models and to a "single-lane" distribution scenario is of particular interest. Additionally, comments regarding the elastic behavior of the structure and the validity of superposition can be made by comparing the results from the single truck tests to the results from tests involving multiple trucks. This commentary is presented in Section 3.3.2 following the discussion of single truck test results.

#### *3.3.1.1. Lane 1 Test Results*

The first load test results presented are those which used a single truck, Truck 1, at eight longitudinal positions in Lane 1. These tests are denoted L1W-P1 through L1W-P8 for the WB bridge and L1E-P1 through L1E-P8 for the EB bridge. The Lane 1 tests are not consistent with normal traffic patterns but were selected to maximize the response of the exterior portions of the bridge under a single lane of traffic. The test truck placed in Lane 1W is shown in Figure 3.10.

For comparative purposes, the response of the WB and that of the EB bridges are both presented in Figure 3.11. The plot consists of the deflected shape due to the truck at positions P1 and P2. By examining the deflected shapes, one can determine that the general load distribution pattern is the same in both bridges. The one anomaly is the distinct divergence of the L1E-P2 data of the EB bridge from that of the WB bridge. This divergence is only present in beams 1 and 2 and may be due to span length differences and/or simple behavioral differences between the two bridges.

The response of the center span will now be discussed for both bridges. Instrumentation is placed across the bridge at all three of the 1/4 points in the center span of both bridges for a more accurate characterization of the bridge. The deflected shapes at the center span 1/4 point for loads at the 1/4 point, P4, and midspan, P5, are compared in Figure 3.12 for both the WB and EB bridges. Due to concerns about the accuracy of the first reading, two readings were taken with the test truck at midspan of the center span of the WB bridge, these are referred to as L1W-P5(A) and (B) in the subsequent graphs and discussion.

**Figure 3.10. Test Truck Positioned in Lane 1.**

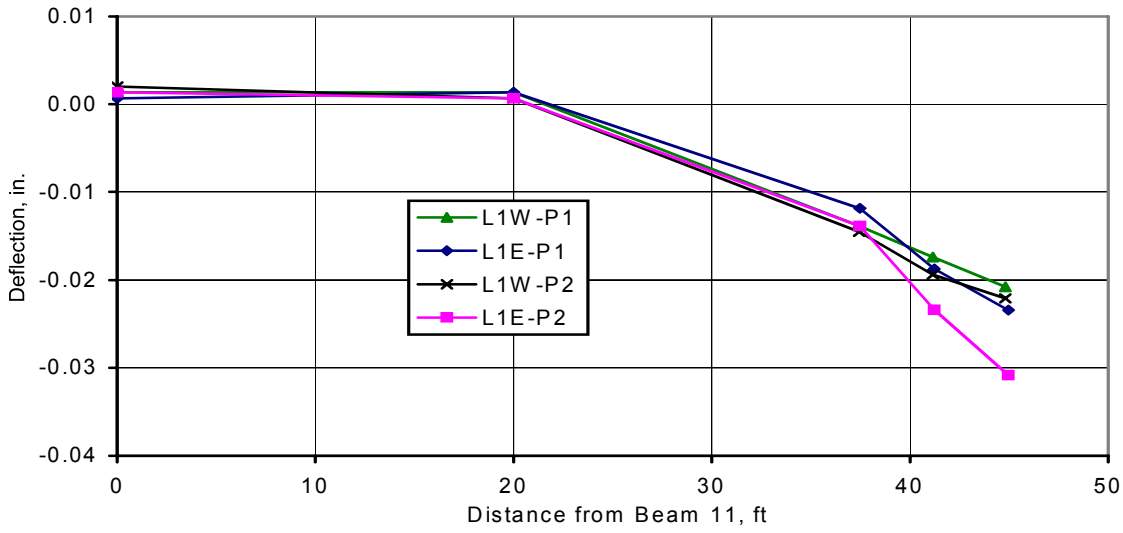


**Figure 3.11. Comparison of Deflections at Transverse Sections W1 and E1: Truck in First Span.**

In Figure 3.12, deflections at transverse sections W2 and E2 are compared. The WB and EB bridges behave differently in these tests. The WB bridge has a characteristic reverse curvature in the deflected shapes while such a reversal is not present in the EB bridge. Beams 3, 5 and 7 of the WB bridge, undamaged as in the EB bridge, deflect more than their counterparts in the EB structure. This increase is indicative of a greater share of the applied load, i.e., redistribution of load, being carried by the stiffer portions of the WB bridge due to the presence of damage in the exterior beam lines. The same trend was observed at sections W4 and E4.

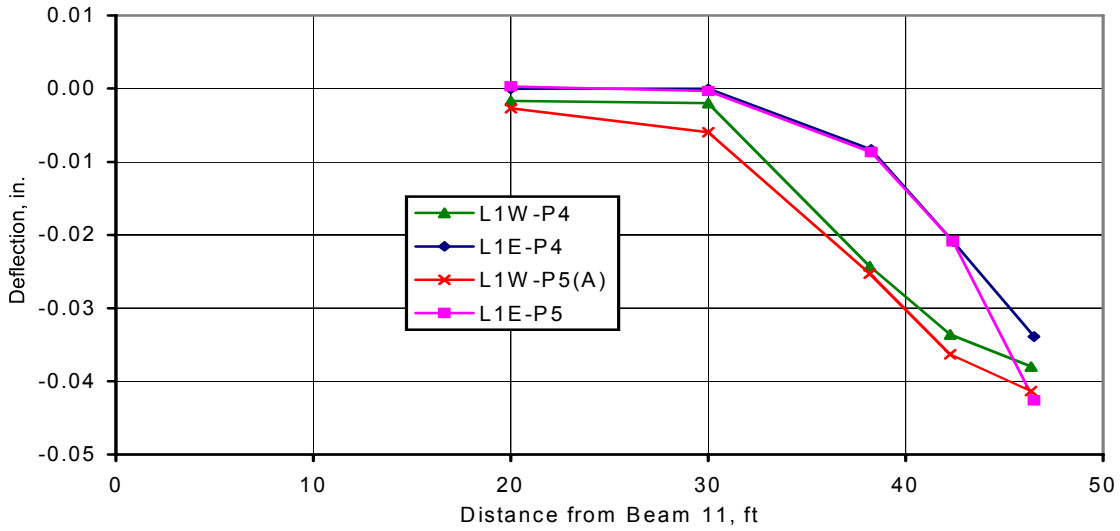


**Figure 3.12. Comparison of Deflections at Transverse Section W2 and E2: Truck in Center Span.**

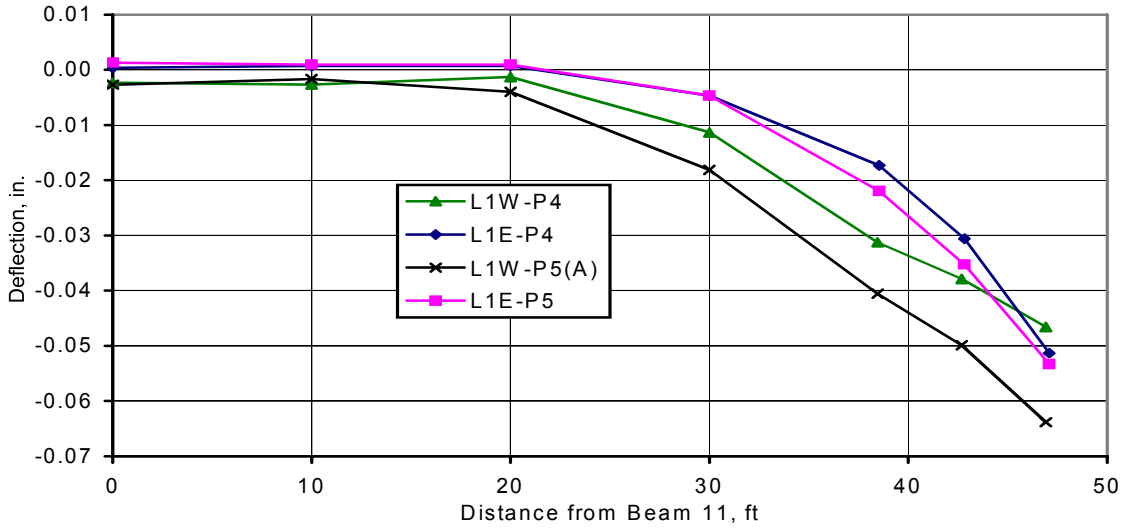


**Figure 3.13. Comparison of Deflections at Transverse Section W3 and E3: Truck in Center Span.**

One can observe in Figure 3.13 that the reverse curvature behavior present at the quarter points is not apparent at midspan. The expected increase in deflection of the midspan region as the truck moves from P4 to P5 is evident.

One of the load cases, L1W-P5(A), in Figure 3.13, is particularly important as the truck is as close as possible to the damaged beams in the WB span and at the position in the span which causes the most significant response. No attempt was made to position the truck to obtain the absolute maximum moment in a span, which is a function of the center of gravity of the axle loads. For purposes of the discussion herein,

maximum moment placement implies that the rear tandem was centered at midspan. In such a position, the truck is over the damaged region of Beams 1W and 2W in the WB bridge and close to maximum moments are generated.

In examining the test data for the center span, the different responses of the WB and EB bridges are noticeable. Had only the first two beams of the WB structure deflected differently than those in the EB structure, one could conclude that there was not a redistribution of load but simply an increase in deflection of the damaged elements. However, since many beams in the cross-section of the damaged bridge deflect more than in the undamaged structure, one can conclude that the increase of deflection in the undamaged elements is due to a redistribution of load. In essence, the exterior damaged members have less stiffness and thus redistribute load to the interior of the bridge when the exterior lanes are loaded.

Presented in Figures 3.17 and 3.18 are the longitudinal deflections of the WB and EB bridges resulting from Truck 1 positioned at midspan of the center span, L1W-P5 and L1E-P5. These curves clearly illustrate the deflection of the bridge along a particular beam line or lines for given load placements. Whereas the transverse sections indicate the relative distribution of load among beam lines at a particular longitudinal location, the longitudinal deflections are helpful in understanding the influence of alternate span load on deflections, the effect of localized damage and beam end boundary conditions.

Figure 3.14 is the longitudinal deflected shape of Beams 1W – 5W with a test truck positioned at L1W-P5. This figure illustrates the simultaneous deflections of Beams 1W-5W in all three spans of the WB bridge.

To confirm the minimal observed continuity in the WB bridge, an analytical deflected shape corresponding to test L1W-P5 is plotted as series SS Beam for all of the beams depicted. The analytical model presumes simply supported conditions and no damage, i.e. a constant moment of inertia. An arbitrary flexural stiffness, EI, was assigned to the member. Shear distortions were not considered although they may occur in the damaged region.

In order to compare the deflected shapes, the computed analytical deflected shape was normalized to the experimental deflection at the east quarter point for the damaged beams, Beams 1W and 2W, and at midspan for Beams 3W and 5W. Recall that the damage to Beams 1W and 2W was located west of midspan, hence the east 1/4 point was chosen to normalize the shapes for those two beams. Having computed the deflected shape of a simply supported beam of uniform stiffness, it was found that the ratio of the 1/4 point, midspan and 3/4 point deflections had a ratio of 1.0 : 1.478 : 1.052 for the prescribed loading, inertia and support conditions. Comparing the measured and predicted values in Figure 3.14, it appears that the damage does not have a significant effect on the deflection of Beams 1W – 3W because they are part of a highly redundant structural system. The predicted uniform stiffness deflections and measured deflections at the midspan and 3/4 point locations are approximately the same.

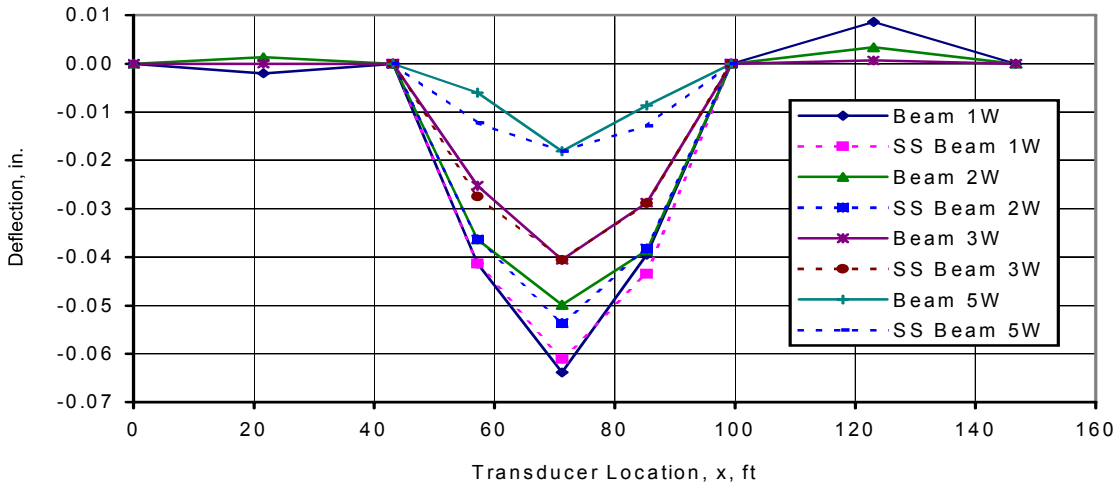


**Figure 3.14. Longitudinal Deflected Shape, Beams 1W-5W: Truck 1 at L1W-P5.**

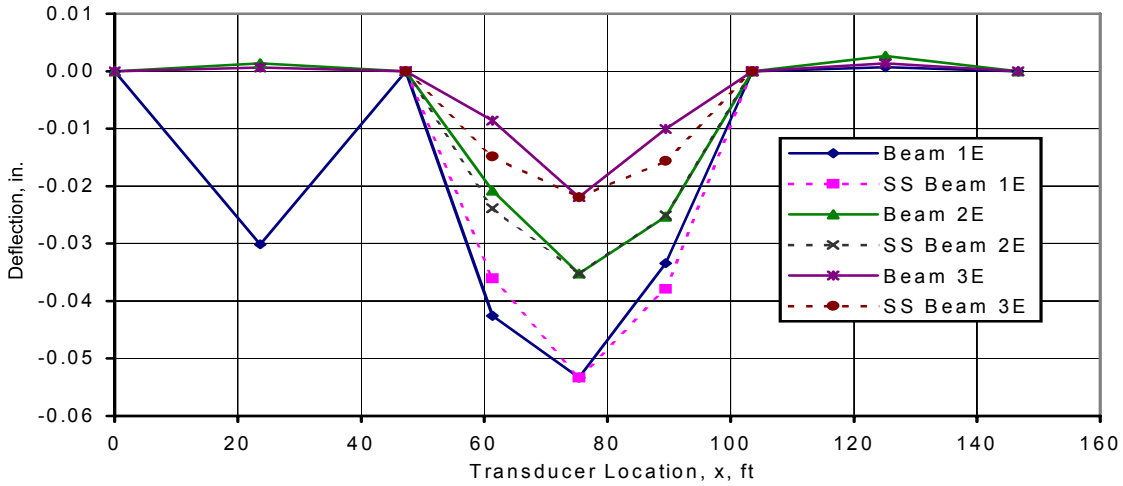


**Figure 3.15. Longitudinal Deflected Shape, Beams 1E – 3E: Truck 1 at L1E-P5.**

Beam 5W is interesting in that unlike Beams 1W – 3W, the deflection pattern is much different than expected for a simply supported beam of uniform stiffness. The deflections appear to be more like that expected of a beam with end restraint. However, with loads placed in Lane 1W, Beam 5W is not subject to direct wheel loads but is drawn down by the loaded beams. As such, a different deflection pattern, i.e. different than the results if the beam were subjected to concentrated wheel loads, is expected.

Figure 3.15 is a similar longitudinal deflected shape but for the EB bridge with the truck at L1E-P5. For this bridge, all deflected shapes have been normalized with respect to the midspan deflections. The ratio of deflections when normalized to the midspan deflection is 0.676 : 1.0 : 0.712 for the test vehicle (Truck 1) at L1E-P5.

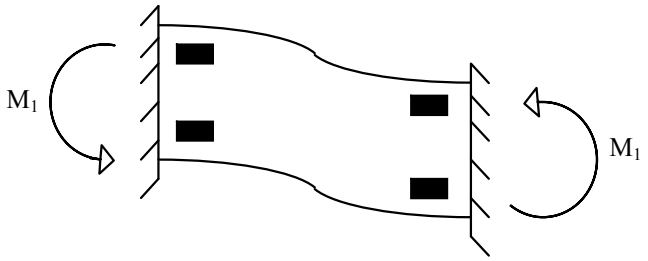


**a.) Displacement Induced Forces Due to Differential Displacement Only.**

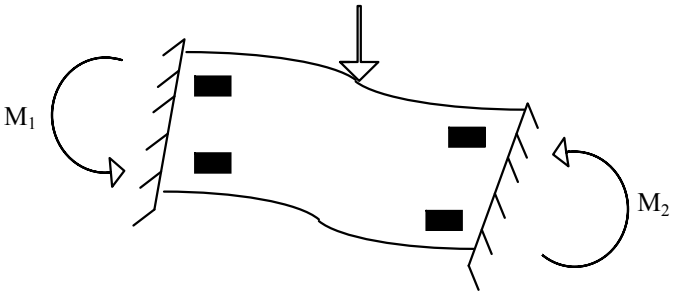


**b.) Effects of Direct Loading and Beam Torsion.**

**Figure 3.16. Behavioral Models for Diaphragms Under Load.**

Comparing the computed and measured response, there is reasonable agreement for both Beams 1E and 2E. However Beam 3E, like 5W in the WB bridge has a markedly different response.

To determine the behavior of the intermediate diaphragms under live load, 12 strain gages were installed on the center span intermediate diaphragms as depicted in Figure 3.5. It was initially anticipated that the stresses in the diaphragm would arise from the structural behavior illustrated in Figure 3.16. This figure illustrates two types of behavior, the first being the classic fixed-fixed beam subjected to differential displacement, Figure 3.16(a), while the second model, Figure 3.16(b), includes torsion of the supporting elements and the presence of direct load.

These two models are only valid for elements that respond in flexure. This is generally accepted by ACI and AASHTO to occur when the aspect ratio, length/height, exceeds 5:2 for continuous beams and 5:4 for simply supported beams. For the instrumented diaphragms, such as shown in Figure 3.5, the clear spacing at midspan is approximately 45 in. between the beam webs. With a depth of 32 in. from the top of the bottom flange to the underside of the deck, the aspect ratio is 1.4:1, which lies between the limits for linear strain distribution for simply supported and continuous beams. An alternate and potentially more appropriate analysis would be to analyze the diaphragm as a deep beam/shear wall.

Graphs illustrating the variation in strain the diaphragms connecting Beams 4W through 1W are presented in Figure 3.17; similar graphs for the EB bridge are presented in Figure 3.18.

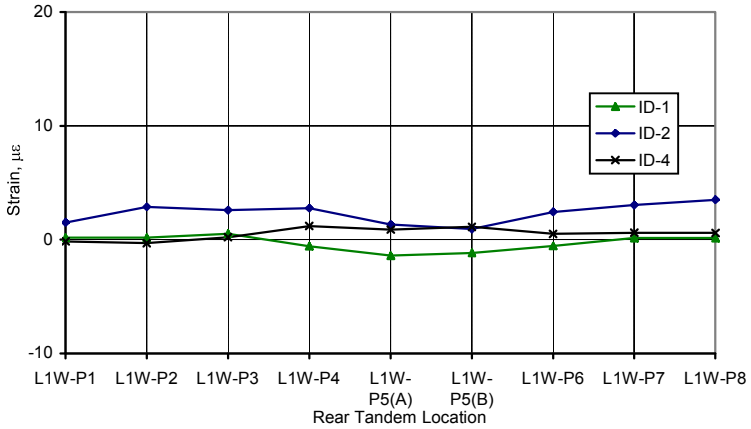


**a.) Diaphragm Strains Between 4W and 3W.**

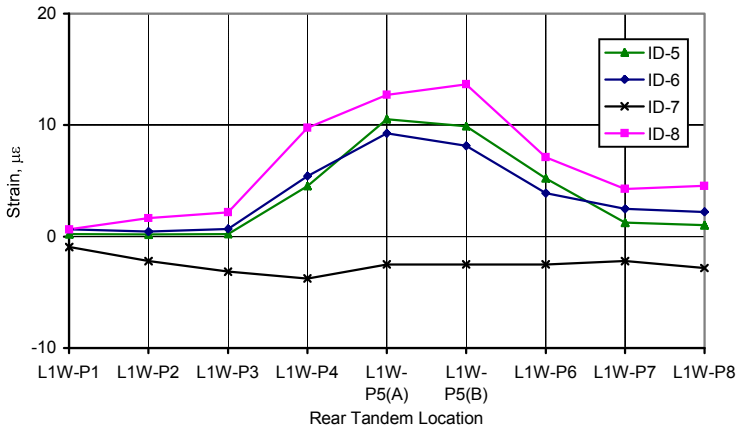


**b.) Diaphragm Strains Between 3W and 2W.**

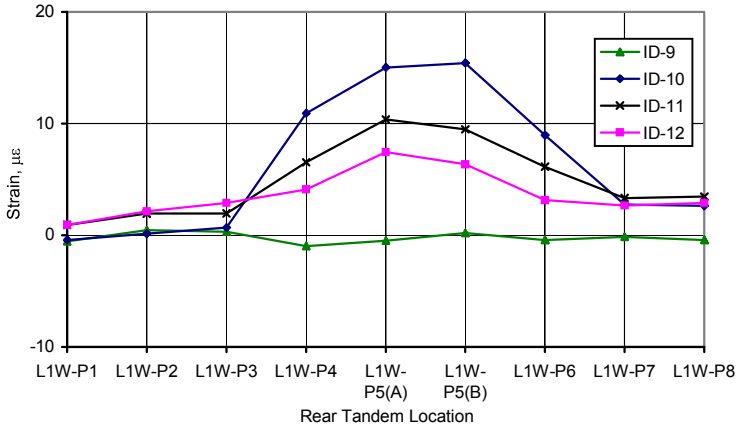


**c.) Diaphragm Strains Between 2W and 1W.**

**Figure 3.17. WB Bridge Diaphragm Strains: Lane 1W Loaded.**

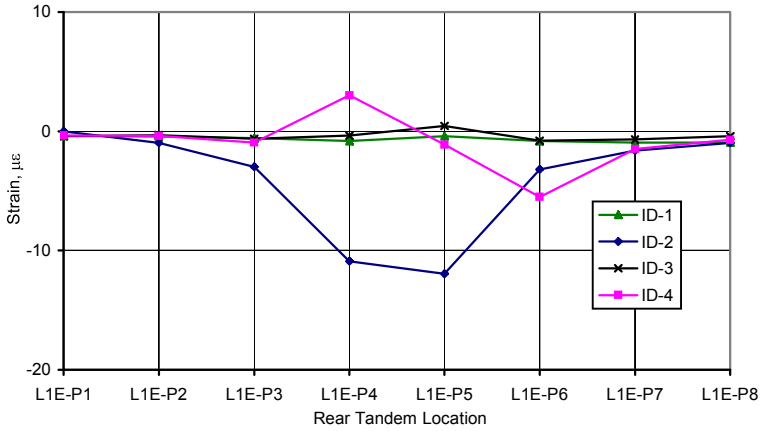


**a.) Diaphragm Strains Between 4E and 3E.**

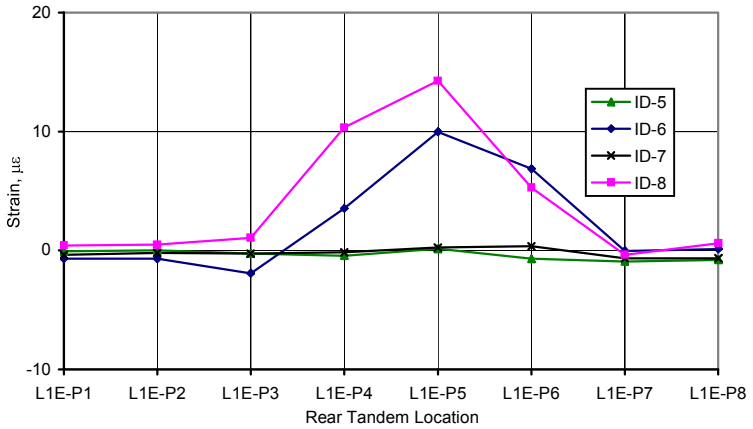


**b.) Diaphragm Strains Between 3E and 2E.**

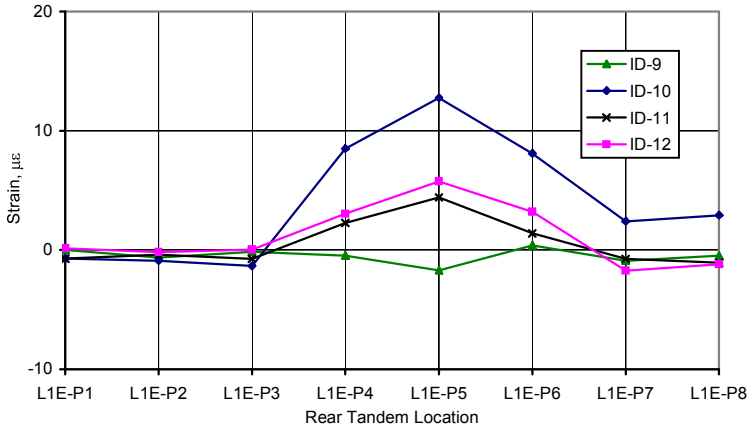


**c.) Diaphragm Strains Between 2E and 1E.**

**Figure 3.18. EB Bridge Diaphragm Strains: Lane 1E Loaded.**

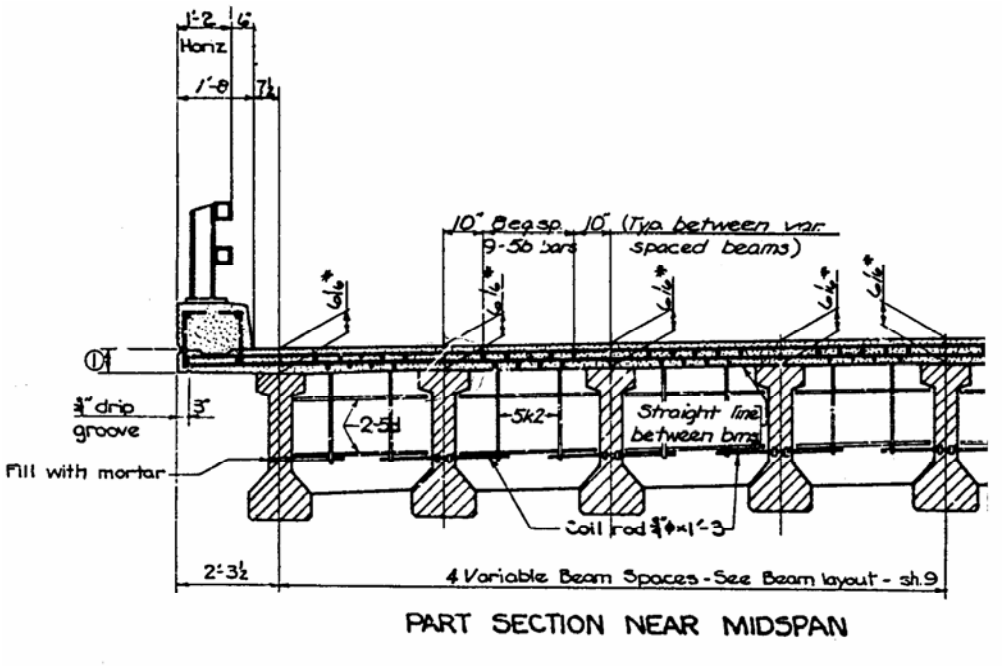


**Figure 3.19. Midspan Intermediate Diaphragm Detail from the Original Design Plans.**

The integrity of the connection between the diaphragms and beams in this bridge is difficult to quantify. Referring to Figure 3.19, the only reinforcing steel that ties the beams to the diaphragms is a coil rod whose main purpose is to provide a form of anchorage and support for the diaphragm reinforcing cage. Other than this connection, the only tie between the beam and diaphragm along the web interface is the very small adhesion/chemical bond between the elements. This lack of true fixity of the diaphragm is another reason, in addition to the aspect ratio, to question a fixed-fixed linear strain distribution analytical model.

There are several important observations to be made from the diaphragm strain data. First, the WB and EB diaphragm strains are nearly identical. The expected larger diaphragm strains in the damaged bridge are not evident. Recall that the hypothesis was that damage in the WB bridge would give rise to higher differential displacements and hence greater diaphragm strain values. In Figure 3.13, the transverse deflected shape at midspan of the center span was plotted for both bridges. In this figure, the differential deflection between beams is evident. In contrast to the hypothesis that damage would cause greater differential displacements, the converse is true. The differential displacement between Beams 1E and 2E in the EB bridge are some 29% greater than in the WB bridge for load position P5. Similarly, the EB differential deflection between Beams 2E and 3E is 43% greater than in the WB bridge. Despite large differences in differential deflections, diaphragm strains in the two bridges are comparable.

Further confirmation of the inaccuracy of the flexural models for diaphragm behavior is found when one computes the theoretical strain in the diaphragm when it is subjected to differential end displacement. For the WB bridge, the displacement of Beam 1W was measured to be –0.0432 in. when the

truck was located at P6. The corresponding displacement of Beam 2W was –0.0332 in. This results in a differential displacement, $\Delta$, of 0.01 in. Admittedly this is a small displacement but in the short diaphragm length, it is sufficient to generate high strains assuming the fixed-fixed condition and flexural behavior exists. The truck located at P6 is important because there are no local bending effects and the strains should be entirely due to differential displacements.

Assuming that diaphragm concrete has a strength of 3,500 psi as specified, the end moment, $M_1$ in Figure 3.16, due to a differential displacement of 0.01 in. is approximately $2.2 \times 10^6$ in-lbs using the formula $M=6EI\Delta/L^2$. This calculated end moment should produce a compressive strain of –244 με in gage ID-10 in sharp contrast to the tensile strain of less than approximately +10 με fairly consistently recorded in both bridges for load cases L1W/E-P6. This indicates that the diaphragm does not behave as assumed as a beam in reverse curvature bending nor does it appear to behave as a beam with fixed end conditions. Thus, the simple flexural models do not explain the behavior of the midspan intermediate diaphragms. However, in both bridges all measured diaphragm strains were small. It was therefore decided that additional analytical modeling of the diaphragms was not warranted and was not within the objectives of the investigation.

The response of the beam end longitudinal strain gages will now be discussed for the Lane 1 tests. The gages are located on the bottom flange, approximately mid-height of the web, and on the top flange of both Beams 1 and 2 of the WB and EB structures. They were placed on Beams 1 and 2 adjacent to the pier diaphragm connecting these two beams together. The gages are only located over the pier adjoining the center and far spans for each bridge. A diagram illustrating the placement of these gages is presented in Figure 3.5.

In the WB bridge, strains at mid-height of the web and in the top flange were negligible. Strains were not linear through the depth of the beam; this is not unexpected since the gages are fairly close to the free end of the beams and also near to the beam bearings which as previously mentioned were corroded and debris laden. The bottom flange strains are consistent with the deflections in that those load cases producing maximum deflection and presumably maximum beam end rotation also produced the maximum bottom flange strains.

Even in the absence of beam continuity, gages P1-3 and P1-6 produced fairly consistent readings on both sides of the pier. The maximum strain recorded in Beam 1W, –30 με, was with the test vehicle in the center span. This corresponds to a stress of –120 psi assuming a Modulus of Elasticity of $4 \times 10^6$ psi for the specified 5,000 psi beam concrete. The consistency of strains on both sides of the pier, especially for Beam 1W, is informative in that it validates the transfer of load into unloaded spans through unintended bearing restraint and/or continuity of the slab, curb and railing. Although a precise accounting of the source of the strains is not possible, it is apparent that the strains are consistent with the deflection data and corroborate the existence of some end restraint in the end of the “simply supported” beams.

For the EB bridge, the strains at the ends of Beam 1E are consistently low, never exceeding ±5 με in any test. The strains in Beam 2E are larger, however the maximum strain is still slightly less than –20 με. After the test, it was determined that gage P2-6 was over a crack and thus provided inconsistent data which is not included in this report. Gage P2-3 is fairly consistent with the readings obtained from the WB bridge though closer to Beam 1W than 2W as might be expected.

The strains in the exposed strands are presented in Figure 3.20. The exposed strand strains recorded in the WB bridge are informative in that they indicate the stress ranges in the exposed strands of the cracked section. Stress range is important in damaged beams and in beams that crack under service load since fatigue of strands in cracked sections has been cited as a failure mode in prestressed concrete beams (Shanafelt and Horn, 1985; Olson, French and Leon, 1992; Khaleel, 1992; Marianos, 1992). Two bottom layer strands in Beams 1W and 2W were strain gaged, gages S1-1, S1-2, S2-1 and S2-2, respectively. The instrumented strands were at opposite ends of the exposed bottom row strands in both beams. Three of the strain gages produce fairly consistent results; gage S2-2 did not function properly. The maximum reliable strains range from 100-150 με. The strain of 150 με corresponds to a stress change of 4,275 psi.

#### *3.3.1.2. Lane 2 Test Results*

The tests in Lane 2 roughly coincide with the normal exit path of vehicles leaving the Interstate. It was unknown at the time of testing whether the beam damage in the WB bridge would be significant enough to affect the load distribution patterns of the bridge. It was anticipated that very little load would be carried by the exterior beams in either bridge since test lane L2 was remote from the first two beam lines.

Similar to the data from the single truck tests in Lane 1, deflection and strain data are presented for Lane 2. Later in this chapter, Lane 1 and Lane 2 data will be combined and compared to the experimental results of loading both lanes simultaneously. Selected data from the center spans are presented in Figure 3.21 and Figure 3.22; only the data from the transverse section at the midspan of both bridges will be presented. Examining this data, one notices several key points.

First, the response of the WB bridge appears to be localized around Beam 5W. The EB bridge appears to deflect in a “smoother” pattern and the magnitude of the deflections are smaller than those in the WB bridge. It is rational to assume that under the action of similar loads a bridge in which the beams deflect in a “smooth curve” would have smaller deflections than a bridge with a highly localized response.

Secondly, neither bridge appears to distribute much load to Beam 1. Beam 1W deflects more than Beam 1E which is probably due to the damaged members. No inference can be drawn about the relationship between deflection and moment fraction for beams of different stiffness. No indications of uplift of the center span of the WB bridge are apparent; there is however, a small uplift in Beam 1E of the EB bridge.

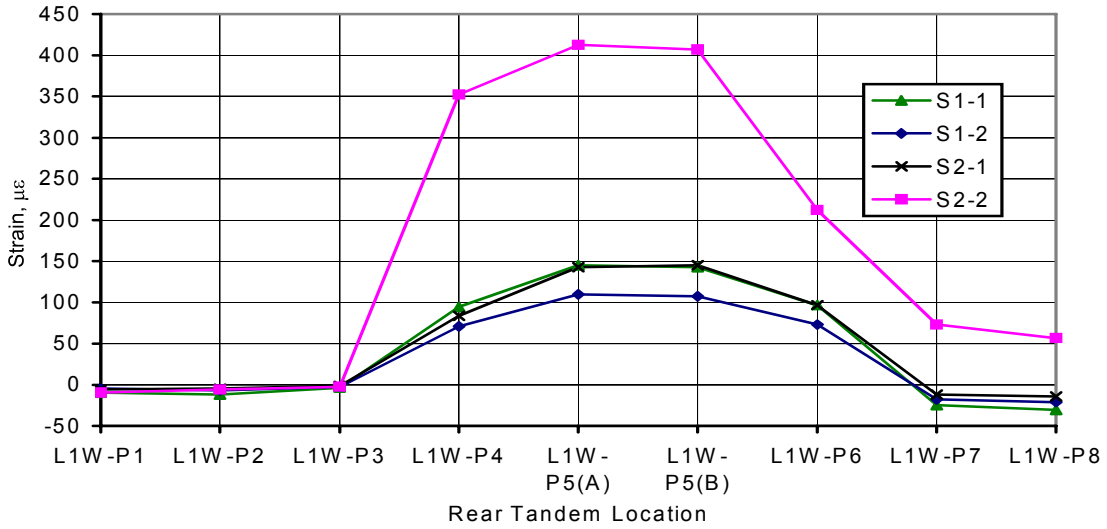


**Figure 3.20. Exposed Strand Strains: Lane 1W Loaded.**

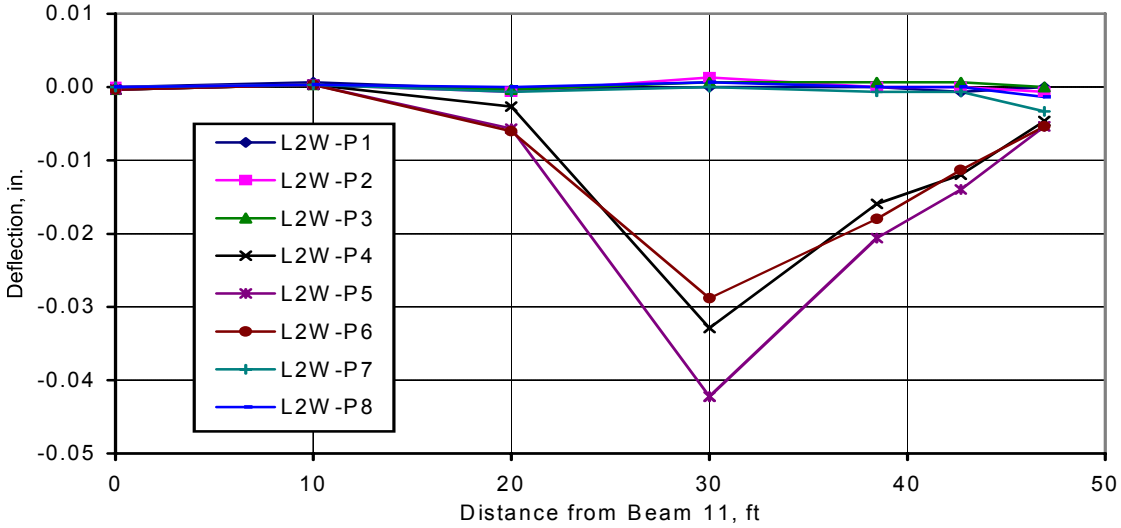


**Figure 3.21. Deflections at Transverse Section W3: Lane 2W Loaded.**

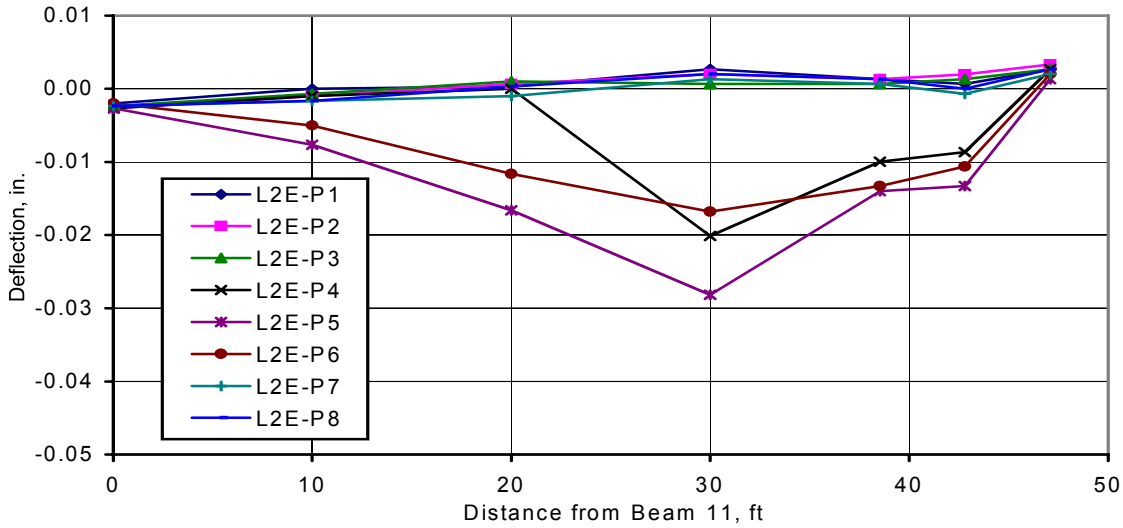


**Figure 3.22. Deflections at Transverse Section E3: Lane 2E Loaded.**

The diaphragm strain readings for the WB bridge were small in this test; the maximum reading was ±5 με but in contrast to the Lane 1W test results previously presented in Figure 3.17, the recorded strains were predominantly compressive. The reversal of sign is consistent with the transverse deflected shape in that when the exterior beam deflects the most, there are tensile strains in most diaphragm gages while for interior lane loading with small exterior beam deflections there are compressive strains. This lends credence to the strains being related to differential deflections and rotations of the longitudinal beams at the diaphragm location.

For the EB bridge, the behavior of the diaphragms was different as depicted by the strains plotted in Figure 3.23. In this figure, the variation in strain in the gages connecting Beams 3E and 4E is recorded with respect to the position of the rear tandem of the test vehicle. The recorded strains are much higher than those in the WB bridge and also much higher than those measured in the Lane 1E tests previously discussed. In the WB bridge, the strains were mostly compressive while for the EB bridge, the strains are tensile. The diaphragm strains are smaller towards the exterior beam. For instance, the highest strain between Beams 3E and 2E is +13 με in gage ID-6 and between Beams 2E and 1E is +3 με in gage ID-10. It is difficult to correlate the diaphragm strains with differential deflection; the smallest diaphragm strains occurred between Beams 2E and 1E, the beams which experienced the greatest differential deflection. The beam end strains measured at all gage locations for the WB and EB bridges were consistently small, never exceeding ±5 με.

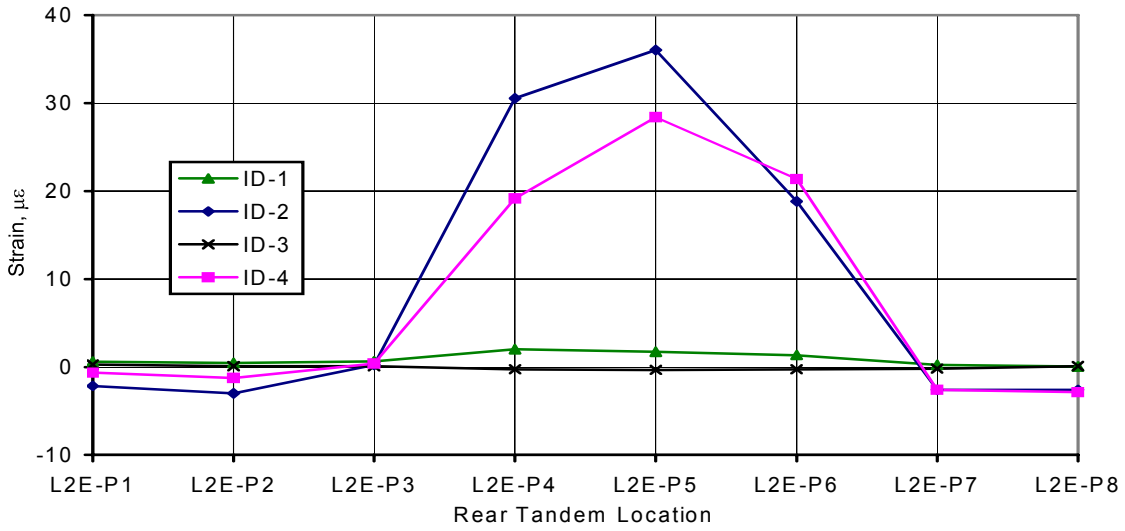


**Figure 3.23. Diaphragm Strains, EB Bridge: Lane 2E Loaded.**

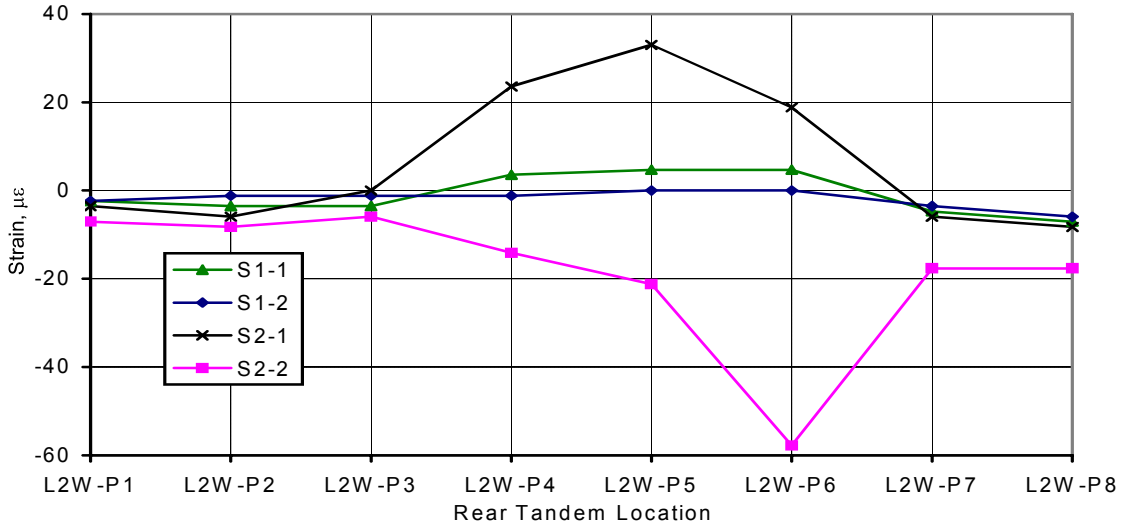


**Figure 3.24. Exposed Strand Strains: Lane 2W Loaded.**

Strains from the exposed strands in the WB bridge are presented in Figure 3.24. The strains in the instrumented strands in Beam 2W are inconsistent; S2-2 is suspect. The data indicate that essentially no load is transferred to the exterior beam of the damaged WB bridge, Beam 1W, and very little to Beam 2W. Comparing the response of gage S2-1 in Tests 1W and 2W, the measured strain decreases from a maximum of +145 με during the Lane 1W tests to +33 με in the Lane 2W tests, a reduction of approximately 75%. Considering loading, the amount of live load carried by Beam 2W is only 1/4 that carried in the Lane 1W tests. This indicates that damage to exterior or near exterior beam lines, even if severe, is not a significant

structural problem as long as traffic is diverted so that it is not in "close proximity" to the damaged element.

#### *3.3.1.3. Lane 3 and Lane 4 Test Results*

Lane 3 is a test position that coincides with the right driving lane on both bridges. The test vehicles were positioned such that the driver's side tandem was 2 ft from the centerline of the through lanes. This test simulates a typical through traffic pattern in the right lane and was believed to be remote enough from the damage that there would not be any difference in the WB and EB bridge responses. At this location in both structures, the beam lines are parallel at a constant spacing of 5 ft. Deflections in the center span were essentially zero except for beam lines 5 and 7 in both bridges. The maximum deflection in the WB bridge was 0.03 in. in Beam 7W and in the EB bridge, 0.02 in. in Beam 5E.

Lane 4 is somewhat analogous to the test conducted in Lane 1 in that the test vehicle was positioned as close to the barrier curb and rail as possible. However, unlike the Lane 1 test positions, there is no beam damage in either bridge at this location. The beam lines are parallel at a spacing of 5ft. The constant spacing, lack of flare and remoteness from damage will allow for the most accurate assessment of "sameness" between the two bridges. Any experimental differences can be attributed to true differences in behavior of undamaged bridges with all other variables having been isolated.

Beam 11W of the WB bridge deflects approximately 0.03 in. with the rear tandem at L4W-P5. Beam 11E of the EB bridge under the action of a similarly located test truck deflects approximately 0.02 in. Oddly, in both of the bridges, these deflections are less than recorded on the flared side of the bridge where the beam spacing is closest. No explanation is presented for this anomaly.

### *3.3.2. Multiple Truck Test Results and Validity of Superposition*

A series of tests were conducted in which both test trucks were employed simultaneously. Tests in which trucks were placed adjacent in Lanes 1 and 2 were intended to simulate multi-lane loading. The tests with two trucks in the same lane were conducted to check for continuity as well as maximum positive moment in the center span. Selected results from these multi-truck tests are presented. The multi-truck data will be compared to the sum of the data obtained from Lanes 1 and 2 for both the WB and EB bridges. The validity of superposition will be established using both deflection and strain data.

**Figure 3.25. Photograph of Test Trucks 1 and 2 in Adjacent Lanes on the EB Bridge, WB Similar.**

### *3.3.2.1. Lanes 1 and 2 Loaded Simultaneously*

A load test was conducted in all three spans where the two test trucks were placed side-by-side with their tandems at midspan as shown in Figure 3.25. This load case was intended to represent a multiple lane loading and distribution scenario and was one of the critical load cases. In these tests, Truck 1, which is slightly heavier than Truck 2, was placed adjacent to the railing. In evaluating the validity of superposition, the results from Truck 1 located in Lane 1 will be directly added to the effects of Truck 1 located in Lane 2. Although this represents a total effect somewhat greater than that due to Trucks 1 and 2 superimposed, the error is small with the total load from superposition measuring approximately 1% higher than the weight of the combined test trucks.

In order to differentiate between the tests in which two trucks were used versus those in which superimposed data is plotted, unique designations are used. Test designations in which the "&" symbol is used are from tests using two test trucks while result designations containing the "+" symbol are superimposed results of Truck 1 in Lanes 1 and 2 independently.

Deflections at transverse section W3 are presented in Figure 3.26. Additionally, the single lane test results, L1W-P5(A) and L2W-P5, have been included so that their relative contribution can be assessed along with the multi-lane and superimposed responses. The validity of superposition is important in regions of damage because it confirms that the bridge has not been stressed into the inelastic region and that the damage is not significant in terms of the load vs. deflection behavior of the structure.

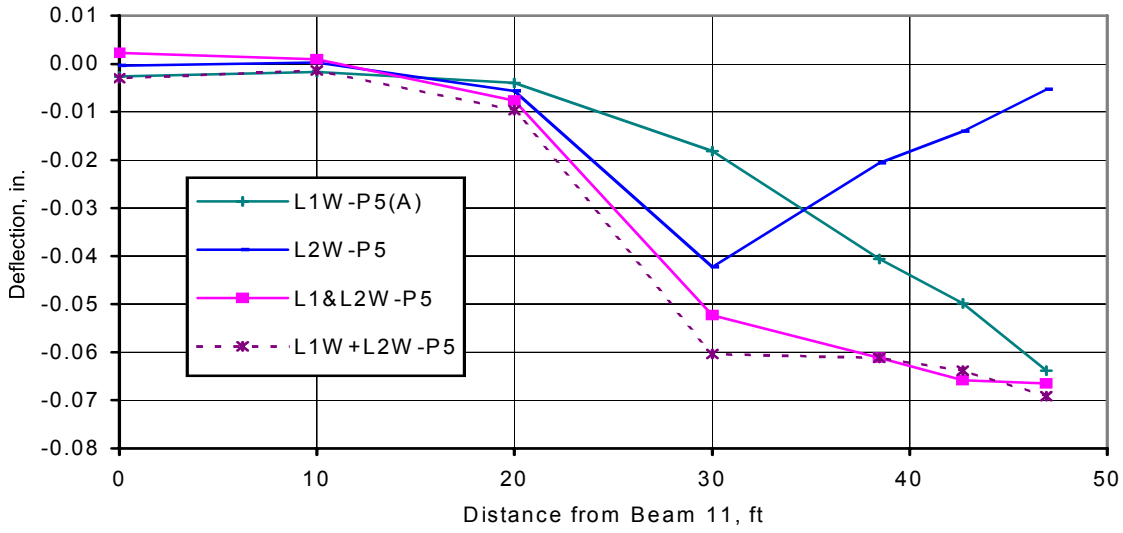


**Figure 3.26. Deflections at Transverse Section W3: Lanes 1W and 2W Loaded.**

In most load cases, the results of two trucks placed simultaneously on the structure was replicated by superimposing the responses from two different single lane tests. This is also important in that it indicates that the results from both the Lane 1W and Lane 2W tests were repeatable. From examination of the data, it is apparent that most of the load carried by Beams 1W and 2W comes from vehicles placed in Lane 1W. The negligible response recorded in the first two beam lines for the Lane 2W tests indicates that even with vehicles in the normal driving position, very little load is distributed to the exterior beam lines.

The EB bridge center span deflected shapes for various load placements are presented in Figure 3.27. The EB bridge exhibits the same characteristic deflected shape as the WB bridge with a reverse curvature profile and a fairly flat response in the region of beams 1 through 5. Both bridges have a pronounced deflection gradient across the width indicating the load distribution in the structures. For the EB bridge, data from Beam 7E during the L1&L2E tests is questionable due to its significant deviation from the superimposed results. A comparison of the superimposed and multi-lane strain results for both bridges indicates a similar agreement such as observed in the deflection comparisons.

### *3.3.2.2. Lane 1 Loaded with Two Test Trucks*

Following the adjacent lane tests, an additional series of load tests were conducted with Trucks 1 and 2 in the same lane at different longitudinal positions. As indicated by Table 3.2, first, Trucks 1 and 2 were placed at midspan of the first and second spans. Following this test, Truck 1 was moved to the third span while keeping Truck 2 in place in the first span. This test generates positive live load moments in each

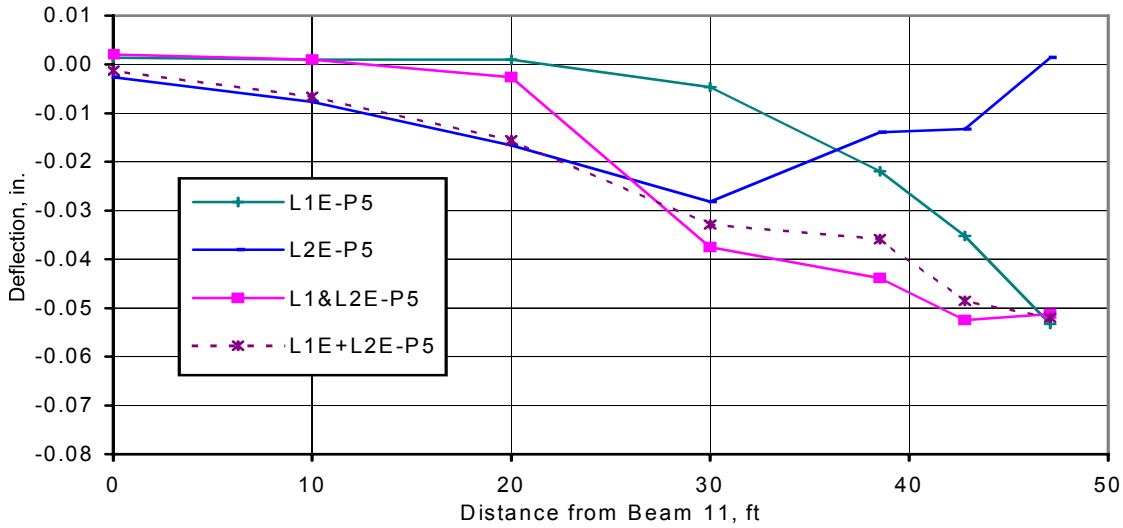


**Figure 3.27. Deflections at Transverse Section E3: Lanes 1E and 2E Loaded.**

of the end spans with no live load in the center span. Truck 2 is then moved to the center span, creating positive moments in the second and third spans simultaneously and maximum negative moment over the pier with the strain gaged beam ends. Finally, both trucks were located in the center span as depicted in Figure 3.28, Truck 1 with its rear tandem at P6 and Truck 2 with its tandem at P4. There was approximately 9 ft between the front axle of Truck 2 and the rear axle of Truck 1. This loading produced the maximum downward deflections along with the maximum beam end strains, exposed strand strains and intermediate diaphragm strains.

Deflections at midspan of the center span of the WB bridge for several load placements are presented in Figure 3.29. During the tests in which only a single truck was positioned in the center span, L1W-P2&P5 as well as L1W-P5&P8, the response is essentially the same. The response compares favorably to that measured during the single lane tests in Lane 1W, load position L1W-P5(A). Also presented is the response of the center span when trucks were positioned at P4 and P6. Test L1W-P4&P6, compares very well to that obtained by superposition of the effects of Truck 1 placed at P4 and P6, L1W-P4+P6. The minor differences are due to the fact that Trucks 1 and 2 are not exactly alike.

Figure 3.30 illustrates the response of the EB bridge due to a series of load tests similar to those conducted on the damaged WB bridge. The center span deflection with a truck located in the center span, tests L1E-P2&P5 and L1E-P5&P8, is essentially the same. The multi-truck test results compare well with the deflections recorded during the Lane 1 test with only Truck 1 on the bridge, plotted as series L1E-P5.

**Figure 3.28. Trucks 1 and 2 at P4 and P6 on the EB Bridge, WB Similar.**

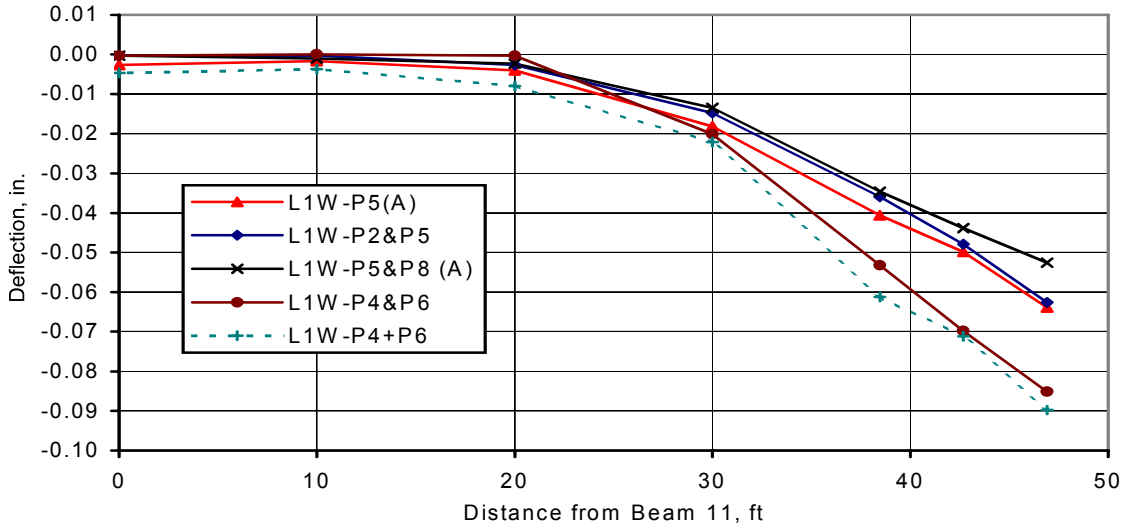


**Figure 3.29. Deflections at Transverse Section W3: Lane 1W Loaded with Trucks 1 and 2.**

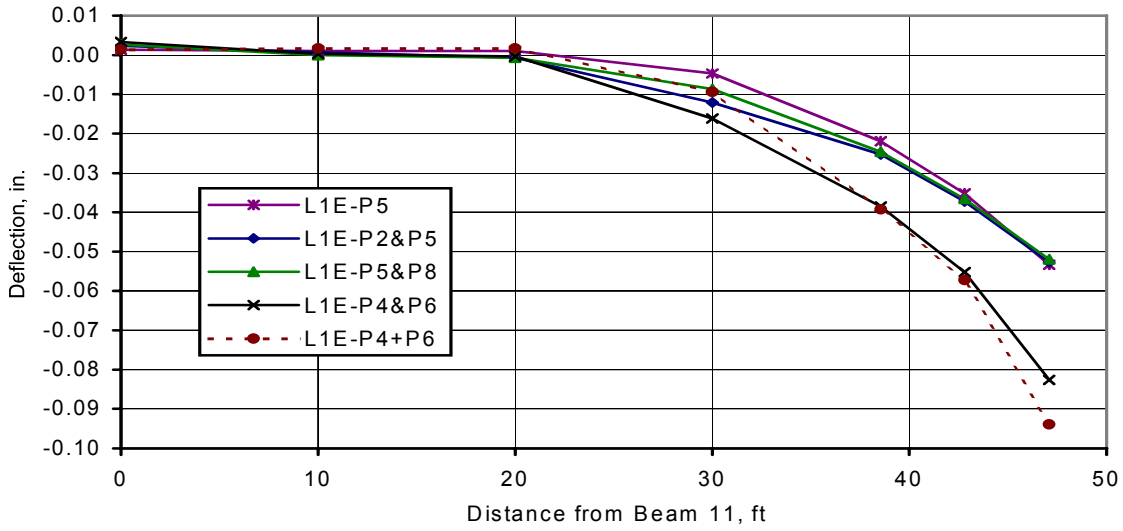


**Figure 3.30. Deflections at Transverse Section E3: Lane 1E Loaded with Trucks 1 and 2.**

The validity of superposition is also apparent in this figure. The results of two trucks located on the bridge, L1E-P4&P6, are nearly the same as the superimposed results of Truck 1 located at two points independently, L1E-P4+P6. Compared to the WB bridge data presented in Figure 3.29, the EB bridge has a greater deflection gradient across the width of the bridge. Although Beams 1W and 1E have nearly the same deflection, this does not indicate similar load distribution since the WB bridge stiffness has been compromised due to damage. The fact the Beams 3W and 5W of the WB bridge deflect somewhat more than in the EB bridge is an indication of "load shedding" in the WB bridge to the stiffer interior beams.

The longitudinal deflected shape of Beam 1W resulting from several load cases is presented in Figure 3.31. Test L1W-P2&P5 involves loading midspan of the east and center spans of the WB bridge simultaneously. As expected, these spans deflect while the west end span remains in essentially a neutral position. As Truck 1 is moved to the west end span for load test L1W-P2&P8, the center span deflects upward while the two end spans deflect downward. Finally, the two test trucks are positioned in the center span for test L1W-P4&P6. This test proved to be critical with the deflections of Beams 1W and 2W being greater than during the adjacent lane tests. The recorded deflections from both test trucks on the bridge are somewhat less than the results of Truck 1 at P4 and P6 superimposed however the agreement is acceptable.

Similar to the single lane tests, the analytical deflected shape of an undamaged beam is plotted as series SS Beam 1W. The analytical shape was normalized to the experimentally recorded deflections at the east quarter point of the beam. For the prescribed inertia and support conditions, the ratio of the analytical 1/4 point, midspan and 3/4 point deflections is 1.0 : 1.398 : 1.015. Noting the differences between the analytical and experimental deflected shapes, it appears that the damage has an effect on the deflection of Beam 1W. Similar analytical/experimental behavior was found for Beam 2W.

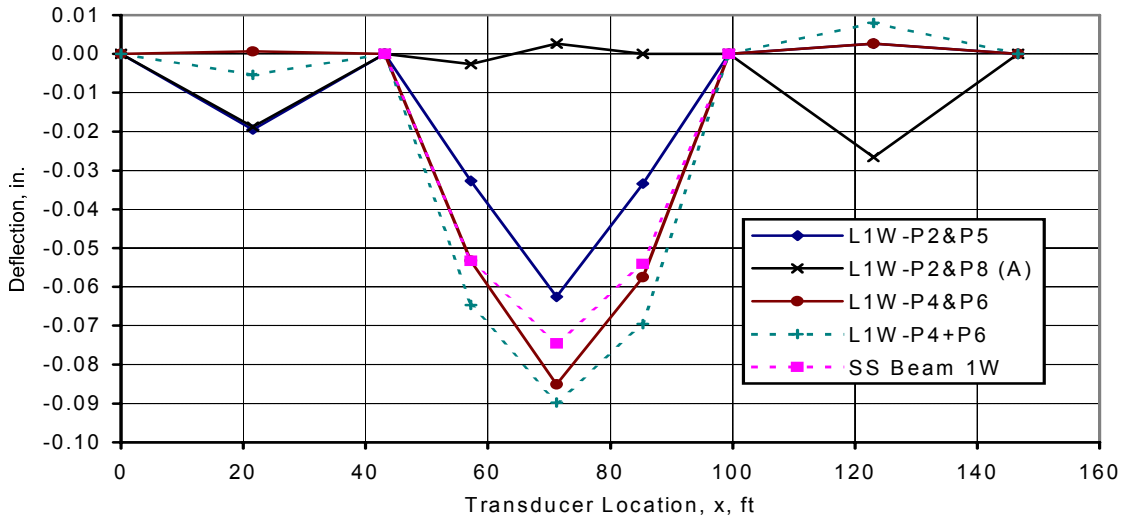


**Figure 3.31. Longitudinal Deflected Shape, Beam 1W: Trucks 1 and 2 in Lane 1W.**

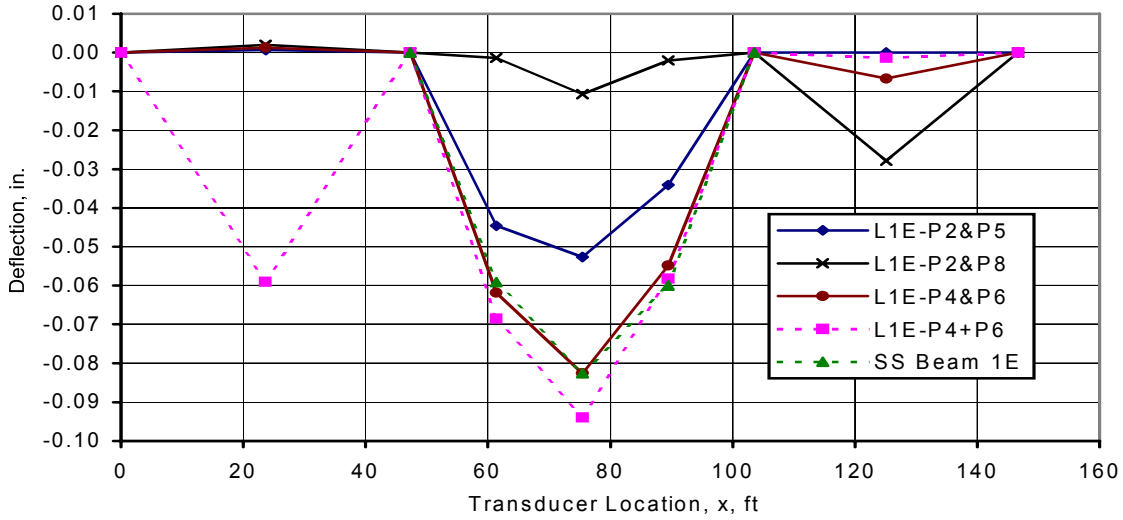


**Figure 3.32. Longitudinal Deflected Shape, Beam 1E: Trucks 1 and 2 in Lane 1E.**

Similar to the deflections in the WB bridge, longitudinal deflected shapes for the EB bridge are presented in Figure 3.32. Presented in this figure is the longitudinal deflected shape for Beam 1E of the undamaged EB bridge. The shape and deflection patterns of are generally consistent with that observed in the damaged WB bridge. There is excellent correlation between the results measured during the multiple truck test, L1E-P4&P6 and those predicted by an analysis of a simply supported beam with a constant moment of inertia. This indicates that the beam behaves essentially like a simply supported beam and confirms that the EB bridge is not damaged. The very close agreement of the analytical and experimental deflected shapes is consistent with that observed for the EB bridge during the single lane tests in Lane 1E.

**Table 3.3. Comparison of Exposed Strand Strains, Lane 1W Loaded with Trucks 1 and 2.**

| Tandem Location | BEAM 1W | | BEAM 2W | |
|---|---|---|---|---|
| | S1-1, με | S1-2, με | S2-1, με | S2-2, με |
| L1W-P2&P5 | 134 | 100 | 132 | -17 |
| (P2+P5) | (133) | (103) | (138) | (407) |
| L1W-P2&P8 | -39 | -28 | -27 | -61 |
| (P2+P8) | (-43) | (-28) | (-19) | (51) |
| L1W-P5&P8 | 93 | 80 | 112 | 179 |
| (P5+P8) | (114) | (89) | (129) | (470) |
| L1W-P4&P6 | 186 | 138 | 169 | 304 |
| (P4+P6) | (191) | (144) | (181) | (565) |

**Table 3.4. Comparison of Beam End Strains, Lane 1W Loaded with Trucks 1 and 2.**

| Tandem Location | BEAM 1W | | BEAM 2W | |
|---|---|---|---|---|
| | P1-3 | P1-6 | P2-3 | P2-6 |
| L1W-P2&P5 | -34 | -23 | -16 | -4 |
| (P2+P5) | (-30) | (-24) | (-12) | (0) |
| L1W-P2&P8 | -13 | -13 | -12 | 1 |
| (P2+P8) | (-12) | (-13) | (-9) | (4) |
| L1W-P5&P8 | -43 | -30 | -20 | -3 |
| (P5+P8) | (-41) | (-37) | (-23) | (2) |
| L1W-P4&P6 | -48 | -32 | -12 | -5 |
| (P4+P6) | (-42) | (-34) | (-17) | (1) |

Examination of the strain data for the WB bridge indicates that in general, there is very good agreement between the superimposed strain results and those obtained by multiple vehicle tests. In Table 3.3 and Table 3.4, results obtained with multiple trucks in Lane 1W are presented on the first line while those obtained by superposition of multiple Lane 1W tests are presented in parentheses on the second line.

The only data in these tables for which the agreement is suspect are the strains in the exposed strand strain gage, S2-2. In examining the results of superposition versus those obtained from the presence of multiple trucks, it is obvious that the data are not correct. Gage S2-2 is believed to be malfunctioning.

The agreement for the diaphragm strains in the WB bridge is not as good as for the beam ends and exposed strands, however, the strains are consistently low, the highest recorded strain being +12 με from multiple test trucks and +20 με from superposition. The agreement of the superimposed and multi-truck diaphragm strains in the EB bridge was better than that found in the WB bridge.

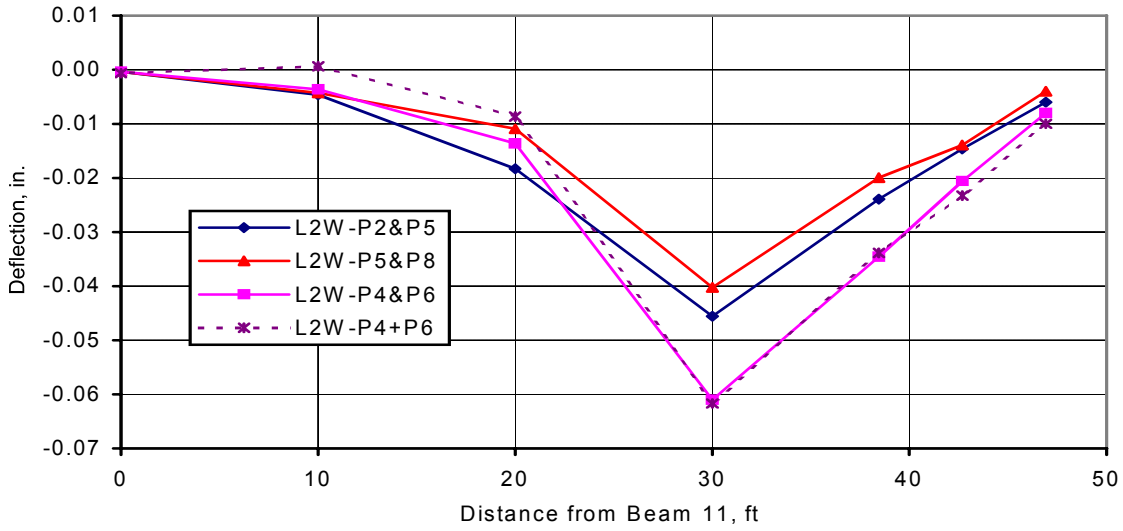


**Figure 3.33. Deflections at Transverse Section W3: Lane 2W Loaded with Trucks 1 and 2.**

### *3.3.2.3. Lane 2 Loaded with Two Test Trucks*

Presented in Figure 3.33 and Figure 3.34 is the deflection response of the center span to several different longitudinal load placements. The response of the two structures is somewhat different. However, like the results presented in the prior section for multiple trucks in Lane 1, the correlation between multiple truck and superimposed results is acceptable across this transverse section. Neither bridge appears to distribute appreciable load to the exterior flared beam, Beam 1W/1E, though the EB bridge appears more likely to do so simply by examination of the measured deflections. This is likely a function of stiffness attracting load and with the damage to beam lines 1W and 2W of the WB bridge, there is little likelihood that they would "draw" moment from interior lanes to an exterior beam line. This is consistent with the "shedding" of load from the exterior beam lines to interior portions of the bridge that occurred in the damaged WB center span.

In terms of longitudinal deflected shapes, in general, they are consistent with the single lane results. Those beams that exhibited a simple support or near simple support behavior continue to do so. The beams whose behavior was inconsistent with simple support conditions continued to behave the same way.

The strains were easily compared to the single lane tests and the effects of superposition. The highest diaphragm strain reading in the WB bridge was less than ±5 με, the highest beam end strain, -12 με and the highest reliable exposed strand reading was +46 με with the tandems at L2W-P4&P6. For the EB bridge, the maximum diaphragm strain was +47 με between beams 4E and 3E. This is significantly higher than the strains measured in the WB bridge but is consistent with the single lane results and with those obtained through superposition. The highest reliable measured beam end strain was –12 με.

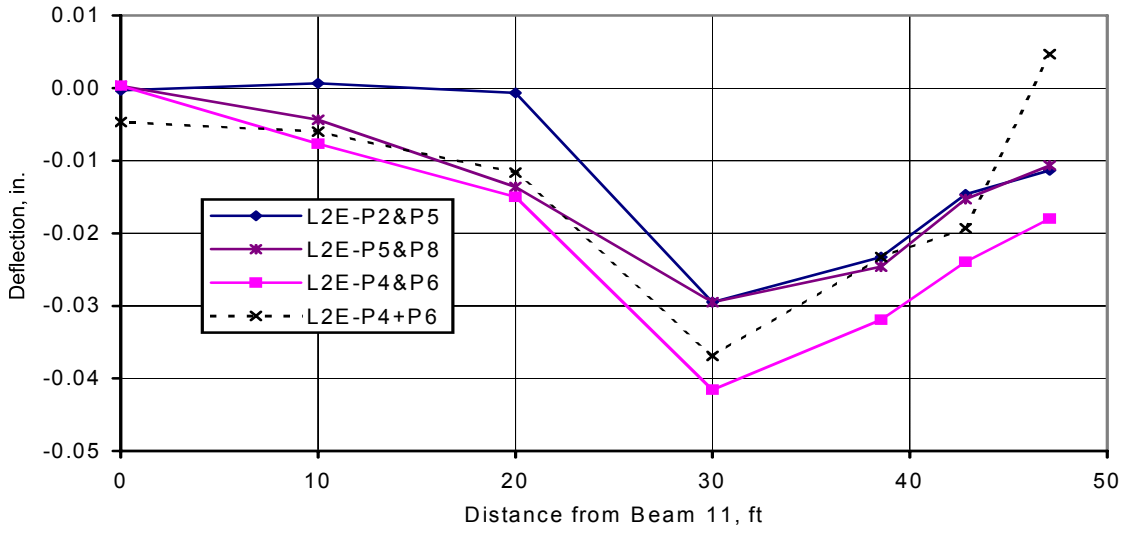


**Figure 3.34. Deflections at Transverse Section E3: Lane 2E Loaded with Trucks 1 and 2.**

### *3.3.3. Baseline Test Result Summary and Conclusions*

A large number of static load tests were conducted on the dual bridges in question. The WB bridge was damaged by overheight vehicle impact while the EB bridge was undamaged. A series of 43 static tests were conducted on each bridge to characterize the response under load and to determine the effect of various load placements on the relative distribution of load in the bridge.

For the tests conducted in Lane 1W/1E, the position where the test truck is closest to the edge beams on the flared side of the bridge, there is reasonable correlation between the deflected shapes of the first span of the WB and EB bridges. Examination of the center span data indicates a different deflected shape in the two bridges with the WB bridge deflecting more over a number of instrumented beam lines including those known to be undamaged. Presuming that the bridge stiffness is the same in undamaged regions, the deflections indicate that load is "shed" from the damaged beam lines in the WB bridge. The maximum deflection in the WB and EB bridges was measured to be 0.064 in. and 0.053 in. respectively. The beams with the most significant deflections in each bridge generally deflected as if they were simply supported and of uniform stiffness. The effect of the damage on the overall longitudinal deflected shape of the damaged beams is slight.

Diaphragm strains in both bridges were small during the Lane 1W/E loading, the maximum being approximately +15 με in both bridges. The strains do not relate well to the magnitude of differential deflection in the beams and generally agree with the findings of others that the diaphragm plays an insignificant role in live load distribution. It also disproves one of the initial assumptions in this project that the response of the diaphragm in the WB bridge would be more pronounced due to the presence of localized damage.

The beam end strains indicate a compressive strain in the bottom flange in those load cases where the center or far spans are loaded. This is consistent with the loss of camber in these beams under load and the corresponding thrust that would develop at the bearings.

The maximum reliable exposed strand strain was approximately +150 με, a change in strand stress of 4,280 psi under static loads. Strains were comparable in both damaged beams and followed the same trend as the deflections and beam end strains.

For tests conducted in Lane 2W/2E, review of the deflected shapes indicates neither bridge distributes a measurable amount of load to the edge beams. This is true for the end spans as well as for the center span. The center span of the EB bridge has a smoother deflected shape than does the WB bridge indicating the EB bridge has better distribution characteristics even in undamaged regions. For beams with the greatest deflections in both bridges, the correlation of the longitudinal deflected shapes to that of an undamaged simply supported beam is fair to good. The maximum downward deflection in the WB bridge center span is slightly greater than 0.04 in. and slightly less than 0.03 in. in the EB bridge.

The diaphragm strains are negligible for the WB bridge however in the EB bridge a maximum strain of +40 με occurred in the diaphragm connecting Beams 4E and 3E with Truck 1 at midspan of the center span, load case L2E-P5. The beam end strains were less than ±5 με in both bridges; the maximum strain in the WB bridge exposed strands was +33 με in Beam 2W.

The exterior beam and to a large extent Beam 2 of both bridges resist minimal live load when the traffic is shifted into Lane 2W/2E. Tests conducted in Lanes 3 and 4 in both bridges were remote from the damage, thus the damage had minimal effect.

The Lane 3W/3E tests indicate different deflections in the two bridges. For the center span, the WB bridge maximum downward deflection is approximately 0.03 in. and for the EB bridge, 0.018 in. Although there is a large difference in these values percentage wise, they represent only minor differences in terms of the significance of the measured values.

The Lane 4W/4E tests are somewhat peculiar in that at this location, all beams in both bridges are parallel and at a constant spacing of 5ft. However, in both bridges, the deflection of Beam 11 is less than for Beam 1 under a similarly located load. This was unexpected since the beam spacing adjacent to Beam 1 is less than that adjacent to Beam 11. This smaller deflection was found in both bridges and for all three spans. Maximum downward deflection in the WB bridge was slightly less than 0.03 in. in Beam 11W and was slightly more than 0.02 in. in Beam 11E of the EB bridge.

Considering the effects of multiple trucks on the bridge simultaneously, the correlation between the effects of two trucks placed in adjacent or in the same lane is excellent compared to the effects of linear superposition of individual truck test results.

With two trucks placed in adjacent lanes, the deflected shapes of both the WB and EB bridges are fairly flat across the first five beam lines. The deflections decrease to essentially zero in the 10 ft from

Beam 5 to 7. This indicates the highly localized response of both bridges and the inefficient lateral load distribution in both structures.

The maximum exposed strand strains were +146 με and +175 με for Beams 1W and 2W, respectively. Diaphragm strains in the WB bridge were very small while those in the EB bridge reached +27 με.

The most significant deflection for beams 1 and 2 in both bridges occurred when the two trucks were placed end-to-end in Lane 1, L1W/E-P4&P6. The deflection of the center span of the WB bridge was 0.085 in., approximately L/7,900 and was 0.083 in., L/8,100 in the EB bridge. Other beams in the WB bridge deflected more than in the EB bridge by a small amount, i.e., 0.01 in. for most of the beams. The beams in both bridges typically deflect as if they are simply supported and have uniform stiffness or only slightly non-uniform as for the WB bridge. Once again, as in the single lane tests, the presence of local damage has only a minor effect on the longitudinal deflected shapes of the damaged beam lines.

The maximum exposed strand strains were also recorded during the test with two trucks in Lane 1. The maximum strain recorded in Beam 1W was +186 με and in Beam 2W, +169 με. These strains correspond to stress increases of approximately 5,300 psi and 4,800 psi in the two strands, respectively. These stress ranges are small and represent a stress range of less than 2% of the ultimate strength of the strand.

The large number of single and multiple truck load tests conducted on the two bridges indicated that neither bridge was overstressed and the differences in their behavior is minor. The fact that the displacements in both bridges are so small may be part of the reason for the disagreement between the test results. To obtain additional data on the effects of the damaged beams, load tests were performed on the WB bridge in August 1998 after the damaged beams were replaced in October 1997. The results from the follow-up tests are compared to the data from the damaged WB bridge and the undamaged EB bridge in the following section.

## ***3.4. WB Bridge Retest (1998) Results***

In August 1998, a series of single and multiple truck load tests were conducted on the repaired WB bridge. These tests were carried out so that a comparison of the behavior of the WB bridge before and after beam replacement could be made. This is the most direct way of assessing the effects of damage in the WB bridge.

Similar to the tests carried out the prior year, both single and multiple truck tests were performed. The single truck tests used a single truck, Truck 3, described in Figure 3.6 while the multi-truck tests used Trucks 3 and 4 simultaneously. Because the 1998 retest vehicle weight is somewhat less than the 1997 baseline truck weight, the retest results have been linearly scaled to represent the effects of the heavier truck. The single truck tests carried out in 1997 used a vehicle with a gross weight of 60,320 lbs while the 1998 tests used a truck weighing 53,100 lbs., approximately 12% less. For tests employing two trucks, the

combined test weight of the 1997 trucks was 119,280 lbs while for the 1998 tests, the combined weight was 104,140 lbs, 12.7% less.

There are slight differences in the retest and baseline test load positions and instrumentation. Due to the fact that the effect of the beam replacement would not be noticeable for trucks positioned in Lane 4W, it was eliminated from the retest. Because there was minimal response on the far side of the bridge for the Lane 1 and 2 tests, displacement transducers were not installed past Beam 7W in the retests. Additionally, since the damaged beams were replaced, obviously there were no exposed strands to instrument. Finally, since the WB bridge diaphragm strains were consistently small, diaphragm strains were not recorded during the retest, however, beam end strains were recorded.

### *3.4.1. Single Truck Test Results*

Similar to the data presentation for the baseline load tests, data from the retests begins with the results of single lane tests. Selected data from this and all subsequent lane and truck positions will be compared to the damaged WB bridge and undamaged EB bridge so that comparisons can be made. The retest results have an (R) designation.

#### *3.4.1.1. Lane 1 Test Results*

Figure 3.35 illustrates the deflection results at transverse section 1 of the WB bridge during the retest as compared to that recorded the prior year in both the WB and EB bridges. As expected, there is very little difference for this span since the damage is in the center span.

Deflections presented in Figure 3.36 indicate that the repaired WB bridge behaves like the undamaged EB structure. The increases in deflection in beam lines 3, 5 and 7 of the WB bridge as compared to the EB bridge, hypothesized to be due to a redistribution of load to interior portions of the bridge in the damaged span, are no longer present. Hence, the assumption of load redistribution in the damaged WB bridge was sound. Since the stiffness of Beams 3W and 5W has not changed, the reduction in deflection is a direct reflection of the reduction in live load to these beams due to the beam replacement.

Deflections at transverse section W4/E4 are presented in Figure 3.37 for all three bridge tests. As may be seen, the repaired WB and EB structures behave “exactly” the same and much differently than the damaged WB bridge. This further confirms the effect of the replacement beams in restoring the original deflection/live load distribution patterns in the previously damaged WB bridge.

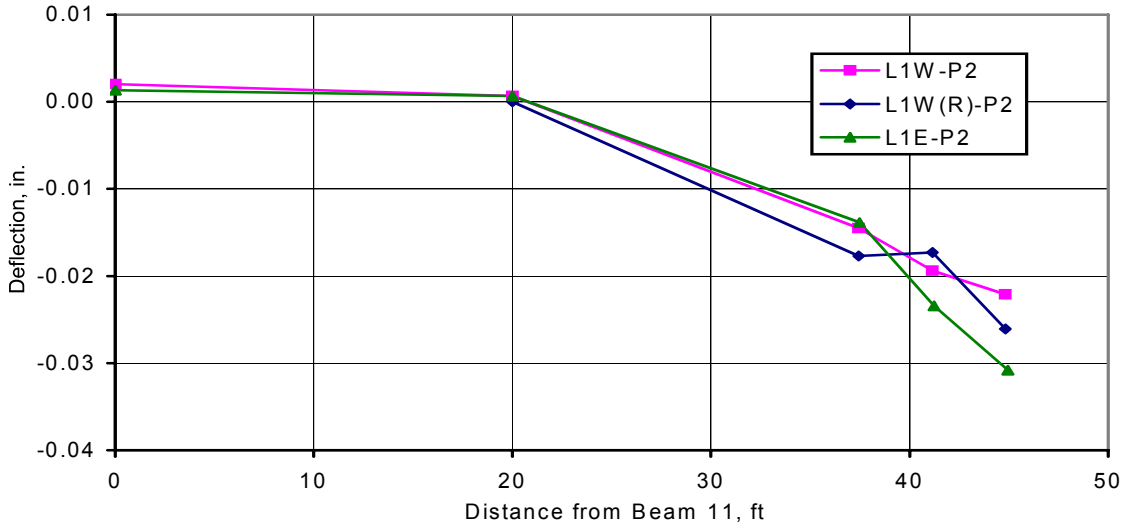


**Figure 3.35. Deflection Comparisons at Transverse Section W/E1: Lane 1W/1E Loaded.**

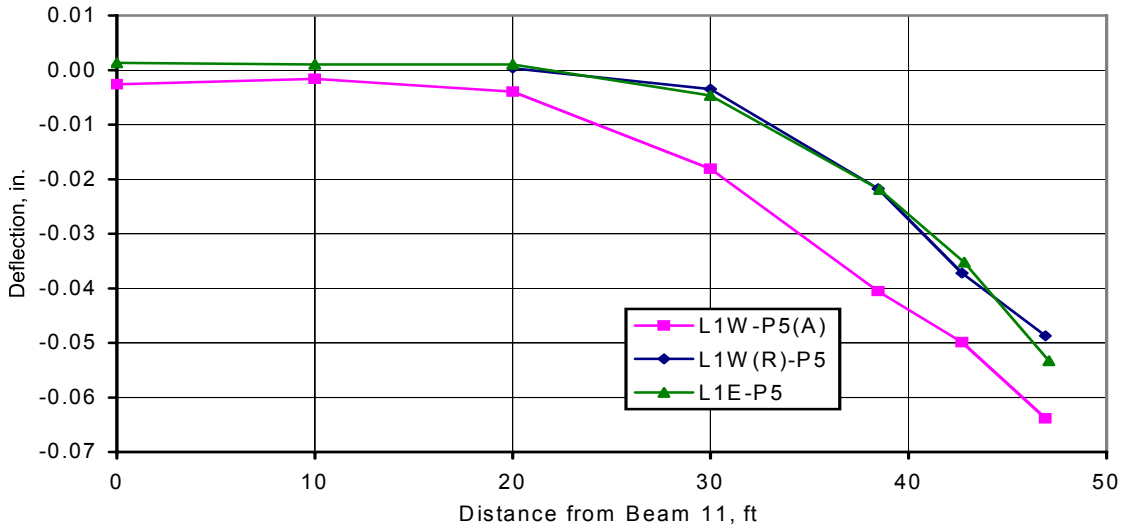


**Figure 3.36. Deflection Comparisons at Transverse Section W/E3: Lane 1W/1E Loaded.**

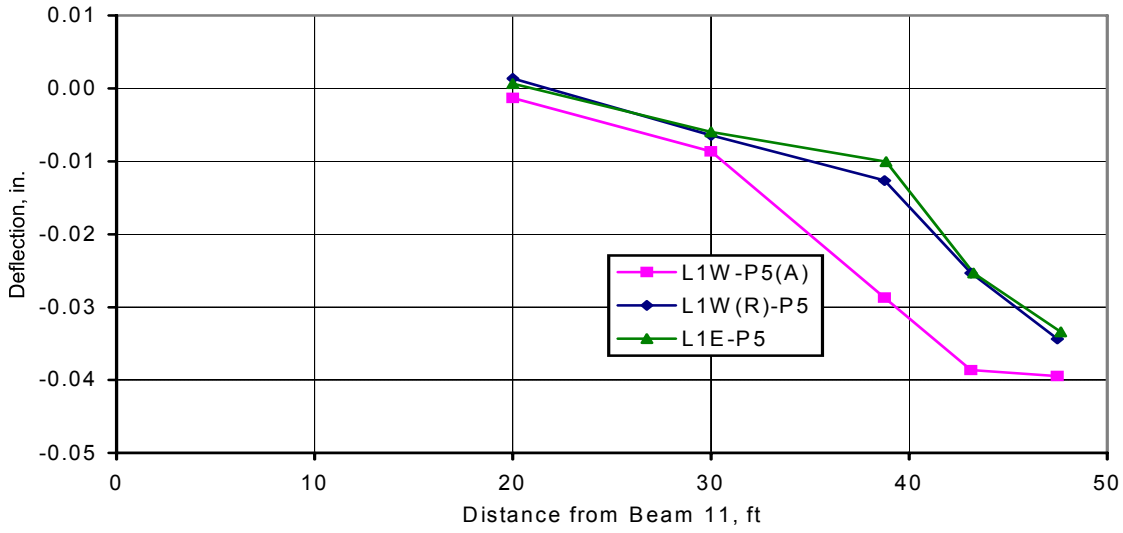


**Figure 3.37. Deflection Comparisons at Transverse Section W/E4: Lane 1W/1E Loaded.**

In addition to confirming the effectiveness of the replacement beams in changing the deflection response of the WB bridge, Figure 3.37 in conjunction with Figure 3.36 provides other useful information. For instance, the increase in load (via deflection increases) apparent in Beams 3W, 5W, and 7W at midspan due to the damage appears to dissipate to a great degree as one moves down the span to the 3/4 point of the WB bridge center span. At midspan, Beam 5W deflects much more in the damaged bridge than in the undamaged or EB bridges, a sign of a redistribution of load. However, at the 3/4 point, there is little difference between any of the three tests. This indicates that load distribution is not a constant along a span. The "extra" load carried at midspan by Beam 5W is not present to the same degree at the 3/4 point.

As further documentation of the effects of the replacement beams, several longitudinal deflected shapes are presented. These deflected shapes are used to reaffirm that the bridge behaves as a series of three simply supported spans and for comparisons to the longitudinal deflection patterns in the damaged WB structure. Because all beams in the repaired structure are undamaged, the analytical deflections are based on normalizing the computed midspan deflection to the experimentally obtained midspan deflection and using the ratio of 0.676 : 1.000 : 0.712 to compute the value of the 1/4 and 3/4 point deflections.

The results of the measured and computed responses for the WB bridge are presented in Figure 3.38. Only beam lines 1W through 3W are presented since they had the largest displacement under Lane 1W loading. The figures contain both measured and computed deflected shapes for both tests. As the data indicate, there is a significant reduction in overall deflection due to the replacement of the damaged beams. This reduction is expected in Beams 1W and 2W since their stiffness was initially compromised by the impact damage. The reduction in Beam 3W deflections is confirmation of the decrease in load to this beam due to the presence of the replacement beams.

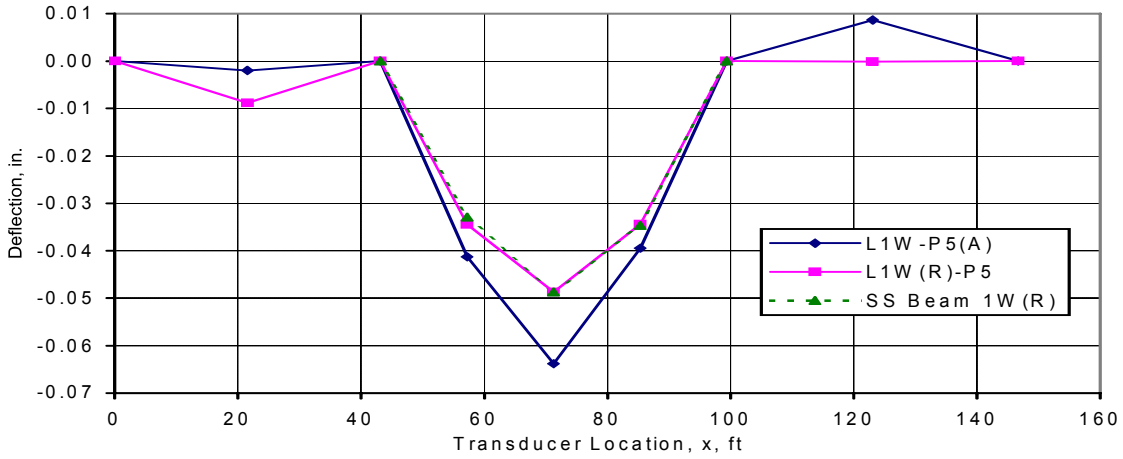


**a.) Beam 1W**

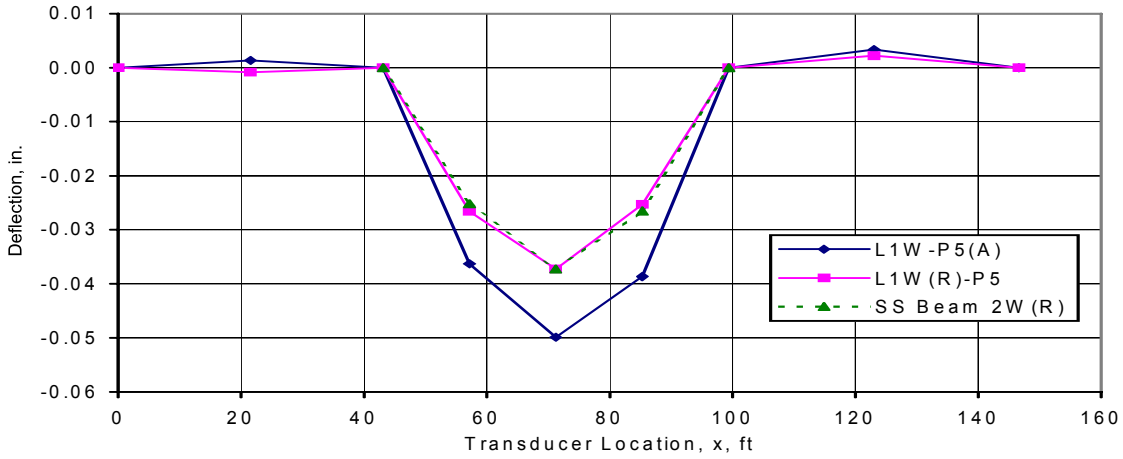


**b.) Beam 2W**

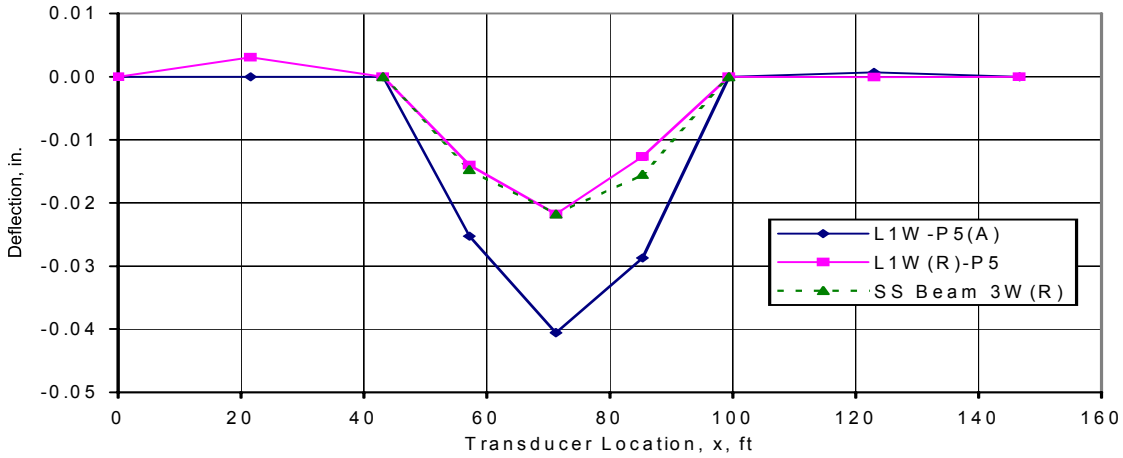


**c.) Beam 3W**

**Figure 3.38. Longitudinal Deflected Shapes, Beams 1W-3W: Lane 1W Loaded.**

By examining the measured beam end strains and comparing them to the prior year's baseline test results it is apparent that the strains are much less following the beam replacement. During the Lane 1W tests conducted on the damaged bridge, bottom flange strains were as high as –30 με and the strains were fairly consistent on both sides of the west pier. During the retest, strains were zero in the midspan beam end gages and –15 με for gage P1-6, bottom flange of the west end span beam. This lack of restraint at the beam end of the new center span beam is consistent with the prior statement that restraint is likely due to a partially frozen bearing condition. When the old beams were removed, the masonry plate on the pier tops was cleaned and new beams with curved sole plates were installed. These beams were only in place approximately ten months when tested, not long enough for the bearings to deteriorate.

#### *3.4.1.2. Lane 2 Test Results*

Due to the erratic behavior of several critical transducers in the center span during this test, only brief statements can be made about the behavior of the repaired bridge during the Lane 2W tests. In general, the center span of the repaired bridge behaved somewhat stiffer than the damaged WB bridge. The data obtained in the end spans was also inconsistent so no conclusions can be drawn about the behavior of these spans. The beam end strains were low in Beams 1W and 2W, the maximum strain being –4 με.

### *3.4.2. Multiple Truck Tests and Validity of Superposition*

This section describes the response of the repaired WB structure under the action of multiple test trucks. Tests are similar to those conducted the prior year. Several tests were conducted with trucks in adjacent lanes and several additional tests with multiple trucks in the same lane. Due to instrumentation problems during the single truck tests conducted in Lane 2W, little can be said about the validity of superposition in the repaired WB structure.

#### *3.4.2.1. Lanes 1 and 2 Loaded Simultaneously*

The midspan deflected shapes of the damaged WB, repaired WB and undamaged EB bridges under the action of two trucks in adjacent lanes are presented in Figure 3.39. The data for Beams 1W and 2W are not believed to be reliable since they are less than the deflection measured in these beams when Lane 1W alone was loaded with a single test truck. These transducers along with that at midspan of Beam 5W were problematic throughout the test though the inaccuracy/unreliability of the readings was not discovered until post-processing of the data. The deflection transducers used on Beams 1W and 2W produced reliable results during the Lane 1W tests but not during the Lane 2W tests where they both remained at zero regardless of load position.

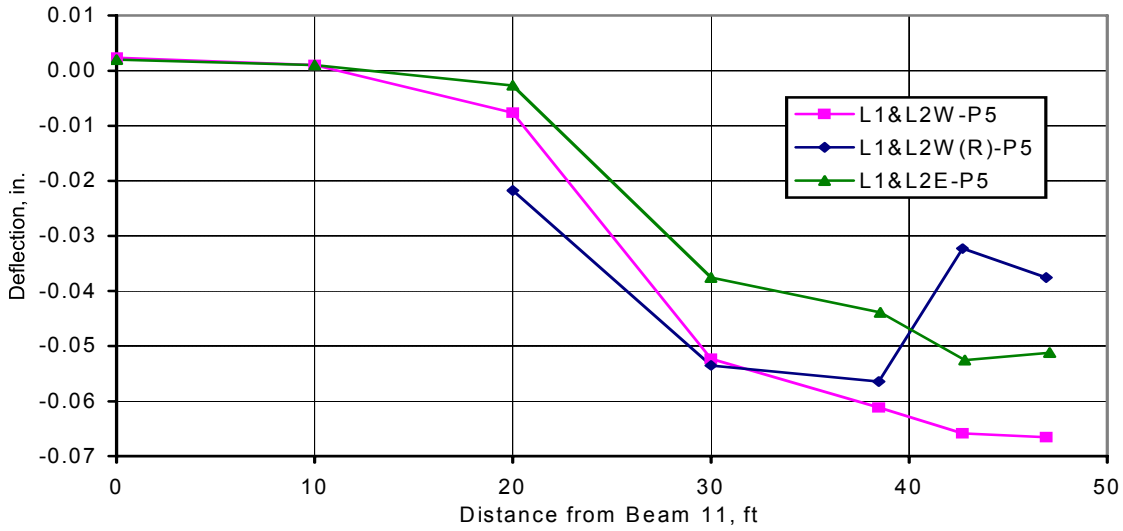


**Figure 3.39. Deflection Comparisons, Transverse Section W/E3: Lanes 1 and 2 Loaded.**

The problems with the poor data notwithstanding, if one extrapolates the trend of the deflected shape of the repaired bridge, the extrapolated deflections appear to be somewhat closer to the EB bridge than the damaged WB bridge. It is important to note however that regardless of the level of damage or which bridge was tested, the deflections are consistently very small and indicate only minor differences in behavior.

The strains measured in the beam ends were typically close to zero for the center span beams while they were as high as –19 με in the end span beam. The end span data are the same as that which would be obtained through superposition of the Lane 1W and 2W effects measured individually. Superposition of strains further confirms that the anomalous deflections recorded in Beams 1W and 2W during the WB bridge retest are not reliable. The measured strains in the center span beams are consistent with that observed in other tests; there is no compressive stress induced in the bottom flange under live load. The strains measured in the 1998 retest are less even in the end span beam than measured during the 1997 baseline tests.

### *3.4.2.2. Lane 1 Loaded with Two Test Trucks*

A comparison of the center span response is presented in Figure 3.40. There is reasonable correlation between the repaired WB and EB bridges except for Beams 2W and 1W where the malfunctioning transducers were located. The kink in the deflected shapes was present at this transverse section for all tests involving multiple test vehicles in Lane 1W of the repaired bridge. The trend of the repaired bridge data indicates that it behaves more like the EB bridge than the damaged WB bridge, further confirmation of the effect of the beam replacement. The longitudinal deflected shapes for the beams with

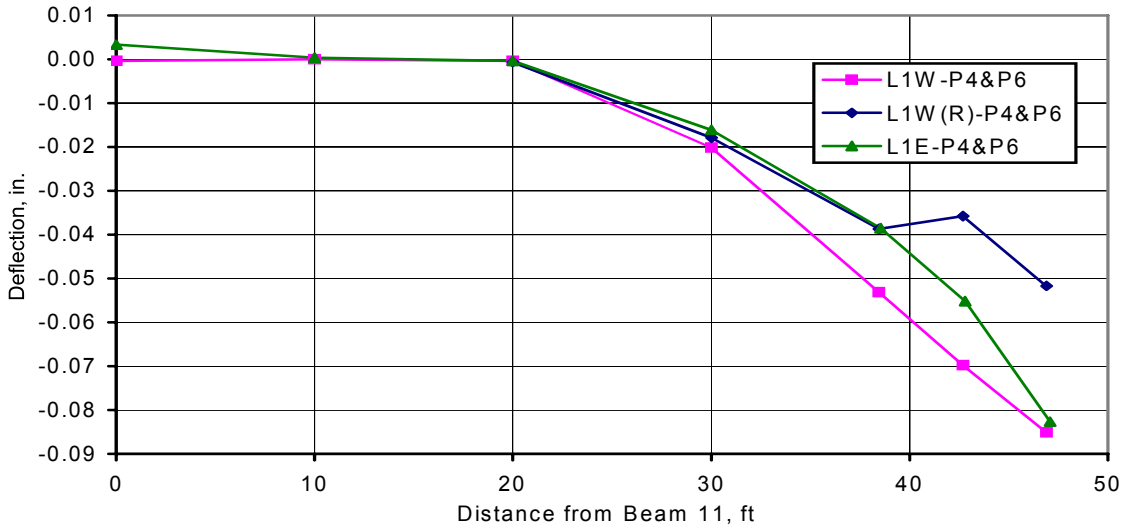


**Figure 3.40. Deflection Comparisons, Transverse Section W/E3: Lane 1 Loaded with Trucks 1 and 2.**

reliable deflections once again indicate simply supported, prismatic conditions. The strains in the center span are again less than ±5 με while in the end span they are a maximum of –25 με at test position L1W(R)-P4&P6. These strains are less than in the damaged WB bridge where strains of –48 με and –32 με were recorded in the center and far spans, respectively.

#### *3.4.2.3. Lane 2 Loaded with Multiple Trucks*

The final test to be discussed involved two test trucks placed end to end in test Lane 2. The results of this load test are presented in Figure 3.41. In this figure, the data indicate that the repaired WB bridge appears somewhat stiffer than the damaged WB bridge but is not as stiff as the EB bridge. However, the difference in behavior is small. The data from Beams 1W and 2W were unreliable.

### *3.4.3. WB Bridge Retest Summary and Conclusions*

The retest conducted on the WB bridge in the summer of 1998 confirmed that majority of the difference in response between the damaged WB bridge and undamaged EB bridge was due to the presence of the damaged beams. However, following replacement of the damaged beams, the two bridges still did not agree perfectly though the differences are small.

The most informative test results are those from Lane 1. In these tests, it was observed that the end span behavior was the same regardless of whether the WB bridge was in the damaged or repaired condition and the end span data generally agreed with the EB bridge. The center span deflections with loads in Lane 1W are less in the repaired WB bridge than in the damaged WB bridge. There are no significant differences between the repaired WB bridge and the undamaged EB structure. This confirms that the replacement of

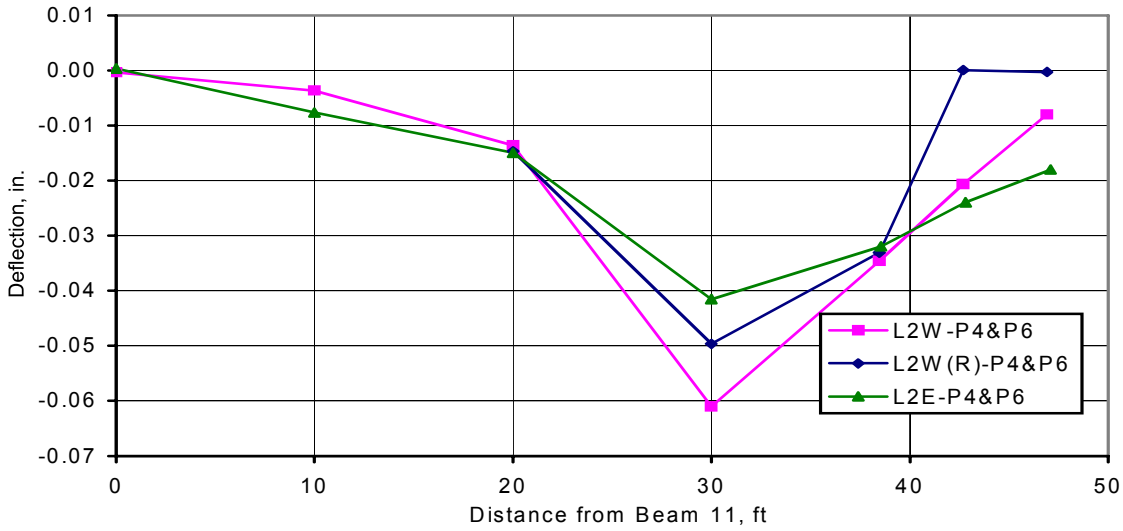


**Figure 3.41. Comparative Deflected Shape: Lane 2 Loaded with Multiple Trucks**

the damaged beams has restored the stiffness and original load distribution characteristics to the WB structure. The comparison of deflected shapes confirms that the increased deflection of the interior beam lines was in fact due to live load redistribution away from the damaged beams.

The installation of the new beams seems to have altered the beam end strain values recorded in the WB bridge. The strains at the top flange, web, and bottom flange in the center span are all essentially zero for Beams 1W and 2W. There are still compressive strains in these same beams in the bottom flange on the opposite side of the pier but not as high as in the baseline load tests. The elimination of bottom flange strain in the 1998 retest indicates that the source of the bottom flange compression strain was likely related to the bearing condition of the removed beams.

# *CHAPTER 4*
# *LABORATORY BRIDGE TEST RESULTS*

This chapter describes the results of a laboratory test conducted on a full scale bridge constructed of prestressed concrete girders. For additional details see Paradis (1999). The bridge had been constructed several years ago as part of a different research project, Project HR-319 (Abendroth et al., 1991).

The overall bridge deck dimensions are 40 ft-4 in. long by 18 ft wide. The center to center bearing length is 38 ft-4 in. The concrete deck is 4 in. thick. A 1-1/2 in. thick haunch was placed above each P/C beam to facilitate the deck formwork, and to provide additional cover for the lifting hooks embedded in the beams. The 4 in. deck thickness did not provide a significant amount of cover for this purpose. Overall dimensions of the bridge model are presented in Figure 4.1.

It was not the intent of the researchers in Project HR-319 to replicate an actual bridge. The limited space at the laboratory dictated that certain modifications be made. The number of beams was reduced to decrease the width of the bridge. Three beams were chosen so that an "interior beam" would exist within the model. The beams were placed 6 ft on centers leaving a 3 ft overhang on the exterior beams (see Figure 4.1). The concrete deck was reduced to 4 in. so that the response to horizontal loading would increase. The deck thickness was not a critical variable in the analysis, so this reduction was justified. This reduced the deck stiffness and permitted the various diaphragms to carry a larger percentage of the horizontal load.

The three P/C beams were Iowa DOT size LXA38; a cross section of this beam is illustrated in Figure 4.2. The beams were modified in Project HR-319 by inserting coil tie inserts at the time the concrete was cast to facilitate the installation of various diaphragms. Pipe sleeves to accommodate the horizontal loading mechanism were also inserted. These inserts were placed at midspan and at the 1/3 points.

The beams were placed on 17 in. long by 12 in. wide by 1 in. thick elastomeric bridge bearing pads. The pads were set on top of 42 in. high by 18 in. wide R/C abutments. After the abutments, pads, and P/C beams were set in place, full-depth R/C end diaphragms were cast around the ends of the beams. The ends of the beams were encased by 8 in. of concrete.

As noted earlier, a 1-1/2 in. haunch was placed monolithically with the 4 in. concrete deck. This provided 5-1/2 in. of clearance for the lifting bars in the P/C beams. At the time the P/C beams were cast, the top surface was intentionally roughened. The combination of the roughening of this surface and the vertical stirrups projecting up through the beam provided the composite action between the beams and the deck. The concrete deck was reinforced with No. 5 reinforcing bars (ASTM A615 Grade 40) throughout. Two layers were used in the longitudinal direction. The top layer had the bars at 12 in. on center between the beams and 9 in. on center near the beams, and the bottom layer had bars at 12 in. on center except at the beams. The transverse reinforcement spacing was 12 in. throughout. Four R/C diaphragms were located at the 1/3 points of the span.

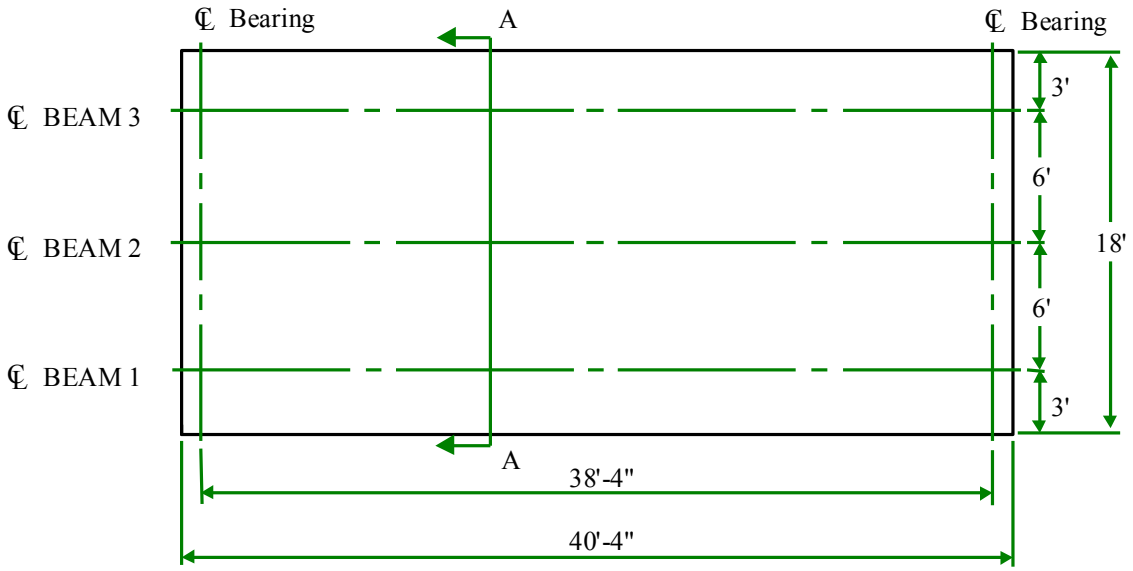


**a.) Plan View**

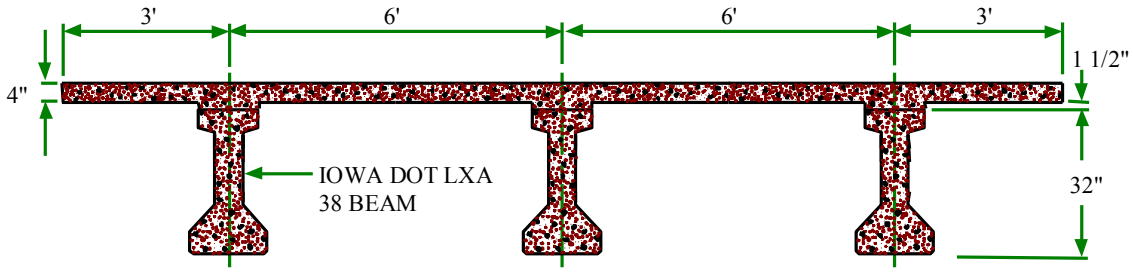


**b.) Section A-A**

**Figure 4.1. Overall Dimensions of the Bridge Model.**

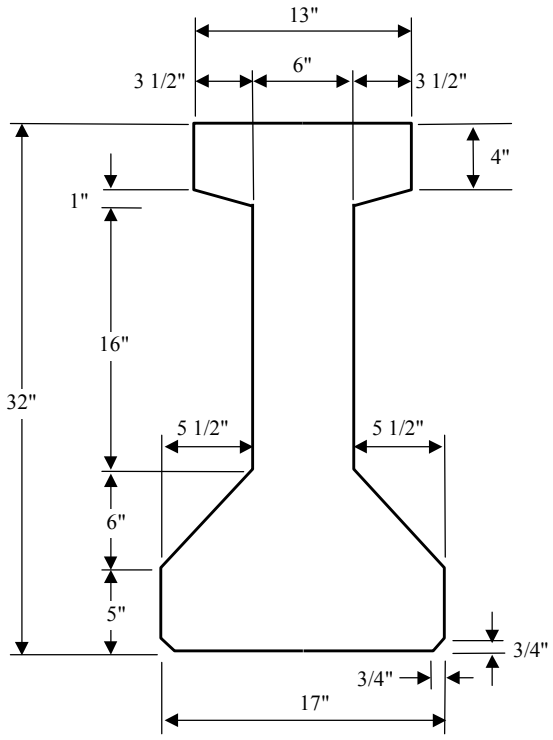


**a.) Normal Cross Section**

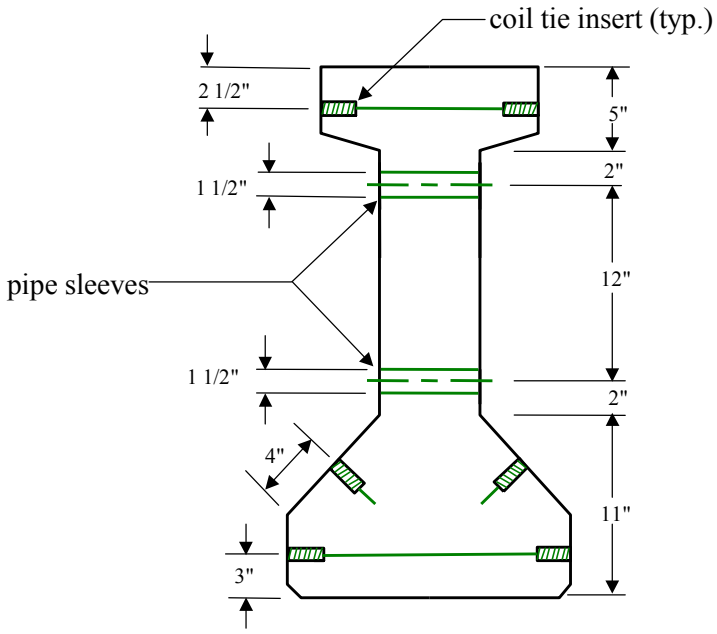


**b.) Modified Cross Section**

**Figure 4.2. Prestressed Beam Cross Sections.**

## *4.1. Test Objectives*

The testing program for this part of the investigation was designed so that a comprehensive record of the behavior of the bridge could be obtained. Baseline tests were completed on the undamaged bridge for comparison purposes; these results are presented in Section 4.3.1. Inflicted damage consisted of both the removal of concrete and the severing of prestressing strands. The focus of the testing program was to gather sufficient data so that accurate comparisons could be made from one level of damage to another. This task was accomplished by loading the bridge at predetermined points and recording the corresponding deflections and strains at critical locations. Sufficient deflections and strains were measured so that the overall behavior of the bridge could be evaluated.

## *4.2. Test Procedures and Instrumentation Description*

A self contained loading frame was required to apply vertical loading to the bridge model; a prototype of this loading frame connected to the bridge abutments is presented in Figure 4.3. The abutments used to support the horizontal loading beam in Iowa DOT Project HR-319 (on the east side of the bridge) were still in place after removal of that beam. The main loading beams were oriented parallel to the longitudinal direction of the bridge. Reinforced concrete was chosen as the material for the main loading beams because it could be cast in place and easily connected to the abutments. The abutments on the east side of the bridge were used as the tie downs/supports for one of the R/C beams. On the west side of the bridge, several reinforcing bar "hoops" were still in place after originally being cast protruding from the abutments. These provided connection for the west R/C loading beam to the abutments. The two R/C beams parallel to the longitudinal direction of the bridge were designed and constructed to act integrally with the existing abutments and formed the basis of the loading frame.

The bridge model was initially loaded at twelve load points. As shown in Figure 4.4, these points were the 1/4 point, 3/8 point, midspan, and 3/4 point of Beams 1, 2, and 3. It was decided that these load points were sufficient to obtain a global response of the bridge. With this configuration, behavior comparisons could be made with respect to the longitudinal and transverse lines of symmetry of the bridge. Loading of a damaged beam on one side of the bridge could be compared to the loading of an undamaged beam on the other side. Therefore, after every level of damage inflicted on the bridge, load was applied to each of these twelve load positions.

**Figure 4.3. Loading Frame for Applying Loads to the Bridge Model.**

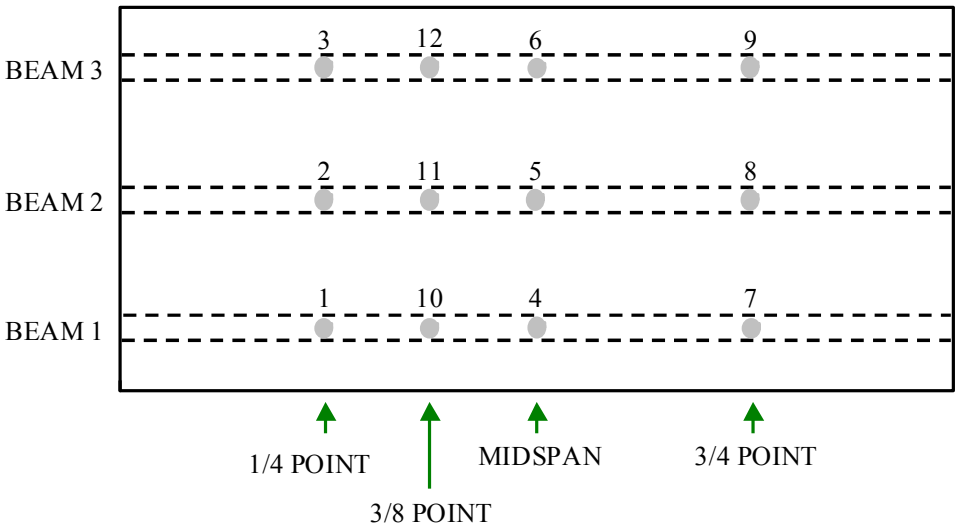


**Figure 4.4. Load Positions Used to Test the Bridge Model.**

All tests consisted of a single point load applied to one of these locations. The maximum load applied to the bridge in these tests was 60 kips; the load was applied in 5 kip increments until the maximum load was reached. Available clearances limited the size of the loading frame, thus the R/C beams in the loading frame could only be designed to resist 60 kips load placed anywhere on the bridge deck. Also, due to the thickness of the bridge deck, it was not possible to apply AASHTO truck loads (i.e. HS20-44) to the bridge. The intent of the project was not to simulate actual truck loadings, but to investigate the effect of a damaged bridge beam on the behavior of the bridge.

The bridge model was instrumented with electrical resistance strain gages and string potentiometer displacement transducers. A computer controlled data acquisition system (DAS) was used to record all of the data gathered in the testing program. The P/C beams were instrumented with a minimum of 12 gages; additional gages were installed on Beams 1 and 2. The basic gage configuration for each beam consisted of gages placed on both sides of the beams at the top and bottom flanges at the 1/4 point, midspan, and 3/4 point. The additional gages were applied to the top and bottom flanges of the east face of Beam 1 on the south end and the west face of Beam 2 on both the north and south ends. The additional gages were placed near the beam ends so that any end restraint at the supports could be detected. It was assumed that all supports would have the same degree of restraint because of similar construction details, therefore, not every beam end was instrumented. The location of strain gages on all three of the P/C beams is presented in Figure 4.5.

As shown in Figures 4.6 and 4.7, concrete gages were also applied to the R/C bridge deck and diaphragms. A total of 12 gages were mounted on the bridge deck, 8 oriented longitudinally (4 each at the 1/4 point and midspan) and 4 oriented transversely at the midspan. Diaphragm gages (4 on each diaphragm) were applied on one side only of the two northern diaphragms. The diaphragm gages were applied 8 in. from the vertical face and 2 in. from the horizontal face of the diaphragm edges. The bridge deck and diaphragm gages were installed so that the transverse load distribution determined using P/C beam strains could be checked.

Strain gages were placed on the seven-wire prestressing strand to observe two different types of behavior. First, the gages measured the strain in the strands during the various load tests. These strains provided information about the effects of damage on strain levels in the strands. Secondly, the strain gages provided a measurement of the remaining effective prestressing force when some of the strands were severed. This process has been used by Olson, French, and Leon (1992) in their work on the repair of damaged P/C girders, as well as in a study by Labia, Saiidi, and Douglas (1997) on pretensioned concrete box girders.

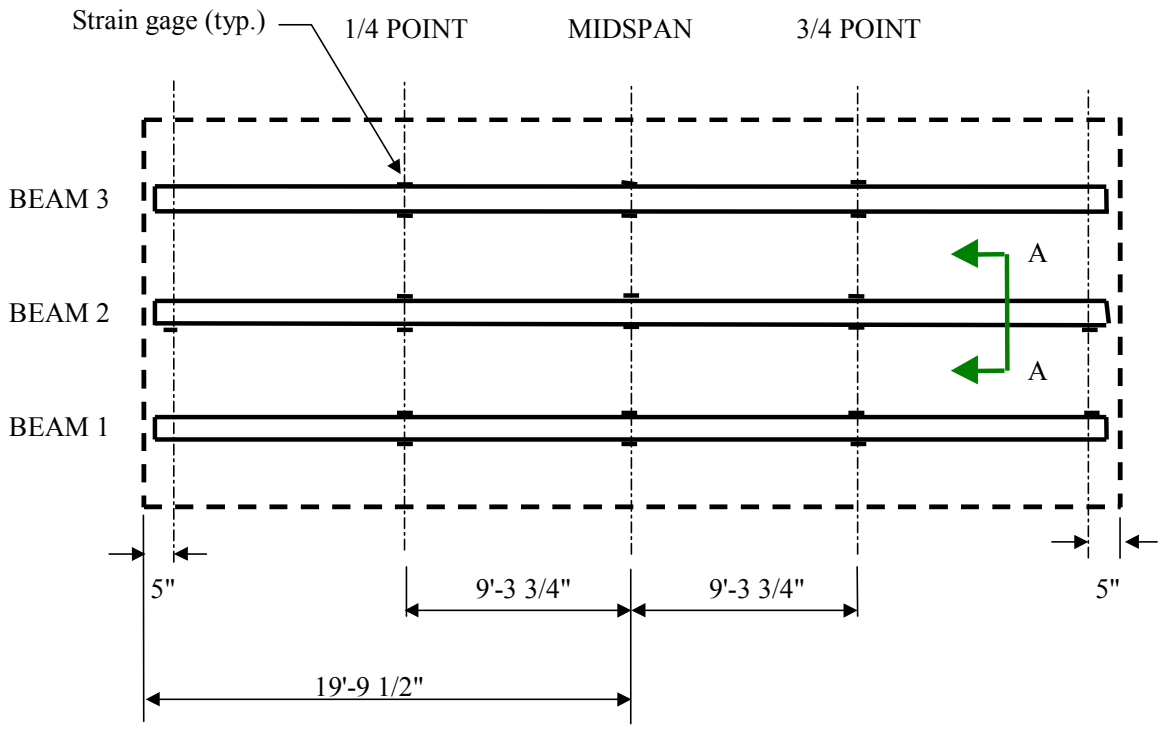


**a.) Plan View**

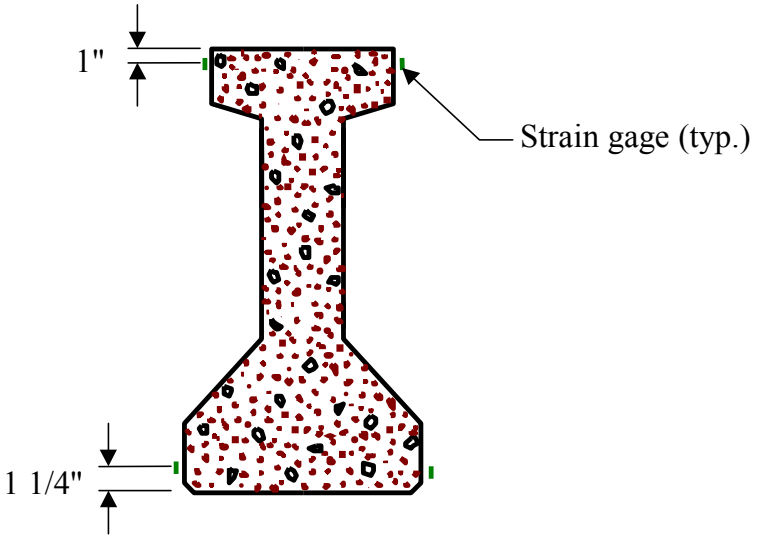


**b.) Section A-A**

**Figure 4.5. Location of Strain Gages on Prestressed Concrete Beams.**

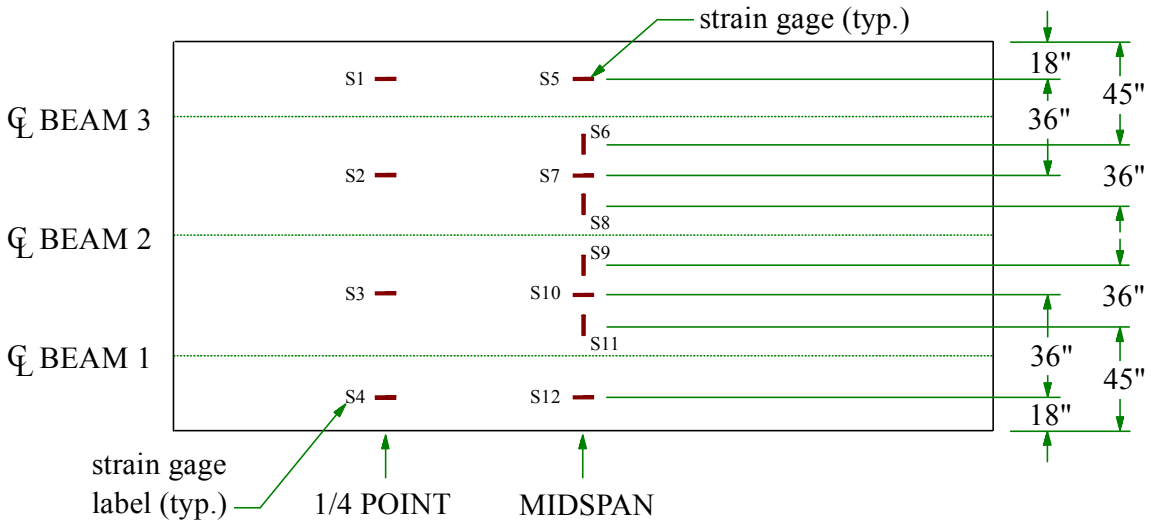


**Figure 4.6. Location of Bridge Deck Strain Gages.**

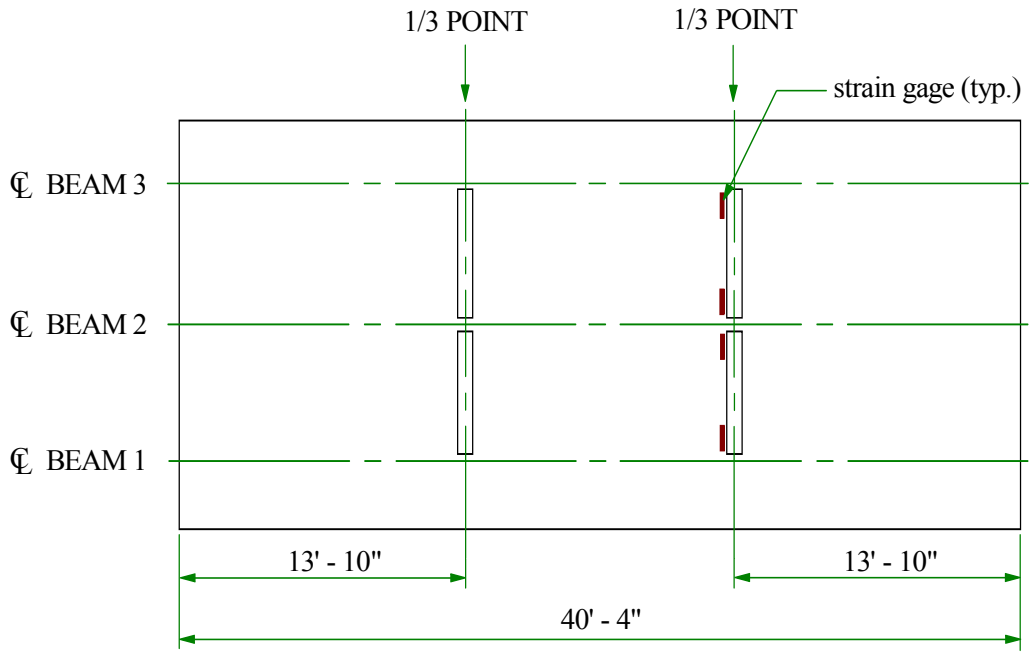


**Figure 4.7. Location of Diaphragm Strain Gages.**

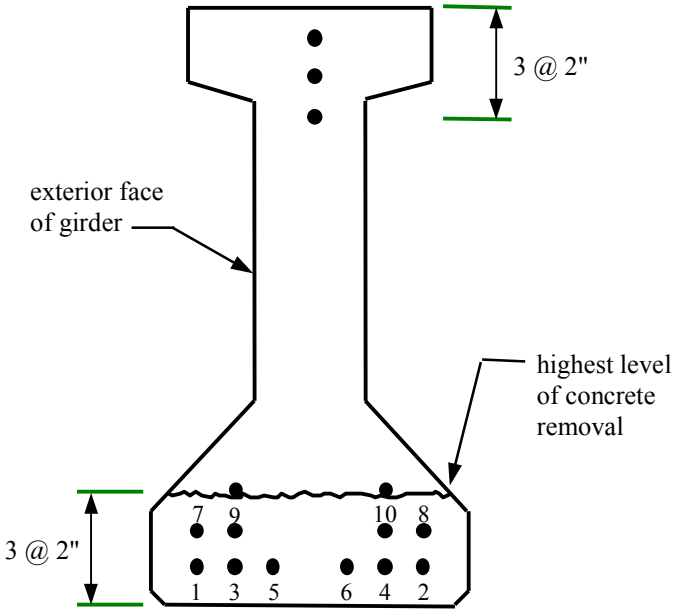


**a.) Strand Numbering System**

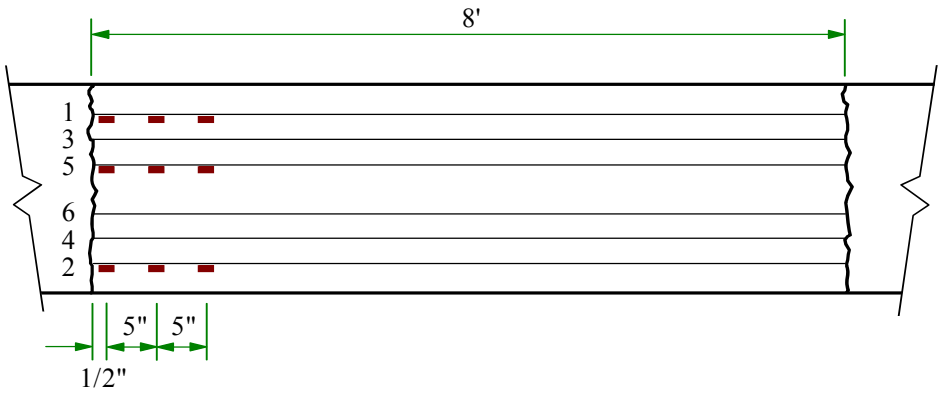


**b.) Location of First Row of Steel Strand Strain Gages**

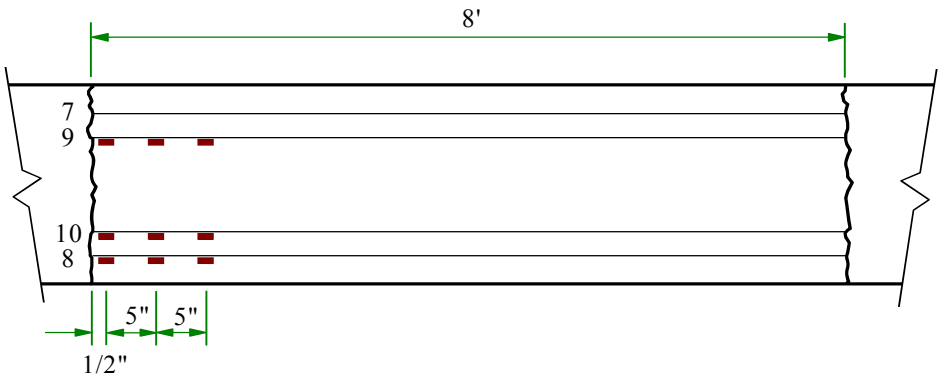


**c.) Location of Second Row of Steel Strand Strain Gages**

**Figure 4.8. Layout of Prestressing Strand Strain Gages.**

The strain gages were not placed on the seven-wire strand until it was desired to sever the strands, which took place after all concrete had been removed. Due to accessibility problems, the gages were placed at two different times. The first set of gages was applied to the bottom row of strands only. As shown in Figure 4.8, a total of nine gages, with three gages on each strand, were applied to Strands 1, 2, and 6. After the severing of Strands 1 through 6 was completed, three gages were applied to Strands 7, 9, and 10 in the next row, for a total of nine. In Figure 4.8a the strands are numbered in the order in which they were severed; the longitudinal location of the strain gages is presented in Figure 4.8b and Figure 4.8c for rows 1 and 2, respectively.

Displacement transducers were placed at the same locations as the first nine load points on the bridge deck; that is, at the 1/4 point, midspan, and 3/4 point of each beam (see Figure 4.4). If the beam ends are included, (where vertical displacement is zero) this configuration provides five known coordinates on the deflection curves for each beam.

Prior to any damage being inflicted on a P/C beam, the bridge was tested in the undamaged state. The maximum 60 kip load was applied in 5 kip increments to the 12 load positions previously described. At each load interval, including the initial zero reading, all instrumentation was read and recorded using the DAS. After testing the bridge in the undamaged state, damage was inflicted on Beam 3 of the bridge model, and the bridge was re-tested.

The intent of damaging the bridge was to simulate actual field damage conditions on the laboratory bridge model. Typically, the exterior girders sustain the most damage in bridge impacts, unless a significant grade is present on the roadway below. It is possible for the interior girders to sustain damage when the impact from the first collision causes a vehicle to rebound and strike additional girders as it travels along the highway. In some cases, the rebounding action causes the vehicle to strike the interior girders with more force than in the original impact. However, this condition was not feasible to model in the laboratory bridge because it had only three beams. Therefore exterior Beam 3 was selected as the beam to damage. With only three beams in the bridge, it was decided to damage only one beam. Damage to one beam simplified comparisons between the various levels of damage. A more complex situation exists when multiple beams are damaged, thus increasing the number of variables in the analysis.

The location of inflicted damage to the beam was decided by simulating field conditions. In reality, a bridge of this type may have a 2-lane highway traveling beneath it. An overheight vehicle traveling under the bridge in one lane would collide with the structure at approximately the 3/8 point. It should be noted that there are numerous variables in the field (lane widths, barriers, bridge length, etc.) which would influence where a given girder might be impacted.

It was important that the damage be applied in small increments so that each level of damage could be evaluated as to its effect on the behavior of the bridge. With large increments of damage, one could not determine when critical damage occurs.

The initial levels of damage consisted of removing a portion of the bottom flange concrete. Various depths and lengths of the P/C beam were removed using a demolition (or chipping) hammer. Concrete was removed until a section 8 ft in length and 6 in. in height was removed from Beam 3. Photographs of four of the damage levels up to this point are presented in Figure 4.9. At this point, it was determined that further concrete damage would be highly unlikely in an actual bridge without some damage occurring to the prestressed strands. Therefore, subsequent damage levels consisted of severing strands.

Strands were severed in Beam 3 with a cutting torch, heating the strands slowly to minimize any "whipping action" that may occur; reducing movement of the strands was done primarily for safety reasons. As previously noted, the prestressing strands were instrumented with strain gages; the sudden release of energy caused by severing these strands causes a large amount of vibration. If precautions were not taken, vibrations could have destroyed the solder connections between the strain gages and lead wires.

Two steps were taken to minimize the vibration. The gages were placed as close as possible to the existing concrete, where the restraining action of the surrounding concrete would reduce vibrations. Secondly, the gradual heating of the strands allows the release of energy to occur at a slower rate, which also reduced the vibration. A photograph of one of the severed strands is shown in Figure 4.10; one can see the "necking down" that occurs in a steel specimen under tensile loads when it is heated gradually. The exposed strands were cut at the end opposite the strain gages to minimize the effects that heat from the cutting torch might have on the strain readings.

While cutting the strands, the tension force is released and thus compressive strains occur in the strands. Initial and final strain readings were recorded during the severing of the strands, which were used to calculate the prestress force in the tendon.

A total of thirteen levels of damage were inflicted on Beam 3. They ranged from a small amount of concrete removal to the severing of ten of the original fifteen prestressing strands. A profile view of the P/C beam for Damage Levels 1 through 7 (concrete removal damage, centered around the 3/8 point of the beam) illustrating the variable dimensions of the damaged region is presented in Figure 4.11. The dimensions shown in Figure 4.11 are listed in Table 4.1 for the given levels of damage. In Figure 4.11, the prestressing strands are not shown for clarity. Cross sections of the P/C beam for Damage Levels 8 through 13 (strand removal damage) are presented in Figure 4.12.

**a.) Damage Level 1.**

**b.) Damage Level 2.**

**Figure 4.9. Damage Levels Consisting of Concrete Removal Only.**

**c.) Damage Level 5.**

**d.) Damage Level 7.**

**Figure 4.9. continued.**

**Figure 4.10. Severed Prestressing Strand Exhibiting Necking Down Behavior.**

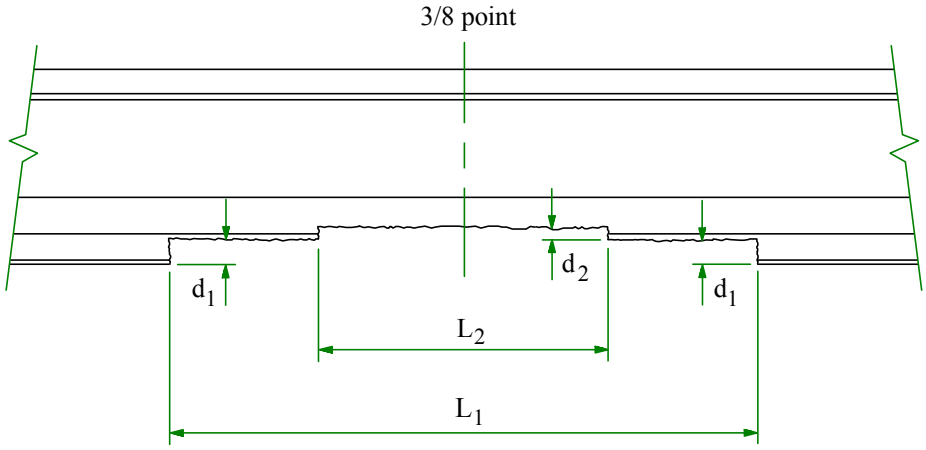


**Figure 4.11. Profile View of the Damaged Region of Beam 3.**

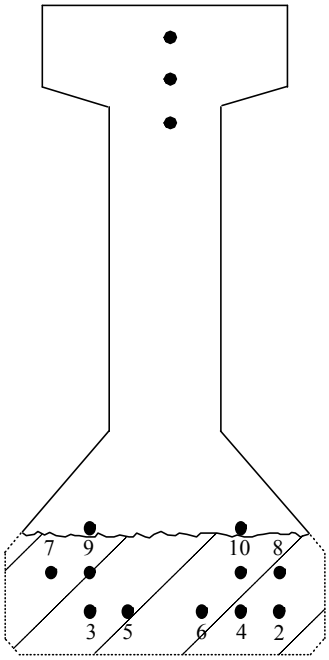


**a.) Damage Level 8**

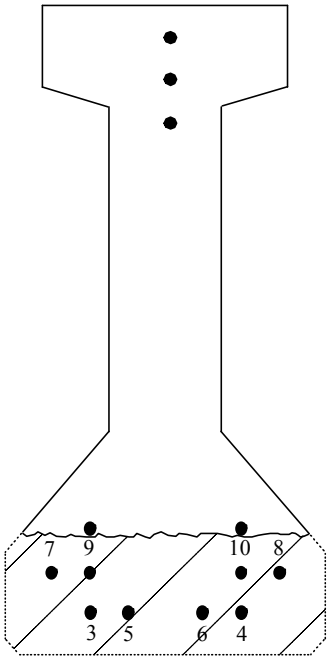


**b.) Damage Level 9**

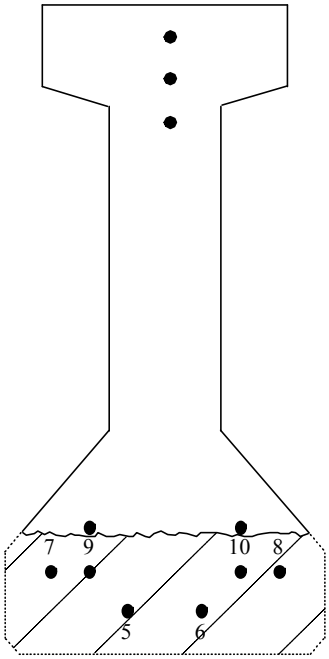


**c.) Damage Level 10**

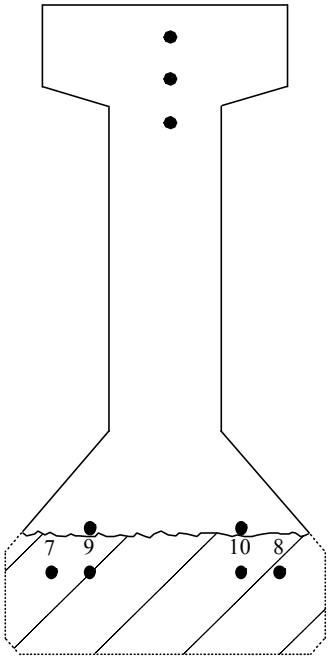


**d.) Damage Level 11**

**Figure 4.12. Strand Removal in Prestressed Concrete Beam 3.**

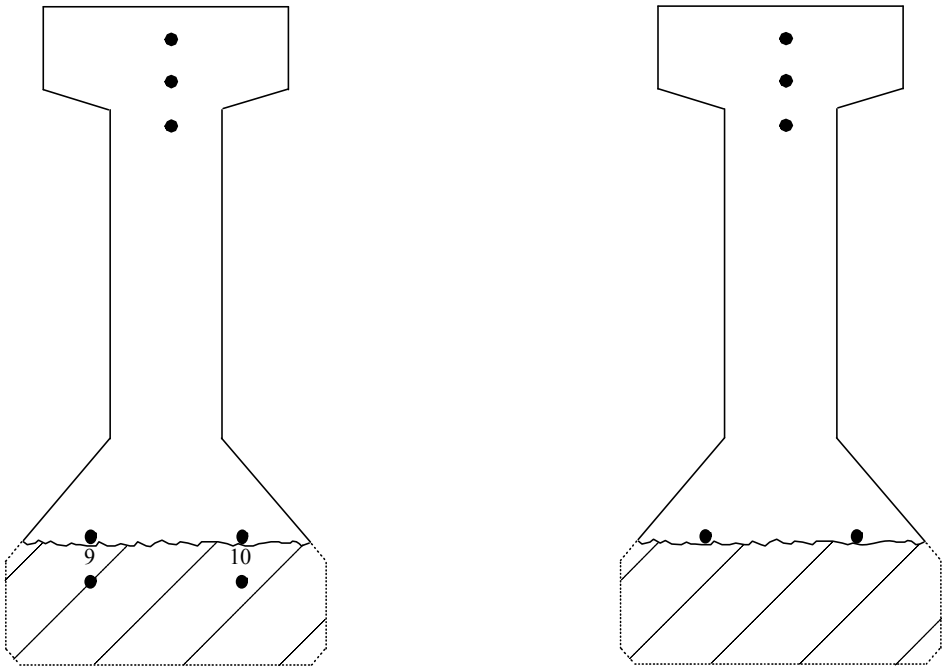


**e.) Damage Level 12** **f.) Damage Level 13**

**Figure 4.12. Continued.**

**Table 4.1. Dimensions of the Damaged Region in Beam 3.**

| Damage Level | Length of Concrete Removed, $L_1$ (ft) | Depth of Concrete Removed, $d_1$ (in.) | Length of Concrete Removed, $L_2$ (ft) | Depth of Concrete Removed, $d_2$ (in.) |
|---|---|---|---|---|
| 1 | 2 | 2 | 0 | 0 |
| 2 | 4 | 2 | 0 | 0 |
| 3 | 4 | 4 | 0 | 0 |
| 4 | 8 | 2 | 4 | 4 |
| 5 | 8 | 4 | 0 | 0 |
| 6 | 8 | 4 | 4 | 6 |
| 7 | 8 | 6 | 0 | 0 |

The concrete removal was terminated at a length of 8 ft-6 in. After reviewing the test data, there was not a significant increase in the deflections for Beam 3 with damaged inflicted on the concrete only (Damage Levels 1 through 7). The conclusion was made that a significant amount of concrete would have to be removed before any noticeable change occurred in the strength and/or stiffness of the bridge. In the authors' opinion, it would be extremely difficult, if not impossible, to accurately model the extensive

cracking that typically occurs in severely damaged P/C members. Therefore, further damage levels concentrated on only severing strands. It should be noted that the damage inflicted on the bridge model is not typical of damage found in actual field conditions. As the damage intensifies, extensive cracking of the concrete propagates away from the damaged location, thus affecting a larger portion of the beam. With available equipment, it was not possible to inflict this type of damage. The scope of the investigation then focused on the strength reduction resulting from severing the strands.

Severing ten of the fifteen prestressing strands without the extensive damage described above occurring to the concrete is highly unlikely. In addition, it is also difficult to imagine a situation where a bridge with a damaged girder losing over 50% of its prestressing force would have to carry heavy truck loads. However, this condition could be applied to the laboratory bridge model for research purposes. The removal of this number of strands and the corresponding loss of prestress provided some insight into the behavior of the bridge model at severe levels of damage, even though such a condition would not normally exist in the field.

## *4.3. Experimental Results and Analysis*

In this section, the results of the various experimental tests and relevant analysis are presented. Tests were conducted on the bridge model in the undamaged condition and with the model subjected to thirteen different levels of damage. For each level of damage, including the undamaged state, load was applied to the twelve different load points previously described. Reference will be made to the various load points throughout this chapter; the reader is referred to Figure 4.4 for the location of these points. A total of 180 tests were completed on the bridge model in the damaged and undamaged condition. Unless otherwise noted, all results correspond to the maximum applied load of 60 kips. In the interest of brevity only selected portions of the data results are presented and discussed. More comprehensive data results are provided in Paradis (1999).

### *4.3.1. Undamaged Bridge Tests*

#### *4.3.1.1. Strains in the P/C Beams*

During the testing in the undamaged state, several factors were investigated to obtain baseline behavior data on the bridge. These included the investigation of maximum magnitudes of strains for various load points, variation in strains between the east and west faces of a given beam at a particular location (Figure 4.5), symmetry of the strain readings about the longitudinal and transverse axes of the bridge, and repeatability of the readings from the two tests in the undamaged state.

Shown in Figure 4.13 are typical load-strain relationships for the three beams. The bottom longitudinal beam strains are shown at the 1/4 point, midspan, and 3/4 point of each beam (on the west face) when the load is applied at the midspan of each beam. Midspan loading corresponds to the maximum moment condition in the beams. Readings were taken at various load increments up to the maximum applied load of 60 kips. The highest magnitude of strain recorded during the undamaged tests was 193 micro- in./in. ($\mu\varepsilon$), which occurred at the midspan of Beam 1 on the east face of the bottom flange.

Similar results were found for strain data on the west face of the beam. Therefore, all subsequent analyses in the report used average strain values on the east and west beam faces.

#### *4.3.1.2. Deflections in the P/C Beams*

The initial deflection data from the undamaged bridge model were investigated similarly to the strain gage data by considering maximum deflection magnitudes, symmetrical behavior, and repeatability of results. Although the number of strain gages used was significantly higher than the number of deflection transducers employed on the P/C beams, the deflection data provided additional insight as to the overall behavior of the bridge. The results of each set of data (strains and deflections) were in general agreement.

Shown in Figure 4.14, is the load-deflection data for Beam 1 with the load placed at the 1/4 point, midspan, and 3/4 point. As can be seen in this figure, loading at midspan produces the greatest deflections. This is consistent with the strain behavior at midspan (which is the maximum moment location) described earlier. The load-deflection data for Beam 3 were not included, but displays similar behavior. The deflections of Beam 2, are somewhat smaller due to different boundary conditions; specifically, the longitudinal edge restraint from the slab that is present on both sides of Beam 2 (as opposed to only one side of Beams 1 and 3). The largest deflection recorded in the undamaged tests was 0.155 in., which occurred at the midspan of Beam 1 with the load at the midspan of Beam 1.

The deflection data obtained during the undamaged tests shows the same symmetrical behavior of the bridge that was obtained with the strain data. Shown in Figure 4.15 are longitudinal deflection curves for all three beams when the load is placed at midspan of the individual beams. A symmetrical loading condition exists with the load at midspan; the 1/4 point and 3/4 point deflections exhibit this symmetry. The deflection values at these points are nearly identical for all three beams at all magnitudes of load. There are small differences in the 1/4 point and 3/4 point deflections, but the difference is small and can be attributed to minor variances in construction details at the supports. The variances in construction details changes the degree of restraint at each support, which causes the 1/4 point and 3/4 point deflections to differ slightly. As one would expect, exterior Beams 1 and 3 deflect than interior Beam 2.

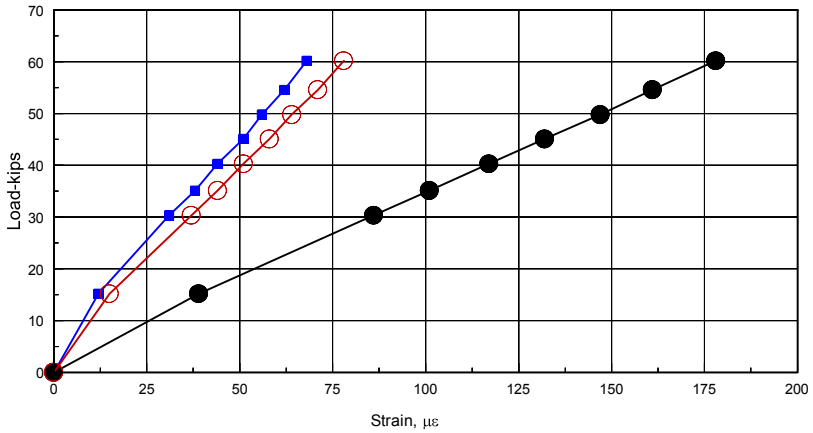


**a.) Load on Beam 1**

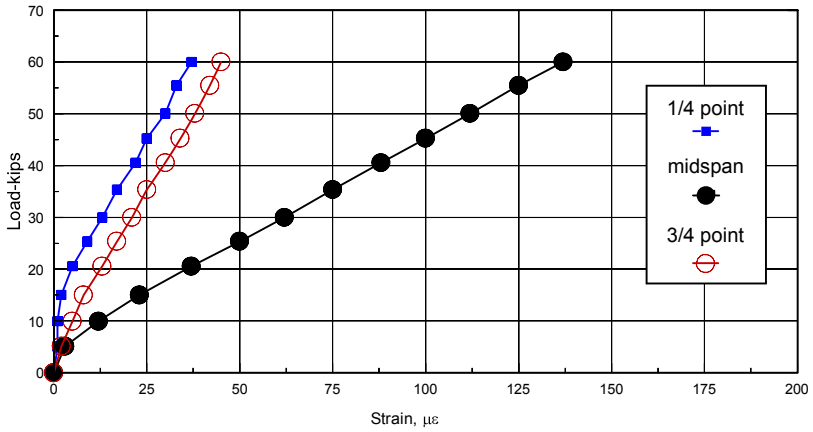


**b.) Load on Beam 2**

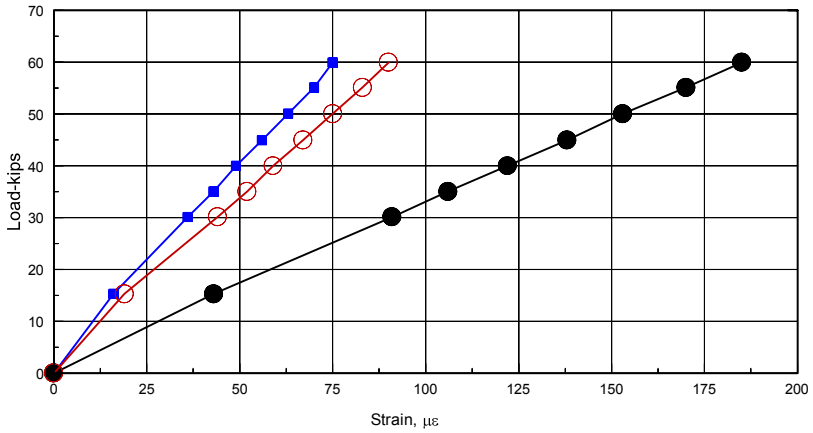


**c.) Load on Beam 3**

**Figure 4.13. Beam Strains: Load at the 1/4 Point, Midspan and 3/4 Point of Each Individual Beam, Undamaged Condition.**

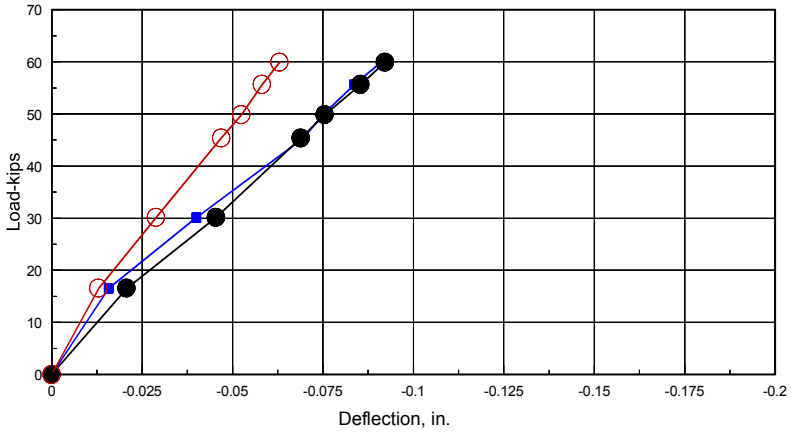


**a.) Load at 1/4 Point**

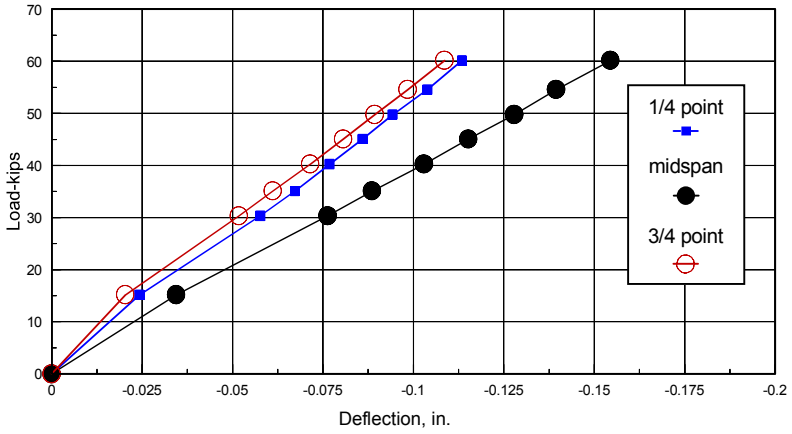


**b.) Load at Midspan**

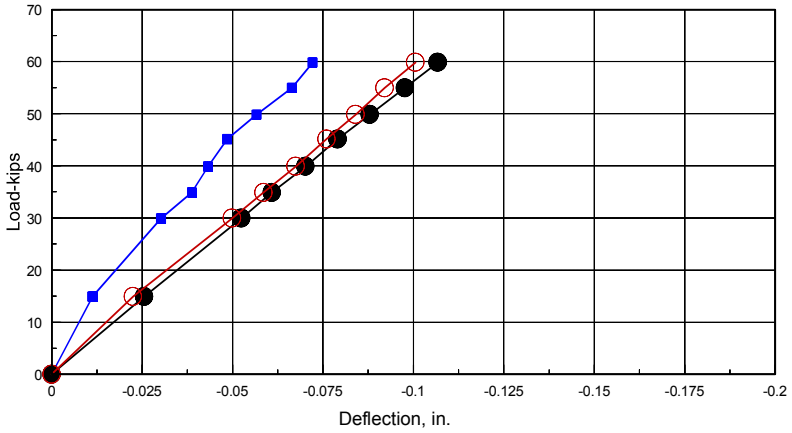


**c.) Load at 3/4 Point**

**Figure 4.14. Beam 1 Deflections at the 1/4 Point, Midspan and 3/4 Point, Undamaged Condition.**

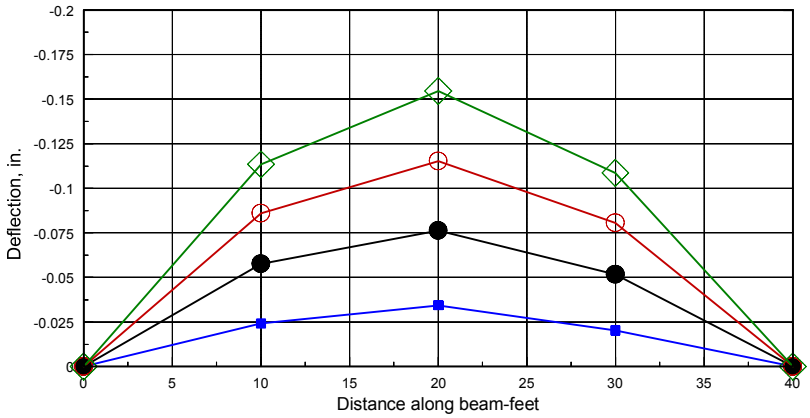


**a.) Load on Beam 1**

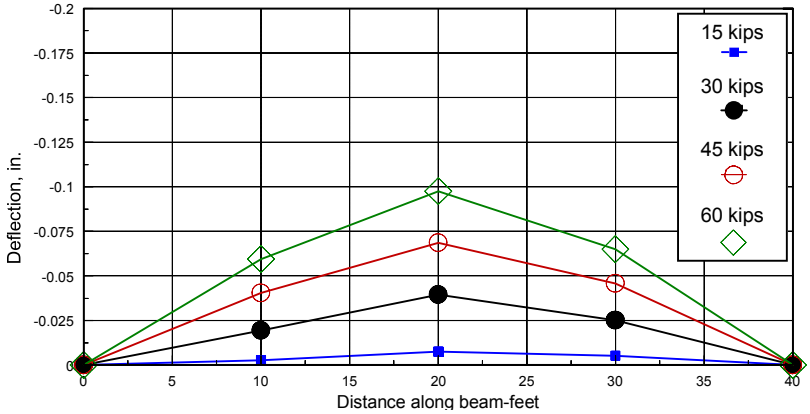


**b.) Load on Beam 2**

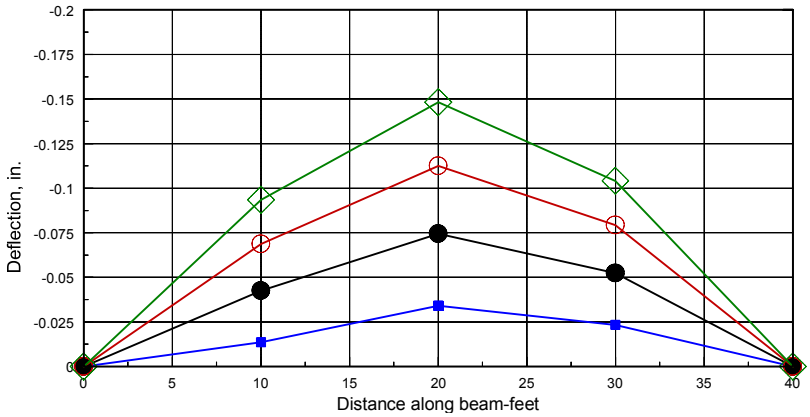


**c.) Load on Beam 3**

**Figure 4.15. Beam Deflections: Load at Midspan of Each Individual Beam, Undamaged Condition.**

#### *4.3.1.3. R/C Diaphragms*

Only strains were recorded for the R/C diaphragms, as all deflection transducers were mounted directly to the P/C beams. The diaphragm strains never reached significant levels. During service load testing of the bridge in the undamaged state, the highest strain recorded in the diaphragms was 9 με. This was recorded with the 60 kip load at position 6. The low level of strain in the diaphragms is in agreement with the results of Iowa Dot Project HR-319 (Abendroth et al., 1991), which found similar behavior.

These relatively low strain readings made it difficult to accurately compare with subsequent strain data as the damage levels increased. Errors recorded in strain gage measurements are of greater concern with small levels of strains. The errors can be due to a variety of environmental factors, generally classified as electrical "noise" or experimental error. The smaller magnitude readings can have a higher percentage of electrical noise, thus making the readings unreliable. Obviously, the percent error is significantly reduced when larger magnitudes of strains are measured. For these reasons, the R/C diaphragm strains were not used in the comparisons.

#### *4.3.1.4. R/C Bridge Deck*

The longitudinal strains (Gages S1 through 4, S5, S7, S10, and S12 in Figure 4.6) in the concrete bridge deck were similar in magnitude to the strains measured in the P/C beams. However, the values were smaller because the strain gages were not located directly above the beams, but between them (see Figure 4.6). Shown in Figure 4.16 is a typical load-strain plot for the bridge deck. The figure shows the strains at four gage locations when load is placed at the midspan of the three beams. The highest magnitude of strain recorded in the concrete slab during the undamaged testing was 118 με. This strain occurred at the location of Gage S12, which is between the free edge of the bridge deck and Beam 1. Comparing the strains in Figure 4.16a and Figure 4.16c shows that symmetry does not exist to the degree exhibited earlier by the P/C beam strains and deflections, however the two sets of strains do follow the same general pattern.

### *4.3.2. Damage Level Comparison*

At the conclusion of the undamaged baseline tests, damage was inflicted to Beam 3 of the bridge model. Inflicted damage first consisted of concrete removal from the bottom flange of the beam centered at the 3/8 point of the bridge model. Damage then focused on severing of the prestressing steel strands. Additional strain gages were applied to the strands prior to severing them. The bridge model was tested twice in the undamaged condition at every load position (twelve). As previously noted, after each level of damage was inflicted, the bridge was tested again with the load being applied at all load positions.

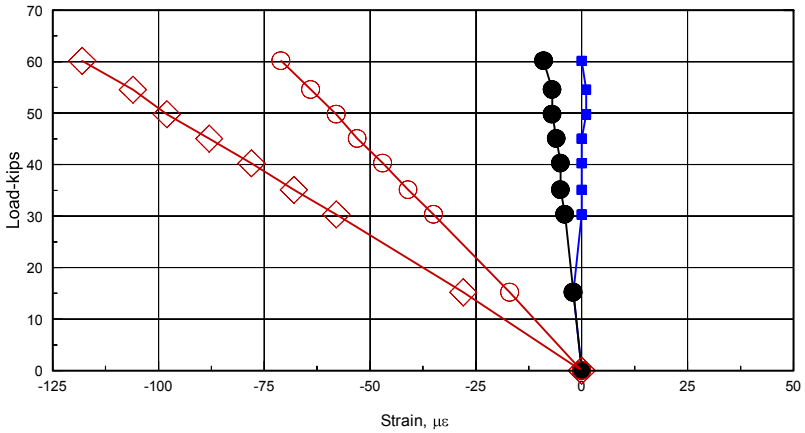


**a.) Load on Beam 1**

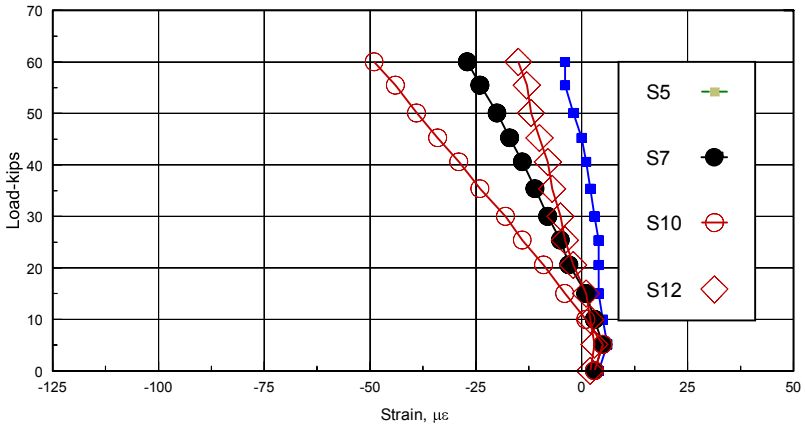


**b.) Load on Beam 2**

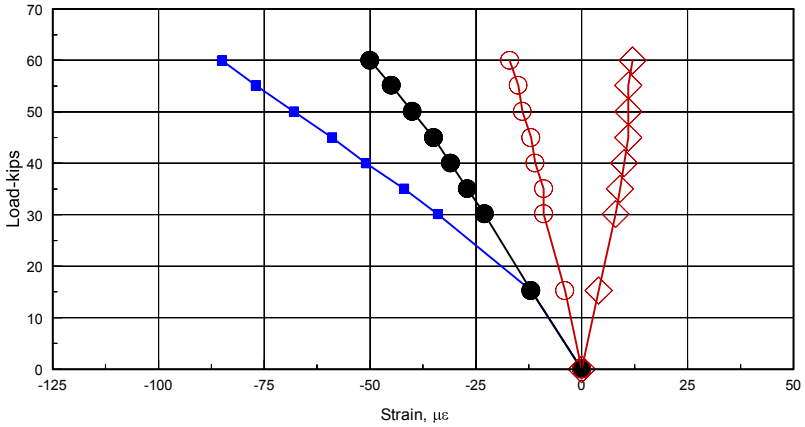


**c.) Load on Beam 3**

**Figure 4.16. Bridge Deck Longitudinal Strains: Load at Midspan of Each Beam, Undamaged Condition.**

#### *4.3.2.1. Influence of Damage on P/C Beam Strains*

P/C beam strains could not be compared for Beam 3, due to the inflicted damage affecting the measured strain results in localized regions of damage. Despite this limitation, P/C beam strains could be compared for Beams 1 and 2. These beams remained uncracked throughout the duration of testing, therefore the measured strains were assumed to be valid. In the following figures, only bottom beam strains in Beams 1 and 2 are presented. Bottom beam strains are presented because they are larger than the strains at the top of the beams.

Shown in Figure 4.17, are the maximum bottom beam strains for Beams 1 and 2 at each damage level when the load is at Position 5 (midspan of Beam 2). This figure shows that the strains are relatively unchanged as the damage to Beam 3 increases. Similar behavior is observed for all other load positions where load is applied away from the damaged beam. However, when the load is moved to Positions 3 and 6 (shown in Figure 4.18 and Figure 4.19, respectively) an increase in measured strain is noted. As is evident for Position 3 (Figure 4.18), the first noticeable increase in strain occurs in Beam 2 at Damage Level 11. Likewise for Position 6 (Figure 4.19), the first noticeable increase in strain occurs in Beam 2 at Damage Level 10. The strains for Position 9 are not included, but are similar to Position 3 results. The magnitude of measured strains are higher with the load at Position 6 than with the load at Position 3.

The higher strains with the load at Position 6 agree with expected behavior, as the moment in Beam 3 is greatest when it is loaded at midspan. It is interesting to note that Beam 1 strains remain unchanged at even the highest levels of damage. This suggests that beams located a distance away from areas of concentrated damage are not significantly affected by the reduction in strength and stiffness of a damaged beam. This strain behavior is observed for all load positions.

Shown in Table 4.2 are midspan strains that were presented in Figure 4.18b and Figure 4.19b and the percent increase in the midspan strains from the undamaged state at each level of damage. Note that increases in Beam 2 strains don't occur until extreme levels of damage occur. It is interesting to observe that at Damage Level 7, which consisted of the maximum concrete loss with no severed strands, the percent increase in strain is negligible. The percent increase that is present at Damage Level 7 (5.0% and 3.8% for Positions 3 and 6, respectively), can be attributed to noise in the strain gage circuits just as easily as it can be attributed to an actual increase in strain. Not until a significant amount of prestress force is removed at Damage Level 10 (4 of 12 strands or 33% severed), do the midspan strains in Beam 2 start to increase. The maximum percent increase, occurring at Damage Level 13 (10 of 12 strands or 83% severed), is 120.0% and 203.8% for Positions 3 and 6, respectively.

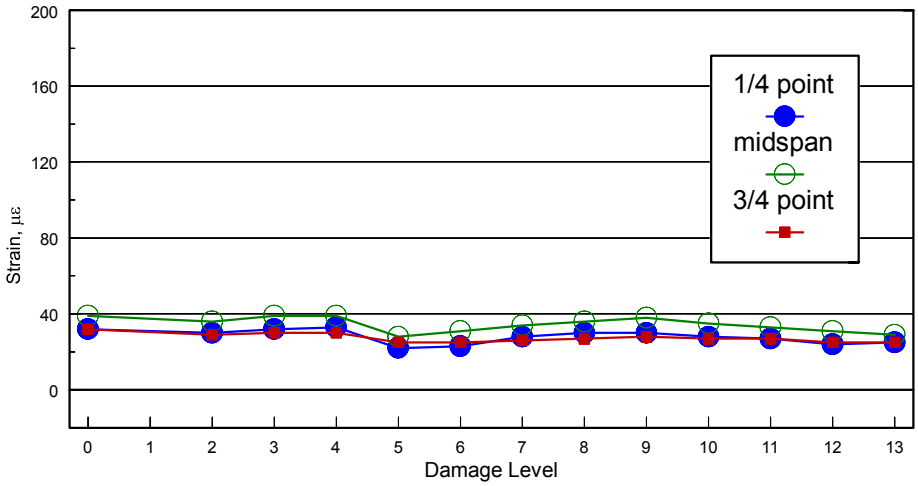


**a.) Beam 1**

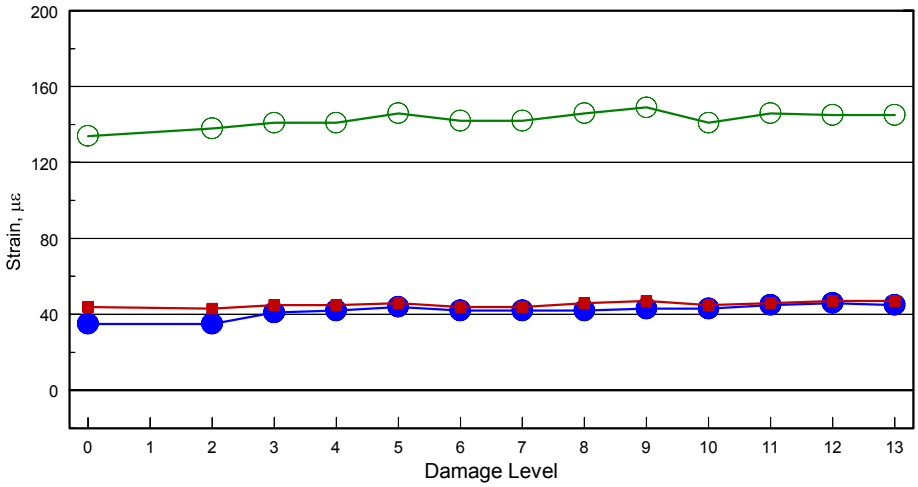


**b.) Beam 2**

**Figure 4.17. Maximum Bottom Beam Strains: Load at Position 5.**

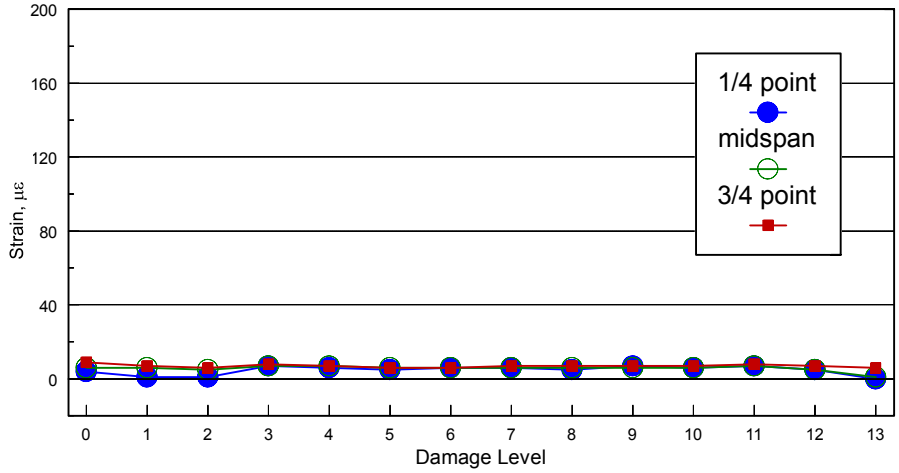


**a.) Beam 1**

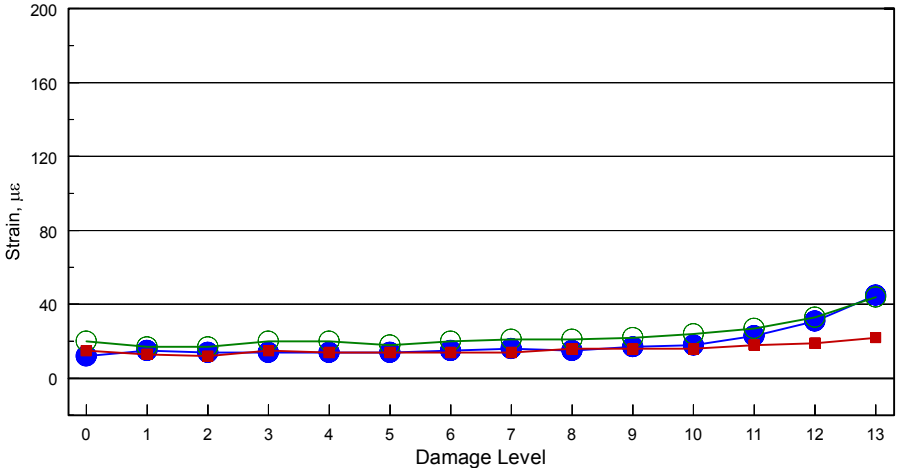


**b.) Beam 2**

**Figure 4.18. Maximum Bottom Beam Strains: Load at Position 3.**

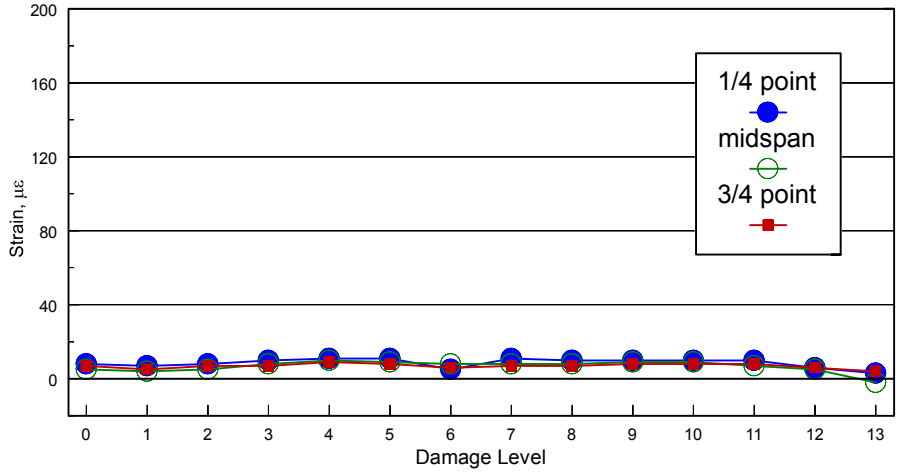


**a.) Beam 1**

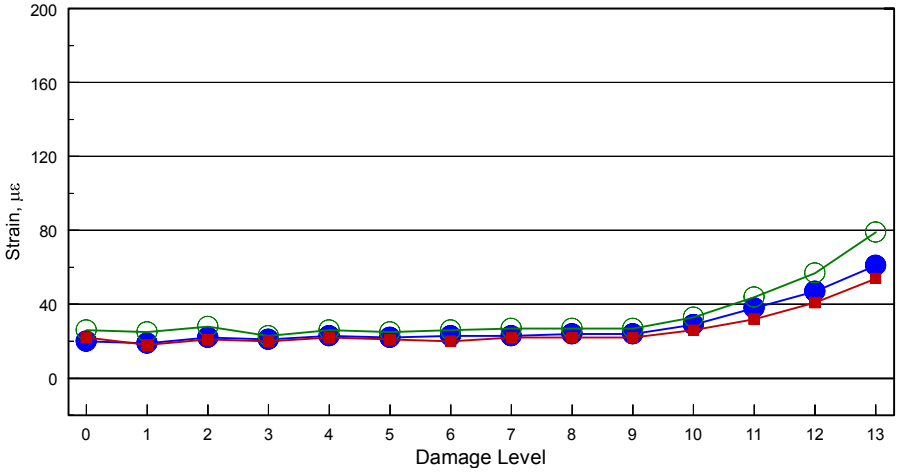


**b.) Beam 2**

**Figure 4.19. Maximum Bottom Beam Strains: Load at Position 6.**

**Table 4.2. Influence of Damage on Midspan Bottom Beam Strains in Beam 2.**

| Damage Level | Load at Position 3 (1/4 Point Beam 3) | | Load at Position 6 (Midspan Beam 3) | |
|---|---|---|---|---|
| | Measured Strain (με) | % Increase | Measured Strain (με) | % Increase |
| Undamaged | 20 | - | 26 | - |
| 1 | 17 | -15.0 | 25 | -3.8 |
| 2 | 17 | -15.0 | 28 | 7.7 |
| 3 | 20 | 0.0 | 23 | -11.5 |
| 4 | 20 | 0.0 | 26 | 0.0 |
| 5 | 18 | -10.0 | 25 | -3.8 |
| 6 | 20 | 0.0 | 26 | 0.0 |
| 7 | 21 | 5.0 | 27 | 3.8 |
| 8 | 21 | 5.0 | 27 | 3.8 |
| 9 | 22 | 0.0 | 27 | 3.8 |
| 10 | 24 | 0.0 | 33 | 26.9 |
| 11 | 27 | 35.0 | 44 | 69.2 |
| 12 | 33 | 65.0 | 57 | 119.2 |
| 13 | 44 | 120.0 | 79 | 203.8 |

Based on the strain results, it appears that minor damage does not have an effect on the distribution of strains (and therefore loads) in beams away from the damaged area. As previously noted, strains were not obtained in the damaged beam, however strains in other beams in the bridge did not increase until major damage was inflicted on Beam 3. When undamaged beams are loaded, there is no noticeable change in the strains in Beams 1 and 2. No P/C beam strain data are available to determine the behavior of the damaged beam when undamaged beams are loaded.

### *4.3.2.2. Influence of Damage on P/C Beam Deflections*

P/C beam deflections exhibited behavior similar to the measured strains. The nine deflection locations monitored during the tests provided additional insight into the global behavior of the bridge. Unlike the strains on the damaged P/C beam, which were unreliable after damage was inflicted, the measured deflections were valid after damaging the beam. The deflection data were valid for all damage levels and load positions.

As the levels of damage increased, longitudinal beam deflections varied depending on their position in the bridge model. The load-deflection curves for Beams 1, 2, and 3 are shown in Figures 4.20

through 4.22, respectively. Each figure shows the longitudinal beam deflections with the load placed at the 1/4 point, midspan, and 3/4 point of the given beam. As may be seen in Figures 4.20 and 4.21, there is relatively little change in the beam deflections for any level of damage for the three load positions.

The deflections in Beam 1 between the undamaged condition and Damage Level 13 actually decreased a very small amount, indicating that uplift was occurring. However, this deflection behavior was not consistent between all damage levels (increases in deflection were occasionally recorded). Additionally, the measured changes in deflection were so small that definite behavior could not be determined. The measured Beam 2 deflections increased as the levels of damage increased, but as with Beam 1, changes were so small that they were insignificant.

In contrast to the behavior of Beams 1 and 2, Beam 3 displayed significant increases in deflections as the amount of damage increased. At Damage Level 13, deflections of the beam were approximately double the values measured in the undamaged condition with the load at midspan (see Figure 4.22b). However, Damage Level 13 corresponds to the highest level of damage, which is not typical of damage found in the field (as described in Section 4.4.1). It is interesting to compare the deflections at lower levels of damage. Table 4.3 shows the midspan deflections of Beam 3 when the load is placed at the 1/4 point, midspan, and 3/4 point of that beam (i.e. data shown in Figure 4.22) and the percent increase in deflections at each level of damage.

Due to the deflection magnitudes being very small, a slight change in deflection produces a large change in the percent increase (or decrease) in deflection. This explains the large fluctuations in the values shown in Table 4.3. It should be noted that large increases in deflections (greater than 40%) do not occur until the level of damage has reached critical levels (after severing of several of the strands). Damage levels consisting of concrete removal only (up to and including Damage Level 7), show a maximum of 30% increase in deflections.

Deflection data were also investigated for Beam 2 with the load placed on Beam 3, and for Beam 3 with the load placed on Beam 2. These results indicated that deflections increased somewhat for each case, but the values were inconsistent and too small to make any conclusions about bridge behavior.

In summary, for loading away from the damaged region, Beam 1 appeared to be unaffected by the inflicted damage while Beam 2 showed some changes, but were not significant. However, Beam 3 deflections at Damage Level 13 increased by 113.6% when it was loaded at midspan. Noticeable increases in Beam 3 deflections did not occur until Damage Level 7 or higher. For loads applied to the damaged beam, Beam 1 remained unaffected throughout the damage level tests. Beam 2 deflections did increase however, with certain deflections nearly doubling at Damage Level 13.

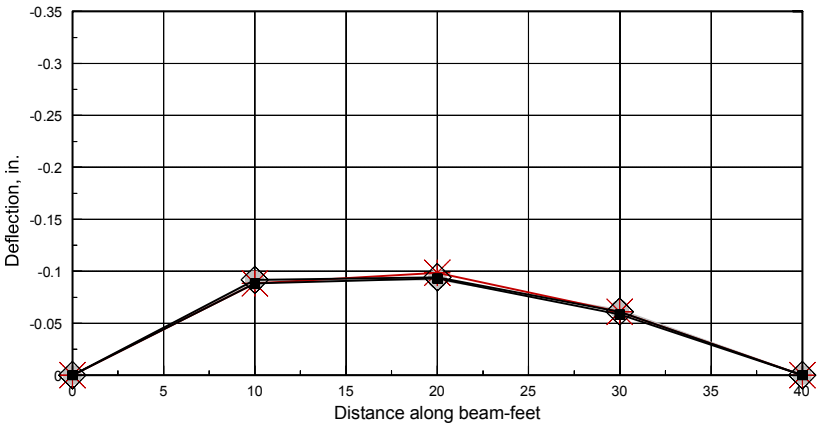


**a.) Load at 1/4 Point**

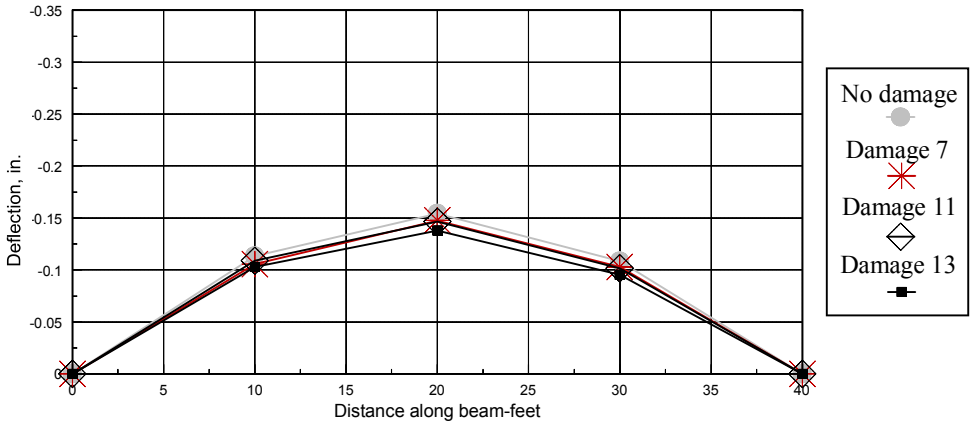


**b.) Load at Midspan**

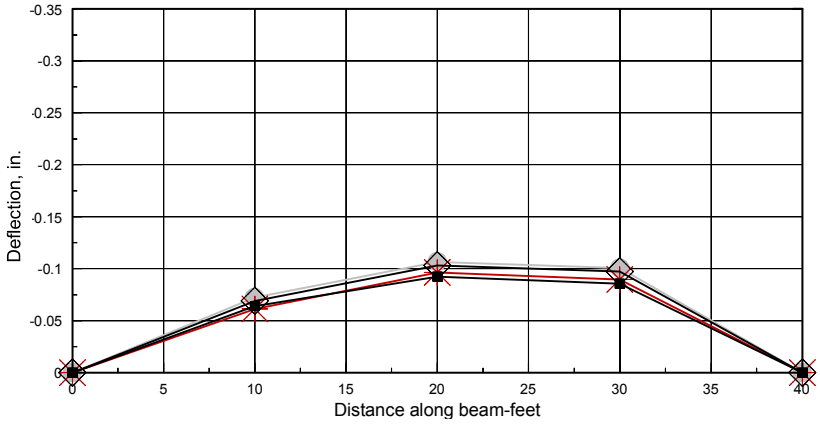


**c.) Load at 3/4 Point**

**Figure 4.20. Influence of Damage on Longitudinal Beam 1 Deflections: Load on Beam 1.**

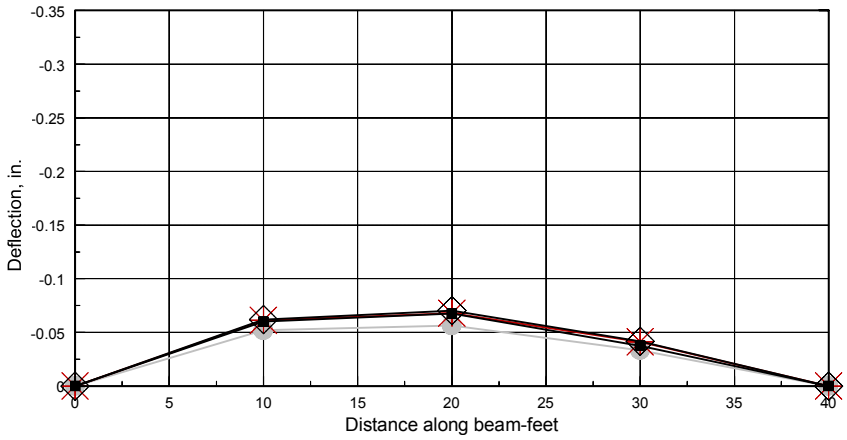


**a.) Load at 1/4 Point**

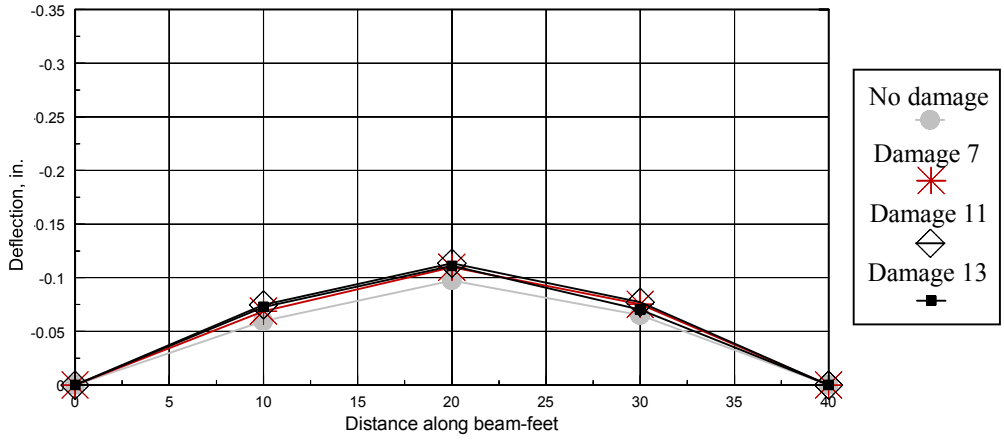


**b.) Load at Midspan**

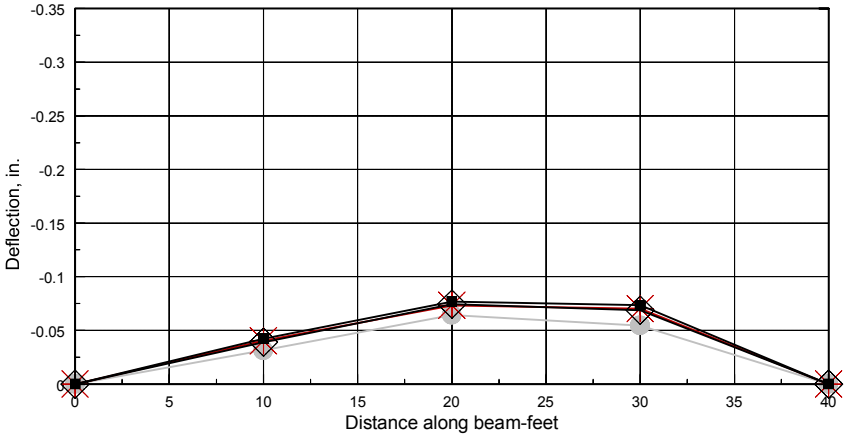


**c.) Load at 3/4 Point**

**Figure 4.21. Influence of Damage on Longitudinal Beam 2 Deflections: Load on Beam 2.**

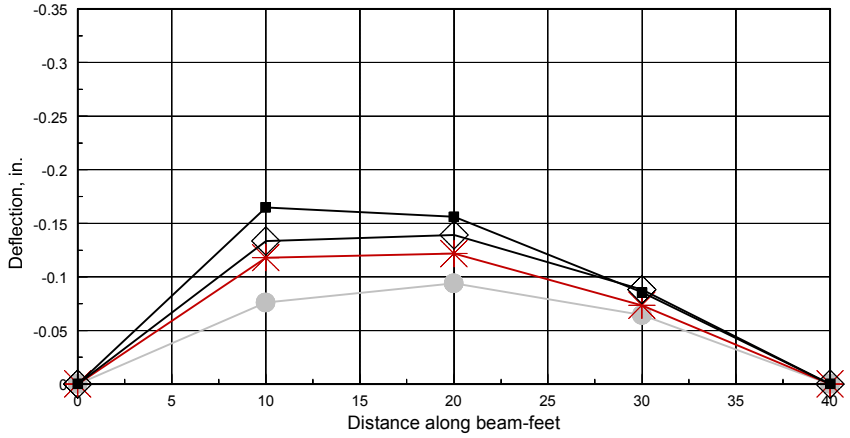


**a.) Load at 1/4 Point**

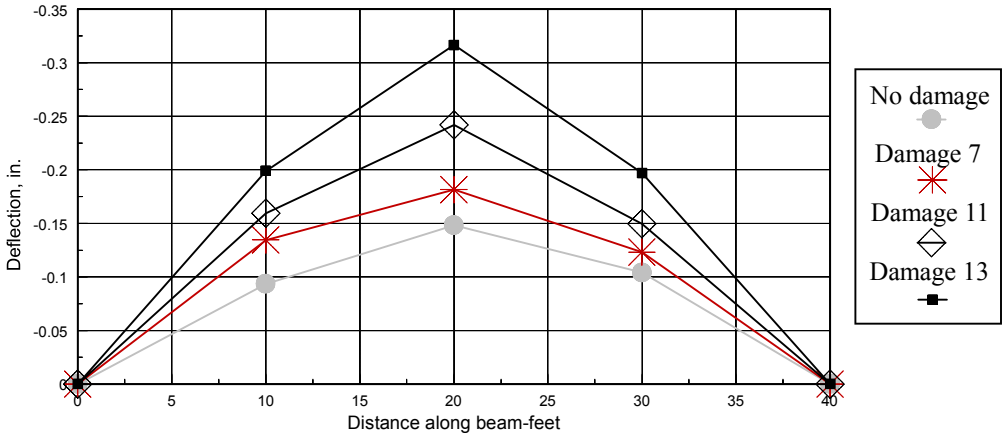


**b.) Load at Midspan**

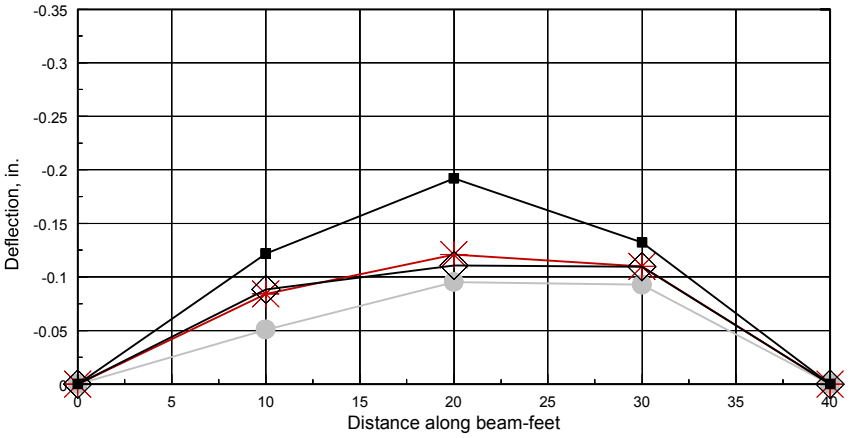


**c.) Load at 3/4 Point**

**Figure 4.22. Influence of Damage on Longitudinal Beam 3 Deflections: Load on Beam 3.**

**Table 4.3. Influence of Damage on Beam 3 Midspan Deflections.**

| Damage Level | Load at Position 3 (1/4 Point Beam 3) | | Load at Position 6 (1/4 Point Beam 3) | | Load at Position 9 (1/4 Point Beam 3) | |
|---|---|---|---|---|---|---|
| | Measured Defl. (in.) | % Increase | Measured Defl. (in.) | % Increase | Measured Defl. (in.) | % Increase |
| Undamaged | -0.094 | - | -0.148 | - | -0.095 | - |
| 1 | -0.083 | -11.9 | -0.135 | -8.7 | - | - |
| 2 | -0.091 | -.32 | -0.138 | -6.9 | -0.104 | 9.1 |
| 3 | -0.101 | 7.2 | -0.156 | 5.1 | -0.103 | 8.2 |
| 4 | -0.114 | 21.4 | -0.170 | 14.3 | -0.111 | 16.4 |
| 5 | -0.119 | 26.4 | -0.169 | 14.0 | -0.110 | 14.9 |
| 6 | -0.117 | 24.3 | -0.176 | 18.4 | - | - |
| 7 | -0.122 | 29.5 | -0.182 | 22.4 | -0.121 | 26.9 |
| 8 | -0.129 | 37.6 | -0.170 | 14.9 | -0.126 | 32.2 |
| 9 | -0.133 | 41.9 | -0.186 | 25.1 | -0.118 | 23.6 |
| 10 | -0.128 | 36.3 | -0.208 | 40.1 | -0.121 | 27.3 |
| 11 | -0.139 | 48.0 | -0.242 | 63.1 | -0.111 | 16.2 |
| 12 | -0.142 | 51.1 | -0.305 | 106.0 | 0.000 | -100.0 |
| 13 | -0.156 | 66.0 | -0.317 | 113.6 | -0.192 | 101.8 |

#### *4.3.2.3. Influence of Damage on R/C Bridge Deck Strains*

The R/C bridge deck strains followed the same overall behavior as the P/C beams. As the distance from the gages to the region of damage decreased, there was an increase in the measured strains. The largest recorded increase was 98.0% at Damage Level 13 with the load at Position 6 (see Table 4.4). However, the lower levels of damage did not affect the measured strains. Significant increases in deck strains were not detected until Damage Level 10.

#### *4.3.2.4. Influence of Damage on Prestressing Strands*

Strains recorded in the prestressing strands indicated that Beam 3 did not experience any significant effects when load was applied away from the damaged region. When Beam 3 was loaded, significant increases in strain were first detected at Damage Level 10. The largest percent increase was 131.0% at Damage Level 12 (see Table 4.5). However, even at this critical level of damage, the total stress

in the strands was found to be approximately 164 ksi. This stress level is well below the yield strength of the Grade 270 ksi steel strands, indicating that yielding had not occurred.

It was possible to calculate accurate stress levels in the strands due to the fact that the modulus of elasticity of the prestressing strands was determined by experimental tensile tests on severed strand specimens. Knowing the modulus of elasticity, it was also possible to determine the effective prestressing force remaining in the strands as well as the prestress losses by measuring strains in the strands at the time of severing. These values were calculated as 143 ksi and 27%, respectively. For further information, see Paradis (1999).

#### *4.3.2.5. Influence of Damage on Transverse Load Distribution*

Transverse load distribution results generally verified the results obtained from the P/C beam strains, deflections, R/C deck strains, and prestressing strand strains (see Table 4.6 through Table 4.8). Moment fractions (or load distribution factors) are used as a means of measuring transverse or lateral load distribution. They are obtained from measured deflections, computed moments of inertia, and deflection constants. One of the more common approaches is to define the moment fraction as the moment in one beam divided by the sum of all beam moments at that particular bridge cross section:

$$MF_i = \frac{M_i}{\sum M} \tag{4.1}$$

where

$MF_i$ = moment fraction for beam i

$M_i$ = moment in beam i

$\sum M$ = sum of all beam moments at the cross section

However, because of the relative difference in stiffness amongst the three beams due to damage, the moments cannot be computed directly. For this presentation, the experimental deflections are used to determine moments in the beams. A relationship between deflection and moment can be given as:

$$\delta = q\frac{PL^3}{EI} \tag{4.2}$$

$$M = rPL \tag{4.3}$$

**Table 4.4. Influence of Damage on Reinforced Concrete Deck Strains with Load at Position 6.**

| Damage Level | Gage S5 | | Gage S7 | | Gage S10 | |
|---|---|---|---|---|---|---|
| | Measured Strain (με) | % Increase | Measured Strain (με) | % Increase | Measured Strain (με) | % Increase |
| Undamaged | -85 | - | -50 | - | -17 | - |
| 1 | -93 | 9.4 | -45 | -10.0 | -16 | -5.9 |
| 2 | -86 | 1.2 | -39 | -22.0 | -12 | -29.4 |
| 3 | -91 | 7.1 | -47 | -6.0 | -17 | 0.0 |
| 4 | -84 | -1.2 | -44 | -12.0 | -15 | -11.8 |
| 5 | -78 | -8.2 | -43 | -14.0 | -14 | -17.6 |
| 6 | -87 | 2.4 | -48 | -4.0 | -18 | 5.9 |
| 7 | -89 | 4.7 | -49 | -2.0 | -16 | -5.9 |
| 8 | -95 | 11.8 | -50 | 0.0 | -18 | 5.9 |
| 9 | -92 | 8.2 | -49 | -2.0 | -18 | 5.9 |
| 10 | -100 | 17.6 | -57 | 14.0 | -18 | 5.9 |
| 11 | -115 | 35.3 | -67 | 34.0 | -18 | 5.9 |
| 12 | -133 | 56.5 | -82 | 64.0 | -23 | 35.3 |
| 13 | -155 | 82.4 | -99 | 98.0 | -20 | 17.6 |

**Table 4.5. Influence of Damage on Average Strand Strains at Given Load Positions.**

| Damage Level | Load at Position 5 (Midspan Beam 2) | | Load at Position 3 (1/4 Point Beam 3) | | Load at Position 6 (Midspan Beam 3) | |
|---|---|---|---|---|---|---|
| | Average Strain (με) | % Increase | Average Strain (με) | % Increase | Average Strain (με) | % Increase |
| 7 | 65 | - | 236 | - | 284 | - |
| 8 | 70 | 7.7 | 266 | 12.7 | 313 | 10.2 |
| 9 | 70 | 7.7 | 263 | 11.4 | 305 | 7.4 |
| 10 | 70 | 7.7 | 273 | 15.7 | 398 | 40.1 |
| 12 | 97 | 49.2 | 362 | 53.4 | 656 | 131.0 |

Therefore $$\delta = \frac{q}{r}\frac{ML^2}{EI} = s\frac{ML^2}{EI} \tag{4.4}$$

and then $$M = \frac{EI\delta}{sL^2} \tag{4.5}$$

where:

$\delta$ = deflection

P = load

L = span length

E = Modulus of Elasticity

I = Moment of Inertia

q, r, s = constants for any given loading condition

The Modulus of Elasticity and the span length are constant for all beams. Therefore a moment fraction for a single beam can be computed based on a ratio of the computed moments of inertia, the measured deflections, and the appropriate deflection constant. For further discussion on moment fractions and the method used to compute the moments of inertia, see Paradis (1999).

$$MF_i = \frac{\frac{I_i\delta_i}{s_i}}{\sum\frac{I\delta}{s}} \tag{4.6}$$

where

$MF_i$ = moment fraction for Beam $i$

$I_i$ = moment of inertia for Beam $i$

$s_i$ = deflection constant for Beam $i$ loading

$\sum\frac{I\delta}{s}$ = sum of $\frac{I\delta}{s}$ terms for all beams

As previously noted, transverse load distribution results generally verified the results obtained from the P/C beam strains, deflections, R/C deck strains, and prestressing strand strains (see Table 4.6 through Table 4.8). For loads applied away from the damaged region, no changes in lateral load distribution were observed. However, significant changes in distribution for Beams 2 and 3 were observed when the load was placed on the damaged beam.

As the level of damage progresses, the moment fraction for Beam 2 increases while Beam 3 decreases. Beam 2 carries a larger percent of the load at higher levels of damage. Increases in moment fractions generally become significant when severing of the strands occurs. The largest percent increase in the moment fraction for Beam 2 was 118.8%, which occurred at Damage Level 13.

Combining the transverse load distribution results with the strand stress levels indicates that changes in load paths are occurring in the bridge model. As the levels of damage progress, the increase in moment fractions for Beam 2 indicates that this beam is carrying more of the applied load than it did in the undamaged state. Beam 3 loses strength as a result of damage, which produces the increase in moment in Beam 2. The mechanism for this load transfer can be attributed primarily to the R/C bridge deck and, to a lesser degree, the R/C diaphragms.

Observing the stress in the prestressing strands indicates that significant strength is left in the damaged beam when theoretical calculations show that failure of the remaining strands should have occurred from applied loads. From the changing transverse live load distribution, it is logical to conclude that a significant degree of redundancy exists in the bridge model. Even at the highest levels of damage (10 of 12 strands or 83% severed), the stress levels in the prestressing strands of the damaged beam indicate that they have not yielded due to the applied load. Beam 2 is carrying a significant percentage of the load originally resisted by Beam 3. At Damage Level 13, with the load at Position 6, Beam 2 carries approximately 22% of the moment originally carried by Beam 3 in the undamaged condition.

The results show that bridge behavior is not significantly affected by the loss of the 8 ft section of concrete. Additionally, the loss of a small amount of prestressing force does not produce overload conditions in the damaged beam because of transverse load distribution and redundancy in the bridge model. Therefore at lower levels of damage, the P/C beam is structurally adequate. However, additional issues such as aesthetics and serviceability are involved in the repair/replacement problem. Due to problems with concrete patching and corrosion of the remaining prestressing steel, repair may not be feasible even though replacement of the damaged girder(s) is not necessary. Additional work is necessary before any conclusions can be made about the serviceability and endurance of repair options.

**Table 4.6. Influence of Damage on Moment Fractions: Load at Position 3.**

| Damage Level | $MF_2$ | % Increase | $MF_3$ | % Increase |
|---|---|---|---|---|
| Undamaged | 0.283 | - | 0.719 | - |
| 1 | 0.310 | 9.5 | 0.692 | -3.7 |
| 2 | 0.268 | -5.3 | 0.734 | 2.1 |
| 3 | 0.247 | -12.8 | 0.742 | 3.2 |
| 4 | 0.268 | -5.4 | 0.705 | -1.9 |
| 5 | 0.244 | -13.7 | 0.754 | 4.9 |
| 6 | 0.251 | -11.4 | 0.742 | 3.2 |
| 7 | 0.286 | 1.0 | 0.695 | -3.3 |
| 8 | 0.257 | -9.3 | 0.733 | 2.0 |
| 9 | 0.272 | -3.9 | 0.711 | -1.2 |
| 10 | 0.290 | 2.5 | 0.698 | -2.9 |
| 11 | 0.355 | 25.5 | 0.632 | -12.0 |
| 12 | 0.420 | 48.5 | 0.558 | -22.4 |
| 13 | 0.470 | 66.1 | 0.528 | -26.5 |

**Table 4.7. Influence of Damage on Moment Fractions: Load at Position 6.**

| Damage Level | $MF_2$ | % Increase | $MF_3$ | % Increase |
|---|---|---|---|---|
| Undamaged | 0.293 | - | 0.676 | - |
| 1 | 0.296 | 1.1 | 0.684 | 1.2 |
| 2 | 0.297 | 1.5 | 0.685 | 1.4 |
| 3 | 0.305 | 4.2 | 0.654 | -3.2 |
| 4 | 0.300 | 2.6 | 0.659 | -2.5 |
| 5 | 0.286 | -2.1 | 0.689 | 2.0 |
| 6 | 0.301 | 3.0 | 0.672 | -0.6 |
| 7 | 0.317 | 8.5 | 0.653 | -3.4 |
| 8 | 0.368 | 25.8 | 0.594 | -12.1 |
| 9 | 0.347 | 18.6 | 0.616 | -8.8 |
| 10 | 0.352 | 20.3 | 0.612 | -9.5 |
| 11 | 0.377 | 28.7 | 0.588 | -13.0 |
| 12 | 0.398 | 35.9 | 0.575 | -15.0 |
| 13 | 0.458 | 56.4 | 0.529 | -21.7 |

**Table 4.8. Influence of Damage on Moment Fractions: Load at Position 9.**

| Damage Level | $MF_2$ | % Increase | $MF_3$ | % Increase |
|---|---|---|---|---|
| Undamaged | 0.217 | - | 0.776 | - |
| 1 | - | - | - | - |
| 2 | 0.207 | -4.7 | 0.751 | -3.2 |
| 3 | 0.283 | 30.4 | 0.724 | -6.6 |
| 4 | 0.277 | 27.5 | 0.719 | -7.3 |
| 5 | 0.321 | 47.5 | 0.657 | -15.3 |
| 6 | - | - | - | - |
| 7 | 0.321 | 47.9 | 0.656 | -15.4 |
| 8 | 0.297 | 36.6 | 0.664 | -14.4 |
| 9 | 0.325 | 49.6 | 0.639 | -17.7 |
| 10 | 0.315 | 45.0 | 0.660 | -14.9 |
| 11 | 0.367 | 68.9 | 0.594 | -23.4 |
| 12 | 0.407 | 87.2 | 0.545 | -29.7 |
| 13 | 0.476 | 118.8 | 0.503 | -35.2 |

## *4.4. Model Bridge Test Summary and Conclusions*

It is important to remember the limitations and conditions under which this research was performed before any conclusions can be made about impact damaged P/C girder bridges in general. The bridge model exhibits behavior for a specific type of bridge with its own unique characteristics, which vary from structure to structure. Span length, deck thickness, number of girders (this bridge model had three), diaphragm configuration, skew angle, support conditions, etc. all may have an effect on the behavior of a bridge under damaged conditions. In addition, simulated damage does not replicate actual damage conditions, where extensive cracking of the concrete section is present. However, with these restrictions in mind, several conclusions can be made from the experimental testing of this bridge model in its undamaged and damaged conditions.

1. Throughout the comparisons for the P/C beams, the R/C deck and the prestressing steel strands, bridge behavior was not significantly affected until strands were removed from the damaged beam. Concrete damage alone was not sufficient to cause relative changes in behavior.
2. Bridge behavior in general is not significantly affected until critical levels of damage are reached (Damage Level 10 or higher, which corresponds to a 33% loss of prestress force in the tensile zone).

3. When load is placed a distance away from the damaged region, bridge behavior remains relatively unchanged. The beam on the opposite side of the bridge model is not adversely affected by the load placed at any location even at the highest levels of damage. In addition, loading of the beam adjacent to the damaged member (i.e. the interior beam) produced no changes in observed bridge behavior in nearly all cases. This indicates that undamaged regions of the bridge are not affected when loads are applied away from the damaged member.
4. Even with a large loss of prestress force (over 80%), significant strength remains in the damaged beam indicating that changes in load paths and/or lateral load distribution have occurred.
5. The investigation of transverse load distribution by moment fractions reveals that the moment in Beam 2 (an undamaged beam) approximately doubles between the initial and final damage conditions. At the same time, stress levels in the damaged beam remain well below the ultimate strength of the section. This indicates that a significant degree of redundancy is present in this bridge model.
6. The amount of transverse load distribution in this bridge model is most likely at the minimum expected level for the type of testing performed in this investigation. Increases in deck thickness and span length would significantly increase the degree of lateral load distribution at the levels of damage tested.

# *CHAPTER 5*
# *ISOLATED BEAM TESTS*

This Chapter presents the results from tests conducted on four isolated P/C beams. Two of the beams were removed from the I-680 WB bridge over County Road L34 near Beebeetown, Iowa. These beams are Iowa DOT standard beam type B55R installed in 1985 (see Figure 3.3). The damaged B55R beams presented an opportunity to obtain stiffness and strength characteristic of the beams in the damaged and repaired condition. Two other beams are also described in this chapter; they are from the bridge model tested and discussed in Chapter 4. The beams from the bridge model are Iowa DOT LXA38 standard beams (see Figure 4.2).

## *5.1. Beebeetown Beam Tests*

In October 1997, the damaged prestressed beams in the WB I-680 bridge over County Road L34 near Beebeetown, Iowa were replaced. Refer to Figures 5.1 and 5.2 for details of the beam removal. The removal process and geometry of the removed beams are briefly described in the following text.

The B55R beams have a total length of 56 ft; the distance between the centerline of beam bearings is 55 ft. Because the longitudinal slab steel needed to be exposed for the subsequent bridge repair, the entire slab was removed for the first 4 ft-9 in. from each end of the beams as depicted in Figure 5.1.

At the request of the researchers, the curb and concrete rail section were removed from the damaged exterior beam, Beam 1W. This was so that these large elements would not influence the stiffness and/or strength of the damaged beam during subsequent testing. Roughened and slightly cracked/spalled concrete existed along the entire top surface of the slab along the north side due to barrier rail removal. The remaining intact slab on Beam 1W had an average width of approximately 5 ft and was unsymmetrical. The width of the portion of the slab under the rail measured 2 ft-3 1/2 in. from the centerline of beam while that part between Beams 1W and 2W measured 2 ft-8 1/2 in. In Beam 2W, the total slab width was approximately 3 ft-1 in. total and was symmetric about the centerline of beam.

The total slab thickness including the originally specified 6 in. slab plus subsequent overlay was slightly more than 9 in. close to the beam web. Significant feathering of the underside of the slab was found along essentially the total length of Beam 2W. The feathering was not present to the same degree in Beam 1W.

In the summer of 1998, Beams 1W and 2W, removed from service the prior October, were tested at the facilities of Wilson Concrete in LaPlatte, Nebraska. At this facility, Wilson Concrete and the University of Nebraska jointly operate an outdoor test facility capable of testing full-size specimens.

**Figure 5.1. Beams 2W and 1W Isolated in Preparation for Removal from the WB Bridge.**

**Figure 5.2. Beam 1W During Removal from the WB Bridge.**

Both beams were loaded symmetrically by two actuators each placed 4 ft from centerline thus creating an 8 ft long constant moment region. With the prescribed loading arrangement, the maximum shear and moment occur under the actuators. Also with this arrangement, the damaged region was subjected to maximum shear and moment simultaneously. Due to the presence of web damage in both beams and the fact that the beams are not designed for such large shears near midspan, it is reasonable to expect a shear failure rather than a flexural failure in this region.

### *5.1.1. Beam 1W*

At the time of the test, both beams were inspected for the first time since the original damage inspection approximately two year's prior. Following the initial damage and eventual removal of the beams from service, a protective tarp was installed to prevent loose debris from falling onto the county road below. It is known that the beams were hit several more times prior to removal due to the presence of several tears in the tarp. The amount of additional damage could not be documented.

An assessment of the beams prior to the test indicates that Beam 1W had significantly more damage than due to the initial collision. The notes from one of the researchers written the day of the test indicated that it was possible to see completely through the web. *"With a minor amount of effort it would have been fairly easy to create a large void in the web simply by removing the fractured concrete"*. The researcher goes on to communicate that *"the tension region damage is extreme…one load point is right over the damage. The damage extends over three stirrups and most of the three stirrups are exposed…I think this will be the source of failure in this test"*. These comments indicate damage much more severe than apparent from the initial inspection photos and description. Photos depicting the test setup and the beam prior to testing are presented in Figures 5.3 through 5.6.

Figure 5.3 is an overall view of the test setup where the location of one of the actuators in the damaged region is clearly visible. Figures 5.4 and 5.5 illustrate the condition of the damaged beam prior to load testing. The bottom flange concrete was significantly fractured along with numerous web cracks. Figure 5.6 is an end view showing the asymmetric composite slab.

Prior to testing of the beam, analytical predictions of the strength of the specimen were made. These predictions are presented in Table 5.1. Theoretical strengths are presented for the beam in an undamaged condition and with two strands missing based on nominally specified material strengths. Prior to the test, an additional strand was severed to determine the effective prestressing force in the strand; thus the damaged beam was believed to have 16 intact strands prior to the ultimate load test. The purpose for the 18 strand calculations was for a point of reference illustrating the effects of the loss of 2 of the original 18 strands on the flexural strength of the beam. The last scenario in the Table considers 3 missing strands; a third strand fractured during the ultimate load test of Beam 1W, see Section 5.1.1.1.2 for details.

**Figure 5.3. Overall View of Test Setup; Beam 1W in Position for Testing.**

**Figure 5.4. Close Up View of Damaged South Face of Beam 1W Prior to Testing.**

**Figure 5.5. Close Up View of Damaged North Face of Beam 1W Prior to Testing.**

**Figure 5.6. End View of Beam 1W Prior to Testing.**

**Table 5.1. Predicted Strengths of Beam 1W.**

| Scenario | # of Effective Strands | $y_{ps}$, in., from beam bottom | $f_c'$ slab, ksi | $b_{eff}$, in. | ≈3 in. Overlay Effective ? | $\phi M_n$, ft-kips |
|---|---|---|---|---|---|---|
| 1 | 18 | 4.00 | 3.5 | 52 | N | 2,285 |
| 2 | 18 | 4.00 | 3.5 | 52 | Y | 2,470 |
| 3 | 16 | 4.25 | 3.5 | 52 | N | 2,040 |
| 4 | 16 | 4.25 | 3.5 | 52 | Y | 2,205 |
| 5 | 16 | 4.25 | 7.92 | 52 | N | 2,140 |
| 6 | 16 | 4.25 | 7.92 | 52 | Y | 2,305 |
| 7 | 15 | 4.40 | 7.92 | 52 | Y | 2,160 |

[1] Undamaged beam, specified material strength, overlay disregarded in "d" distance
[2] Undamaged beam, specified material strength, overlay included in "d" distance
[3] 2 strands missing in bottom row, specified material strength, overlay disregarded in "d" distance
[4] 2 strands missing in bottom row, specified material strength, overlay included in "d" distance
[5] 2 strands missing in bottom row, $f_c'$ of slab/overlay = 7.92 ksi, overlay disregarded in "d" distance
[6] 2 strands missing in bottom row, $f_c'$ of slab/overlay = 7.92 ksi, overlay included in "d" distance
[7] 3 strands missing following ultimate test, $f_c'$ of slab/overlay = 7.92 ksi, overlay included in "d" distance

In Table 5.1, the variable $y_{ps}$ is the location of the centroid of the strand group measured from the bottom of the beam. The column titled $f_c'$ slab refers to the strength of the concrete in the slab/overlay. No distinction between the strength of concrete in the two materials is made. Subsequent to the beam tests, cores were obtained from the web and slab of Beam 1W to determine in-situ concrete strengths. The cores were obtained and tested in accordance with ASTM C 42 and C 39 procedures. The average strength of the cores obtained from the beam web was 8,220 psi and that of the slab and overlay, 7,920 psi. These strengths are in contrast to the specified compressive strengths of 5,000 psi and 3,500 psi for the beam and slab, respectively. A Modulus of Elasticity, E, was not obtained from the cores so a theoretical E has been computed based on the formula for high strength concrete, $E = 1{,}000{,}000 + 40{,}000\sqrt{f_c'}$ . Using this formula results in a predicted E of 4,627 ksi for the beam concrete and 4,560 ksi for the slab/overlay concrete. A modular ratio of 1.015 results from these two values, thus a reasonable average E of 4,600 ksi could be used for both materials.

The dimension $b_{eff}$ represents the effective flange width of an isolated T-beam. It is assumed that the web width referred to in the AASHTO Standard Specification provisions of Article 8.10.1.3 refers in this case to the width of the rigid top flange, 1 ft-1 in., similar to that allowed by Article 9.8.3 for beams with wide top flanges. The column related to the overlay allows for consideration of the overlay up to the ultimate moment. Finally, the last column presents the predicted flexural design strength of the beam. The strength was computed in accordance with Equations (5.1) and (5.2). One should note that although the slab concrete strength increased by 126% over that specified, the theoretical flexural design strength increases by less than 5%.

$$\phi M_n = \phi\left[A_s^* f_{su}^* d\left(1 - 0.6\frac{\rho^* f_{su}^*}{f_c'}\right)\right] \tag{5.1}$$

$$f_{su}^* = f_s'\left[1 - \left(\frac{\gamma^*}{\beta_1}\right)\left(\frac{\rho^* f_s'}{f_c'}\right)\right] \tag{5.2}$$

Where:

$A_s^*$ = area of prestressing steel
$f^*_{su}$ = average stress in the prestressing steel at ultimate load
d = distance from the extreme compression fiber to the centroid of prestressing force
$\rho^* = A_s^*/bd$
$f_c'$ = compressive strength of concrete at 28 days
$\gamma^* = 0.40$ for stress-relieved strand
$\beta_1$ = equivalent stress block correction factor

Equations (5.1) and (5.2) are Equations (9-13) and (9-17), respectively from the AASHTO Standard Specifications, 16th edition, with interim specifications up to 1998. The equations presume bonded behavior with only prestressing steel in the tension zone and rectangular section behavior. Because some of the bottom flange and web are destroyed or fractured, the conditions of strain compatibility and linear strain through the depth of the member are not technically correct and the expected strength of the beam should deviate somewhat from the bonded member predictions. A partially bonded element will have less flexural strength than one that is fully bonded.

The shear capacity of this beam is difficult to predict using conventional code-based formulations. As mentioned previously, there is significant section loss in the web within the damaged region. This loss compromises the concrete contribution to shear strength. Additionally, several of the stirrups in the damaged region are debonded from the concrete over a significant portion of their length. Without sufficient web steel development and anchorage, these stirrups are of little value in providing shear resistance. For these reasons, no attempts using code-based formulations were made to predict the shear strength for this beam. A more appropriate analysis of this disturbed region would be through a strut and tie analogy but once again assumptions need to be made regarding the integrity of the load path in the struts and ties.

A schematic of the test frame setup and instrumentation layout for Beam 1W are presented in Figure 5.7. Instrumentation for the testing of Beam 1W consisted of deflection transducers, strain gages mounted on the concrete surface and strain gages on several exposed strands.

Displacements were recorded with string potentiometers. The offset transducer (TD1) at midspan was placed to detect if the asymmetry of the composite slab as well as the damage caused the beam to rotate during the test. Only minor differences were noted between the centerline and offset transducers at midspan; thus, only the centerline deflections are presented.

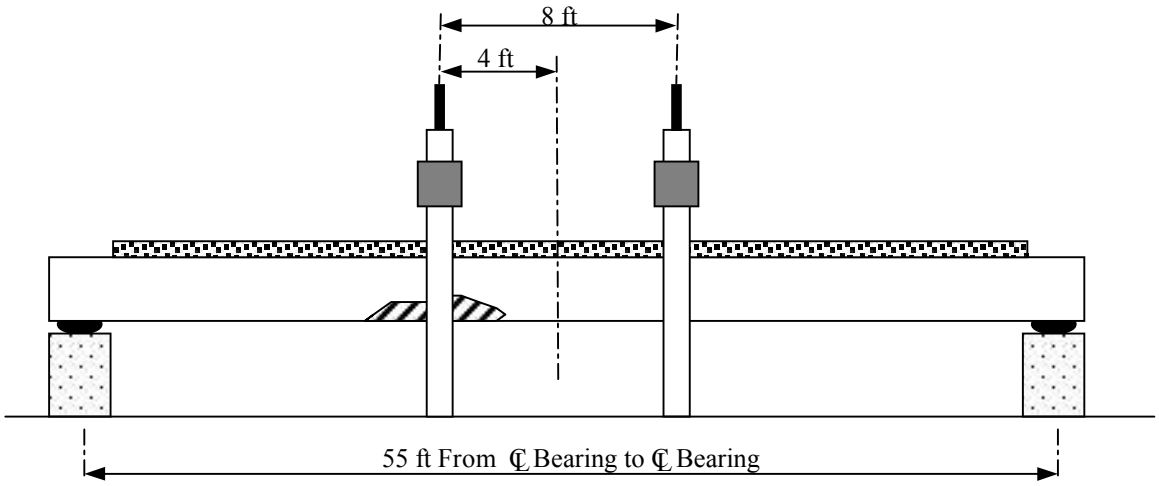


**a.) Elevation View of Load Frame.**

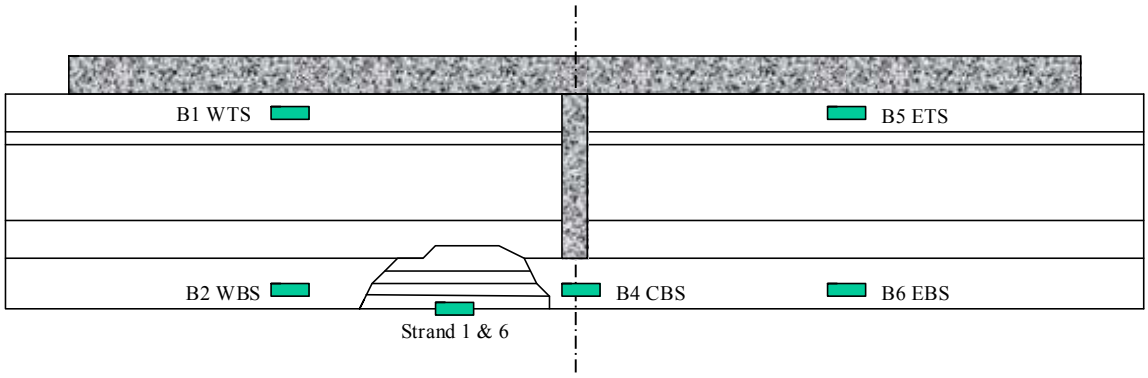


**b.) Instrumentation on South Face.**

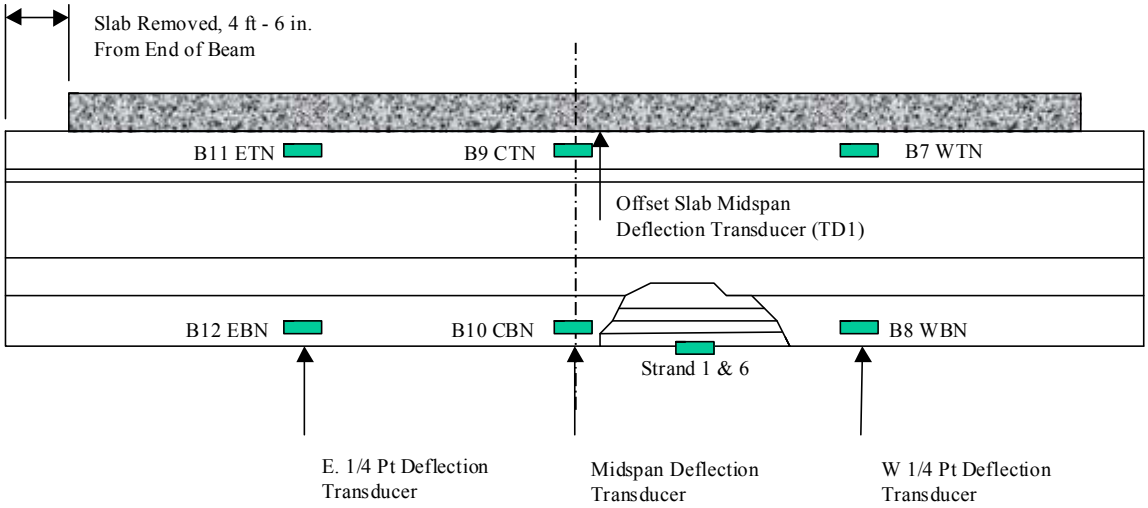


**c.) Instrumentation on North Face.**

**Figure 5.7. General View of Test Setup and Instrumentation Layout, Beam 1W.**

Strain gages for determining longitudinal strains were installed on the top and bottom flange on both the north and south faces of the beam for redundancy. The one exception is that a top flange strain gage was not installed at midspan on the south side of the beam since the diaphragm stub was in the way. Strain gages on the concrete surface are typically located at 2 in. from the bottom and top of the prestressed beam section. The gages were used primarily to compute experimental locations of the neutral axis of the section. The notation used for the gages is first the location along the beam, **W**est, **C**enter or **E**ast quarter point, **T**op or **B**ottom flange, and **N**orth or **S**outh face assuming the orientation of the beam in the bridge.

Three strands were also instrumented. One of the strands was purposely severed prior to the ultimate load test to determine the remaining strain and hence the stress in the strand, therefore only two strands were instrumented for the ultimate load test. The strand severing technique has been used by other researchers with varying degrees of success (Halsey and Miller, 1996; Labia, Saiidi and Douglas, 1997; Olson, French and Leon, 1992). Strand severing was also used in the laboratory testing phase of this research program with some success (Paradis, 1998). A promising nondestructive device for measuring the remaining effective prestress has been developed by the U. of Texas (Civjan, Jirsa, Carrasquillo and Fowler, 1995). This device was previously discussed in Chapter 2.

The strain recorded upon severing of the strand fluctuated significantly before reaching a stable value of -1873 με. This strain corresponds to an effective prestress of 53,380 psi, much less than the effective stress expected following normal prestress losses. This reading may or may not be reliable though a loss of effective stress is expected. The sudden loading from severing the strand may have damaged the gage resulting in unreliable results. If the measured loss is reliable, it is greater than would be experienced in the bridge since the adjacent beams would restrain the beam as the bottom flange is damaged. Additionally, the measured effective prestress, if reliable, invalidates use of the AASHTO equations for moment strength since the effective prestress is less than the $0.5f_s'$, the value used as the lower bound for which the AASHTO equations are applicable. Hence the strengths reported in Table 5.1 would be invalid.

#### *5.1.1.1. Beam 1W Test Results*

5.1.1.1.1. Service Load Test

A baseline load test was conducted to determine the stiffness characteristics of the beam. Both actuators were loaded to approximately 30 kips, creating moments of approximately 420 ft-kips at the quarter points and 718 ft-kips throughout the entire 8 ft long constant moment region. The live load moment of 718 ft-kips is over twice the unfactored design live load and impact moment for this beam in service, 355 ft-kips, based on HS20 live loads and impact and a wheel load distribution factor of S/5.5 = 0.77 for exterior beams spaced less than 6 ft on center. Additionally, a dead load moment of 300 ft-kips and 400 ft-kips due to self weight is resisted at the quarter point and midspan, respectively, during the test.

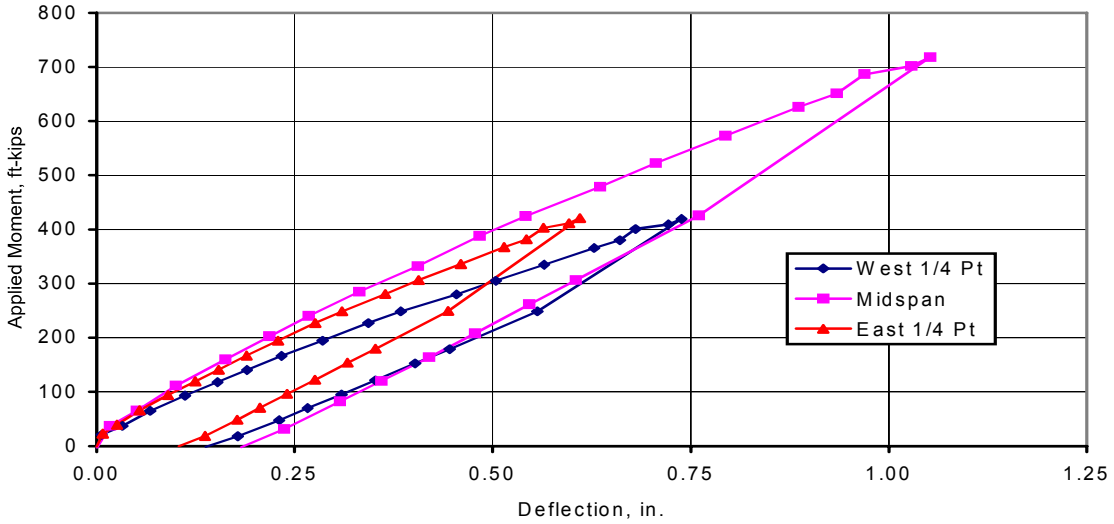


**Figure 5.8. Service Test of Beam 1W: Applied Moment vs. Deflection.**

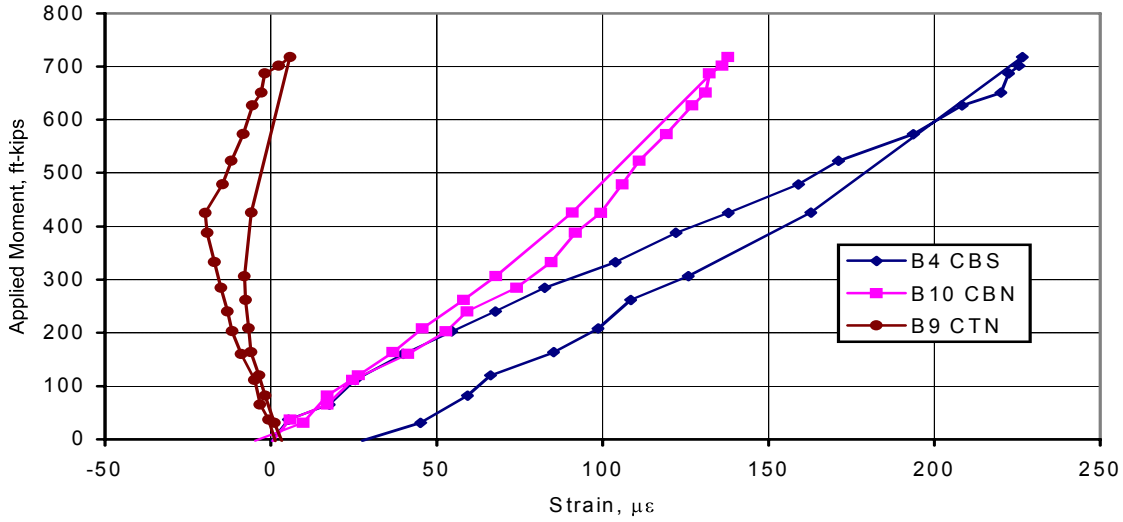


**Figure 5.9. Service Test of Beam 1W: Applied Moment vs. Midspan Strains.**

Figure 5.8 presents the applied moment versus deflection of Beam 1W during the service load test. Even with the large amount of damage in the web and flange regions the deflection behavior of the beam is essentially linear. The effect of the localized loss of section west of the midspan diaphragm is evident in that under symmetric loading, the west 1/4 point deflects approximately 20% more than the east 1/4 point.

Midspan surface strains vs. applied moment are presented in see Figure 5.9. Between an applied moment of 300 and 400 ft-kips, the behavior of gages B9 and B10 changes, likely due to the opening of a crack. The quarter point strains are linear throughout the test.

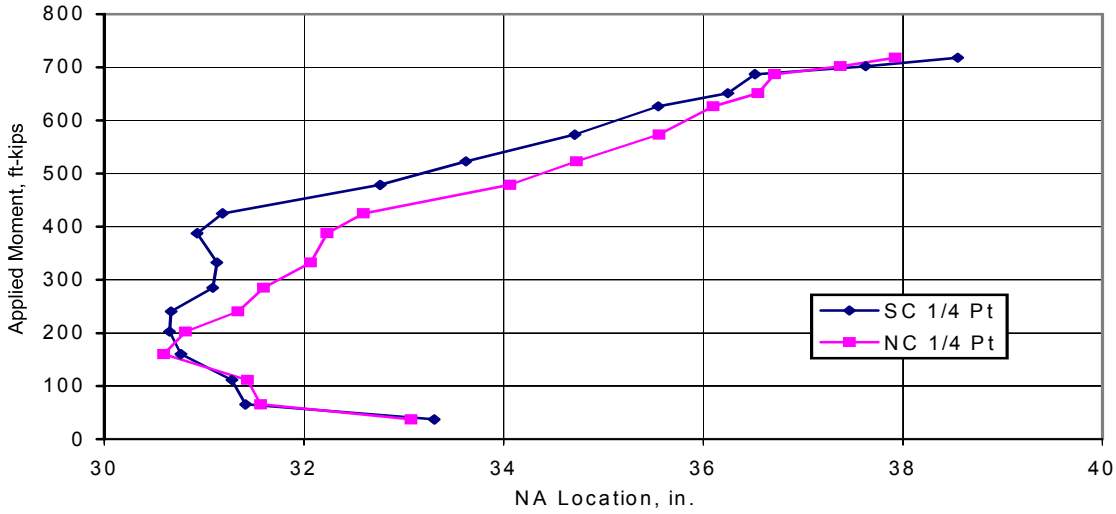


**Figure 5.10. Service Test of Beam 1W: Location of Midspan Neutral Axis.**

Using the measured strains, the experimental neutral axis of the section can be computed. Since the only top flange reading at midspan is gage B9, it is used with both bottom flange gages to compute a neutral axis location. The neutral axis variation at midspan measured from the bottom fiber is presented in Figure 5.10.

Consistent with the fact that the neutral axis is computed based on the strain readings presented in Figure 5.9, one expects to see movement of the live load neutral axis due to the bilinear behavior of gages B9 and B10. Up to an applied midspan moment of approximately 400 ft-kips, the neutral axis for live loads is between 31 and 32 in. from the bottom fiber. Because the only top flange gage is on the north side of the beam, it was used in conjunction with the bottom flange gages on the north and south side of the beam for the neutral axis location calculations. The behavior exhibited in Figure 5.10 is consistent with the movement of the neutral axis of a cracked prestressed concrete section under load.

Unlike midspan, the neutral axis at the quarter points is essentially constant throughout the entire range of service loading. Using gages B5 and B6 to compute the neutral axis location at the undamaged east quarter point, the computed value is fairly constant at approximately 32 in. This reading is suspect due to low strain levels in gage B5. Using gages B11 and B6 produces a neutral axis value of approximately 28.2 in. at the peak load. This value is fairly constant throughout the entire range of service loading. At the west quarter point, where one might expect the relative closeness of damage to cause the neutral axis to shift upward, the neutral axis location is lower than at the midspan or east quarter point locations. Using gages B1 and B2, one obtains a neutral axis location of 26.1 in. at maximum load and using gages B7 and B2, one obtains a value of 27.6 in. These peak readings are approximately 1-3/4 in. higher than at low load levels indicating an upward movement of the neutral axis during the test, consistent with cracked section behavior.

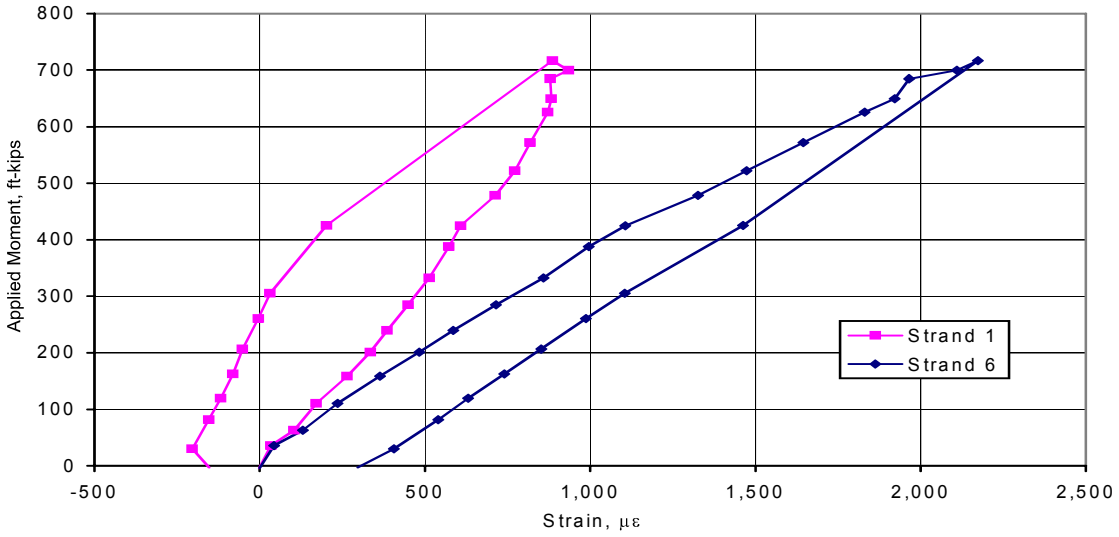


**Figure 5.11. Service Load Test of Beam 1W: Variation in Strand Strains.**

Examining the east and west quarter point neutral axis locations, three of the readings range from 26.1 in. to 28.2 in. with an average of 27.3 in. while the other is approximately 32 in. The neutral axis of an uncracked composite section is at approximately 31 in. from the bottom using the full 9 in. slab and overlay, an effective width of 52 in. as previously discussed and a modular ratio of 1.015. The moment of inertia of this section is 221,400 $in^4$. The lower experimental neutral axis values indicate a source of error in the computed section properties, likely due to an overestimation of effective flange width or contribution of the overlay. If the measured neutral axis of 27.3 in. is accepted, this corresponds to an effective width of 29.4 in., and a moment of inertia of 179,840 $in^4$, much less than predicted by code. If the overlay is discounted and the 52 in. effective width presumed to be correct, the neutral axis is approximately 27.7 in. above the bottom fiber of the beam and the moment of inertia, 176,900 $in^4$. However it should be noted that with the exception of several transverse cracks, the overlay appeared well-bonded to the beam. An assumed moment of inertia of 178,000 $in^4$ at both quarter points of Beam 1W will be used in future discussions.

There are any number of combinations of effective flange width and effective deck thickness that will produce a neutral axis location of 27.3 in. on average. At this point it is more informative to understand that both the west quarter point and midspan region appear to behave as cracked to some degree while the east quarter point has a constant behavior throughout the range of service loading.

The response of the instrumented strands is presented in Figure 5.11. The response of the two instrumented strands, both in the bottom row, is substantially different. No explanation is given for the difference in response, however, the response of the gage on strand 6 is close to the measured response of the strands which were instrumented on subsequent tests carried out on Beam 2W. Refer to Section 5.1.2.1 of this report for the Beam 2W results. For this reason, the response of the gage on strand 6 is believed to

be correct. The maximum strain of +2172 με corresponds to a change in stress of 61,900 psi assuming an E of $28.5x10^6$ psi for the strands.

It is notable that when Beam 1W was still part of the I-680 WB bridge, the maximum recorded exposed strand strain was +150 με under the action of a single truck producing a moment of 655 ft-kips which was distributed to several beams. The corresponding deflection was 0.064 in. The strain and deflection in the isolated beam under a similar *directly applied* moment are +1,920 με and 0.92 in., an increase of 12.8 and 14.4 times, respectively. Similarly, with two trucks in the center span, both located in Lane 1W at L1W-P4&P6, producing a maximum applied moment of approximately 790 ft-kips once again distributed to several beams, the exposed strand strain was measured to be +186 με and the deflection, 0.0851 in. The strain and deflection in the isolated beam from the same *directly applied* moment are approximately +2400 με and 1.16 in., an increase of 12.9 and 13.6 times, respectively. Although the barrier rail has been removed thus altering the stiffness of Beam 1W, the in-situ strain and deflection are only a small fraction of those measured in the isolated beam under similar applied moments. This dramatic increase in recorded strains in the isolated beam demonstrates the inherent load distribution and system redundancy in the damaged WB bridge.

5.1.1.1.2. Ultimate Load Test

Following the single loading and unloading service test, the beam was loaded to failure. At this point the beam had two severed strands in the bottom row out of a total of eighteen. During the loading of Beam 1W, an additional strand partially ruptured with three of the wires breaking during the course of loading. This strand should be entirely discounted from the section resistance. Photos of Beam 1W following the ultimate load test are presented Figures 5.12 through 5.15.

In Figure 5.16, the applied moment versus recorded deflections that occurred during the ultimate load test of damaged Beam 1W are presented. The beam behaved in a ductile fashion with significant inelastic response. At ultimate load, the deflection of the west quarter point is 5.22 in. and of the east quarter point, 4.88 in., a 7% difference. These deflections are due to a live load moment of approximately 1210 ft-kips at the quarter points. The ultimate live load moment at midspan and throughout the damaged region was 2067 ft-kips with a corresponding deflection of 8.62 in. When the ultimate load was reached, progressive failure of the beam began with large vertical flexural and diagonal shear cracks propagating up into the top flange. These cracks are noticeable in Figures 5.12 through 5.15. Along with crack propagation, a portion of the overlay crushed and debonded from the original slab and the beam sheared vertically and displaced laterally in the damaged region; the debonded slab overlay is visible in Figure 5.13. Prior to the shear failure, the beam behavior was unstable with increasing displacement under decreasing loads, a sign of impending failure. Once the beam sheared and displaced approximately 10 in. at midspan, the load was held constant for approximately 10 minutes while the beam was photographed and examined. The unloading curve is presented to illustrate the deflection recovery of this beam during unloading.

**Figure 5.12. South Face of Beam 1W West of Midspan Following the Ultimate Load Test.**

**Figure 5.13. South Face of Beam 1W Looking East Following Ultimate Load Test.**

**Figure 5.14. North Face Damage in Beam 1W Following Ultimate Load Test.**

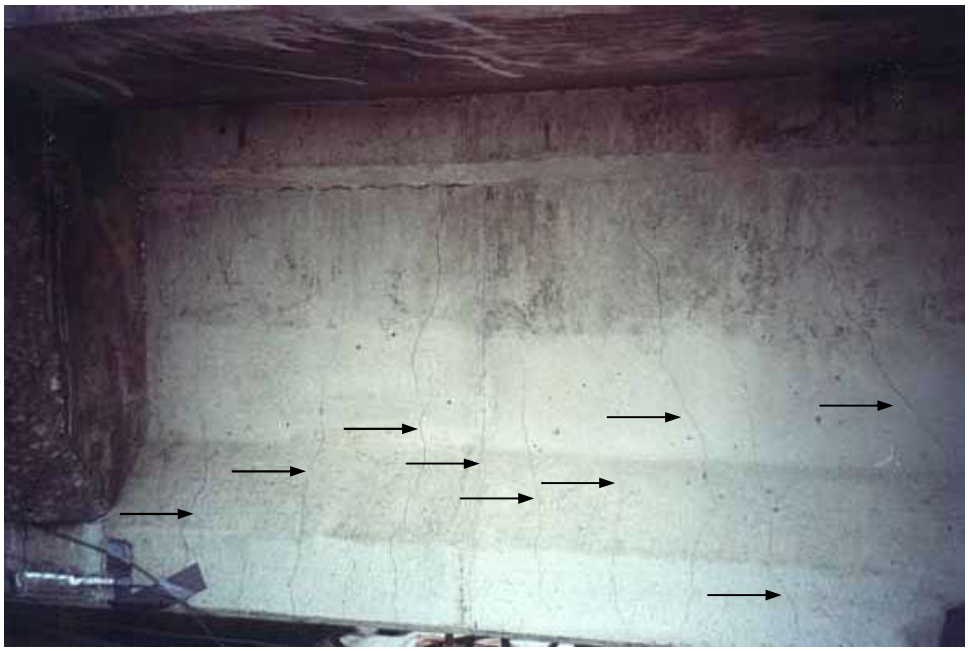

**Figure 5.15. Cracks on South Face of Beam 1W East of Midspan Following Ultimate Load Test.**

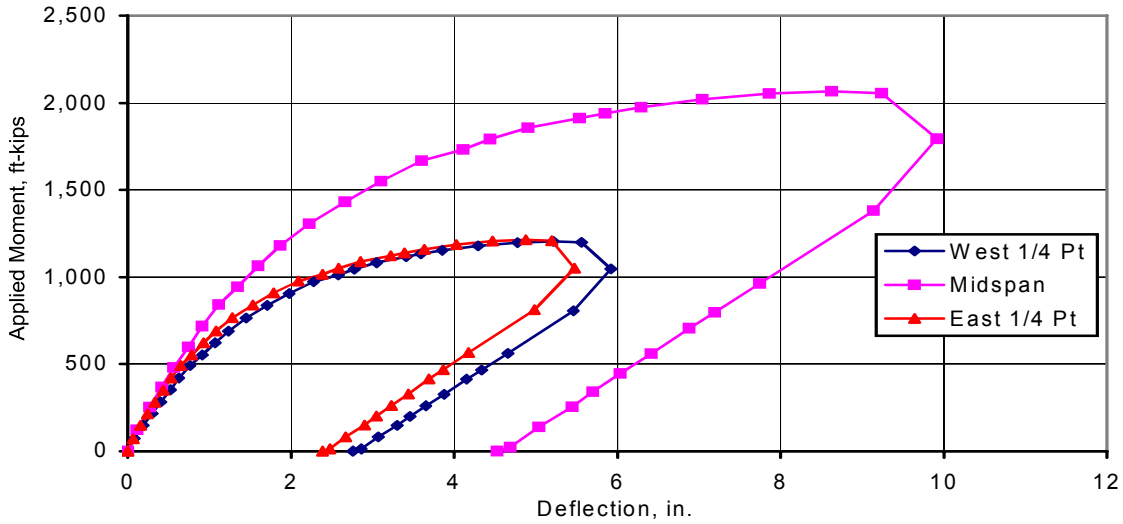


**Figure 5.16 Ultimate Load Test of Beam 1W: Applied Moment vs. Deflection.**

As a comparison of the AASHTO predicted strength and that measured, consider that the ultimate live load moment of 2,067 ft-kips in addition to a dead load moment of approximately 400 ft-kips is a total moment resisted by the damaged beam of 2,467 ft-kips. This is 14% greater than the most optimistic Code-based prediction of the damaged beam strength presented in Table 5.1, 2,160 ft-kips for a beam with three severed/ruptured strands though recall that the code equation approach may potentially be inapplicable due to the suspect effective prestress level.

The live load neutral axis locations vary. The east quarter point data are similar to the service test, 32.4 and 28.6 in. at maximum load for gage combinations B5 and B6 and B11 and B6 respectively. Once again, the 32.4 in. reading is suspect due to the small strains recorded by gage B5. The average computed neutral axis location for these two gage combinations is 32.2 and 28.4 in. respectively throughout the entire loading cycle showing essentially no variation from that recorded at maximum load. The neutral axis at the damaged west quarter point varies as in the service test. At low load levels, the neutral axis varies from 26.2 to 26.5 in. from the bottom fiber. At maximum load, the neutral axis level is recorded to be at 28.4 or 29.6 in. depending on which gage combination is used. These readings are fairly consistent again with the east quarter point lower reading and are also consistent with the upward movement of the neutral axis associated with a cracked section under load.

Figure 5.17 presents the moment, M, versus curvature, $\phi$, response for the west quarter point where $\phi$=M/EI. For a section whose stiffness does not change with applied load, the M vs. $\phi$ response should be linear. A decreasing slope indicates cracking. Figure 5.17 indicates that the M vs. $\phi$ response begins to flatten out at a quarter point live load moment in excess of 500 ft-kips.

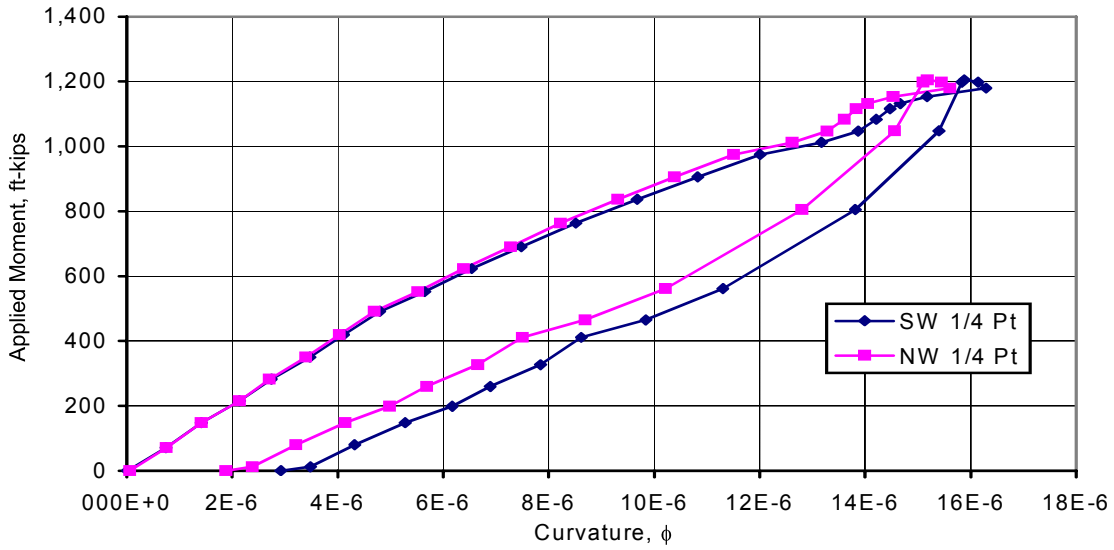


**Figure 5.17 Ultimate Load Test of Beam 1W: Applied Moment vs. Curvature at W Quarter Point.**

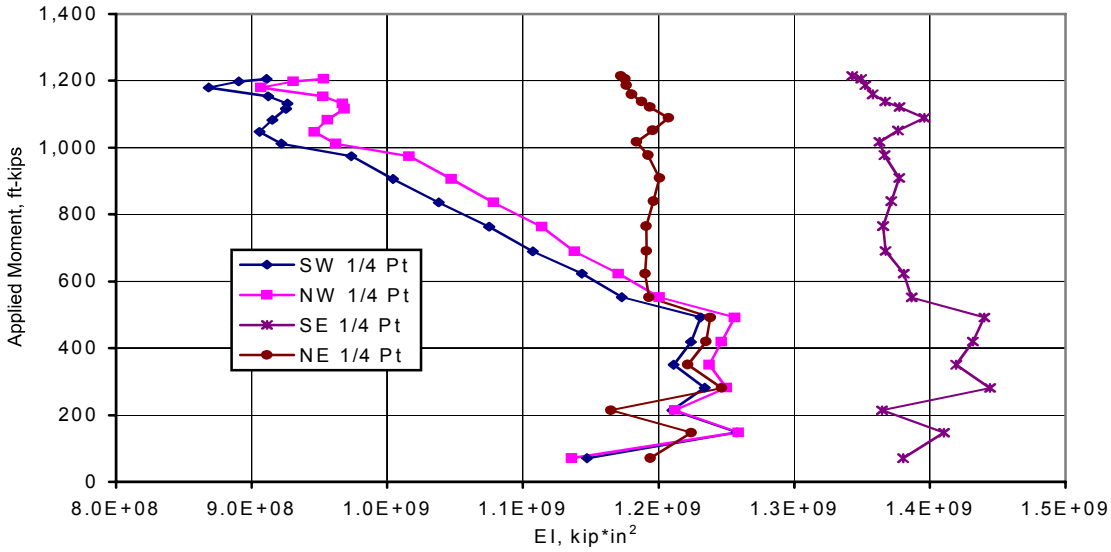


**Figure 5.18 Ultimate Load Test of Beam 1W: Applied Moment vs. EI at Quarter Points.**

As a measure of flexural stiffness, computed values of EI, based on measured load and curvature data, are presented in Figure 5.18. The figure indicates that EI begins to decrease after a moment of 500 ft-kips is applied at the west quarter point. The east quarter point remains at a fairly constant stiffness even at ultimate load. For a lower bound EI of the uncracked section of approximately $1.25 \times 10^9$ kip-in$^2$ and an assumed "I" of 178,000 in$^4$ at the quarter points, the implied Modulus of Elasticity is 7,022 ksi, much different than the value of 4,600 ksi computed based on the core compression test results. This poor correlation of predicted and experimental E values is consistent in all beams tested in this research project.

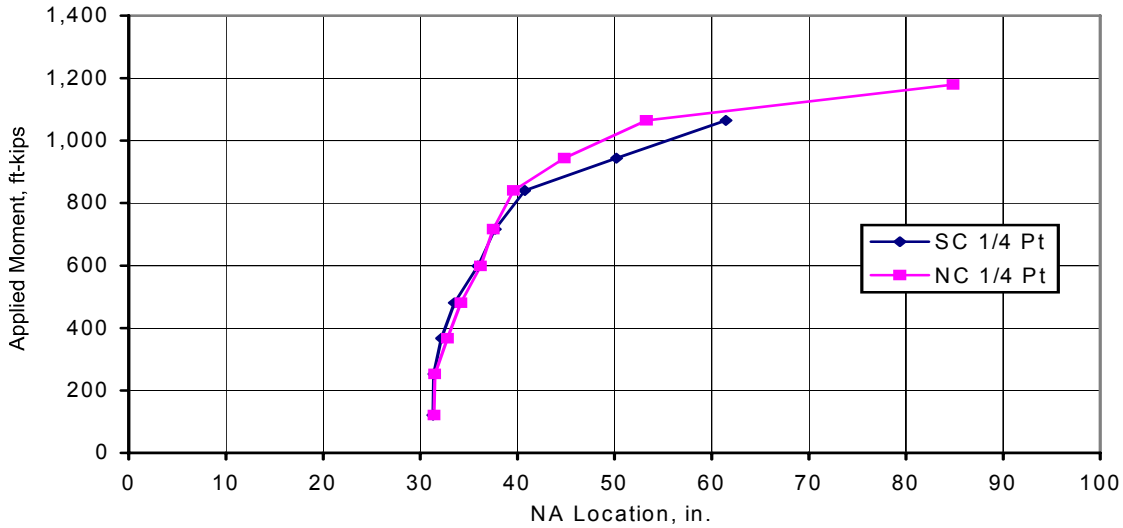


**Figure 5.19 Ultimate Load Test of Beam 1W: Applied Moment vs. Midspan NA Location.**

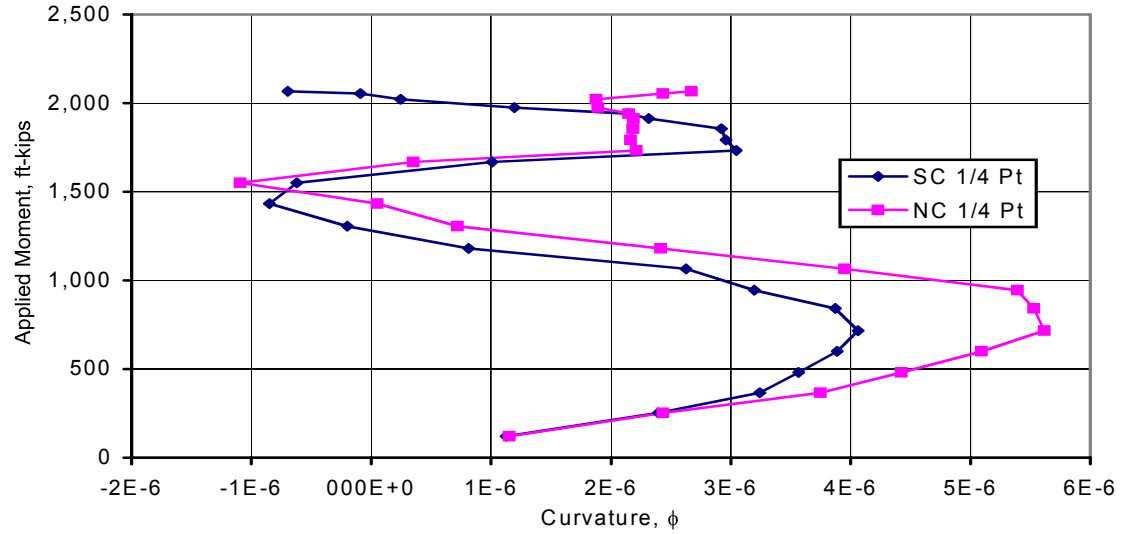


**Figure 5.20 Ultimate Load Test of Beam 1W: Applied Moment vs. Midspan Curvature.**

The midspan region of the beam during the ultimate load test produced little useful strain data as evidenced by the plots in Figures 5.19 and 5.20. These figures illustrate the erratic response of the damaged midspan region due to the advancement of cracks through the section. The strain gages in this region are adversely affected by the opening of cracks and are of little value in characterizing the response of the beam except for low load levels similar to that observed during the service test. Although erratic, a separate comparison of the moment vs. neutral axis location and curvature for the midspan region indicates repeatability between the service and ultimate tests throughout the load range the tests have in common.

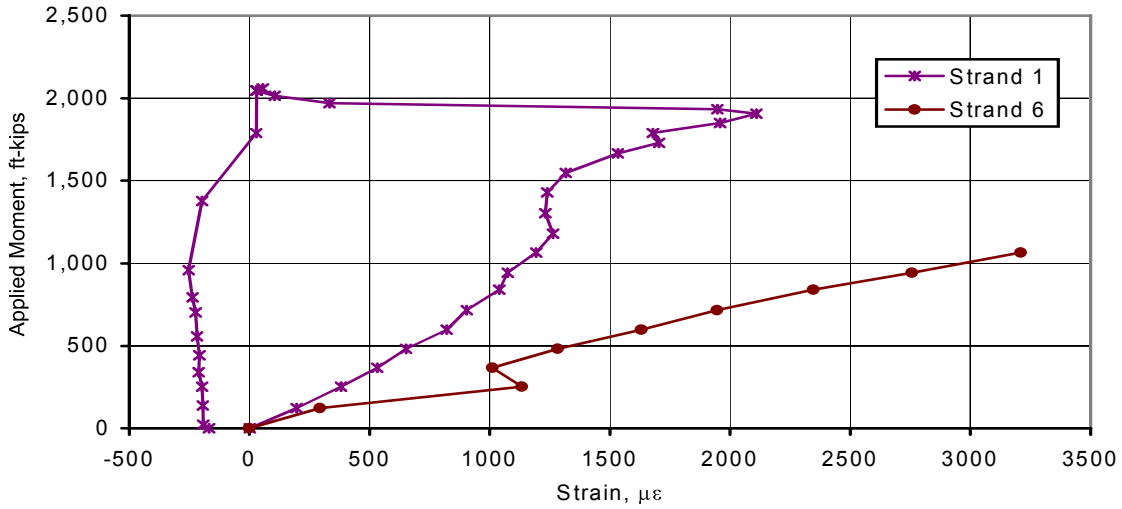


**Figure 5.21. Exposed Strand Strains: Ultimate Load Test of Beam 1W.**

Finally, similar to that presented for the service load test, the exposed strand strains are presented for the ultimate load test. Similar to the service level test, the response of the strand 6 gage is believed to provide more accurate results. Unfortunately, the gage on strand 6 ceased to operate properly after an applied moment in excess of 1,000 ft-kips. The gage on strand 1 was operable but the results are erratic.

#### *5.1.1.2. Beam 1W Test Summary*

The tests conducted on Beam 1W provide valuable information. The service tests indicates that the behavior of the beam as an isolated element is elastic under applied loads equal to the expected dead load and twice the design live load and impact that this beam is expected to carry in service. The service test indicates that the neutral axis is at a constant location at the undamaged east quarter point. The neutral axes in the damaged region from midspan to the west quarter point shift upward under live load.

The ultimate load test resulted in a combined shear failure through the damaged region due to a shear of 112 kips and a total dead load and live load moment of 2,467 ft-kips. As a reference, the Group I Load Combination specified in the AASHTO Standard Specifications results in a design ultimate moment for this beam of 1.3{400+1.67(355)}=1,291 ft-kips, indicating that the beam in the damaged condition still had twice its required flexural capacity.

### *5.1.2. Beam 2W*

Although Beam 1W exhibited significant excess strength over that required in the I-680 bridge, this is a function of the close beam spacing in the bridge. Due to the fact that there may be instances when

the computed capacity of the beam is inadequate, a second beam from the same bridge was repaired using carbon fiber strengthening techniques and then tested.

Carbon fiber was selected for the strengthening system in part because other strengthening techniques such as steel jackets, external post-tensioning and internal strand splicing have been studied in the past. References describing these retrofit techniques were discussed in Chapter 2 of this report. Very little work has been performed to date on carbon fiber strengthening of prestressed concrete elements; most research concerns reinforced concrete. Additionally, the research preformed on reinforced and prestressed concrete strengthening using advanced composites is almost exclusively limited to laboratory-scale specimens. The objective of this work was to demonstrate that large-scale damage to prestressed concrete members could be effectively repaired with field-applied materials.

#### *5.1.2.1. Service Load Tests on Damaged Specimen*

Similar to Beam 1W, Beam 2W had damage to the bottom flange and beam web though not nearly as severe. Several photos of the beam prior to the service load testing are presented in Figures 5.22 through 5.25. The location of the instrumentation used in the testing of Beam 2W is shown in Figure 5.26. Five service tests were conducted on Beam 2W prior to the repair, the first three with all strands intact and the final two with two of the eighteen strands severed. The number of severed strands during service tests 4 and 5 is the same as in Beam 1W prior to the ultimate load test. Figure 5.27 depicts the load vs. displacement response of Beam 2W prior to severing the two strands. Strands 4 and 5 were selected for severing. Strands 5 and 6, of a total of seven bottom row strands, were instrumented, each strand with three strain gages. Gages S1, S2 and S3 were placed on strand 6 while S4, S5 and S6 were on Strand 5. It was anticipated that by severing instrumented strand 5 that the effective prestress in the strand could be determined. Prior to the severing operation, all gages on Strand 6 were operational while only one on Strand 5 was operational.

During the severing of strand 4, both strand 5 and 6 recorded increases in tensile strain as would be expected. The increase in strand 5 was +63 με and in strand 6, +39 με. During the severing of strand 5, the operable gage on strand 5 recorded a compressive strain of approximately -1700 με, a stress of -48,450 psi. However, this reading was while the strand was partially intact. No reliable reading was obtained for the completely severed condition. The gages on strand 6 continued to function and recorded an average increase in strain of +104 με following the complete severing of strands 4 and 5 in the bottom row, an increase in stress of approximately 2,960 psi. Prior to the severing of the two strands, the average change in strain for strand 6 was +1,720 με (49,020 psi) under an applied live load moment of 716 ft-kips. Following severing, the change in strain was an average of +1,870 με (53,295 psi) due to an applied live load moment of 714 ft-kips, an approximate change in stress range of 9% due to removal of 11% (2 out of 18) of the original strands. The change in strain corresponds well with Strand 6 on Beam 1W presented in Figure 5.11.

**Figure 5.22. South Face of Damaged Beam 2W Prior to Repair.**

**Figure 5.23. End Elevation of Beam 2W Prior to Repair (Looking East).**

**Figure 5.24. North Face Damage West of Midspan Diaphragm, Beam 2W.**

**Figure 5.25. Underside of Damaged Flange, Beam 2W, Strain Gages on Strands 5 and 6.**

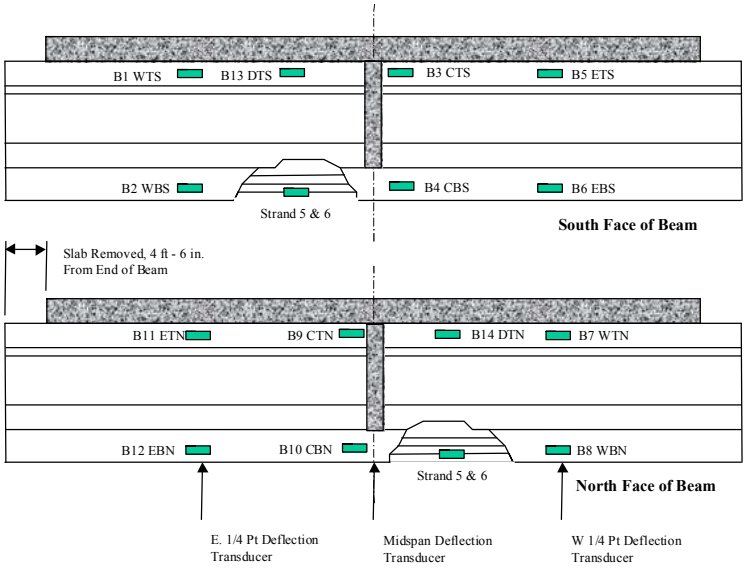


**a.) Instrumentation on Beam 2W Prior to Repair.**

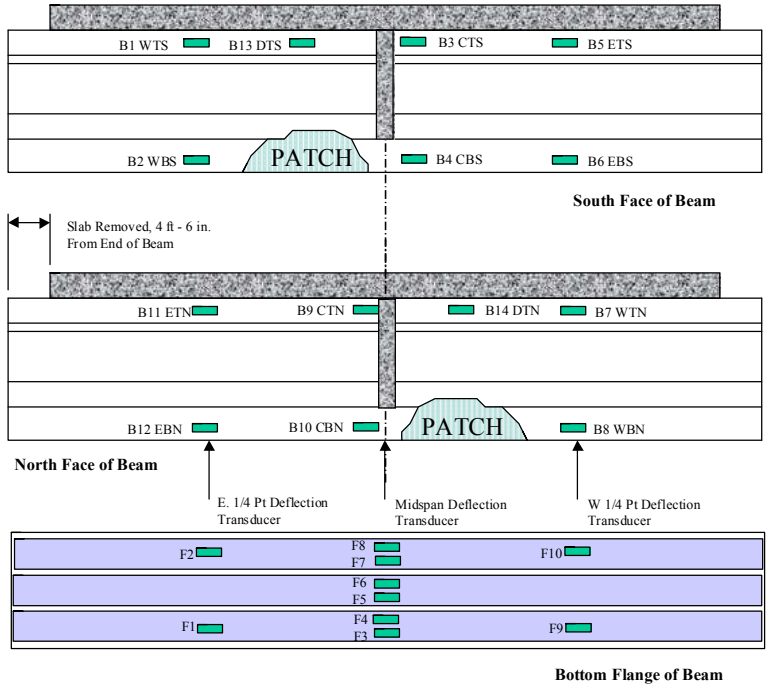


**b.) Instrumentation on Repaired Beam 2W.**

**Figure 5.26. Pre and Post Strengthening Instrumentation on Beam 2W.**

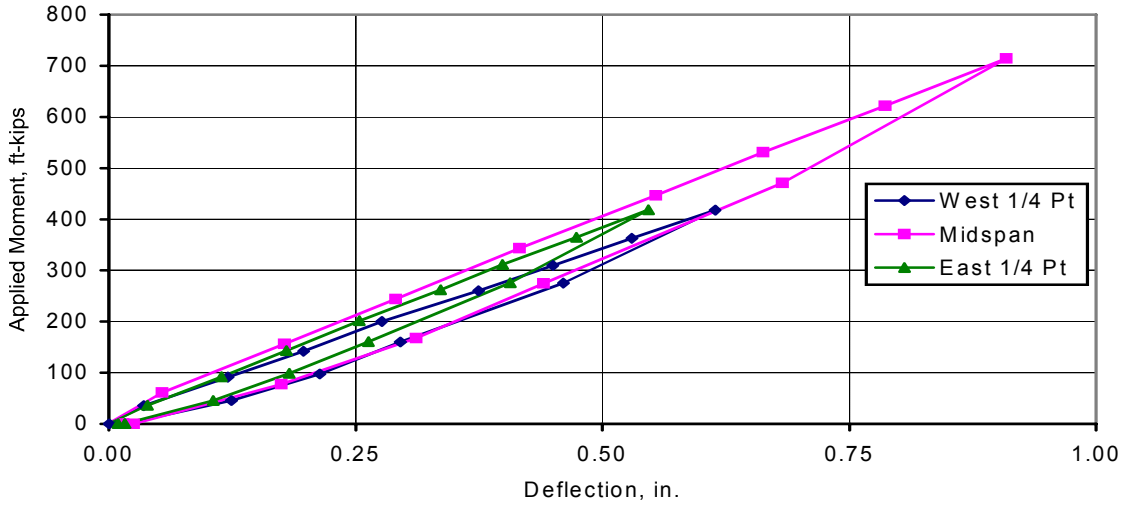


**Figure 5.27. Service Test 3 of Beam 2W: Applied Moment vs. Displacement.**

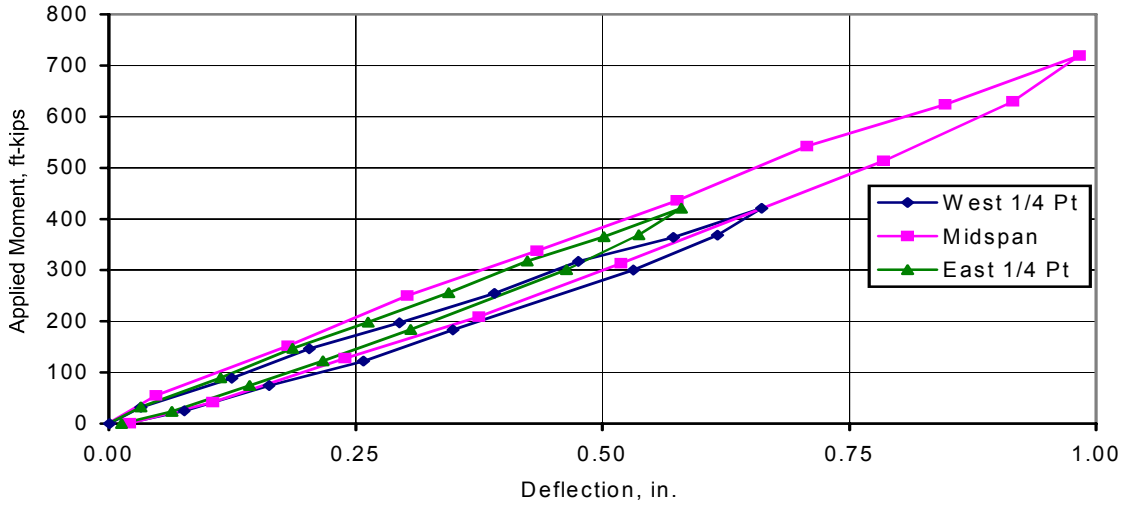


**Figure 5.28. Service Test 5 of Beam 2W: Applied Moment vs. Displacement.**

Figure 5.28 presents the load vs. displacement response of the beam following the severing of two strands and two additional static load tests. As compared to the Service Test 3 results, a deflection increase of approximately 8% occurs due to the removal of approximately 0.3 $in^2$ of prestressing steel from the tension side of the beam. The increase in deflection is consistent with the increase in exposed strand strain. The change in deflection and strain following severing are very sensitive to small amounts of steel removal. This is consistent with the findings of Olson, French, and Leon (1992) previously presented in Chapter 2 of this report and with those of Paradis (1998) which were presented in Chapter 4.

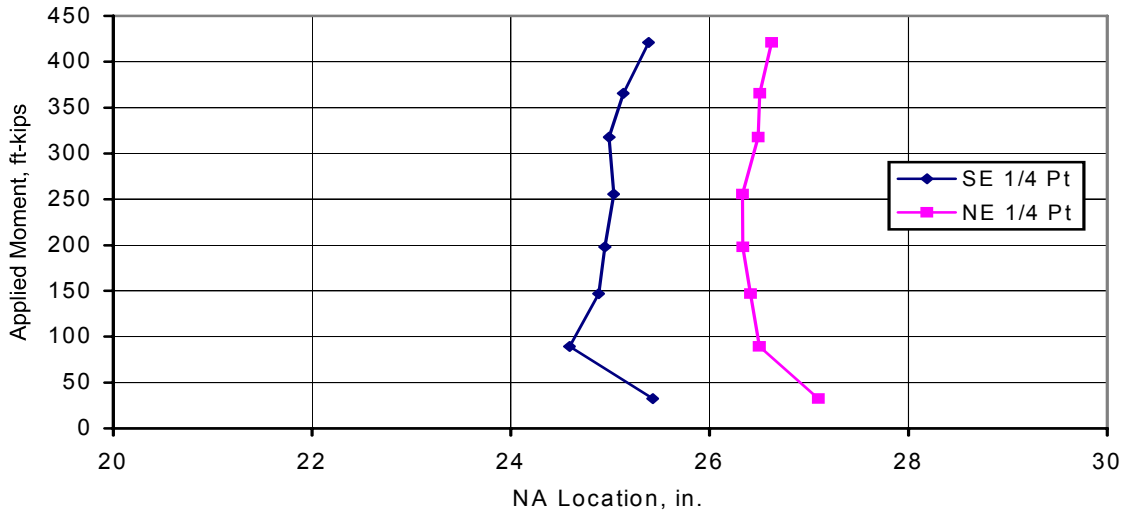


**Figure 5.29. Service Test 5 of Beam 2W: Applied Moment vs. NA Location at E 1/4 Point.**

The neutral axis location at the undamaged east quarter point appears to be insensitive to the amount of applied load as illustrated by Figure 5.29. The response is consistent with the behavior of an uncracked section. The theoretical neutral axis of an uncracked section with the full 37 in. x 9 in. slab is 28.2 in. from the extreme bottom fiber, higher than measured. For a neutral axis location of 26 in., similar to that measured, the moment of inertia is 160,000 $in^4$ with a reduction in effective slab thickness.

The response of the midspan, damaged region and west quarter points is indicative of cracking, especially the damaged region, since the neutral axis moves up with load. An example of the changing neutral axis location is presented in Figure 5.30 for the damaged region.

Figures 5.31 and 5.32 depict the variation in the average measured neutral axis location and EI recorded during the five service tests. Unlike the figures previously presented that depict the variation of a particular measured quantity throughout the course of a single test, these figures are the measured responses at peak load during all service tests. Figure 5.31 indicates that the neutral axis location in the damaged region is the highest measured location, as expected. The west quarter point is close to the damage location as is the midspan region. Figure 5.32 depicts the variation in EI. The undamaged east 1/4 point has the highest EI, an average of $1.25 \times 10^9$ kip-$in^2$ throughout all tests. The EI values for the west quarter point and midspan regions average $1.13 \times 10^9$ and $1.18 \times 10^9$ kip-$in^2$, respectively. Using the assumed moment of inertia of 160,000 $in^4$ for Beam 2W at the quarter points, the upper and lower bounds for E are 7,800 ksi and 7,063 ksi, respectively. The E from Beam 1W was computed to be 7,022 ksi using a similar approach. These values are much higher than the theoretical E for the measured concrete strengths. The EI value in the damaged region is less by a factor of approximately 8 to 9, than the other locations. The average EI in the damaged region is $1.37 \times 10^8$ kip-$in^2$. EI in the damaged region decreases 7% from Service Test 3 to Service Test 5, consistent with the increases in measured deflections and exposed strand strains.

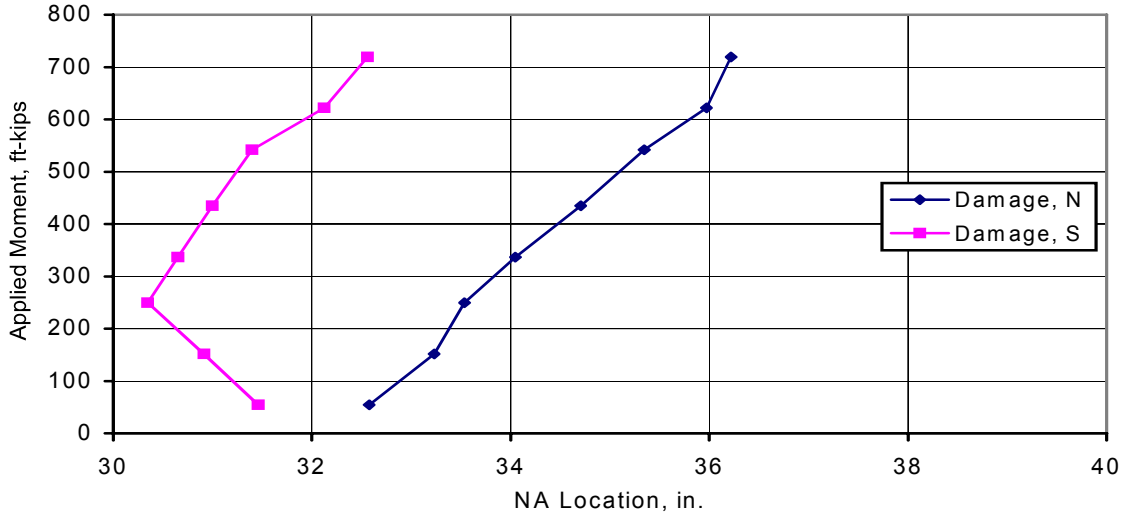


**Figure 5.30. Service Test 5 of Beam 2W: Applied Moment vs. NA Location in Damaged Region.**

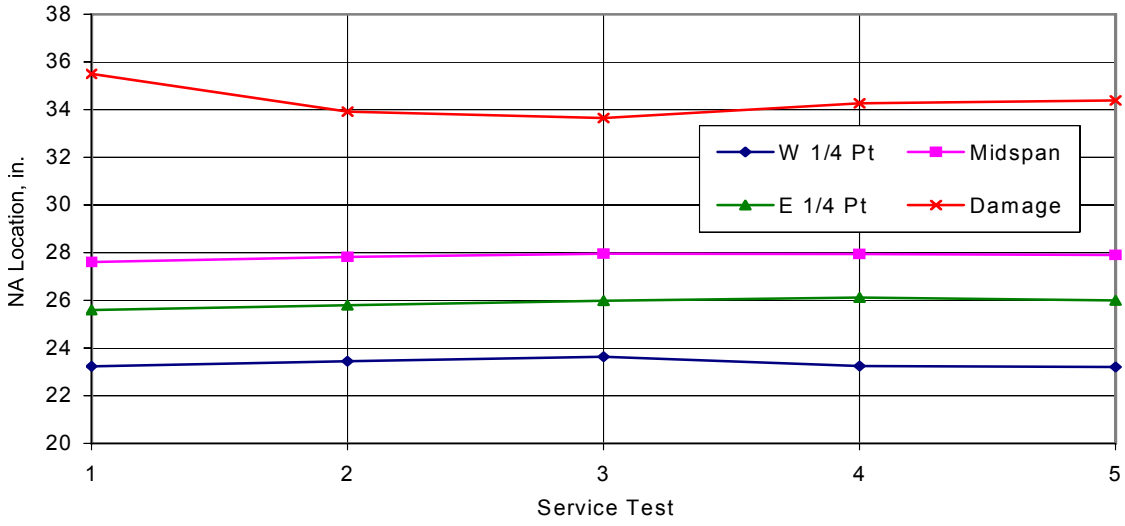


**Figure 5.31. Variation in Beam 2W NA Location with Service Tests.**

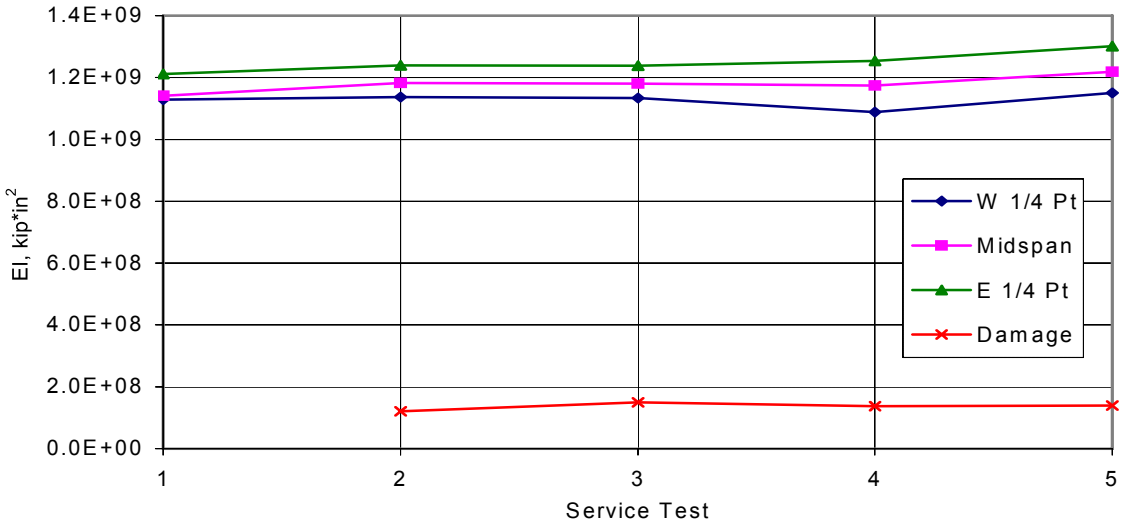


**Figure 5.32. Service Tests of Beam 2W: Variation in EI.**

### *5.1.2.2. Repair of Beam 2W*

Following the service load tests, Beam 2W was repaired. Photos depicting a portion of the repair process are presented in Figures 5.33 through 5.36.

The repair consisted of first patching the significant concrete damage west of midspan. This was accomplished by simply forming the damaged area and hand packing a patch mortar into the void space. Following the placement of the patch mortar and an overnight cure, the composite strengthening system was applied.

The composite strengthening system was supplied by Fiber Reinforced Systems of Columbus, Ohio, and was installed by Lithko Construction, also from Ohio. The material properties for the composite constituents are presented in Table 5.2.

Following patching of the void that resulted from removal of the loose concrete from the bottom flange and web areas, strengthening began with the installation of longitudinal carbon fiber reinforced polymer (CFRP) plates on the bottom flange of Beam 2W as depicted in Figure 5.34. The longitudinal plates are pultruded CFRP that are easily applied in the field with only the tools depicted in Figure 5.33. Prior to installation of the plates, both the substrate, in this case the bottom flange of the beam, and the plate, are coated with a thin layer of epoxy. The plate is then aligned on the bottom of the substrate and the two epoxy layers pressed together with a hard rubber or wooden roller. It is important that adequate pressure be applied so that air bubbles are removed and only a thin glue line remains. A total of three plates were applied to the bottom flange over the full length of the beam. Strain gages were applied to the plates at both quarter points and at midspan.

**Figure 5.33. Trowel, Spatula and Roller Used for Application of Epoxy and CFRP Plates.**

**Figure 5.34. Installation of CFRP Reinforcing Plates to Repaired Bottom Flange of Beam 2W.**

**Figure 5.35. Completed Installation of CFRP Reinforcing Plates on Beam 2W.**

**Figure 5.36. Placement of CFRP Fabric External Stirrups on Beam 2W.**

**Table 5.2. Properties of CFRP Repair Materials Used for the Repair of Beam 2W.**

| Component | Geometry | Tensile Strength | Tensile Modulus | Elongation @ Break |
|---|---|---|---|---|
| Longitudinal Plates | 5 in. x 0.080 in. plate | 143,000 psi | $17x10^6$ psi | 0.85% |
| External Fabric Stirrups | 12 in.(w) fabric | 2.8 kips/in. width | $33x10^6$ psi | 1.8% |

Following installation of the longitudinal plates, the contractor installed the external carbon fiber fabric "stirrups". This is illustrated by Figure 5.36. The external stirrups were 12 in. wide CFRP fabric sheets placed 18 in. on center for the length of the beam. The stirrups enhance the shear strength of the beam and prevent premature debonding of the longitudinal plates, similar to the role of internal steel stirrups. Shear strength enhancement was important due to the shear failure through the web damage region observed in Beam 1W previously depicted in Figure 5.12 and Figure 5.14. External confinement is also important since failure of CFRP strengthened specimens has been commonly observed to be through failure of the glue line or of the substrate itself due to high horizontal shear and peeling forces.

5.1.2.2.1. Service Load Test

Two service tests were conducted on Beam 2W using loads of similar magnitude to those used in the pre-repair tests. Only brief results from the second test are presented.

Figure 5.37 presents the applied moment vs. deflection plot for repaired Beam 2W and the behavior recorded prior to repair during Service Test 5; the repaired beam results are presented as solid lines. The change in response is due to the installation of the CFRP and patching of the web and flange damage. The peak deflection of 0.72 in. is 27% less than that measured prior to repair and 21% less than prior to any strands being severed. The response of the quarter point deflection transducers during the repaired beam tests indicates that the undamaged east quarter point deflects more than the repaired west quarter point. This is believed to be an error in the naming of the gages but no correction has been made.

Figure 5.38 depicts the variation in the neutral axis location in the damaged region measured on the north and south faces of the beam. The trend is similar to the pre-repair results such as those depicted in Figure 5.30 but the neutral axis is approximately 2 in. lower in the repaired specimen at a comparable maximum load. The response is also indicative of the behavior of a cracked section since the patch concrete, installed in a neutral stress condition, is expected to crack under live load. The computed EI values for the repaired beam are essentially the same as for Service Test 3 (prior to strand severing) and Service Test 5 (prior to repair) for the midspan and east quarter point locations. Patching of the void and installation of the CFRP plates increased the EI of the beam by 34% in the damaged region over Service Test 5 and 22% over the beam prior to any strands being severed, Service Test 3.

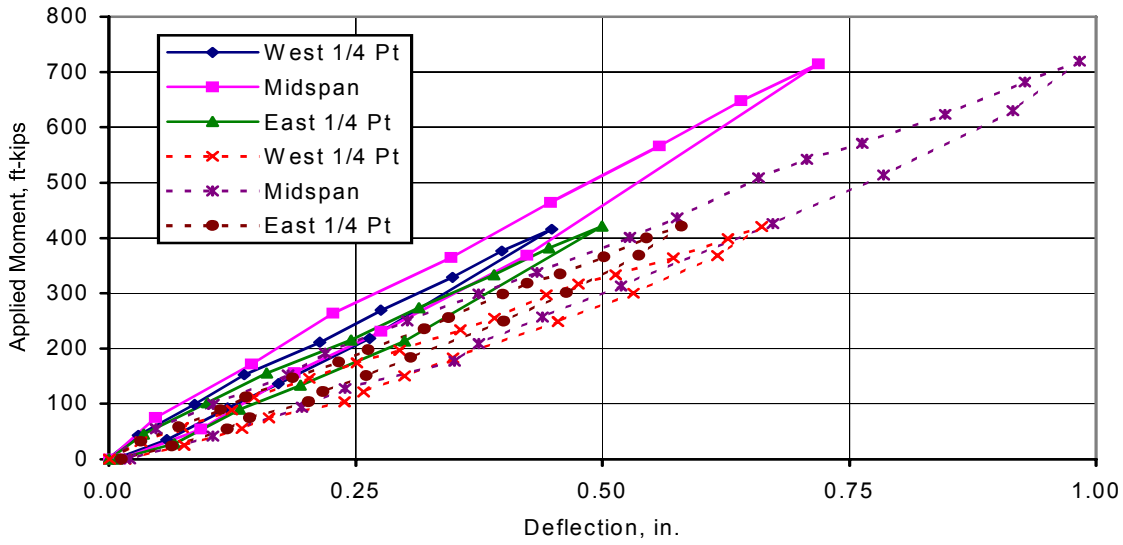


**Figure 5.37. Service Test 2 of Repaired Beam vs. Pre-Repair Service Test 5: Moment vs. Deflection.**

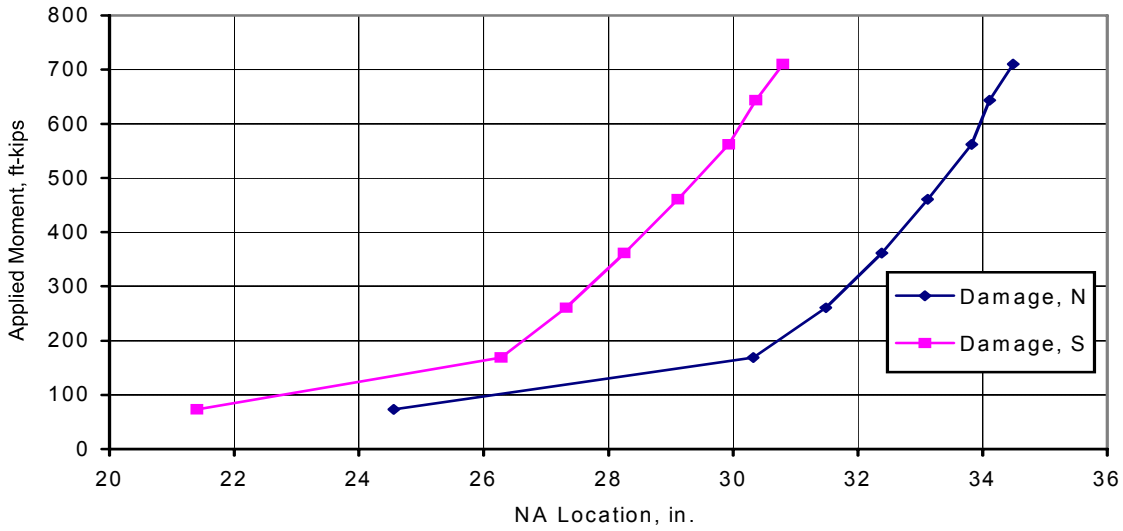


**Figure 5.38. Service Test 2 of Repaired Beam 2W: Applied Moments vs. NA Location.**

A comparison of the bottom flange concrete strains at the quarter points and midspan to those on the CFRP plates indicates excellent correlation. The concrete strains are similar to those recorded in the pre-repair tests however there is an appreciable reduction in the strain increment recorded in the strands in the damaged region. This is reasonable since in areas where the beam section is intact, the concrete in the bottom flange still carries tension. In the damaged region, the tension normally carried by the precompressed bottom flange, which was being carried solely by the intact strands, is now partially resisted by the CFRP plates. At a maximum test moment of 710 ft-kips, the change in strain in strand 6 was

measured to be +1,333 με (37,990 psi) as opposed to a range of +1,908 με (54,380 psi) during Service Test 5 of the damaged specimen under similar loads, a decrease of 30%. Under the service level design live load moment for this beam, 355 ft-kips, the range of stress is approximately 16.5 ksi. The AASHTO LRFD Specifications (Article 5.5.3.3) indicate that the stress range in prestressing strands/tendons be kept to less than 10 ksi for radii of curvature less than 10 ft. Since the damage in this beam is near the hold-down location where there is sharp curvature of the strand, this stress limit seems reasonable. Even in the repaired condition it appears that this section may be susceptible to fatigue under the theoretical live load and impact moment though no such evaluation was carried out. One should bear in mind however that the maximum strain/stress recorded in Beam 2W in-situ was +175 με (≈5 ksi) with two trucks in adjacent lanes, test L1&L2-P5. These two trucks cause a total moment applied to the span of approximately 1,300 ft-kips distributed among the beams in the cross-section. The effects of transverse live load distribution are apparently significant since the in-situ strains of +175 με due to a total span moment of approximately 1,300 ft-kips are only 13% those measured during the isolated beam test, +1,333 με, due to a total beam moment of 710 ft-kips. These findings are similar to those for Beam 1W which were previously discussed (See Section 5.1.1.1.1).

5.1.2.2.2. Ultimate Load Test

The load test to ultimate for Beam 2W was intended to demonstrate the strength increases possible through the use of bonded CFRP plates applied to the bottom flange. To determine the effectiveness of the repair, results from the baseline specimen, Beam 1W, are compared to the strengthened beam, Beam 2W.

At a load per actuator slightly more than 105 kips, a midspan/damaged region live load moment of 2,480 ft-kips, the beam failed catastrophically. This live load is in addition to a dead load moment at the midspan location of approximately 280 ft-kips. Although the failure of the beam was catastrophic, significant inelastic behavior and large deflections preceded the failure. The mode of failure is somewhat analogous to that observed in Beam 1W, failure of the beam directly under the west load point in the damaged region. At the time of failure, the overlay in this beam had partially debonded and spalled. However, this was not until the ultimate load was approached. Beam 2W completely collapsed at ultimate load. The failure was sudden so a primary cause of failure was not observed though it appeared from assessment of the beam following the test that a combined shear/compression failure occurred in the damaged region.

Figure 5.39 illustrates the vertical and inclined cracks that developed in the concrete and propagated through the unidirectional CFRP stirrup. A picture of the debonded overlay immediately preceding the collapse of the beam is presented in Figure 5.40. A photograph of the collapse at a point approximately 4 ft from midspan, directly under the west actuator is presented in Figure 5.41. Finally, Figure 5.42 illustrates the fracture of the CFRP stirrups and corresponding debonding of the longitudinal plates following collapse of the beam.

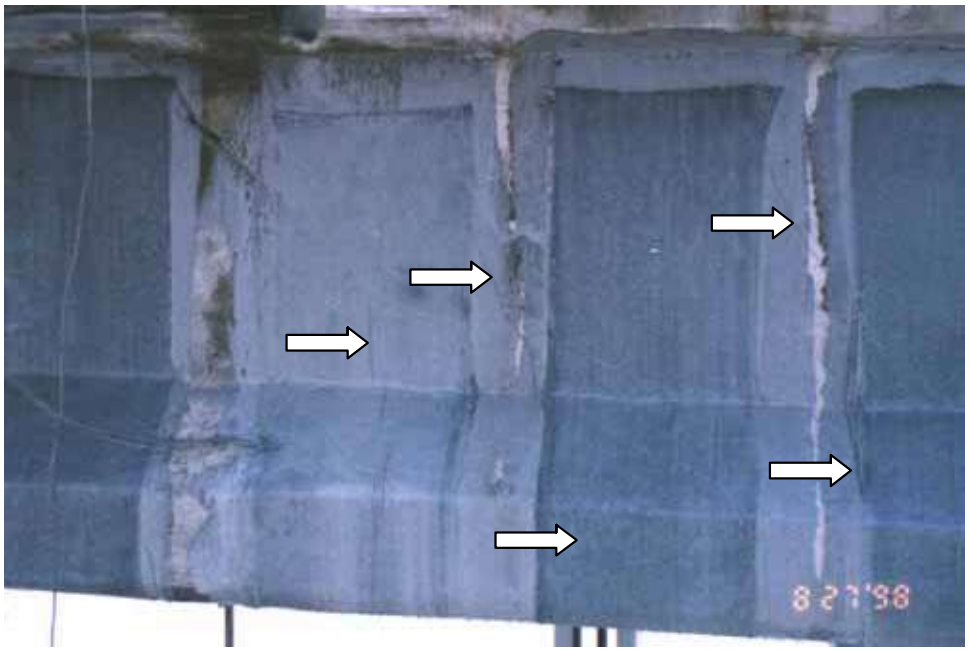


**Figure 5.39. Vertical/Inclined Cracks in FRP Stirrups in Previously Damaged Region of Beam 2W.**

**Figure 5.40. Debonded Overlay in Constant Moment Region of Beam 2W Near Ultimate Load.**

**Figure 5.41. South Face of Beam 2W West of the Midspan Diaphragm.**

**Figure 5.42. Fractured CFRP Stirrups and Debonded Plates Near Midspan of Repaired Beam 2W.**

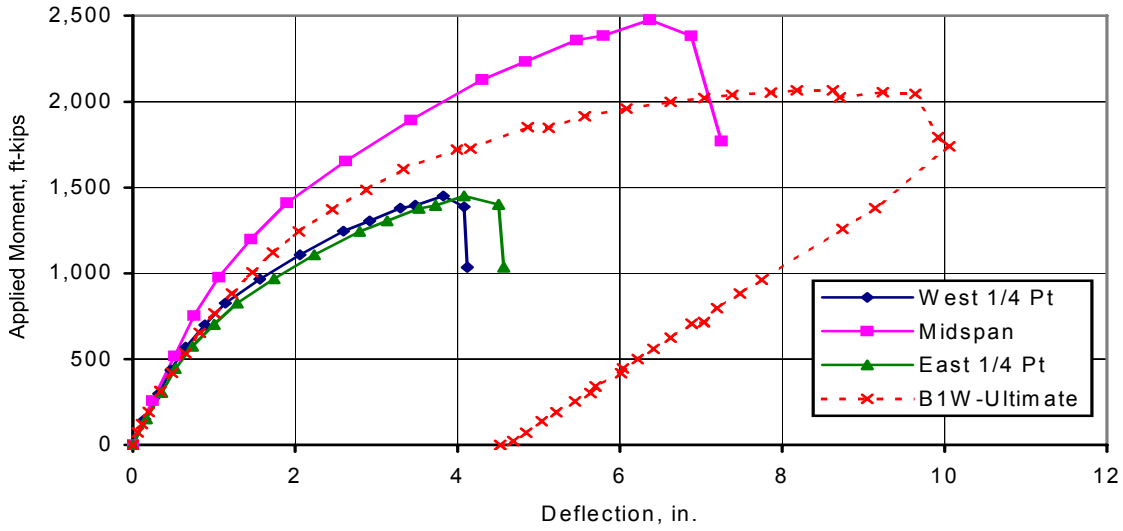


**Figure 5.43. Ultimate Load Test of Beam 2W: Applied Moment vs. Deflection.**

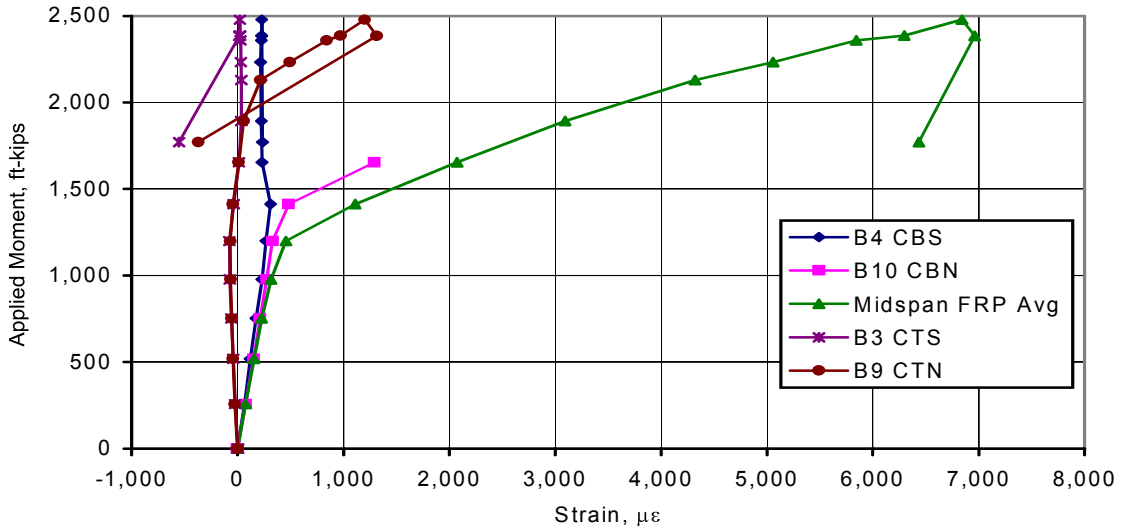


**Figure 5.44. Ultimate Load Test of Beam 2W: Response of Midspan Strain Gages.**

The moment vs. deflection behavior of Beam 2W and Beam 1W is presented in Figure 5.43. Due to the addition of the CFRP plates, a significant increase in strength was attained but at the expense of displacement ductility. However, as previously mentioned, there is still ample ductility in repaired Beam 2W.

The response of the midspan strain gages to the applied live load moment is illustrated in Figure 5.44. Strains in the CFRP were measured using six gages at midspan, two each on all three plates (See Figure 5.26b). The average of these six strain gages is plotted. The peak average strain in the CFRP was

measured to be +7,200 με, approximately 85% of the failure strain of the cured laminate described by Table 5.2. The composite stress in the laminate was computed to be 122,400 psi and the total force in the three plates, close to 147 kips. This is equivalent to the capacity of approximately 3.5, 1/2 in.ϕ, 270 ksi prestressing strands. Having only removed 2 strands from the section, this retrofit attained its design goal of replacing the lost tensile capacity of the damaged strands. A lesser amount of CFRP would have also achieved this objective and ensured a greater amount of displacement ductility.

Up to near collapse the longitudinal plates appeared to be well-bonded to the beam. The numerous external confinement stirrups were effective at ensuring bond between the plates and beam though numerous sounds were heard throughout the load test as the epoxy bonding the stirrups and plates to the beam cracked. Graphs of the strain in the CFRP provide additional insight into the failure of the beam. It appears that at maximum load, the plates begin to debond. This is evident by the decreasing strain in the plates following maximum load. Though not presented, the response of the CFRP strain gages at the quarter points is similar. The maximum strains in the quarter point CFRP gages prior to beam failure and plate slip are approximately +1,500 με, a stress of 25,500 psi.

Other useful data are available in the midspan strain plot. The response of the bottom flange bonded strain gages, B4 and B10, installed on the side of the concrete beam, is essentially the same as that of the CFRP gages until the concrete cracks in the vicinity of the gages. Cracking is apparent from the sharp knee in the moment vs. strain curve at an applied live load moment of approximately 1,300 ft-kips. When the tensile force resisted by the precompressed bottom flange is released due to the progression of cracks, a substantial portion of that force is absorbed by the longitudinal CFRP plates and the rest by the intact prestressing strands. The rapid increase of strain with applied moment is indicative of cracking.

The strains in the damaged region of Beam 2W are presented in Figure 5.45. As the figure illustrates, significant strain was recorded in gages S1, S2 and S3 on the remaining instrumented strand, Strand 6 (See Section 5.1.2.1 for location of strain gages), though the total stress in the strand is somewhat difficult to estimate since no accurate value of the effective prestress force is available. However, at strain levels this high, the strand has likely yielded. The maximum change in strain in the strands is reasonably close to that recorded in the CFRP plates.

The change in EI for the west quarter point is presented in Figure 5.46. The low load stiffness of this cross-section as well as the damaged region is enhanced by the presence of the CFRP plates as previously discussed. Similar to Beam 1W (see Figure 5.18 for details), there is a dramatic drop in stiffness at the onset of significant structural cracking.

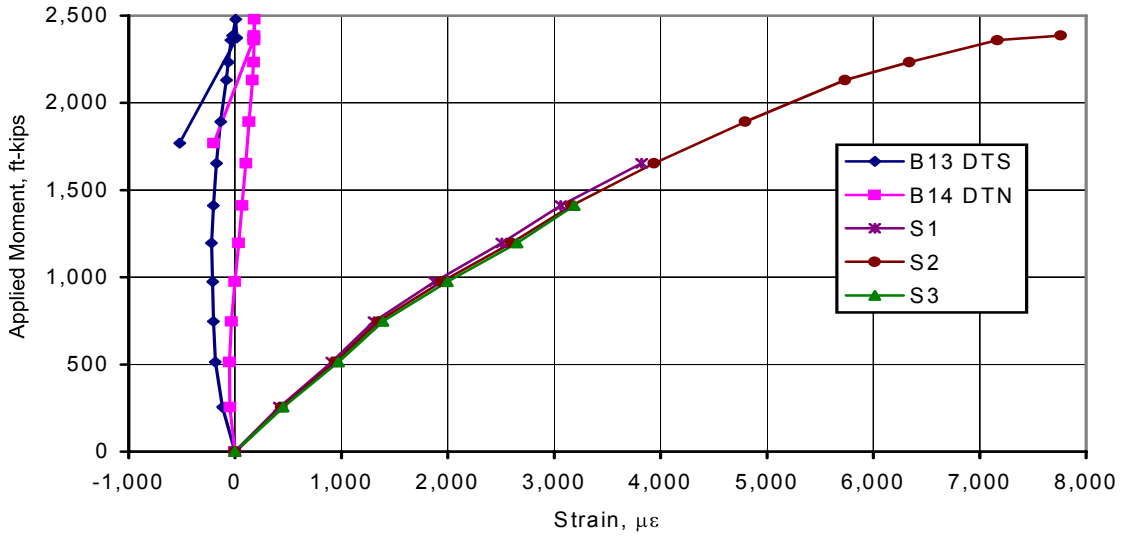


**Figure 5.45. Ultimate Load Test of Repaired Beam 2W: Moment vs. Strains in Damaged Region.**

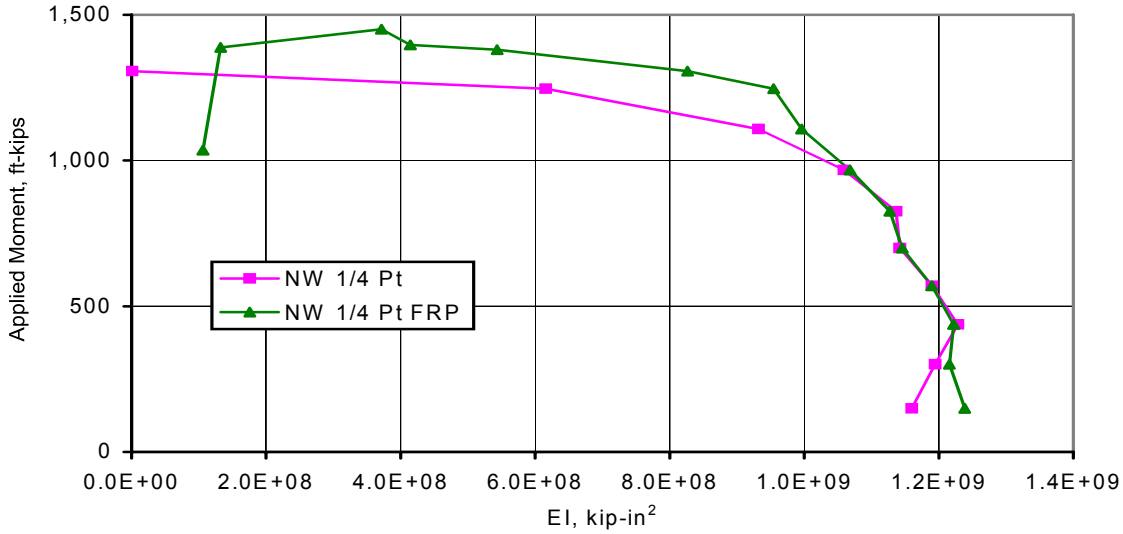


**Figure 5.46. Ultimate Load Test of Repaired Beam 2W: Change in EI, West Quarter Point.**

## *5.2. Summary of Beebeetown Beam Tests*

The results of a number of service and ultimate load tests have been described and compared. The reference specimen, Beam 1W, failed at a total dead and live load moment of 2,467 ft-kips. Failure was through combined shear and slab crushing. Beam 1W had two severed strands prior to the ultimate load test and one that partially ruptured during the test. An attempt to measure the effective prestress by severing a strand produced an effective prestress of 53,380 psi. This value is questioned due to the fluctuations in the strain readings after severing.

The experimental strength is higher than that predicted for a damaged beam. The experimental strength is also higher than that expected of an undamaged beam having all strands intact, discounting the overlay strength, and considering the material strengths to be of the specified values.

Under directly applied moments similar to those applied to a full span in the field, the experimentally recorded strain in the exposed strands and midspan deflection for the isolated beam are 13 to 14 times higher than recorded in-situ. This is a reflection of the significant load distribution in the damaged WB bridge.

Repaired Beam 2W was significantly stronger than Beam 1W. An increase in applied load of approximately 20% was attained. When the lesser dead load moment of Beam 2W, 280 ft-kips at midspan as opposed to 400 ft-kips for Beam 1W is considered, the total resisted moment for Beam 2W, approximately 2,760 ft-kips, is still 12% greater than that for Beam 1W. The effect of the CFRP on structural stiffness was minor except in the web damage region where large increases in stiffness were observed. The external carbon stirrups provided excellent confinement for the longitudinal plates. The longitudinal plates were efficiently used since at maximum moment they were stressed to 85% of their ultimate tensile capacity. The three plates carried a force equal to the strength of 3.5, 1/2 in.$\phi$, 270 ksi prestressing strands in a beam in which only 2 were originally removed.

The strains and deflection in the isolated beam are again much less than recorded in-situ when the moment in the isolated beam is equal to the moment applied to the entire test span. At a test moment of 655 ft-kips, the exposed strand strain and midspan deflection for Beam 2W were +1,540 $\mu\varepsilon$ and 0.82 in. prior to repair and +1,221 $\mu\varepsilon$ and 0.66 in. following repair when tested as an isolated beam. These reductions are on the order of 20%. The in-situ strain and deflection were measured to be +145 $\mu\varepsilon$ and 0.052 in., respectively. The dramatic difference between the in-situ and isolated beam test results is a reflection of the transverse live load distribution characteristics of the WB bridge.

## *5.3. ISU Model Bridge Beams*

Because it is somewhat difficult to quantify the amount of damage in Beams 1W and 2W that were removed from the Beebeetown bridge and because the beams had different geometric proportions, (i.e., different composite deck widths), the comparison of Beams 1W and 2W was complicated. Additionally, only the increase in strength of Beam 2W vs. Beam 1W could be determined; no beam was available to be tested in an undamaged condition. In order to obtain a more accurate “A” vs. “B” comparison of two beams, one damaged and one damaged and repaired, two of the beams from the model bridge described in Chapter 4 were tested.

### *5.3.1. Beam 1 – Control Specimen*

Beam 1 was part of the bridge model tested and discussed in Chapter 4 of this report. Beam 1 had never been damaged and was considered to be a "new" beam for all practical purposes. Beam 1 served as a baseline specimen that provided the stiffness and strength characteristics of an undamaged prestressed concrete beam.

Following completion of the bridge tests discussed in Chapter 4, the deck was sawn midway between Beams 1, 2 and 3 of the model bridge. Additionally, the deck was sawn transversely for its full depth in front of the abutment diaphragms. This created three "simply supported" beams with the exception that the beams themselves were still encased in the abutment diaphragm which was continuous for the width of the bridge. It should be noted that the abutment diaphragm and abutment footing were constructed using details similar to those used for integral abutment bridges. Additional details concerning the construction of the original bridge can be found in Abendroth, Klaiber and Shafer (1991) as well as Paradis (1998).

Following the cutting of the slab, Beam 1 was tested. Beam 1 was loaded with the actuators located 5 ft from the centerline of the beam. Pictures of the test configuration are presented in Figures 5.47 through 5.49. Since the reaction beams bear against the underside of the prestressed concrete beam, the loading system is self-contained. The beam can be considered for analytical purposes to be elastically restrained at the abutment by a spring of unknown stiffness. Such a model is depicted in Figure 5.50. The distance between the centerline of the beam bearing pads is 38 ft–4 in.

A number of tests were conducted on this beam. Two service load tests were conducted; in the first test, 25 kips per actuator was applied and in the second test, 84 kips per actuator was applied. At the conclusion of the second service test, no cracks were apparent. A subsequent test to 93 kips per jack was required to produce the first flexural cracks near midspan which was considerably greater than the load expected to cause cracking. This was due in part to the amount of end restraint and the increase in concrete strength over time. Based on the 28-day strength results obtained for the beam and slab concrete when the bridge was originally constructed, 7,270 psi and 5,400 psi respectively, the theoretical cracking moment was determined to be 860 ft-kips and the ultimate moment, 1,341 ft-kips. The point loads that will load the beam to cracking and ultimate load, respectively are 61 kips and 100 kips at each actuator if the beam is considered simply supported.

The live load vs. displacement plot for the cracking test is presented in Figure 5.51. The nonlinear behavior above a load of 80 kips is indicative of the onset of cracking. Because of the way the load frame hangs from the beam itself, Beam 1 has a dead load of approximately 6,300 lbs. at each actuator location prior to application of any actuator load. This load and its corresponding displacement are not reflected in the plots that follow. Load, displacement and strain values are only due to live loads. A photo of Beam 1 following the cracking test is presented in Figure 5.52.

**Figure 5.47. Actuator Placement for Beam 1 Load Test.**

**Figure 5.48. Self Contained Reaction Frame Under Beam 1.**

**Figure 5.49. Bearing of Self-Contained Frame on the Bottom of Beam 1.**

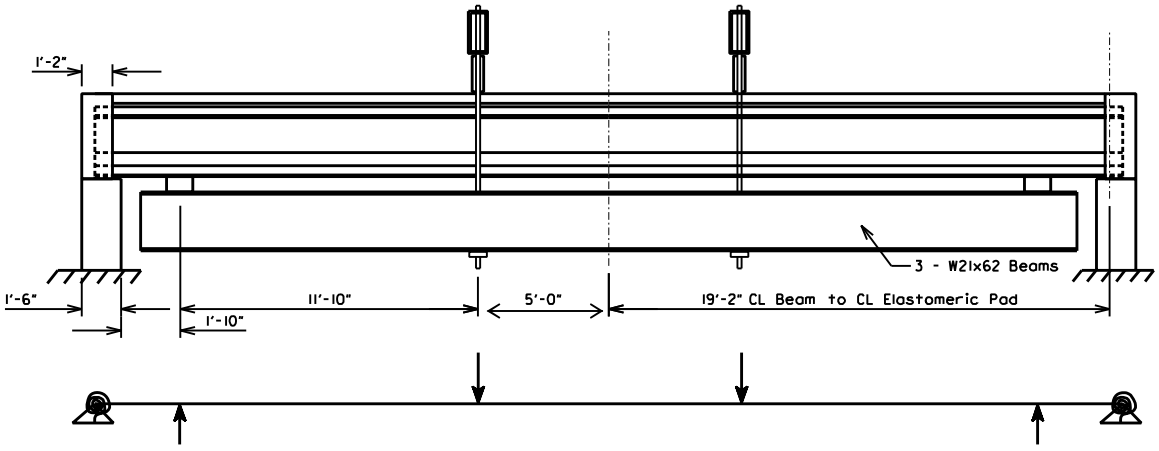


**Figure 5.50. Schematic and Boundary Conditions for Beam 1 Loading.**

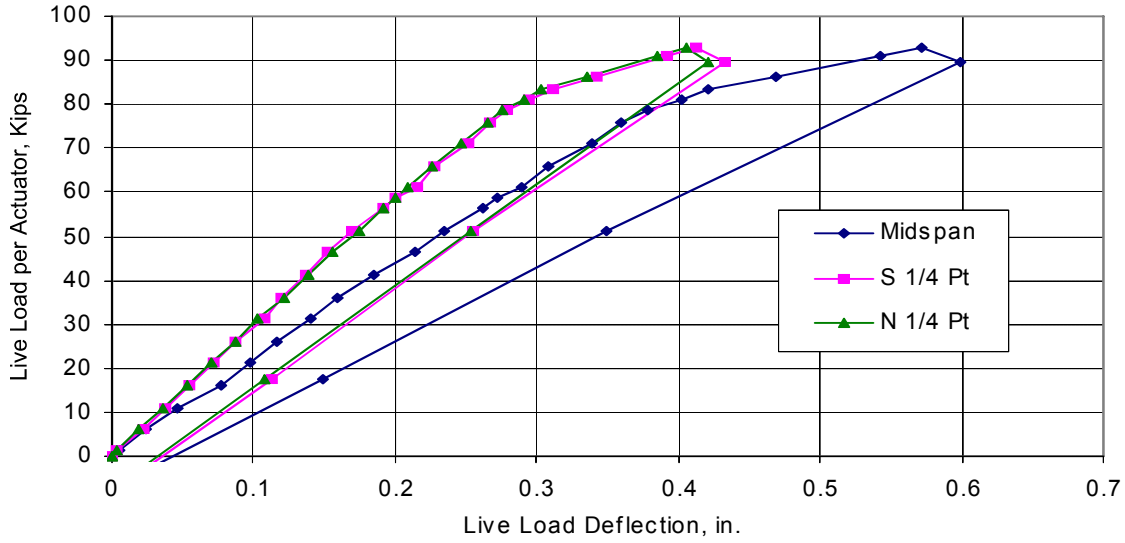


**Figure 5.51. Beam 1 Cracking Test: Load per Actuator vs. Live Load Displacement.**

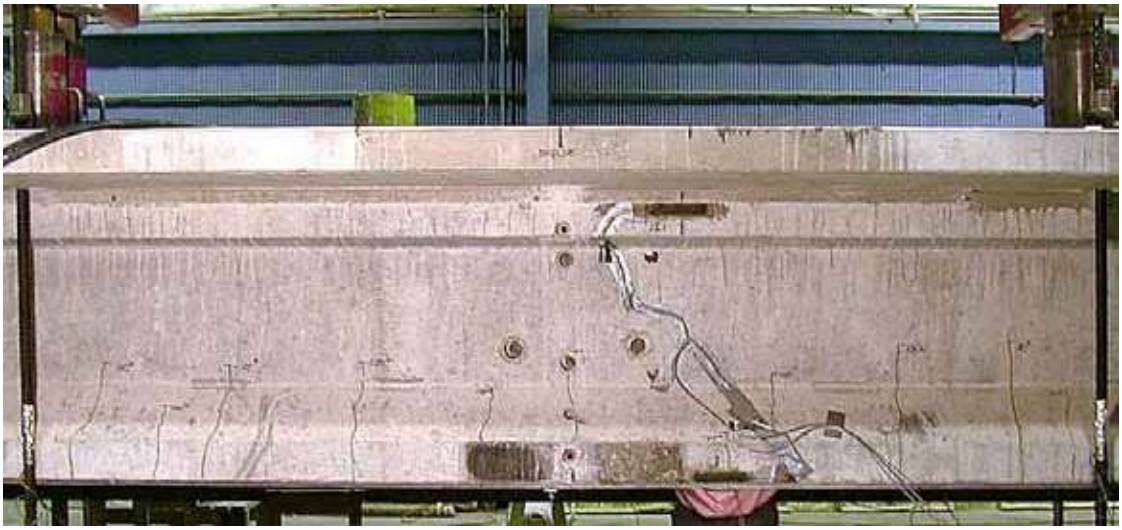

**Figure 5.52. Crack Patterns at 100 kip Total Load Following the Beam 1 Cracking Test.**

The cracks in the beam were marked as depicted in Figure 5.51. The crack pattern is vertical as expected in a region of constant moment/zero shear. There were no cracks outside of the constant moment region. The cracks are fairly constant in length, terminating slightly above the flange to web chamfer. This is an approximate location of the neutral axis of the section under the prescribed loading. The crack terminates slightly below the neutral axis of the internal stress distribution, not to be confused with the centroid of the composite section that resists the actuator loads. Although concrete carries some tension, for all practical purposes the crack tips can be considered to define the neutral axis. The crack spacing

primarily coincides with the spacing of the vertical stirrups in the section. This is consistent with the findings of others in that vertical crack spacing is strongly correlated to the stirrup locations.

Using the strain profile through the depth of the beam, the neutral axis for live loads was computed and found to not vary at the quarter points throughout the cracking load test. The neutral axis locations under live load at the north and south quarter point were an average of 19.5 in. throughout the entire test. The neutral axis location at midspan varies from approximately 18 in. to 21 in., rising throughout the test. An average of 19.8 in. is found for the midspan neutral axis location throughout the test, which is similar to the location at the quarter points. The upward movement of the neutral axis indicates the section was cracked prior to testing. This is reasonable since prior to the test described herein, a series of increasing load service tests were conducted, the maximum live load being 84 kips in the final service test. Though no cracks were visible during these service tests, examination of subsequent test data indicates that the midspan region appears to be cracked prior to the "cracking" test. Paradis (1998) determined a neutral axis location under live loads of 22.71 in. for the same beam prior to the bridge model being separated into individual beams. The lower neutral axis in the separated condition is consistent with the smaller effective flange width of isolated T-beams.

To quantify the amount of end fixity in this beam due to encasement of the beam end in the abutment diaphragm, several different approaches were employed. The experimental results from Service Test 2, prior to the onset of cracking, were used in these analyses. The deflection of the beam with 60 kips at each load point was computed using the STAAD-III program assuming simply supported, fully fixed, and partially restrained end conditions. The partially restrained conditions simulate the presence of an end moment that is some percentage of the fixed end moment. In order to compute the deflections, the EI of the beam is required. Using an average neutral axis value for the quarter points and the midspan region of 19.8 in., an effective slab width was computed to be 27.4 in. The transformed effective width is 26.3 in. using compression strength results from 28-day strength tests to compute a modular ratio, $E_{beam}/E_{slab}$, of 1.04. For an isolated T-beam, AASHTO recommends that $b_{eff}$ be less than the web width plus an additional $4t_s$ where $t_s$ is the thickness of the slab, 4 in. for this beam. For rigid top flange beams such as prestressed I-beams, the web width may be interpreted as the top flange width, in this case, 13 in. A resulting $b_{eff}$ of 29 in. is computed using this flange width, 6% greater than measured. However, an additional AASHTO restriction states that the slab thickness must be at least 50% of the flange width which is not true for this beam. A modified effective web could be considered equal to $2t_s$, or 8 in. Thus a predicted effective slab, $b_{eff}$, equals 8 in. plus $4t_s$, or 24 in. total, 23% less than the experimental value. The experimental value of 27.4 in. is bounded by these two scenarios. Using the computed value for $b_{eff}$ results in a moment of inertia of the transformed composite section of 76,550 $in^4$. The transformed composite section has a modulus of elasticity of 4,411 ksi using the formula $E = 1{,}000{,}000 + 40{,}000\sqrt{f_c'}$ and 7,270 psi for the 28-day beam compressive strength; EI is thus computed to be approximately $338 \times 10^6$ kip-$in^2$.

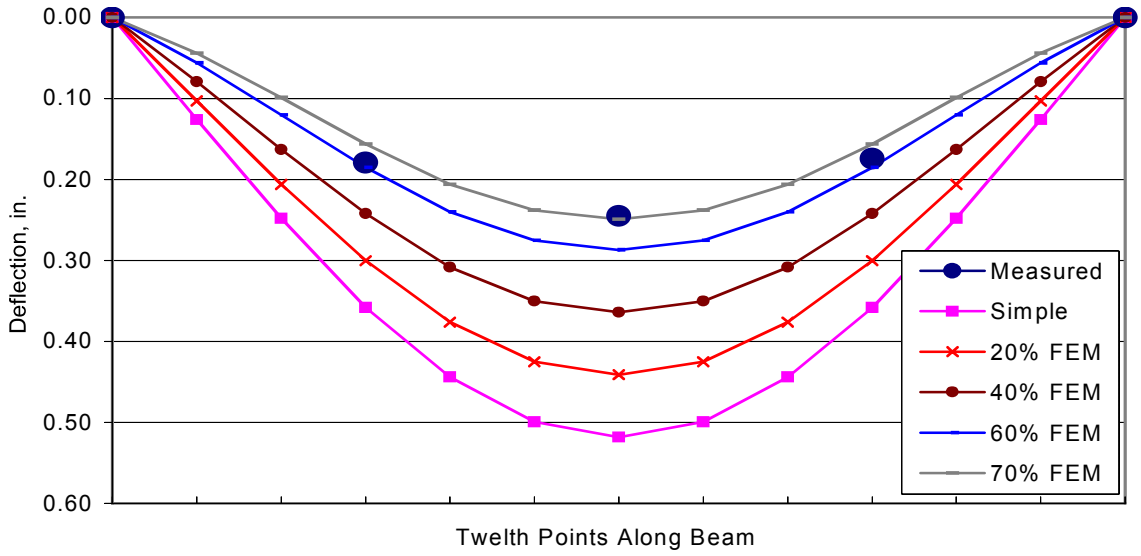


**Figure 5.53. Analytical and Measured Deflections Along Beam 1, 60 Kips per Actuator.**

The deflections at the 1/4 point and midspan with a load of 60 kips at each actuator and this value of EI are 0.36 in. and 0.52 in. presuming simply supported conditions and 0.07 in. and 0.14 in. presuming full end fixity. The measured values are 0.18 in. and 0.25 in. The measured and computed data are presented in Figure 5.53. Using the measured deflection values, one finds that the measured quarter point and midspan deflections correspond to fixity estimates of between 60% and 70%. Paradis (1998) found that the beam end fixity was on the order of 50% prior to the sawing of the slab in the longitudinal and transverse directions. It is unreasonable to expect that fixity of the beam ends increased after transverse and longitudinal sawing of the slab so the fixity estimates presented above have some experimental error associated with them. This error was later determined to be in the EI value. During subsequent tests of these beams as true simply supported specimens, with a known applied moment and measured curvature, an EI of approximately $560 \times 10^6$ kip-in$^2$ was determined, an increase over that previously calculated of 66%. The source of this increased stiffness is likely due to the poor estimation of E. The theoretical value for E used in the prior calculations was based on 28-day strength results from concrete cast in the early 1990's. The concrete strength, and henceforth E, have certainly increased since that time. Additionally, the formulas for predicting E for concrete are subject to a wide scatter. Both of these sources of error contribute to the poor estimation of the structural stiffness.

Predicted deflections for various degrees of end restraint using the measured EI value of $560 \times 10^6$ kip-in$^2$ are presented in Figure 5.54. Using the experimentally determined EI value as an improved estimate, the recorded deflections of the beams agree with a lower assumed end restraint provided by the abutment, somewhere between 20% and 30%. This is reasonable since the restraint should be lower than when the beams were interconnected by the slab, determined by Paradis (1998) to be approximately 50%.

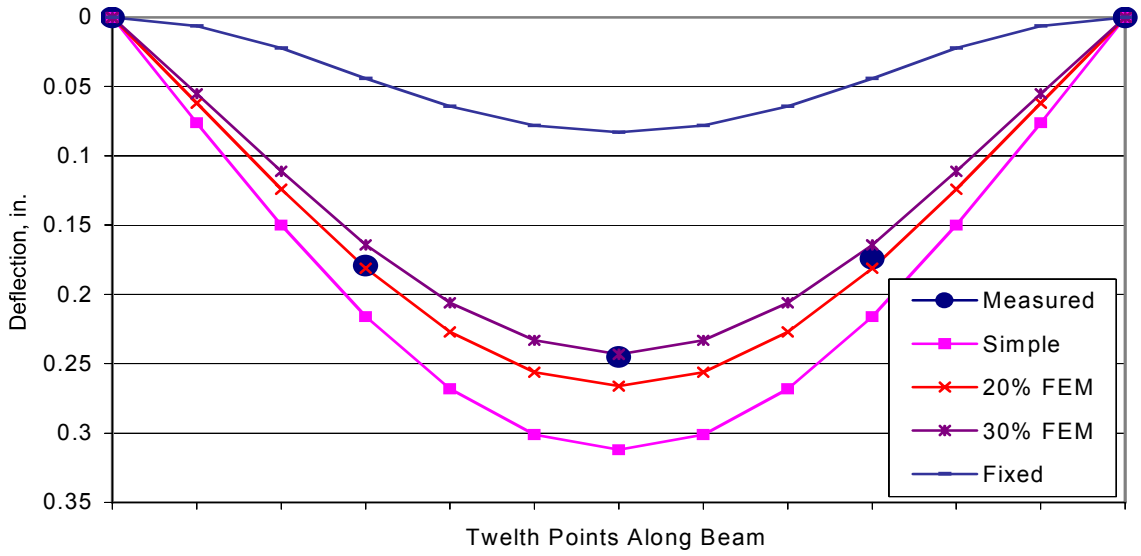


**Figure 5.54. Measured vs. Predicted Deflections Along Beam 1 Using Experimental EI Value.**

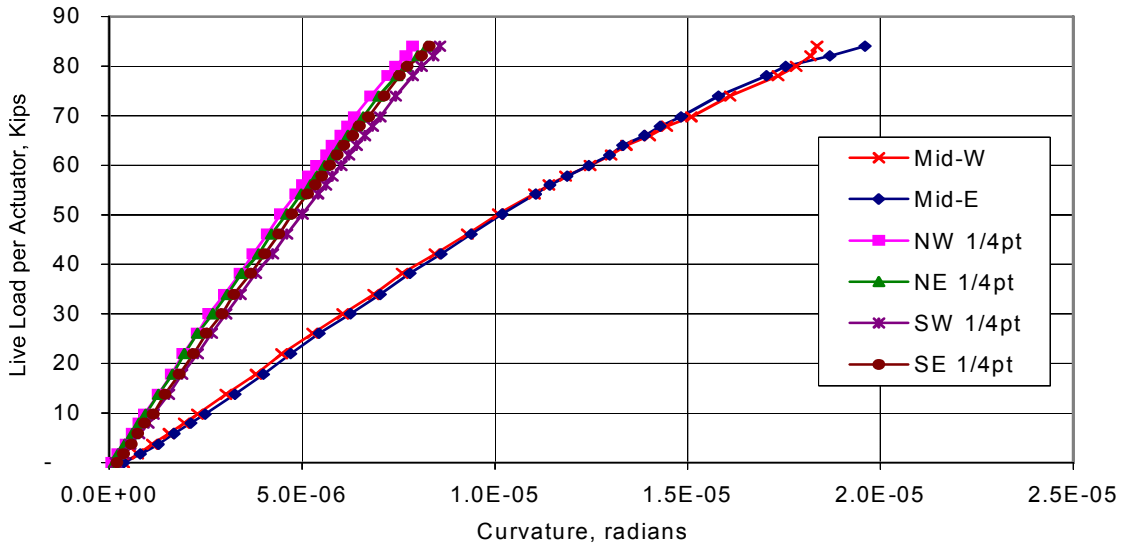


**Figure 5.55. Actuator Load vs. Measured Curvature, Beam 1.**

As an alternate means of determining fixity, the moment-curvature relationship can be used to establish the degree of rotational restraint at the abutments. The ratio of applied moments at midspan to the quarter point can be expressed directly as the ratio of the measured curvatures presuming EI is a constant at both locations. The assumption of a constant EI is reasonable up to cracking. For Beam 1, the ratio of the midspan curvature to the quarter point curvature is approximately 2.1:1 until the applied load exceeds 60 kips. The relationship between the applied load and the measured curvature is presented in Figure 5.55 for

Service Test 2. The ratio of midspan to quarter point moment (curvature) is 1.6:1 for simple support conditions and 9.4:1 for fixed end conditions. A ratio of 2.1:1 corresponds to an end moment that is approximately 50% of the fixed end moment for the prescribed loading condition. This is a substantially higher estimate than that based on the magnitude of the deflections. However, the different approaches, though yielding dissimilar results, indicate that there is some end restraint in the bridge model.

Following the cracking test, an ultimate load test was conducted. During this test, which proved to be unsuccessful, the self-contained load frame failed at an actuator load of approximately 106 kips each. At this point, the beam was heavily cracked as depicted in Figure 5.56. The dotted line crack marks on the beam indicate the progression/development of existing/additional cracks during the ultimate load test.

In Figure 5.57, the load vs. deflection results from the cracking test are presented as dashed lines and those from the ultimate test as solid lines. The figure indicates the expected difference in the ultimate test and cracking test results due to the opening of a number of the existing cracks and the development of additional cracks.

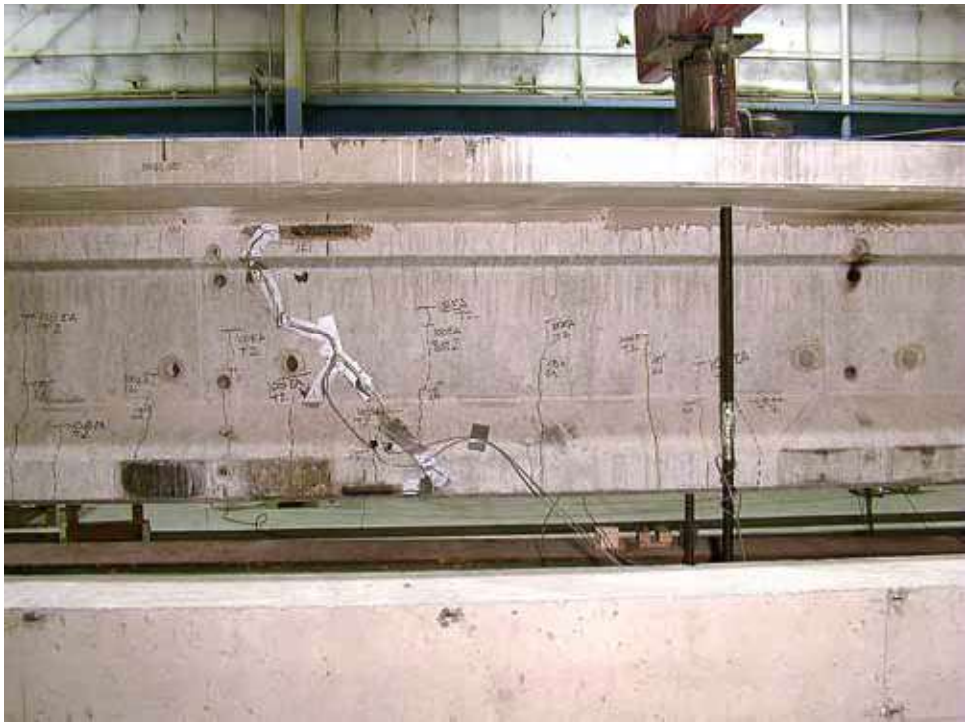

**Figure 5.56. Beam 1 Crack Patterns Following the Unsuccessful Ultimate Load Test.**

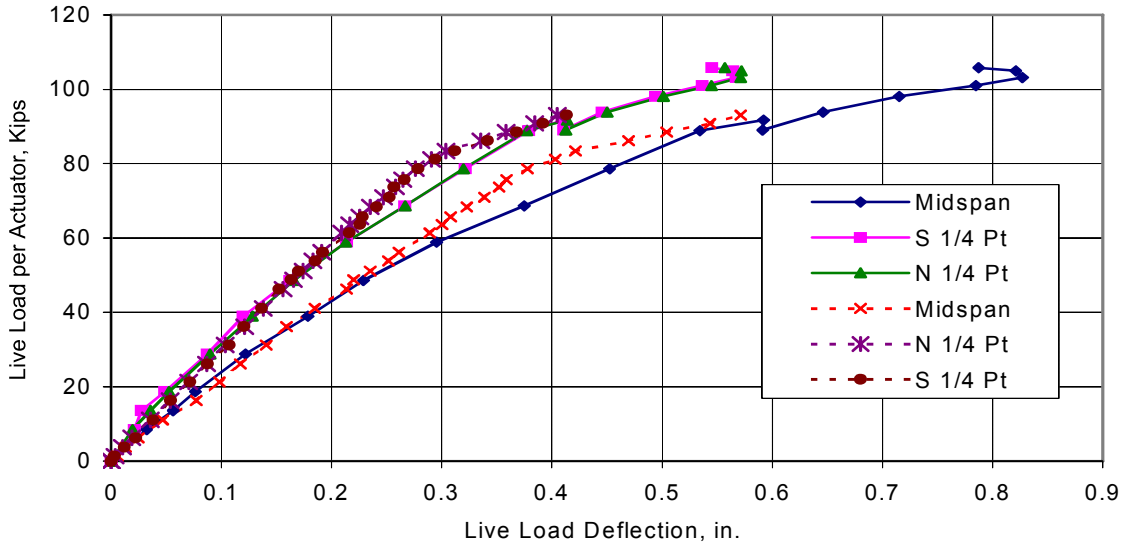


**Figure 5.57. Ultimate Load vs. Cracking Test, Beam 1: Applied Load vs. Deflection.**

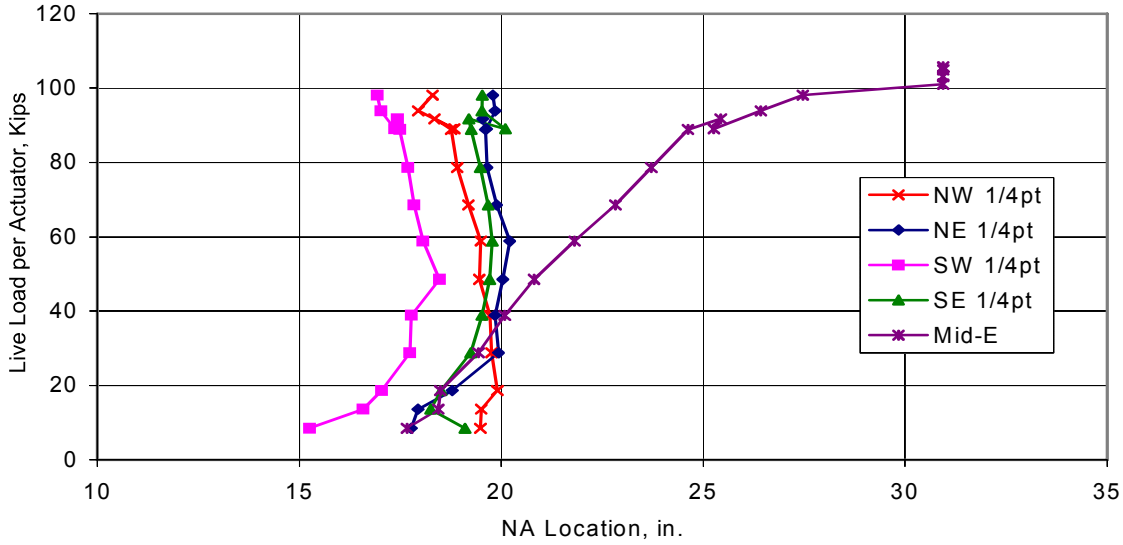


**Figure 5.58. Ultimate Load Test of Beam 1: Applied Load vs. NA Locations.**

The neutral axis locations at midspan and at the quarter points are presented in Figure 5.58. The neutral axis is relatively unchanged at the quarter points while it rises significantly at midspan. This is consistent with the location and degree of cracking observed in the beam during testing.

Because this beam could not be tested to failure at the laboratory facility in which it was located, Beams 1 and 2 were removed from the bridge model and transported to the ISU Structures Laboratory. In removing the beam from the model and testing it in the lab, a true simply supported condition would be obtained and the beam could be loaded to failure.

Following the removal and transportation of Beam 1 to the ISU Structures Laboratory, the beam was tested two additional times. Because of the change in restraint conditions and loading patterns, it is not possible to make a direct comparison of the results from the bridge model tests to those conducted on the isolated specimens. The beam tests prior to removal of the beams from the bridge model abutments used a self-contained load frame that applied equal but opposite point loads to the beam while the simply supported specimen only has two equal point loads applied to the deck. In the bridge model load tests, loads were applied 5 ft on either side of the centerline while in the ISU Structures Laboratory, loads were applied 4.5 ft from center creating a 9 ft long constant moment region.

Before the beam was tested, it was covered with a thin coat of plaster to cover the existing cracks and labels on the beam. The plaster coating allows an easier detection of cracks in the beam. The first test on Beam 1 was to apply a sufficient amount of load so that some of the preexisting cracks would open. At this point, the cracks were marked and the beam unloaded. Several representative plots of the behavior of the beam during this test are presented in Figures 5.59 through 5.65.

Figure 5.59 presents the applied moment vs. deflection response for this beam. The presence of preexisting cracks is evident in the nonlinear response of the section. At the peak moment, the actuator loads were approximately 52 kips each. Though not an exact comparison to the previous bridge model tests due to previously mentioned changes in restraint and load pattern, a comparison of Beam 1 tested as part of the bridge model, Figure 5.57, and the aforementioned simply supported specimen, Figure 5.59, reveals significant differences in deflection at similar actuator loads. This is further confirmation of the presence of end restraint in the bridge model.

The opening of the cracks is confirmed by the variation in neutral axis depicted in Figures 5.60 and 5.61. An upward moving neutral axis is indicative of a cracked section with significant crack openings and the creation of additional cracks at a midspan moment in excess of 500 ft-kips. To determine the neutral axis location for the south side of Beam 1, labeled SC in Figure 5.60, the strain gages on the top flange and top of slab were used for live load moment in excess of 500 ft-kips since the bottom flange gage was adversely affected by the presence of the cracks. The nonlinearity of the strain distribution above a live load moment of 500 ft-kips is evident in the stain profiles of Figure 5.61. The strain profiles are more accurately drawn once the cracks open by connecting the slab and top flange gages with a straight line and extrapolating to a zero strain value. The moment vs. curvature response for midspan is presented in Figure 5.62 and follows the same trend as the variation in deflections and neutral axis location at midspan.

Figures 5.63 through 5.65 refer to the uncracked quarter points. A slight variation in the neutral axis location from the original bridge model tests is noted. The average neutral axis location for the three tightly grouped series is 21.1 in. throughout the entire load range. This is compared to 19.8 in. for the beam while still in the bridge model. The moment of inertia for a section having its live load neutral axis at 21.1 in. from the bottom fiber is 85,790 $in^4$ and the composite area is 491 $in^2$.

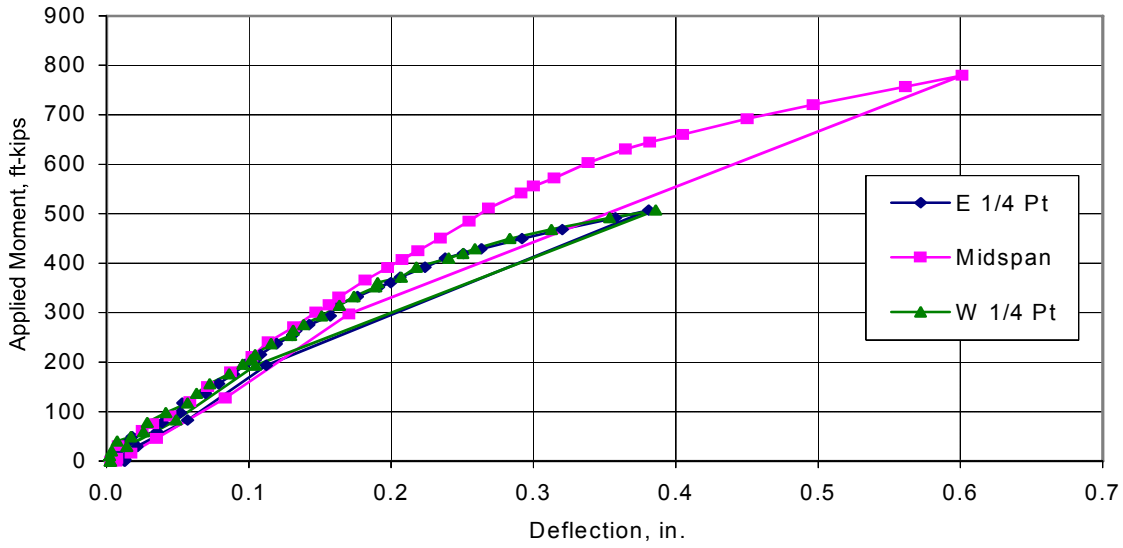


**Figure 5.59. Service Test of Cracked Beam 1: Applied Moments vs. Deflection.**

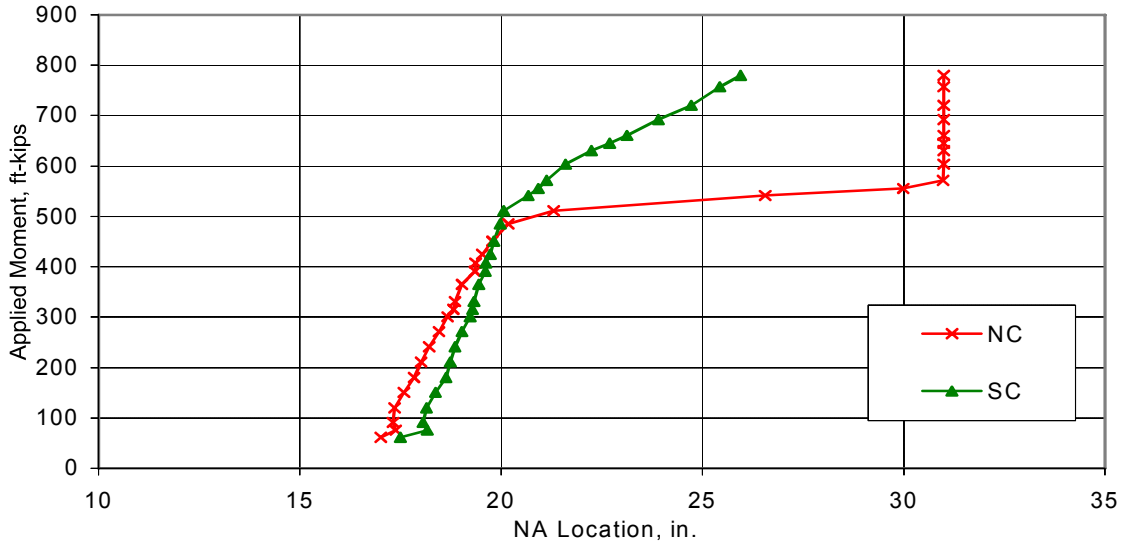


**Figure 5.60. Service Test of Cracked Beam 1: Applied Moment vs. Midspan NA Location.**

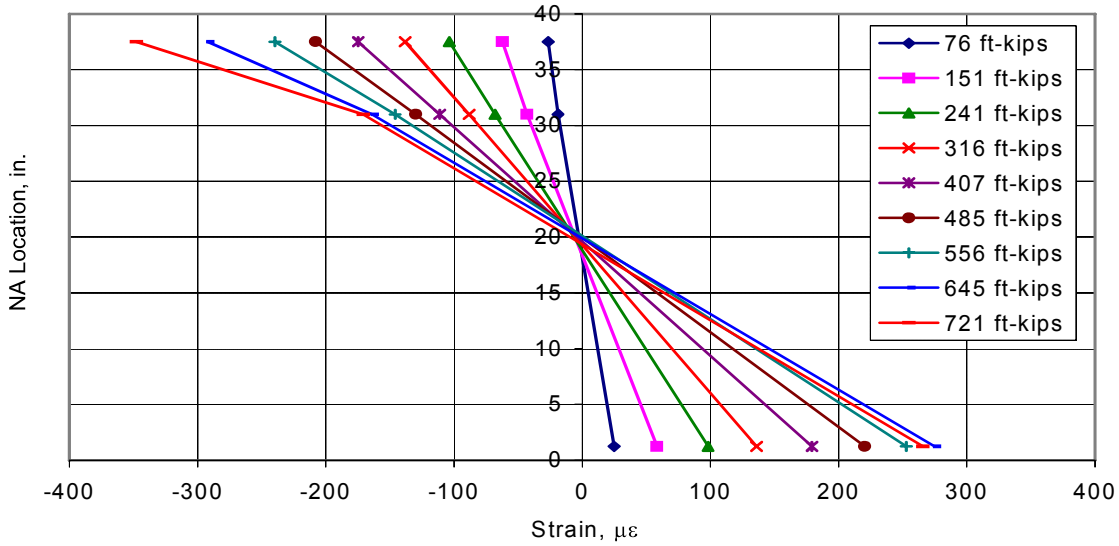


**Figure 5.61. Service Test of Cracked Beam 1: Midspan Strain Profiles.**

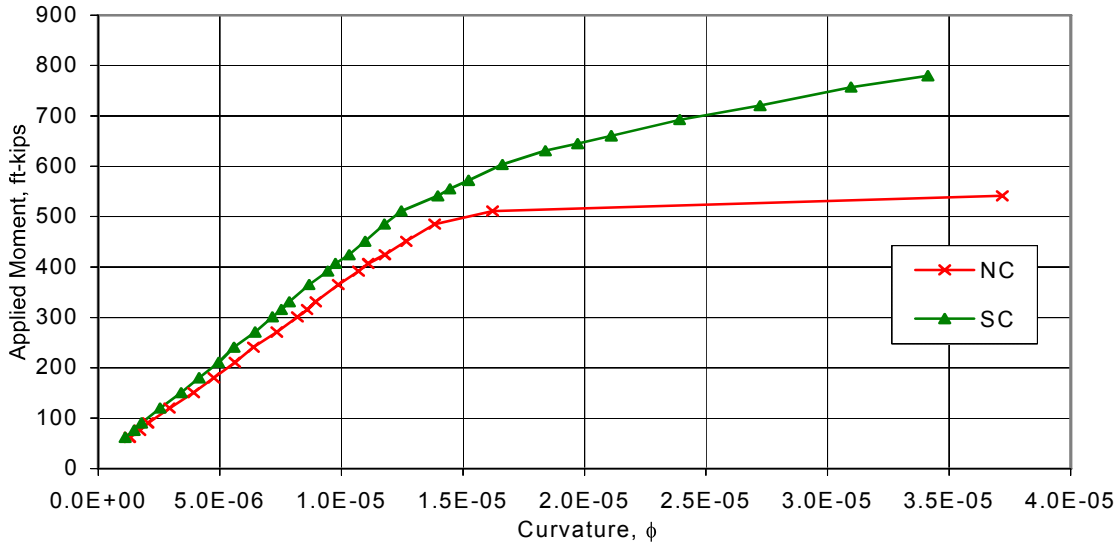


**Figure 5.62. Service Test of Cracked Beam 1: Midspan Moment vs. Curvature.**

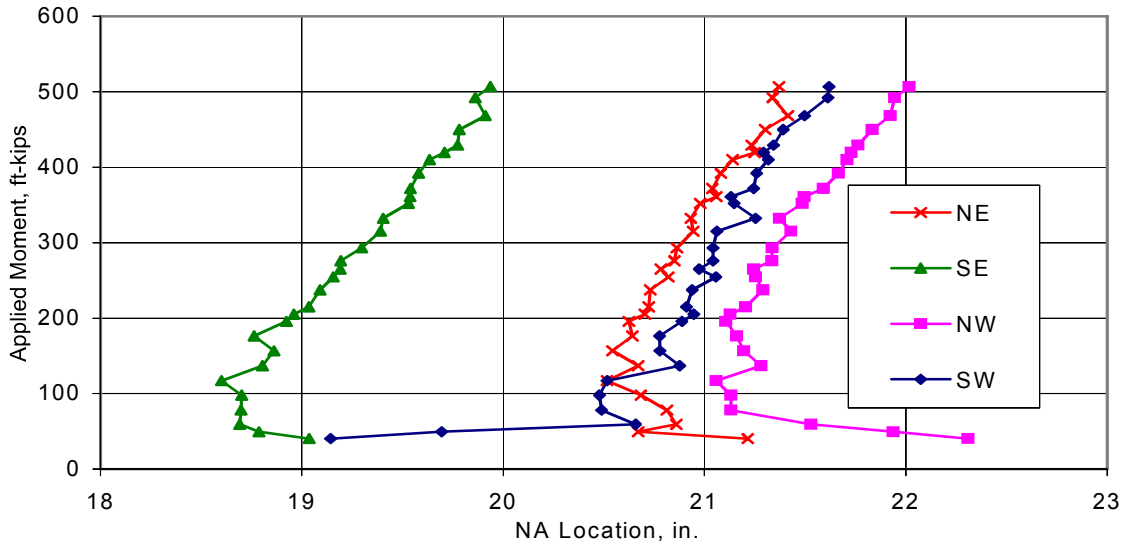


**Figure 5.63. Service Test of Cracked Beam 1: Moment vs. NA Location at Quarter Points.**

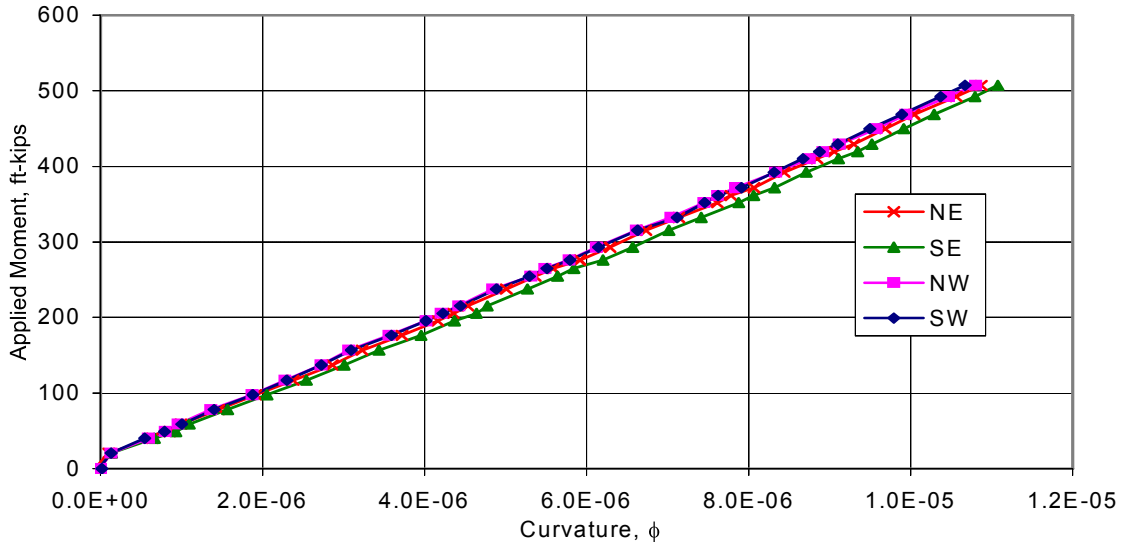


**Figure 5.64. Service Test of Cracked Beam 1: Applied Moment vs. Quarter Point Curvature.**

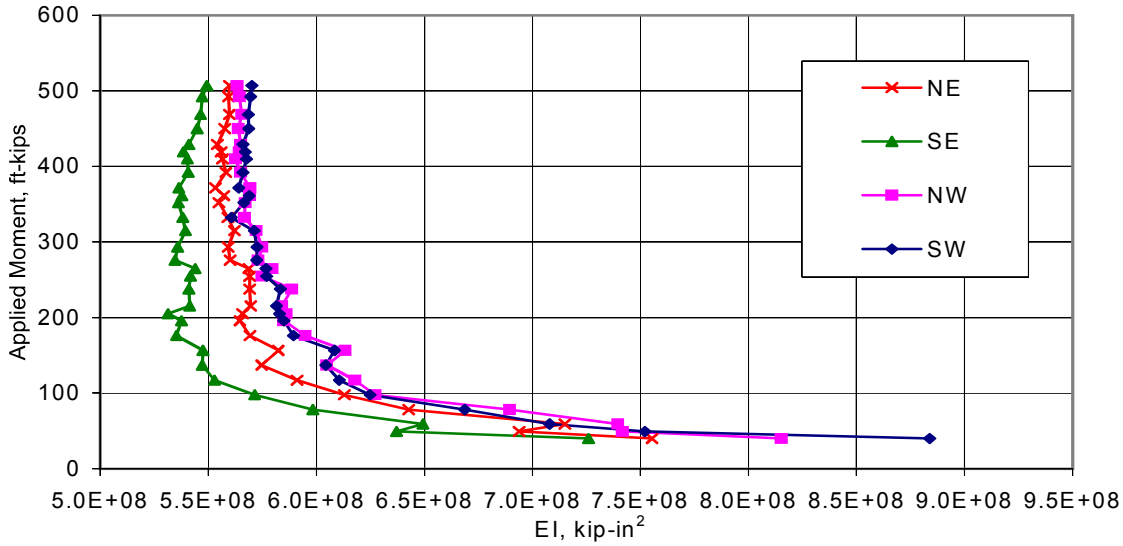


**Figure 5.65. Service Test of Cracked Beam 1: Moment vs. EI.**

Figure 5.64 presents the moment vs. curvature response at the quarter points for Beam 1 in the simply supported condition. The response is linear throughout the entire test indicating no change in the effective EI during the test. This is an indication of uncracked behavior. This confirms an earlier assumption that the ratio of curvatures could be assumed to be the ratio of applied moments at different locations along the beam. From the relationship, $\phi$=M/EI, with both M and $\phi$ known, the effective EI can also be computed. Results from such a computation are presented in Figure 5.65.

In Figure 5.65, the measured curvatures at the uncracked quarter point are used in conjunction with the known applied moment to compute an experimental EI, approximately $5.6 \times 10^8$ kip-in$^2$. This is significantly different than the theoretical EI value, $3.38 \times 10^8$ kip-in$^2$. The measured value is 65% greater than the theoretical value. Though not presented until later in this chapter (see Section 5.3.2.2), the measured EI value of Beam 2 in the area where it was neither damaged nor strengthened is also $5.6 \times 10^8$ kip-in$^2$. Thus, the much higher value for EI than theoretically calculated is credible and repeatable in different beams and in different tests on the same beam.

Following the crack reopening test, an LVDT (linear voltage displacement transducer) was installed across one of the existing cracks near midspan to detect the reopening of the crack. The LVDT was installed on the vertical face of the bottom flange approximately 2 in. above the extreme bottom fiber. Crack reopening is a reliable means of determining the effective prestress in the beam. Although a specimen may be cracked, until a sufficient amount of load is applied to overcome the compressive stresses due to prestress, the crack remains closed and the beam behaves as an uncracked specimen. Once the precompression is overcome, the crack reopens. The load at which the rate of crack opening significantly changes, the crack reopening load, is then used to determine the effective prestress. The applied moment

vs. crack opening displacement is presented in Figure 5.66. The moment at which the crack opens is then used in the following formula to determine the effective prestressing force. The procedure is similar to that used by Pessiki et al (1996) except that their work was on a noncomposite beam.

$$-\frac{P}{A_{N/C}}-\frac{P\,e\,y_{N/C}}{I_{N/C}}+\frac{M_{SW}\,y_{N/C}}{I_{N/C}}+\frac{M_{LL}\,y_C}{I_C}-\left\{\frac{\left[\frac{M_{LL}\,y_{LL}}{I_C}\right]n\,A_{ps}}{A_C}\left(1+\frac{e_C\,y_C}{r_C^2}\right)\right\}=0 \qquad (5.3)$$

where:

| | | |
|---|---|---|
| $P$ | = | Force in prestressing strands |
| $A_{N/C}$ | = | Area of non-composite beam |
| $I_{N/C}$ | = | Moment of inertia of non-composite beam |
| $y_{N/C}$ | = | Distance from non-composite centroid to the fiber of interest |
| $e$ | = | Prestressing strand centroid eccentricity from centroid of non-composite beam |
| $A_c$ | = | Area of composite beam |
| $I_C$ | = | Moment of inertia of composite beam |
| $y_C$ | = | Distance from composite centroid to the fiber of interest |
| $e_C$ | = | Prestressing strand centroid eccentricity from centroid of composite beam |
| $r_c$ | = | Radius of gyration of the composite section |
| $n$ | = | $E_{strand}/E_{beam}$ |
| $A_{ps}$ | = | Total area of prestressing strands |
| $y_{LL}$ | = | Distance from centroid of composite section to centroid of strands |
| $M_{SW}$ | = | Self-weight (non-composite) moment |
| $M_{LL}$ | = | Moments applied to the composite section |

For the terms involving the effect of the initial prestressing force, the geometric properties are that of the noncomposite (N/C) beam since the prestressing force acts on this section alone. Stress acting on the composite section are denoted with a (C). The first three terms relate to the stresses prior to composite action. The fourth term is the effect of live loads acting on the composite section. Finally, the bracketed term is the change in compressive stress in the concrete that occurs due to elongation of the strands under load. The bracketed term is an expanded version of the familiar equation for stress due to prestressing:

$$f=\frac{P}{A}\left(1+\frac{ey}{r^2}\right) \qquad (5.4)$$

Examining Figure 5.66, the crack reopening moment was determined to be 580 ft-kips. This is in addition to a dead load moment of 118 ft-kips due to the beam, slab and haunch at midspan. The total moment is therefore 698 ft-kips. Using the equation (5.3), along with $A_{N/C}$=326 in.$^2$, $I_{N/C}$=36,336 in.$^4$, $y_{N/C}$=12 in., e=5.98 in., $A_c$=491 in.$^2$, $I_c$=85,790 in.$^4$, $y_c$=19.1 in., $e_c$=13.03 in., $r_c$=174.7 in.$^2$, n=6.46, $A_{ps}$=2.295 in.$^2$, $y_{LL}$=19.1 in., $M_{SW}$=118 ft-kips, and $M_{LL}$=580 ft-kips, the effective prestressing force, P, can be determined to be 378 kips.

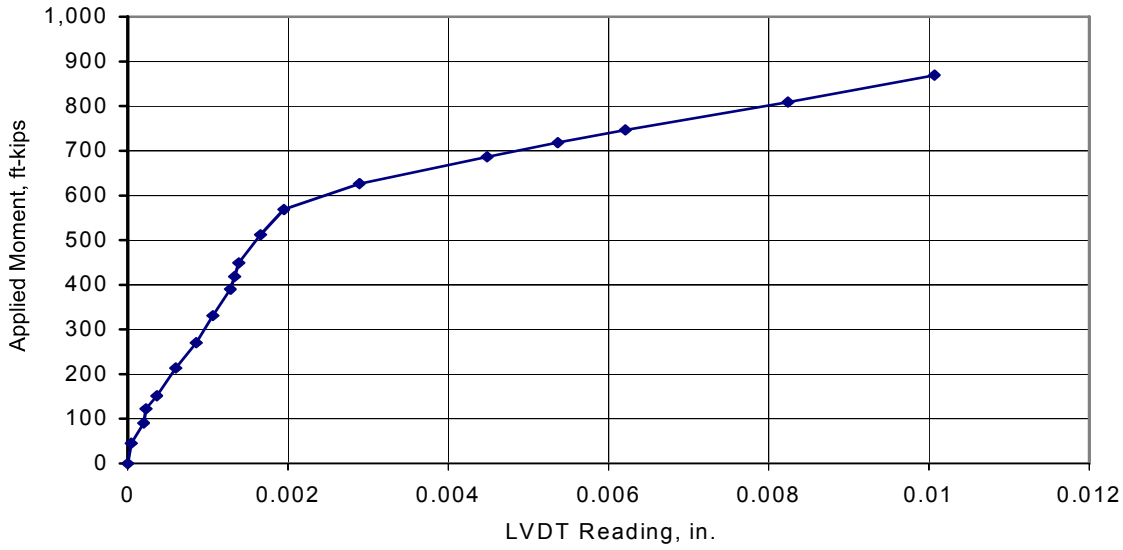


**Figure 5.66. Applied Moment at Midspan vs. Crack Opening Displacement, Ultimate Test of Beam 1.**

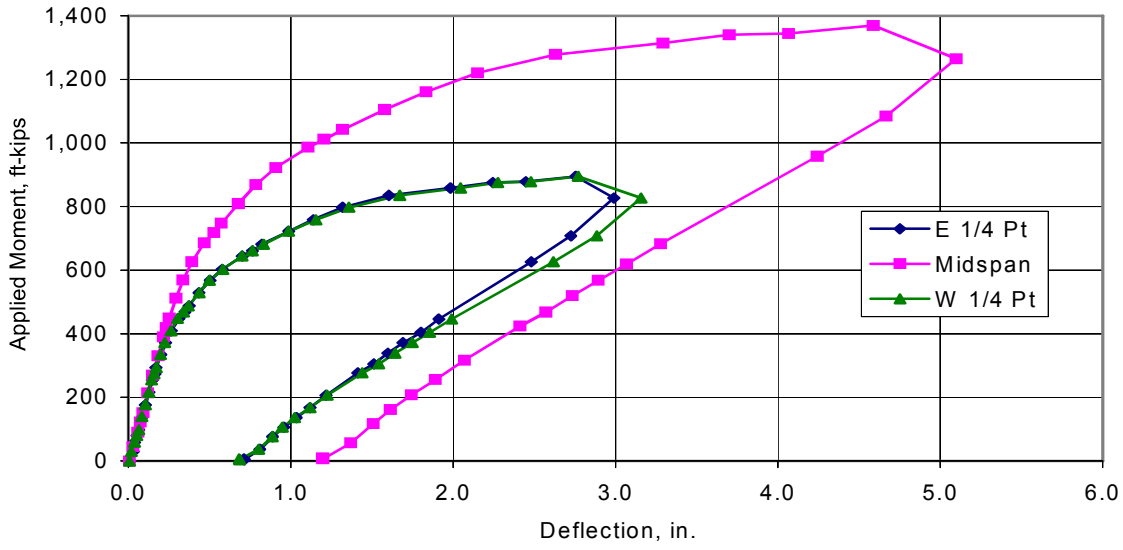


**Figure 5.67. Ultimate Load Test of Beam 1: Applied Moment vs. Deflection.**

For an effective prestressing force in the strands of 378 kips, the effective stress in each strand can be calculated to be 164.7 ksi in each of the 15, 1/2 in. ϕ low-relaxation strands. Assuming an initial jacking stress of 196.2 ksi, this is a loss of 31.5 ksi. The losses were compared to those predicted using the standard Iowa DOT method for loss computations and found to be less than the predicted value of approximately 39 ksi. The measured loss is 80% of that predicted.

The load vs. deflection response of Beam 1 during the ultimate load test is presented in Figure 5.67; several key points are worth noting. It was previously determined that the crack reopening load was at

an applied moment of 580 ft-kips at midspan; this moment is less than the moment between 625 ft-kips and 650 ft-kips at which the bilinear behavior is noticed. This is consistent with the findings of others that the cracks reopen prior to observation of significant bilinear behavior.

The peak live load moment of 1,369 ft-kips, plus the midspan dead load moment of 118 ft-kips equals the total resisted moment of 1,487 ft-kips. The theoretical capacity of this beam using the AASHTO specified approach is 1,341 ft-kips, thus the experimental capacity is 11% higher than the theoretical capacity. The beam exhibited significant ductility as evident by the large region of significant changes in displacement with little change in applied load. Loading was terminated prior to crushing of the slab due to safety concerns. At the time the loading was terminated, numerous cracks were present, the slab had slipped relative to the top flange of the beam at the beam end and several loud noises were heard from the beam.

Figure 5.68 presents the variation in the neutral axis location for the quarter points with applied live load. The neutral axis locations are consistent with those measured during the service load test (see Figure 5.63). The variation in the computed EI, as a function of the applied live load is presented in Figure 5.69. Once again, this value is consistent with that determined during the service load test however significantly different than the theoretical value.

Figure 5.70 is a photograph of the overall condition of Beam 1 following the ultimate load test. Extensive cracking was present. Many of these cracks were pre-existing cracks from the previous unsuccessful ultimate load test. These cracks propagated under application of the ultimate load. However, a number of additional cracks also developed. The cracks consistently terminated near the junction of the top flange and the web. Crack formation typically followed the tension stiffening model whereby the concrete loses its capacity to carry tension directly at a crack but the concrete “tooth” between the cracks carries tension until it develops secondary cracks. This explains the pattern of major cracks extending the full depth of the web with shallower secondary cracks between the primary cracks.

Figure 5.71 is a close up view of the constant moment region of Beam 1. Consistent with a constant moment/zero shear region, the cracks are primarily vertical and are fairly uniformly spaced. A vertical crack passed directly through the bottom flange strain gages in the midspan area rendering them useless.

Figure 5.72 depicts the cracks in the shear span; the cracks are inclined and normal to the direction of the principal tension stress in the web. The angle of inclination of the cracks varies from near vertical adjacent to the load to close to 45 degrees for the crack closest to the supports.

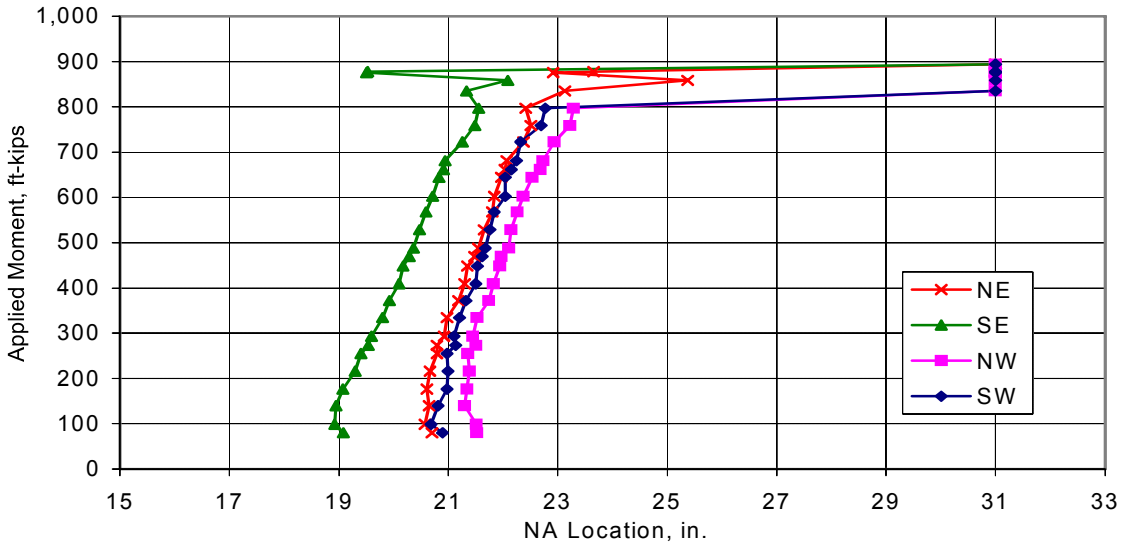


**Figure 5.68. Ultimate Load Test of Beam 1: Applied Quarter Point Moment vs. NA Location.**

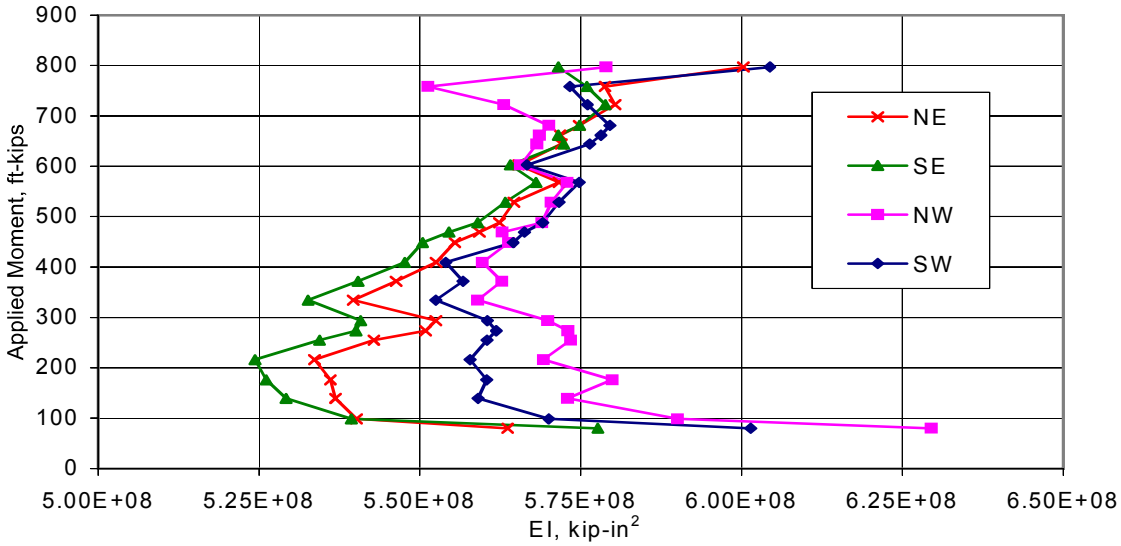


**Figure 5.69. Ultimate Load Test of Beam 1: Moment vs. Computed EI.**

**Figure 5.70. Overview of Beam 1 Crack Patterns Following the Ultimate Load Test.**

**Figure 5.71. Extensive Vertical Cracking in the Constant Moment Region of Beam 1.**

**Figure 5.72. Diagonal Tension Cracks in High Moment/Shear Region of Beam 1.**

**Figure 5.73. Web Shear Cracks in Beam 1 Adjacent to the Support.**

Finally, Figure 5.73 depicts the crack pattern that developed at the beam supports at ultimate load. Consistent with web shear cracking, the cracks began near the centroid of the beam and progressed toward the flanges under load. Though not clearly visible, the slab and haunch separated slightly from the top of the beam.

## *5.3.2. Beam 2 – FRP Repaired Specimen*

### *5.3.2.1. Repair Details*

This section describes the repair of a damaged prestressed concrete beam, Beam 2, that was intentionally damaged in the laboratories of Iowa State University. The damage to this beam, though not as severe as that inflicted to Beam 3 described in Chapter 4, was significant. Concrete was removed in a section 8 ft long, the full width of the bottom flange and 3 in. high. The "damage", extending from midspan toward the quarter point, exposed the bottom layer of six prestressing strands. Three of the strands in the bottom layer were removed leaving 9 of the original 12 prestressing strands in the bottom flange. This resulted in a decrease in flexural capacity of approximately 25%.

The objective of the damage and repair program was to assess the ability of CFRP strengthening to restore stiffness and strength to a damaged specimen. Beam 2 was service and ultimate load tested and compared to Beam 1 discussed in the previous section. In order to assure maximum quality in the repair, a professional contractor certified to install the manufacturers product was used to repair the beam.

Repair of Beam 2 began with removal of the three severed strands from the cross-section, the resulting beam is depicted in Figure 5.74. The exposed concrete to be patched was wet numerous times to a saturated/surface-dry condition to assure that the beam did not draw the moisture out of the repair material.

Following saturation, Sika Armatec® 110 EpoCem® was brush-applied to the exposed concrete as well as the reinforcing and prestressing steel. Armatec is three-component cementitious bonding agent/corrosion inhibitor. After a short cure period, the beam was patched using a SikaTop® 123 Plus Mortar which is a polymer-modified two-component non-sag mortar that can be used in vertical and overhead repair applications in lifts up to 1-1/2 in. The mortar also contains a penetrating corrosion inhibitor. After patching, the beam was allowed to cure for approximately two weeks although the CFRP repair could have begun within several days. A picture of the patched beam is presented in Figure 5.75. Properties of these patch materials as supplied by the manufacturer are presented in Table 5.3.

**Figure 5.74. Damaged Bottom Flange of Beam 2, Removed Strands in Foreground.**

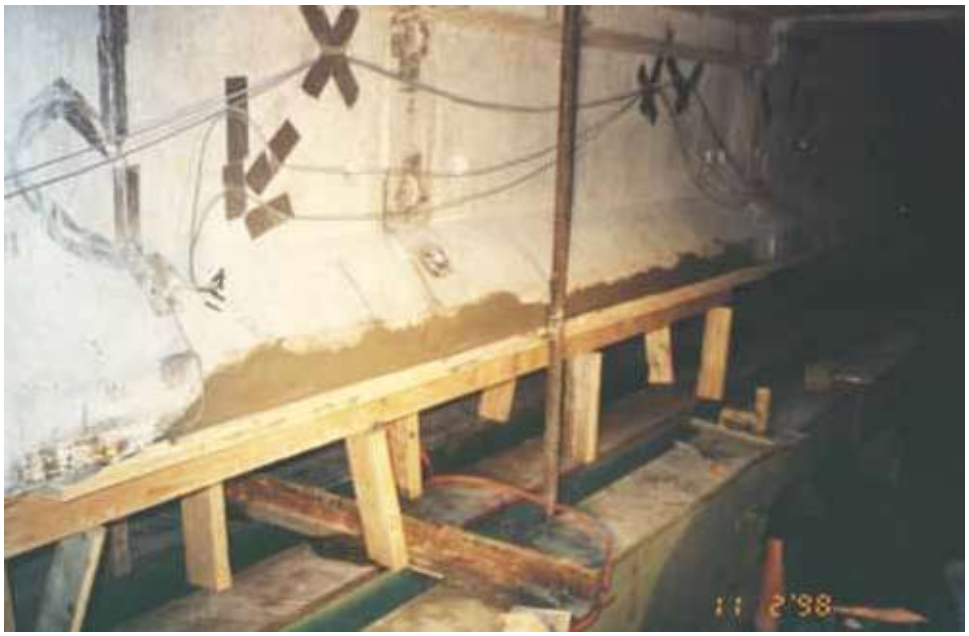

**Figure 5.75. Completed Concrete Repair on Beam 2.**

**Table 5.3 Cementitious Patch Material Properties Used on Beam 2.**

| Product | 28 Day Compressive Strength (psi) | 28 Day Splitting Tensile Strength (psi) | 28 Day Flexural Strength (psi) |
|---|---|---|---|
| Sika Armatec® 110 EpoCem® | 8,500 | 600 | 1,250 |
| SikaTop® 123 Plus | 7,000 | 900 | 2,000 |

The rough corners of the patch and original concrete were ground smooth with a hand-held grinder. In preparation for installation of the Sika CarboDur® reinforcing plates, the beam was cleaned with water to remove any dust from the surface that may hinder the bond of the epoxy used to attach the composites.

The beam was repaired with five CarboDur reinforcing plates – three S1012 plates bonded along the bottom of the bottom flange and two S812 plates bonded to the vertical faces of the bottom flange. The S812 plates are 80 mm wide x 1.2 mm thick (3-1/8 in. x 0.047 in.) with a tensile strength of 51,700 lbs. The S1012 plates are 100 mm wide x 1.2 mm thick (4 in. x 0.047 in.) with a tensile strength of 64,700 lbs. The plates were attached to the flange with Sikadur® 30, a structural epoxy paste specifically formulated for use with the CarboDur system. The CarboDur plates were intended to strengthen the beam to its original flexural strength. The plates were proportioned to replicate the strength of the three damaged strands when the plates were stressed to approximately 40% of their ultimate tensile strength. This arrangement of material was determined following consultation with the manufacturer and review of previous test results. The inability to stress the plates to higher levels of their ultimate capacity is a function of the delamination of the plates from the substrate or failure of the substrate itself at high stress levels.

The installation of the plates follows a procedure similar to the one previously described in Section 5.1.1.2 of this report. A predetermined thickness of the Sikadur 30 mortar was applied to the bottom flange of the beam and to the reinforcing plates. The plates were then placed against the substrate and pressed into place using a hard rubber roller. The installation of the three S1012 plates on the bottom flange is shown in Figure 5.76.

In an effort to eliminate debonding at the ends of the plates, each end was transversely confined with a 24 in. wide glass fiber reinforced polymer (GFRP) wrap. A similar wrap was placed in the middle of the constant moment region. This central wrap was to help restrain peeling of the longitudinal plates from the substrate as flexural cracks developed in the maximum moment region. These cracks have been documented by other researchers to be a common source of initiation for plate debonding. Installation of the glass wrap is depicted in Figure 5.77. Properties of the fiber materials and epoxies as supplied by the manufacturer are presented in Table 5.4.

**Figure 5.76. Installation of S1012 Reinforcing Plates on Beam 2 Bottom Flange.**

**Figure 5.77. Installation of GFRP Wrap on Bottom and Sides of the Bottom Flange of Beam 2.**

**Table 5.4. FRP and Epoxy Properties Used in the Repair of Beam 2.**

| | | | | | |
|---|---|---|---|---|---|
| Longitudinal Plates | Sika CarboDur | Tensile Strength<br>348,000 psi | Modulus of Elasticity<br>22.5 x $10^6$ psi | Elongation at Break<br>1.9% | Fiber Volumetric Content<br>>68% |
| | Sikadur 30 | Tensile Strength<br>3,600 psi | Elongation At Break<br>1% | Shear Strength<br>3,600 Psi | Bond Strength<br>3,200 Psi |
| External Glass Fiber Wrap | Unidirectional Glass Fiber | Tensile Strength<br>330,000 psi | Tensile Modulus<br>10.5 x $10^6$ psi | Elongation at Break<br>4% | Density<br>0.092 lbs/$in^3$ |
| | Cured Laminate, Fiber Content = 9 oz/sy | Tensile Strength<br>29,000 psi | Modulus of Elasticity<br>1.26 x $10^6$ psi | Thickness<br>0.040 in. | Strength per Inch Width<br>1,160 lbs./layer |

The properties of the CarboDur reinforcing plates were independently verified by the researchers. A sample of material removed from Beam 2 following completion of all load tests was tested. In these tests, the Modulus of Elasticity was determined to be 22.6 x $10^6$ psi and the tensile strength, 355 ksi. These values are in excellent agreement with those published by the manufacturer.

### *5.3.2.2. Service Load Tests*

This beam was never tested in the repaired condition while still a part of the bridge model due to previous damage to the self-contained loading frame. The first tests conducted on the repaired specimen, Beam 2, were subsequent to its relocation to the ISU Structures Laboratory. In this location, true simply supported conditions exist.

Instrumentation for the testing of Beam 2 was similar to that used for the testing of Beam 1. However, at midspan and the west quarter points, the strain gages on the bottom flange were not on the concrete since it had been previously removed. The strain gages were installed instead on the CFRP plates placed on the vertical surface of the repaired flange. Additionally, strain gages were installed on the CFRP plates on the underside of the bottom flange. The instrumentation used on Beam 2 is presented in Figure 5.78.

At the east (unstrenghened) quarter point, there are strain gages on top of the slab, on the top flange of the beam, and on the vertical face of the bottom flange of the prestressed concrete beam. At midspan, gages were placed on the top of slab, top flange of the concrete beam and on the CFRP plates on the vertical surface and horizontal surface of the repaired bottom flange. Finally, at the west quarter point, gages were placed on the top flange of the beam as well as on the CFRP plates bonded to the vertical and horizontal surfaces of the repaired flange.

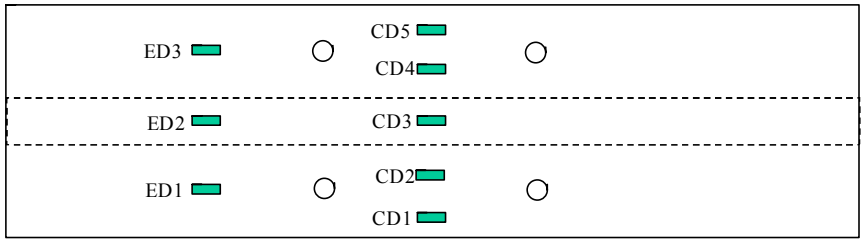


**a.) Top Surface of Deck**

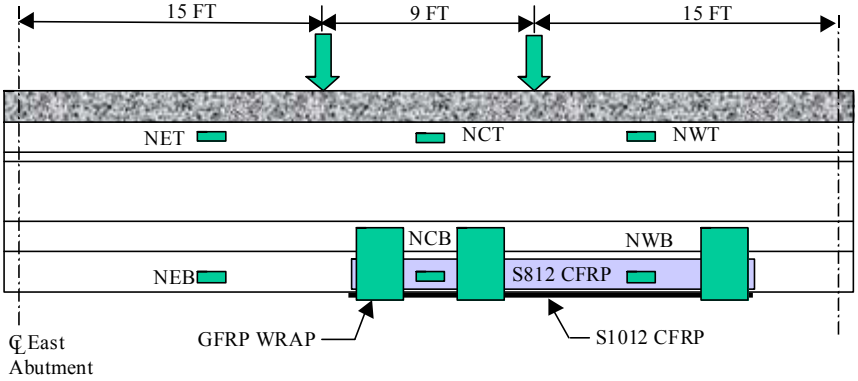


**b.) North Face of Beam**

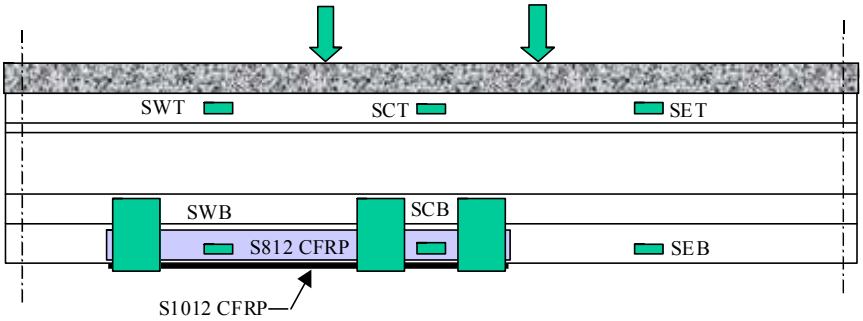


**c.) South Face of Beam**

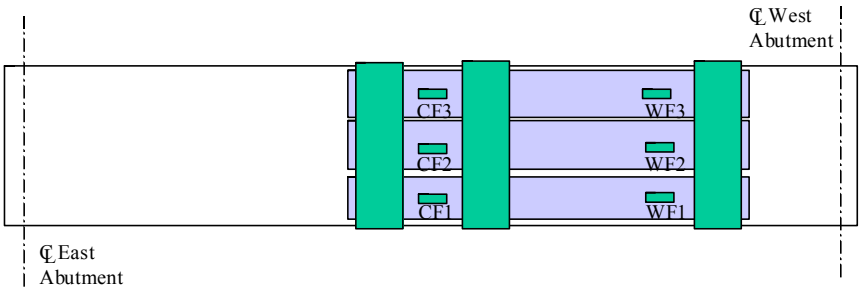


**d.) Bottom Surface of Bottom Flange**

**Figure 5.78. Instrumentation Layout, Repaired Beam 2.**

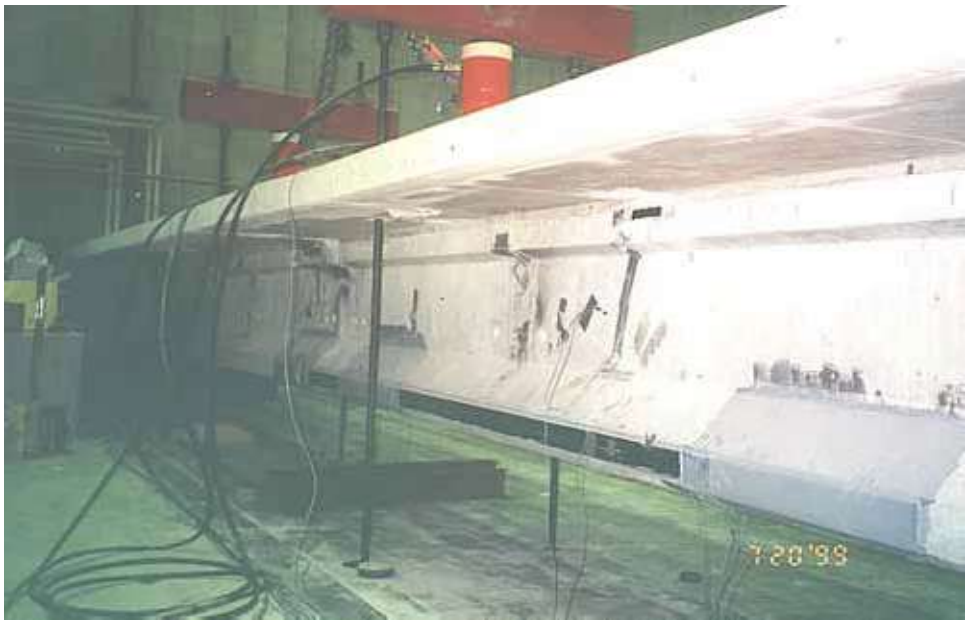


**Figure 5.79. Beam 2 Prior to Testing; CFRP Plates and GFRP Wrap Visible on Bottom Flange.**

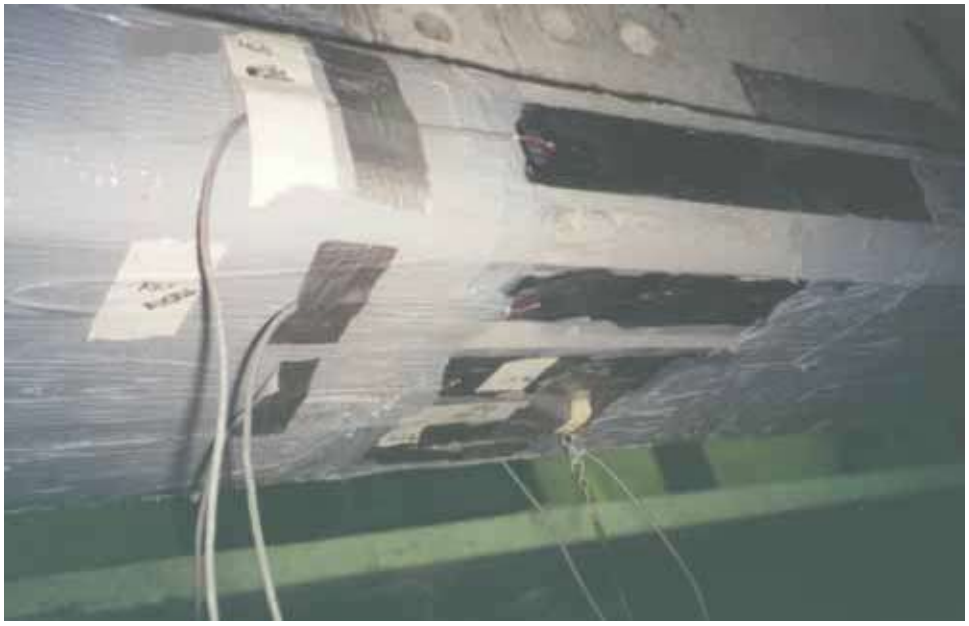

**Figure 5.80. Strain Gages on CFRP Plates at Midspan of Beam 2.**

In the service test on Beam 2, a total load of 88 kips was applied, 44 kips at each load point. These actuator loads produced an applied moment at midspan of 648 ft-kips and 423 ft-kips at the quarter points. These moments correspond to the first noticeable flexural cracks in the midspan region. At this load, the cracks were marked and the beam unloaded.

Several plots of the experimental data, Figures 5.81 through 5.83, are presented to explain the response of the specimen. Figure 5.81 presents a portion of the data collected at the undamaged east quarter point of Beam 2 during the service test. In part (a) of the figure, the variation in strain in several of the gages is presented with respect to the magnitude of applied moment. Of the three gages on top of the deck at the east quarter point, gage ED2, located over the beam centerline, is believed to be most representative of the correct strain at this location. Gages ED1 and ED3, located further away from the beam centerline are typically only 50-60% of that recorded at centerline, likely due to shear lag effects. The response of the two strain gages located on the top flange is similar, as is the response of the bottom flange strain gages. In part (b) of Figure 5.81, the strain profile through the depth of the beam is presented using gages ED2, NET and NEB, respectively. This combination of gages produced the most consistent linear strain profile through the depth of the beam. A neutral axis for live loads of between 18.8 and 21.9 in. was recorded with an average value of 20 in. Finally, in part (c), measured curvatures (not presented herein) along with known applied moments are used to compute an EI value for the beam under live load. Depending on which gage combination is used for computational purposes, there is variability in the result. An average of all four results yields a predicted EI of $5.6 \times 10^8$ kip-in$^2$, the same value as measured previously for Beam 1 prior to it being cracked.

Figure 5.82 presents the response of the midspan region. Part (a) presents a measured neutral axis location based on a variety of scenarios. For the series labeled NCT&NCB and SCT&SCB, gages on the vertical face of the top and bottom flange were used. The top flange gages were bonded to concrete and those on the bottom flange bonded to the S812 CFRP plates. For the series labeled “Avg. Deck & NCB/SCB”, an average of the five strain gages on the deck at midspan, gages CD1 to CD5, was used along with the CFRP strain gages on the vertical surface of the bottom flange. Finally, the series entitled “Avg. Midspan Deck & Plates” uses average strain from the five concrete strain gages on the deck surface as well as the three CFRP strain gages mounted on the underside of the bottom flange. There is a wide scatter in the deck strain gages with the highest and lowest values ±20% from the mean. The three bottom plate CFRP gages have a scatter of ±10% from the mean. Due to the variety of gage combinations used, there are various predicted values for the experimental neutral axis under live load. However, examining the strain components used to derive the neutral axis locations, those predictions based on gage SCB are suspect. The authors believe the best prediction of the neutral axis location in the midspan region is between 21 and 23 in. from the extreme bottom fiber. The EI value presented in part (c) is also subject to scatter though an average of $6.3 \times 10^8$ kip-in$^2$ is found by summing all of the predicted values throughout the test. This is 12% higher than the value determined at the east quarter point.

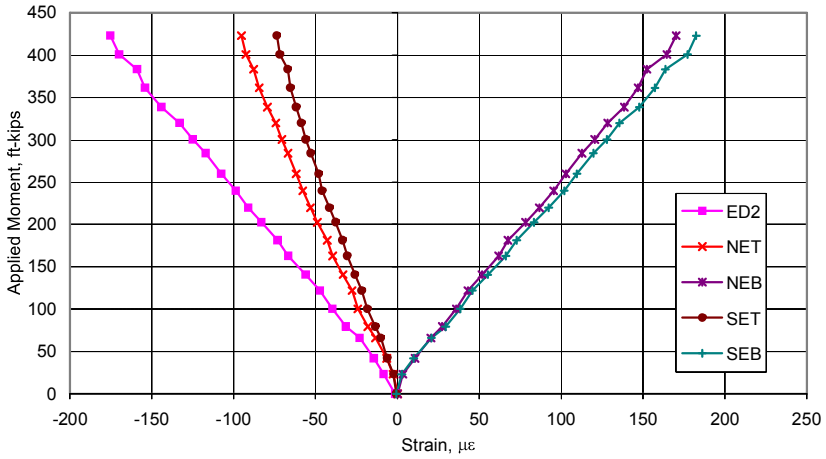


**a.) Strains at East Quarter Point.**

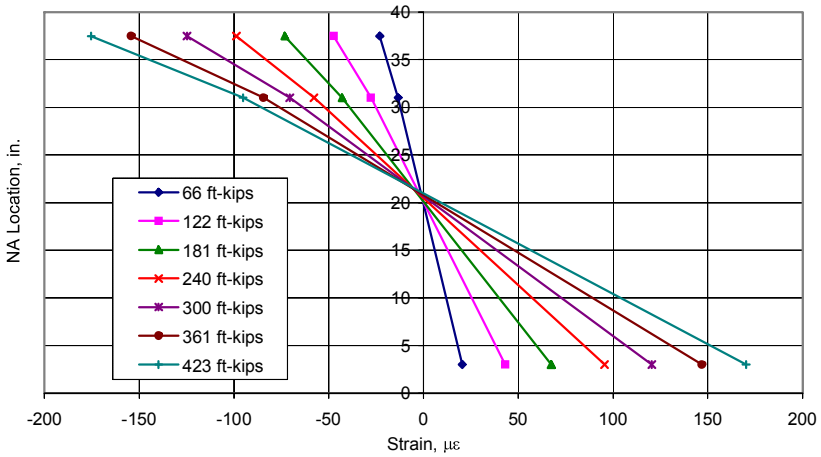


**b.) Strain Profile Through Gages ED2, NET and NEB.**

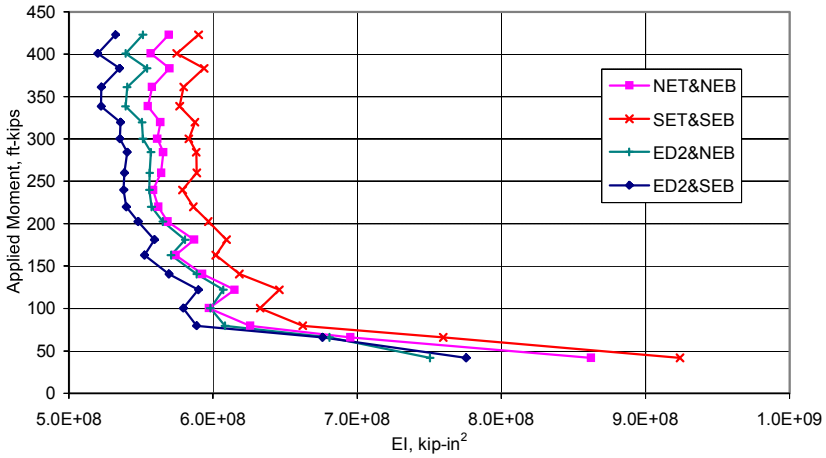


**c.) Applied Moment vs. EI.**

**Figure 5.81. Service Test of Undamaged/Unstrenghened Beam 2: East Quarter Point Data.**

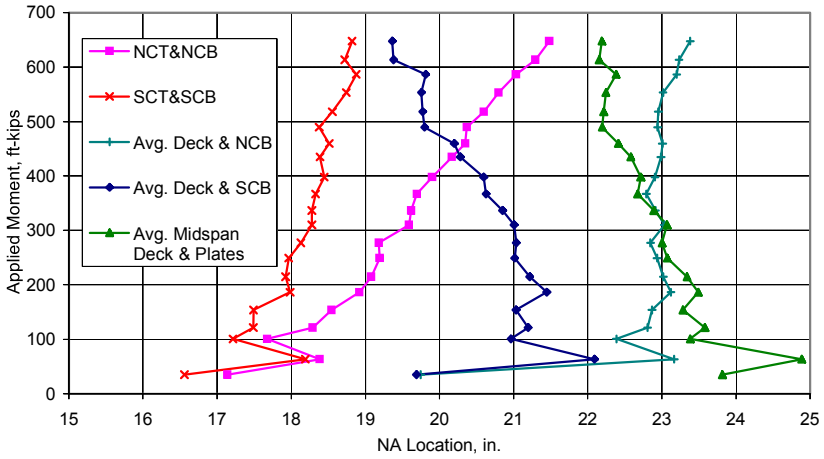


**a.) Predicted Neutral Axis Based on Various Gage Combinations.**

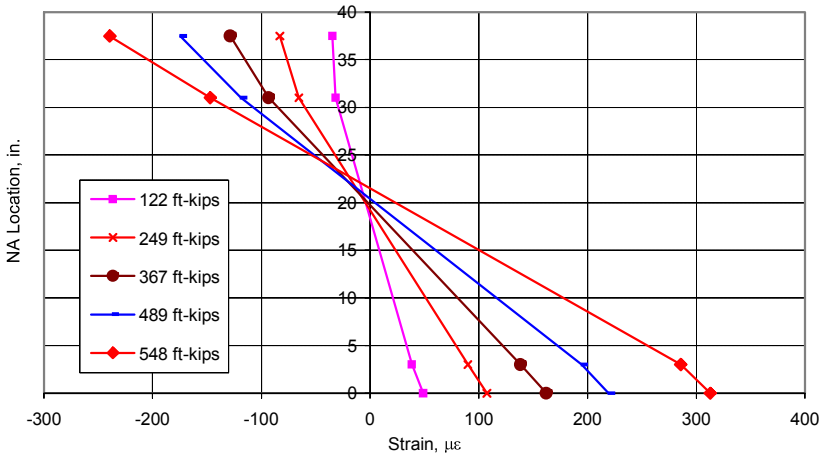


**b.) Strain Profiles Using Gages CD2, NCT, NCB and CF1.**

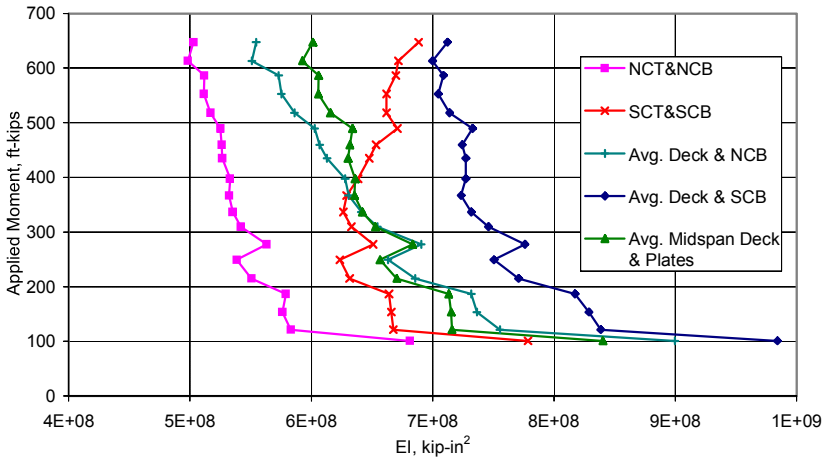


**c.) Applied Moment vs. EI.**

**Figure 5.82. Service Test of Beam 2: Response of Midspan Region.**

Finally, Figure 5.83 provides a portion of the experimental data from the repaired west quarter point location. This data can be compared to that of the east quarter point. In part (a), the strains in various gages are presented. As compared to the east quarter point, the strains on both the top flange of the P/C beam and on the vertical portion of the bottom flange are somewhat smaller in magnitude. Although, as part (b) indicates, the neutral axis under live loads is slightly higher at the repaired quarter point, 21.7 in., than at the undamaged quarter point, the curvature is less at the repaired quarter point for comparable moments. This is reflected in the EI values presented in part (c). The average of three clustered values is $7x10^8$ kip-in$^2$, an increase of 25% over the undamaged/unstrenghened east quarter point. Explanation of the difference in EI values can be found in the difference in moment of inertia of a section whose neutral axis is at 20 in. versus one whose neutral axis is 21.7 in. from the extreme bottom fiber. For the section with the 20 in. neutral axis, the moment of inertia is 77,980 in$^4$ and for the section with the 21.7 in. neutral axis location, 90,060 in$^4$, an increase of 15%. This does not account for the stiffening effects of the addition of the CFRP plates that are the likely source for some of the additional stiffness. The axial rigidity, EA, of the CFRP plates is equivalent to approximately 4.4, 1/2in. $\phi$ prestressing strands. However, only three strands were severed implying a net increase in axial stiffness of 1.4 strands. The neutral axis and moment of inertia values have been obtained through the use of engineering judgements in interpreting the experimental data and thus should be only considered to be average or representative properties.

#### *5.3.2.3. Ultimate Load Test*

Beam 2 was successfully load tested to failure. The primary interest was to determine the mode of failure and strength of the repaired specimen. FRP strengthened concrete beams can fail in a number of different ways. The most common failure modes are fracture of the FRP, failure of the epoxy or of the substrate, and crushing of the concrete slab due to over-reinforced conditions. The GFRP transverse confinement at each end of the CFRP plates, as well as the supplemental wrap in the constant moment region, was intended to delay the debonding of the strips from the bottom of the beam.

To determine the crack reopening load, the LVDT was installed approximately 6 in. from the bottom fiber on the sloping face of the bottom flange of the P/C beam. In order to determine the crack reopening load, a computation similar to that used for Beam 1 was performed with the exception that the area of the CFRP has been included in the section properties. For a crack reopening moment of 450 ft-kips (See Figure 5.84), the effective prestressing force is 288 kips, an effective stress in the strands of 157 ksi compared to 164.7 ksi in undamaged Beam 1. The accuracy of the computation for resulting prestress in Beam 2 is questioned due to the change in cross-section stress distribution from the severing of three of the strands.

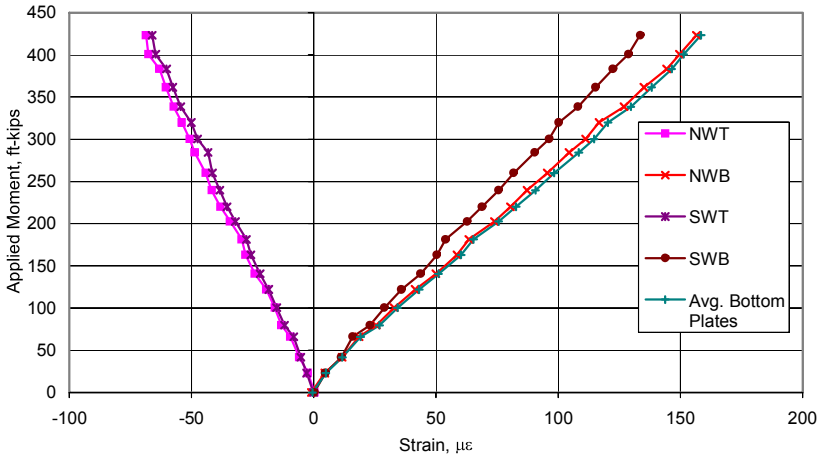


**a.) Strains at West Quarter Point.**

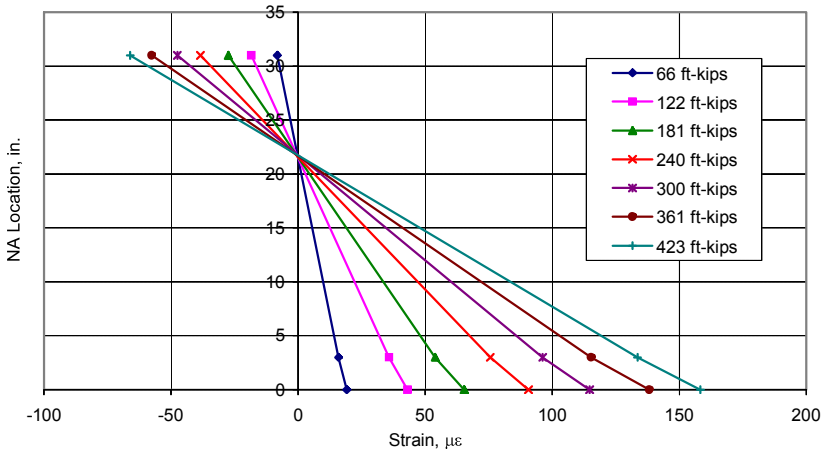


**b.) Strain Profiles Using Gages SWT, SWB, and the Average Bottom Plate Value.**

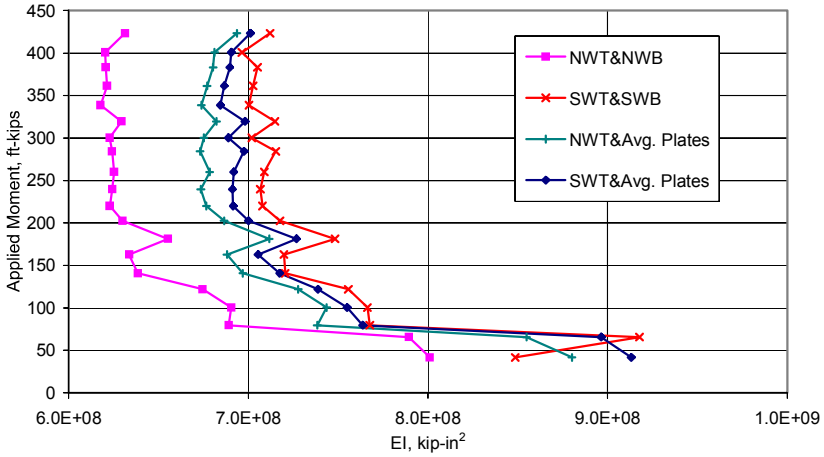


**c.) Applied Moment vs. EI.**

**Figure 5.83. Beam 2 Service Load Response: Repaired West Quarter Point.**

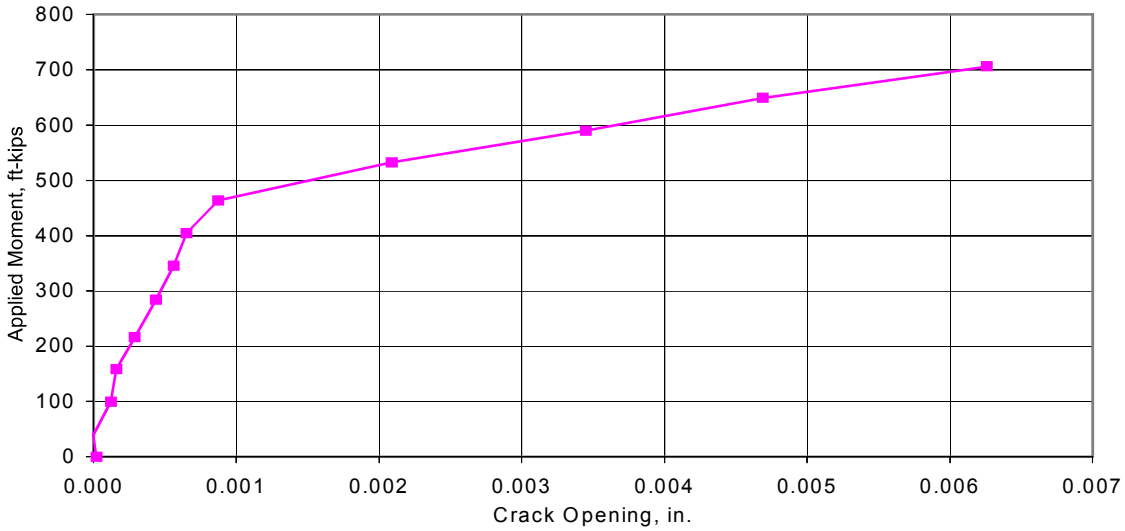


**Figure 5.84. Applied Midspan Moment vs. Crack Opening, Beam 2.**

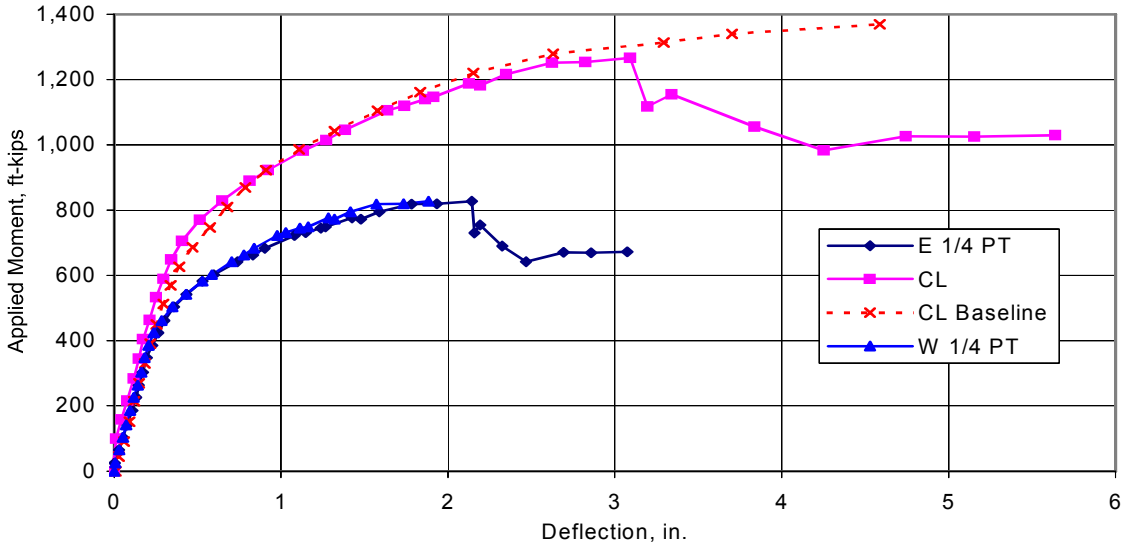


**Figure 5.85. Beam 2 Ultimate Load vs. Baseline (Beam 1) Results: Applied Moment vs. Deflection.**

Figure 5.85 presents the applied moments vs. deflection for the repaired beam. The displacement of the baseline specimen, Beam 1, is also presented as "CL Baseline". The repaired beam demonstrated substantial displacement ductility. The peak moment applied to the beam, 1,266 ft-kips, plus the self-weight moment of 118 ft-kips, results in a total resisted moment of 1,384 ft-kips. The design strength of an undamaged beam using the AASHTO approach is 1,341 ft-kips. The strengthening used on this beam was able to restore the strength to that of a theoretically undamaged specimen. As a comparison, the undamaged control specimen was subjected to a combined dead and live load moment of 1,487 ft-kips prior to failure.

The capacity of the strengthened beam is only 90% of the strength of the control specimen. However, the original design objective was to restore the strength of the beam to its theoretical undamaged capacity based on code-specified equations; in this regard, the repair was successful.

The cause of the lesser strength in the repaired beam as compared to the baseline specimen is failure of the interface between the CFRP and the concrete substrate. At the peak live load moment, the CFRP plates on the underside of the bottom flange peeled away from the bottom of the beam. This is shown in Figure 5.86. The plates must have also slipped longitudinally in order for the bow in the plates to occur. Once the plates peeled from the flange, the horizontal shear load transfer from the plate to the substrate was destroyed over a significant length and presumably a much larger portion of the load was transferred through the ends of the plate and henceforth the GFRP confining wrap. The drop in load capacity from the peak to an approximate moment of 1,100 ft-kips is coincident with the beginning of the debonding of the bottom plates. One should note that prior to this debonding, the repaired and baseline specimen followed essentially the same load-displacement path. As additional load was applied, progressive debonding of the bottom plates occurred until they fell away from the bottom of the beam.

When the plates completely debonded and fell away from the beam, the actuator loads decreased to approximately 69 kips each resulting in a midspan moment of 1,000 ft-kips. Tearing of the plates from the bottom of the beam occurred near the west quarter point where the GFRP transverse confining wrap was the only means of anchoring the peeled plates to the beam. Concurrent with loss of the bottom flange plates, the vertical plate on the south face of the beam tore away from the flange at midspan, fracturing the GFRP wrap. It also debonded from the beam for most of its length. As additional load was applied to the beam, the portion of the tensile load initially carried by these partially or fully debonded plates was transferred into the remaining bottom flange vertical plate on the north face and into the remaining prestressing strands. The increase in load into the remaining CFRP plate in conjunction with the destruction of the GFRP confining wrap at the west quarter point and midspan caused the vertical plate on the north face of the beam to peel away at a midspan moment of 1,070 ft-kips (See Figure 5.87). Following this debonding, the specimen continued to deflect with no additional load applied. This is the flat portion of the moment vs. displacement curve presented in Figure 5.85. The applied moment of approximately 1,030 ft-kips, in addition to a dead load moment of 118 ft-kips is a total of 1,148 ft-kips, much less than the 1,384 ft-kips resisted by the beam prior to loss of the plates. The difference between the unstrenghened and strengthened capacities is approximately 17%, which is a substantial gain due to the addition of the CFRP plates and GFRP wrap.

The mode of CFRP failure was not consistent. Examination of the bond failure for the north face plate indicated that failure was in the bond between the plate and the epoxy. The plate separated from the epoxy and the trowel marks were clearly evident in the epoxy bonded to the beam. When the bottom plates were removed from the flange, a large piece of the original P/C beam concrete was still attached to the CFRP indicating excellent bond between the epoxy and the original beam (See Figure 5.88).

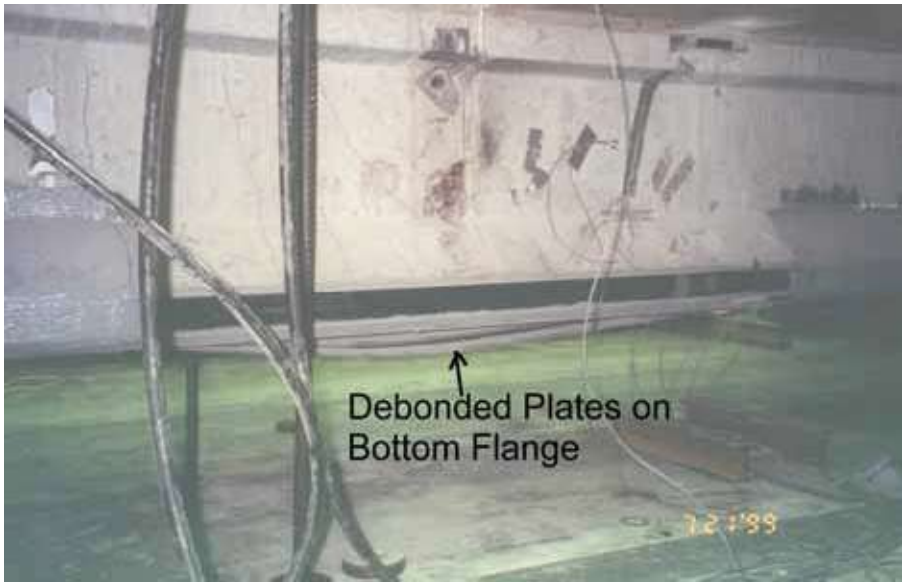


**Figure 5.86. Partial Debonding of the Beam 2 Bottom Plates Between the GFRP Confining Wraps.**

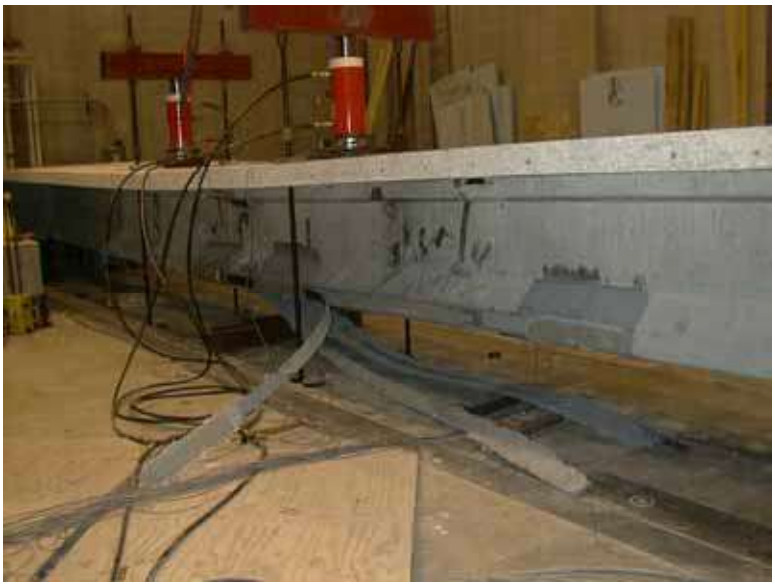

**Figure 5.87. Failure of the Beam 2 Bottom Plates as well as the North Face Plate.**

Finally, examination of Figure 5.89 indicates not only complete fracture of the GFRP confinement but also a large voided area in the patch concrete. When the south face plates debonded they removed much of this concrete. It is still well-adhered to the plates. Once again, this demonstrates excellent bond between the epoxy and the substrate, in this case the patch material.

Figure 5.90 presents the strains, measured neutral axis and effective EI at the undamaged east quarter point for the ultimate load test. The response of this location until near the ultimate load is linear. At live load moments in excess of 700 ft-kips at the quarter point, some nonlinearity is present due to the progression of cracks through the section. The value of the neutral axis and EI for this location are essentially the same as the values determined in the service load test (see Figure 5.81).

The response of the midspan region is presented in Figure 5.91. Because of the various degrees of plate debonding, only average strains for the bottom flange plates are presented. The response of the strain gages in part (a) of the figure is consistent with the progressive failure of the CFRP system previously described. For instance, examining the series labeled NCB, the strains on the vertical CFRP plate on the north face of the bottom flange, following the peak moment when the bottom plates debond, this plate has a dramatic increase in strain with little additional load. As previously mentioned, with four of the five plates debonded at this time, the remaining plate on the north face would experience a significant increase in tensile force.

Unlike the east quarter point which responds essentially linearly and with constant stiffness, the midspan region has a significant change in the neutral axis location and EI during the course of the test. This is a reflection of the significant amount of cracking present at midspan during the ultimate load test and is also a function of the failure of the CFRP strengthening system.

Finally, the west quarter point data are presented in Figure 5.92. The west quarter point behaves in many ways like the midspan region with a linear region up to the development of significant cracks followed by a much more flexible response as the cracks progress and the debonding of the plates commences.

The maximum strain induced in the CFRP plates was 6,020 με. This strain corresponds to a stress of 135,450 psi, approximately 39% of the ultimate tensile strength of the plates. As a point of reference, the plates were originally designed assuming they could attain 40% of their ultimate tensile strength before debonding.

## *5.4. ISU Model Bridge Beam Test Summary and Conclusions*

A number of static load tests were conducted on two separate Iowa DOT standard prestressed concrete I-beams. The beams had previously been load tested a number of times during the bridge model experimental testing program. These loads never exceeded 60 kips so that the beams would not be damaged during that portion of the experimental program.

**Figure 5.88. Failure of the Original P/C Beam 2 Substrate Near Midspan.**

**Figure 5.89. Fracture of GFRP Wrap and Voided Flange in Beam 2 Following Plate Debonding.**

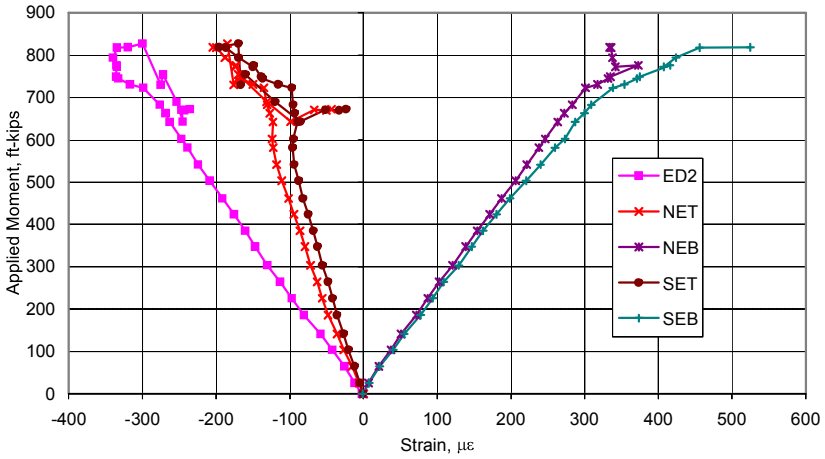


**a.) Strains at East Quarter Point.**

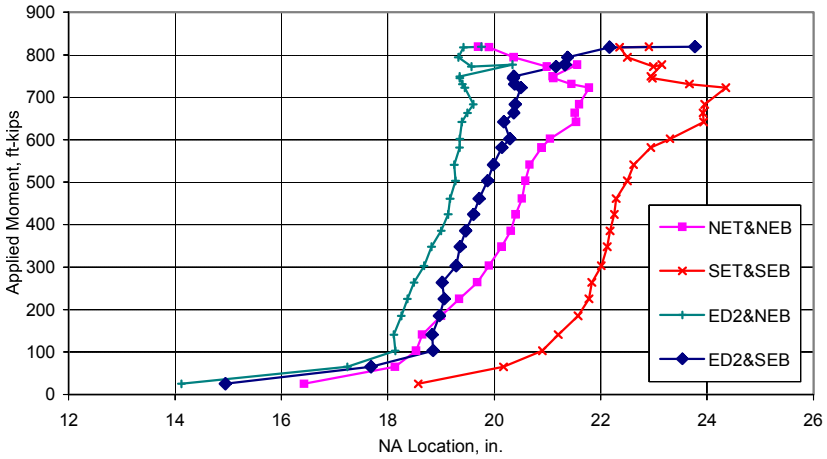


**b.) Computed Neutral Axis Under Live Loads.**

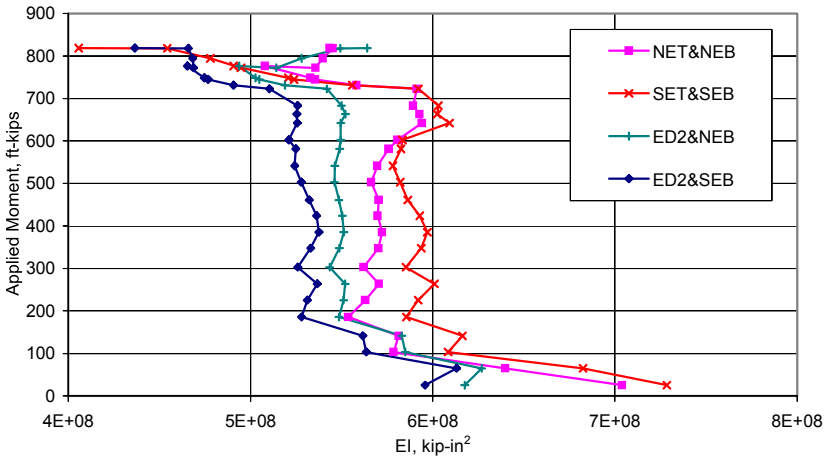


**c.) Applied Moment vs. EI.**

**Figure 5.90. Ultimate Load Test of Beam 2: Undamaged East Quarter Point.**

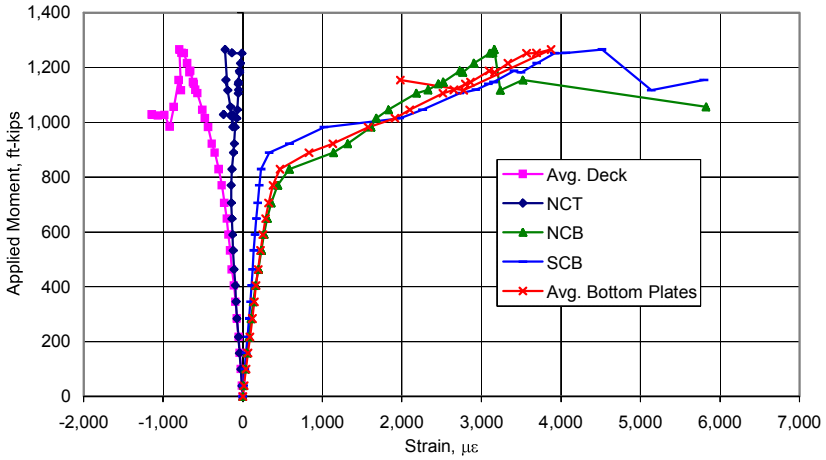


**a.) Variation in Midspan Strains.**

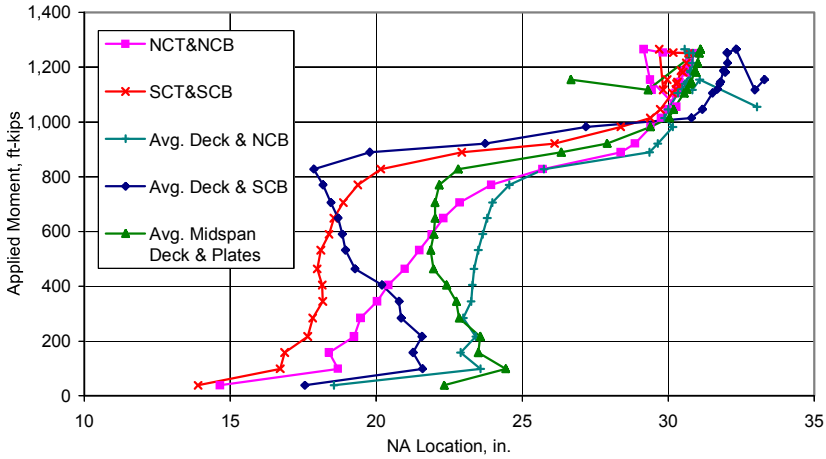


**b.) Computed Neutral Axis Location.**

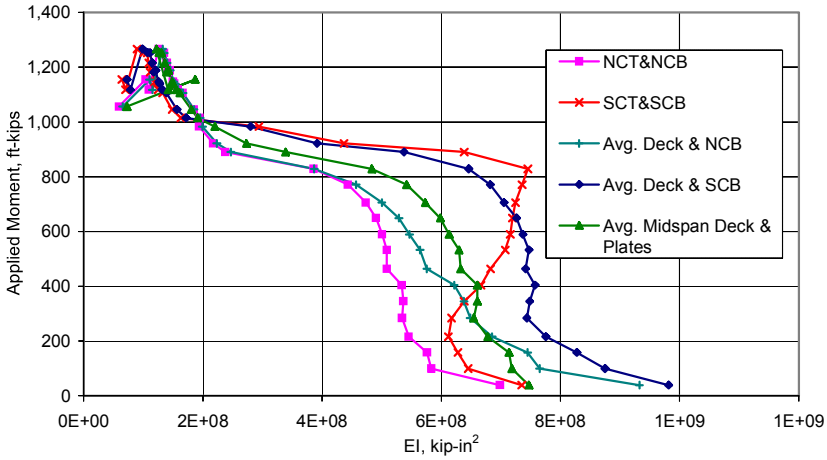


**c.) Applied Moment vs. EI.**

**Figure 5.91. Ultimate Load Test of Beam 2: Midspan Region.**

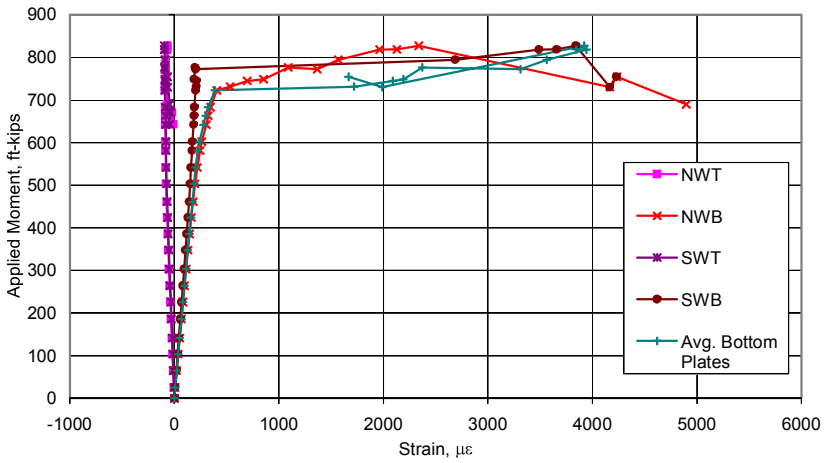


**a.) Variation in West Quarter Point Strains.**

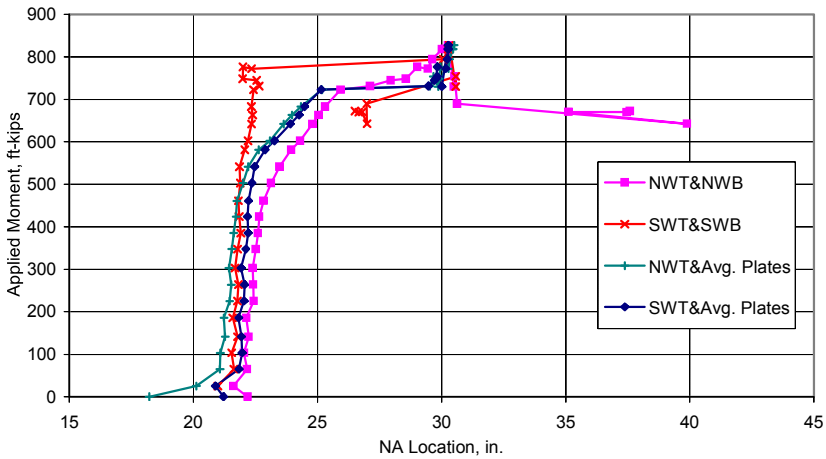


**b.) Computed Neutral Axis Location.**

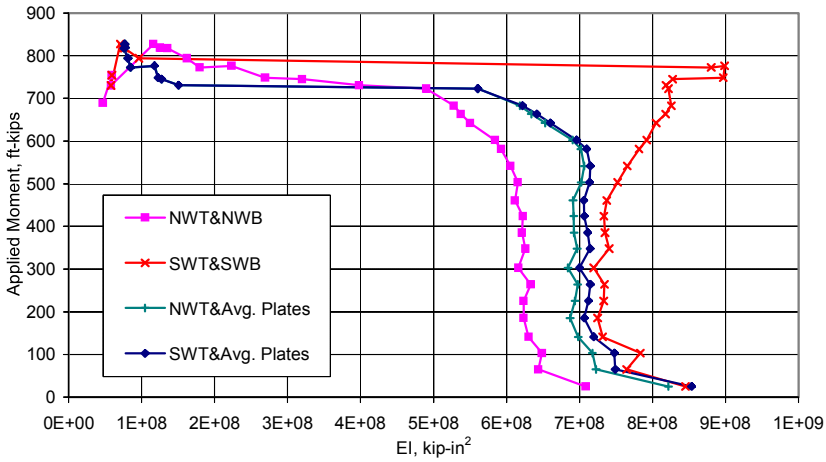


**c.) Applied Moment vs. EI.**

**Figure 5.92. Ultimate Load Test of Beam 2: Repaired West Quarter Point.**

An unsuccessful attempt was made to test Beam 1 while it was still partially restrained in the bridge model. Due to appreciable amounts of end restraint, the beam could not be loaded to its ultimate capacity prior to failure of the self-contained load frame. However, nonlinear behavior of the beam was recorded and the beam was significantly cracked throughout the constant moment region.

Following transportation of the isolated beam and slab to the ISU Structures Laboratory the beam was successfully load tested to failure. Significant ductility of the beam was present. The ultimate strength of the beam was determined to be 11% higher than predicted using standard AASHTO methods of strength prediction. The prestressing force in this beam was estimated using crack reopening methods. The prestress losses were estimated to be 31.5 ksi as opposed to a predicted loss of 39 ksi. The loss is 80% of that predicted.

The experimental EI value of this beam and subsequently Beam 2, is substantially higher than predicted. The source of uncertainty is in the value for E predicted by code equations. Using the moment-curvature relationship from the simply supported beam test, an estimate of fixity in the original lab model was made. Depending on whether deflections or ratios of curvature are used in the analysis of fixity, estimates of end restraint vary. For deflection based analysis, the end moment appears to be between 20-30% of the fixed end moment value. Using curvature ratios, the estimate is higher, approximately 50%. Although there is scatter in the predicted value, both approaches yield an estimate of end restraint that is significant.

Beam 2 was the CFRP strengthened specimen. Following removal of the entire flange width for a depth of 3 in. and a length of 8 ft, three of the exposed strands were severed. The beam was repaired using CFRP plates that when operating at approximately 40% of their ultimate tensile strength, provide a force similar to the ultimate tensile strength of the removed strands. The repair was easily installed using cementitious patch materials to repair the damaged flange and simple tools to install the CFRP plates and GFRP wrap.

The beam was service tested to cracking, unloaded, and subsequently loaded to failure. Prior to the beginning of plate bond failure, the response of the repaired and baseline specimen, Beam 1, was essentially the same. At a total applied dead and live load moment greater than the theoretical beam capacity predicted by AASHTO for an undamaged beam, the failure of the strengthening system was initiated by debonding of the plates on the underside of the bottom flange. A progressive failure then occurred such that at the conclusion of the testing, the plates were completely separated from the beam and the resulting capacity was that of an unstrengthened section.

The failure mode was a combination of bond related failures. The majority of the plates debonded and removed a thin layer of the patch and/or original P/C beam concrete during failure. A significant length of the north face flange plate debonded from the epoxy with the epoxy remaining attached to the substrate. On the south face flange plate, debonding of the strip was due to significant tearing of the patch concrete from the repair. A portion of the bottom flange plates near midspan pulled a piece of the original P/C beam

concrete out of the flange at failure. The plates attained a strain of approximately 39% of ultimate prior to debonding. The design criteria employed which assumed failure at 40% of ultimate strain appears sound for this beam.

## ***5.5. P/C Beam Strengthening Conclusions***

Based on the success of the retrofit of Beam 2W removed from the Beebeetown bridge as well as the intentionally damaged beam, Beam 2, removed from the ISU model bridge, strengthening of damaged P/C beams with FRP materials appears to be a viable repair option. From observations of the behavior of both retrofit specimens as compared to their unstrengthened companion beams, the repair is effective in restoring stiffness in the damaged beams and in providing increases in strength over the damaged state. Both retrofit beams exceeded the theoretical strength of an undamaged specimen.

One of the significant differences in the two retrofitted beams is the amount and location of external transverse confinement. In the case of Beam 2W removed from the Beebeetown bridge, external CFRP wraps, 12 in. wide spaced 18 in. on center, were placed over the length of the beam. For Beam 2, strengthened in the ISU Structures Laboratory, the confinement was composed of a GFRP wrap, 24 in. wide, placed at the ends as well as at one location in the maximum moment region. The longitudinal plates in the Beam 2W tests were able to sustain a stress of approximately 122 ksi, 85% of their ultimate tensile strength of 143 ksi, prior to the beam failing. The laboratory strengthened Beam 2 was able to sustain stresses of approximately 135 ksi in the longitudinal plates, or 39% of the ultimate tensile strength (348 ksi) of the Sika CarboDur plates. The mode of failure for both retrofit beams can be partially or entirely attributed to failures that began in the bond between the beams and longitudinal plates yet the failure of the Beam 2W retrofit was such that a much greater capacity of the longitudinal plates was mobilized. This can be attributed to the enhanced bond between the plates and beam through the application of numerous well-spaced external CFRP stirrups along the length of the beam. From this investigation, the use of well-distributed transverse strips throughout much of the retrofitted length, particularly in areas where significant cracks might develop, was shown to be beneficial.

# *CHAPTER 6*
# *STRUCTURAL ANALYSIS AND MODELING*

This chapter presents a literature review concerning the analytical modeling of bridge structures, models calibrated to the work of others for software validation, and the results from analyses conducted on the I-680 bridge structures. The results of an eccentrically stiffened plate finite element model are presented and compared to the experimental response of the damaged and undamaged/repaired bridges. Additionally, analytical results from a simplified grillage model are compared to the results from the more complicated model and to the experimental results. The intent of the analytical modeling portion of this project was to assess the live load distribution characteristics of the damaged and undamaged/repaired bridges.

## *6.1. Mechanics of Live Load Distribution*

The main objective of this project was to examine the two sides of the common structural design equation, namely load effect and anticipated strength. Because a damaged bridge has a local change in stiffness (flexural, shear, torsional, and axial) in the damaged region, there was a question about how damage would affect the local and global response of the structure. This project included the testing of two bridges in the field, one of which was tested with damaged beams in place and again following replacement of the damaged members. The other structure was an adjacent undamaged structure and is used for comparison. In addition to the field tests of the accidentally damaged structure, a significant testing program was conducted on a model bridge in the ISU Structures Laboratory. This chapter only discusses the analytical modeling of the I-680 bridges. For analytical results corresponding to the laboratory bridge tests, refer to Mateega (1997).

A theoretical understanding of live load distribution is important in interpreting the experimental behavior and in providing analytical modeling guidelines which practicing engineers can use to characterize the effects of local damage to prestressed concrete elements. In order to determine the effects of isolated damage on the load distribution characteristics of a multi-girder prestressed concrete I-beam bridge, it is first important to understand the mechanics of live load distribution in multi-beam systems. This section will examine several references that address the live load distribution in such structures.

The live load distribution characteristics of a bridge are dependent on a number of factors, most important of which is the beam spacing. Additional characteristics of a bridge that are important in determining the degree to which live loads are effectively distributed are:

- beam area, flexural and torsional stiffness, eccentricity from the center of the deck, and span length,
- slab thickness and effective slab span,

- the amount of flexural and torsional restraint, and,
- the location and stiffness of intermediate diaphragms/cross frames.

The degree to which these various effects contribute to the distribution of applied live load varies from bridge to bridge but it is commonly understood that they all participate to some degree. It is important to understand that live load distribution is not constant along a span, i.e., for load in a given position, the live load distribution factor is different for a beam at midspan than at the quarter point. The distribution factor varies depending on the type of applied load, i.e., point versus distributed loads. It also varies based on the magnitude of load. For instance, live load distribution factors presently specified in design codes are based on the behavior of the structure in the elastic condition. It has been shown that if one is concerned about the behavior of a bridge and distribution of load at the ultimate level, the code-specified live load distribution factors are inherently conservative. This is because they do not account for the sequential formation of failure mechanisms and the redistribution of load to members whose ultimate capacity has not been reached. For instance, Heins and Kuo (1975) compared the elastic live load distribution to interior stringers in a steel bridge versus the live load distribution at the onset of slab crushing and determined that the live load fraction to the most heavily loaded beam was roughly S/5.5 at the service level but decreased to S/7 at ultimate. This reduction in live load factor at ultimate load is due to the inelastic redistribution of load to adjacent but not yet overloaded elements. It was hypothesized at the start of this research project that this redistribution (or change in expected distribution) of load would even be apparent at the elastic level since members of lesser stiffness were present in the bridge.

In a paper by Tamberg (1968), the relative influence of torsional stiffness was examined as it relates to the distribution of load in a variety of structures. A portion of the paper reviews the computation of torsional stiffness properties of prestressed concrete I-girders and the relative influence of torsional versus flexural stiffness on the structural behavior of multi-beam bridges. Tamberg contends that a proper estimate of torsional stiffness must be made. A common mistake is to assume that the torsional stiffness coefficient, $K_T$, is equal to the polar moment of inertia but that is only true for circular sections. Determination of $K_T$ for stocky sections such as a prestressed beam is typically more difficult to ascertain than flexural or axial stiffness. Tamberg presents results from a finite difference analysis of the torsional stiffness of an AASHTO Type III girder plus composite slab. He concludes that the conventional assumption of summing the torsional stiffness of individual segments of a structure as commonly done for thin open-walled cross sections such as plate girders, known as Bach's method, significantly underestimates the stiffening effect due to interconnection of the individual pieces. This is true if Bach's method is used to compute the stiffness of a girder idealized as a series of rectangular elements as opposed to a combination of trapezoidal flanges and a rectangular web. It is also true if having computed $K_T$ for the girder using refined methods, Bach's method is used to compute $K_T$ of the composite system. No method is proposed as an alternate to this approach but a comparison of an interconnected composite section analysis versus Bach's method illustrates the significant underestimation of $K_T$ by Bach's method.

Following the discussion on estimating $K_T$, Tamberg discusses the relative contribution of flexural and torsional stiffness to the distribution of live load in a right, simply-supported, five beam structure using the term H, the characteristic flexural stiffness ratio, as well as $K_G$, the torsional stiffness of a girder. H is defined as $E_G I_G / E_S I_S L$ where

$E_G$ = Modulus of Elasticity of girder material
I = Moment of inertia of a longitudinal girder
$E_S$ = Transverse Modulus of Elasticity (slab or slab plus diaphragm)
$I_S$ = Transverse inertia per unit length (slab or slab plus diaphragm)
L = Bridge Span

Four possible limiting scenarios were examined for combinations of $K_G$ and H, two of which are discussed herein, namely, $H = 0$, $K_G = 0$ as well as $H = 0$, $K_G = \infty$. A value of zero for H implies that the ratio of beam flexural stiffness to slab flexural stiffness is very small, i.e. can be approximated by zero.

In scenario 1, it is assumed that the bridge is infinitely stiff in the transverse direction and the beams have negligible torsional stiffness. In this case, the bridge will deflect and rotate as a rigid body, analogous to the rigid rotation model currently specified in the AASHTO LRFD Specifications for the determination of live load distribution to an exterior beam. In this scenario, 60% of a load placed directly over the exterior beam of the five beam bridge studied by Tamberg (See Figure 6.1) will be resisted by that beam with distribution percentages of 40%, 20%, 0% and –20% for the other four beams, respectively.

Scenario 2 presumes infinite torsional rigidity of the beams; the bridge will deflect as a rigid body but the cross-section will be prevented from rotating. This implies that all beams share the load evenly; in Tamberg's case the live load distribution is 20% of the total load to all beams.

A comparison of scenarios 1 and 2 illustrates that a reduction of load effect to the exterior beam of 2/3 has been achieved by changing the torsional stiffness of the beam from zero to infinity. The assumption of zero (negligible) torsional stiffness is reasonable for thin open-walled cross-sections such as plate girders and thus live load distribution in plate girder bridges would primarily be a function of the transverse stiffness of the structure. However, closed sections such as box beams or stocky prestressed concrete sections possess significant torsional stiffness that significantly influences the distribution of live loads.

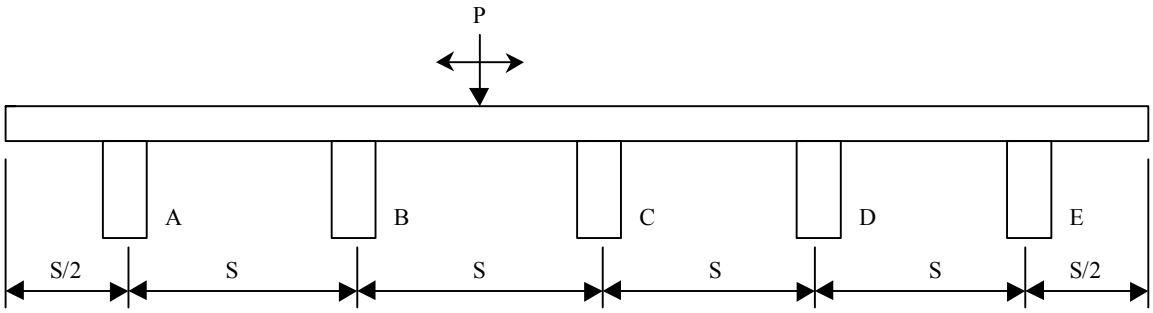


**Figure 6.1. Schematic of 5-Beam Bridge Studied by Tamberg (1968).**

Tamberg presents a series of influence lines where the user may directly calculate the characteristic flexural stiffness ratio, H, as well as several other terms and arrive graphically at an expected amount of live load resisted by a particular beam for various transverse positions of applied load. The influence lines indicate that at best, for an infinitely transverse and torsionally stiff section, the exterior beam resists 20% of the applied load. For infinite transverse stiffness and negligible torsional stiffness, the exterior beam resists 60% of the applied load. However, as the structure becomes less flexurally stiff in the transverse direction with respect to the longitudinal beam stiffness, the load fraction to the loaded beams continues to increase to near 100% for transversely flexible systems. Tamberg cites work that indicates that the benefit arising from multiple flexurally stiff intermediate diaphragms is only apparent once the number of diaphragms per span is three or more. The additional diaphragms only tend to have an effect when the beam spacing exceeds 9 ft up to which point the transverse slab stiffness is dominant.

Eby, Kulicki, Kostem and Zellin (1973) describe the computation of the St. Venant torsional constant for standard AASHTO prestressed concrete I-beams. The reason for the study was explicitly to study the load distribution characteristics of prestressed concrete I-beam bridges for the Pennsylvania Department of Transportation in the early 1970's. The method of analysis used the eccentrically stiffened plate model where the slab is discretized by a series of plate elements and the beams are eccentrically linked to the slab. The beam elements in such a model must be assigned axial, flexural, shear and torsional stiffness properties as part of the analysis. The study by Eby et al. examined the results of a finite difference analysis of standard prestressed concrete I-beams as well as other prismatic sections and compared those results to a series of empirical equations available in the literature at the time. Comparison included examination of the aforementioned Tamberg studies of the 1960's.

Eby et al. determined that Equations 6.1 were accurate when compared to the finite difference results; refer to Figure 6.2 for a description of the variables.

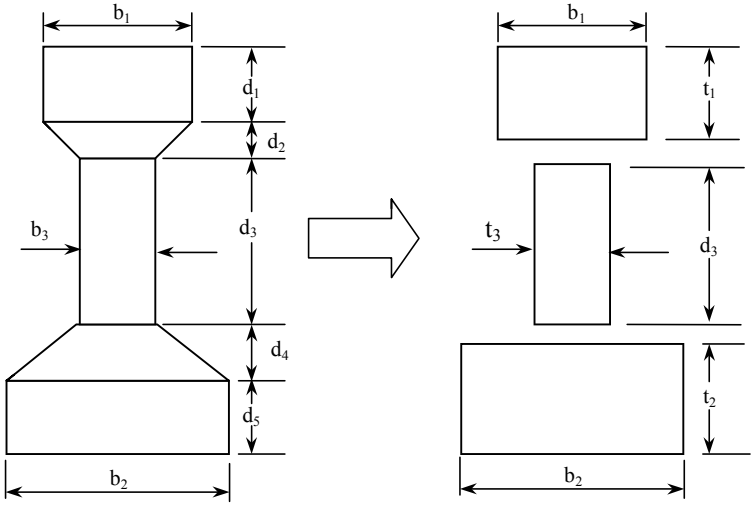


**Figure 6.2. Prestressed Beam Idealization, Eby et al. (1973).**

$$K_T = \frac{1}{3}\left(b_1 t_1^3 + b_2 t_2^3 + d_3 t_3^3\right) + \alpha_1 D_1^4 + \alpha_2 D_2^4 - 0.21(t_1^4 + t_2^4)$$

$$D_1 = t_1 + \frac{b_3^2}{4t_1}$$

$$D_2 = t_2 + \frac{b_3^2}{4t_2} \qquad (6.1)$$

$$\alpha_1 = -0.042 + 0.2204\frac{b_3}{t_1} - 0.0725\left(\frac{b_3}{t_1}\right)^2$$

$$\alpha_2 = -0.042 + 0.2204\frac{b_3}{t_2} - 0.0725\left(\frac{b_3}{t_2}\right)^2$$

In Equations 6.1, "t" represents the smaller of the paired dimensions "b" and "t", i.e., $t_3$ is usually equal to $b_3$. Eby et al.'s approximate equations (Equations 6.1) were compared to the following approximations (Equations 6.2) and found to be in closer agreement with the finite difference results.

$$K_T = \quad I_{polar} \qquad \text{(a)}$$

$$\sum_{i=1}^{3} \frac{A_i^4}{40 I_{polar_i}} \qquad \text{(b)} \qquad (6.2)$$

$$\frac{1}{3}\sum_{i=1}^{3} b_i {t_i}^3 \qquad \text{(c)}$$

The first approximation, Equation 6.2(a), though valid for circular sections, yields results which vary by as much as 1,000% from the finite difference results.

Equation 6.2(b) is given in the AASHTO LRFD Specification, Equation (C4.6.2.2.1-2), as an approximation for the torsional stiffness of a stocky section such as a prestressed beam. AASHTO states that Equation 6.2(b) presented above *"has been shown to substantially underestimate the torsional stiffness of some concrete I-beams and a more accurate, but more complex, approximation can be found in Eby et*

*al."*. Eby's derived equations predict torsional stiffness some 10-20% higher than the AASHTO equations for typical I-girder sections. Hsu (1984) indicates that the AASHTO equation is based on St. Venant's approximations for bulky sections without reentrant corners. Since prestressed concrete I-beams have reentrant corners which tend to stiffen the section, the AASHTO approximation is expected to be a lower bound estimate of the torsional stiffness of a section. Hambly (1977) contests the lower bound assertion and contends that the AASHTO equation overestimates torsional stiffness. The work of other researchers and the commentary in the AASHTO specification do not support this.

Equation 6.2(c) also had significant scatter in the reliability of the results with errors as large as 20% overestimation of the torsional stiffness of prestressed concrete I-beams. The coefficient of 1/3 used in Equation 6.2(c) is technically only valid for very slender elements such as a plate girder flange or web. A more correct representation of Equation 6.2(c) is presented in Figure 6.3 from Bakht and Jaeger (1985). This modified form of the torsional constant equation leads to results that agree with Tamberg's conclusion that Bach's method underestimates the torsional constant for stocky sections.

Using Eby's equations, the torsional constants for standard Iowa DOT prestressed concrete beams were computed and are presented in Table 6.1. These constants are important input to a stiffened plate or grillage computer analysis.

Kostem and DeCastro (1977) comment on the effectiveness of intermediate diaphragms in distributing loads in simply supported prestressed concrete I-beam bridges. In their work, the authors prepared finite element models of two bridges and compared the results to experimental results from field load tests. The first bridge is 71.5 ft long with a 36 ft roadway, has six beams spaced on 6.75 ft centers and a 10 in. x 28 in. reinforced concrete diaphragm at midspan. A safety curb and parapet is on one side only. The second bridge is 68.5 ft long with a 32 ft roadway having five beams on 8 ft centers, and a 9 in. x 34 in. reinforced concrete midspan diaphragm. A safety curb and parapet are on both sides.

The authors concluded via their analytical work that because of numerous gaps in the rail system and lack of full integration with the slab, the curb and rail were only 50% effective in contributing edge stiffness to the bridge. They also concluded via examination of analytical and experimental data that an analytical diaphragm of approximately 20-30% of the calculated composite stiffness produced results in accordance with those measured in the field. This shows the poor efficiency of the diaphragm section in distributing vertical loads. It was determined that this effectiveness was dramatically reduced when multiple lanes of load are applied to the bridge. Virtually no change in live load distribution was observed when the maximum number of lanes were loaded regardless of the presence and configuration of diaphragms in the bridge. For a six beam bridge similar in size to that tested in the field during this research project, diaphragms at midspan were shown to be most effective with loads reducing from slightly more than S/5.5 for a bridge with no diaphragms to slightly more than S/6 for a bridge with diaphragms. Conversely, the exterior beams experience a slight increase in maximum live load with diaphragms in the bridge; with a larger number of diaphragms, the live load carried by the exterior beams increases.

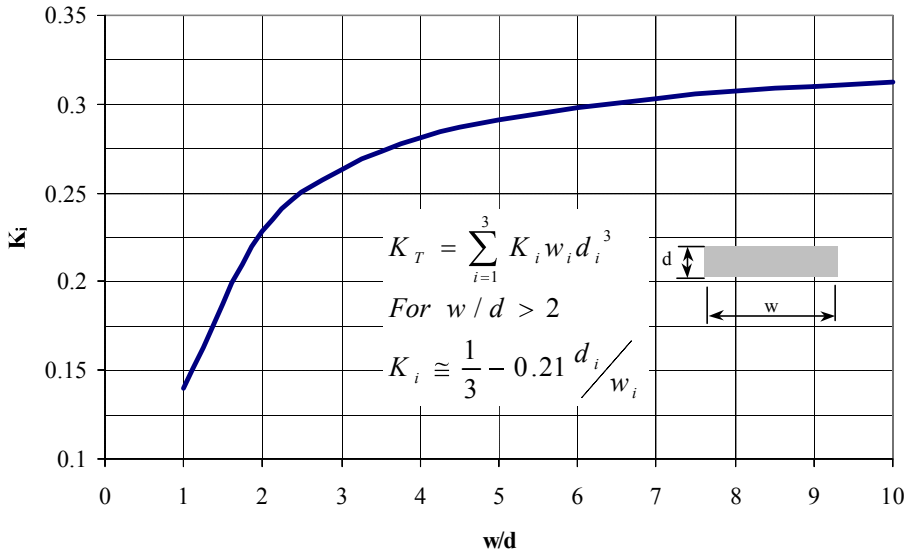


**Figure 6.3. Torsional Constant for Rectangular Sections.**

**Table 6.1. Torsional Constant, $K_t$, for Iowa DOT Standard P/C Beams.**

| Iowa DOT Designation | Torsional Constant, $K_T$, $in^4$ |
|---|---|
| LXA30-46 | 5,275 |
| LXA50-55 | 10,783 |
| LXB34-59 | 7,980 |
| LXB63-67 | 15,444 |
| LXC30-67 | 9,532 |
| LXC71-80 | 18,544 |
| LXD (ALL LENGTHS) | 17,832 |

Deatherage (1987) investigated many of the variables that affect the performance and capacity of beam and slab bridges. There are a number of sources of unintended stiffness that are found to affect load distribution. These include the presence of stiff parapets and railings that tend to edge stiffen a bridge and draw force to the exterior beam lines, partially relieving the interior beams. Additionally, the participation of bracing and the slab in load distribution is discussed as a source of conservatism. Support conditions, typically stiffer than assumed, are mentioned as a source of unintended stiffness. Deatherage indicates that sources of unanticipated strength include material strength in excess of that specified and unintended composite action between the beam and slab.

## *6.2. Computer Modeling*

The behavior of prestressed concrete through its various stages of loading is very difficult to predict. This is due to the complex interaction of a variety of components such as initial stress in the tendons, loss of stress in the tendons, concrete creep and shrinkage, strand relaxation, environmental conditions during service, and level of loading. When coupled with the issue of the effect of damage on the stress state in a damaged beam, the problem becomes more complex. It was not the goal of this research program to answer these very complex behavioral issues on a micro level. Rather, the aim of the analytical modeling portion of the investigation was to develop simple models that assist in understanding the measured response of the field-tested bridges to an acceptable degree of accuracy and to provide practical recommendations regarding the analytical modeling of undamaged and damaged P/C bridges.

The common analytical tool of the researcher is the finite element modeling technique. However, it is unrealistic to assume that the majority of practicing engineers have the time, facilities, or expertise to develop a highly detailed finite element model of a complex damaged bridge structure, refine the model, determine convergence, and interpret the results properly. For these reasons, the analytical tools provided by this research were to be of a somewhat simpler form. The goal was to use simple models, such as grillage analyses or eccentrically stiffened plate models, to predict the global load distribution behavior of prestressed concrete bridges.

The use of various methods of structural analysis for beam and slab as well as solid and voided slab bridges is presented in Hambly (1976). Of particular interest are the recommendations concerning grillage analysis of beam and slab bridges. Two types of grillage models will be discussed, the common plane grillage and a variation known as a downstand grillage. A depiction of these types of idealizations is presented in Figure 6.4.

A plane grillage analysis is one in which all members, longitudinal and transverse, are assumed to be in the plane of the structural model. Hambly recommends that longitudinal elements be placed at the location of main longitudinal structural members. If the beam spacing exceeds 1/10th of the effective span then additional notional longitudinal elements should be used. This is due to the poor distribution characteristics of beam and slab bridges where a large spacing between longitudinal elements will not accurately depict the flow of forces. Even in bridges where the beam spacing does not exceed 1/10th of the span, the distribution characteristics can be improved by inclusion of these notional longitudinal elements.

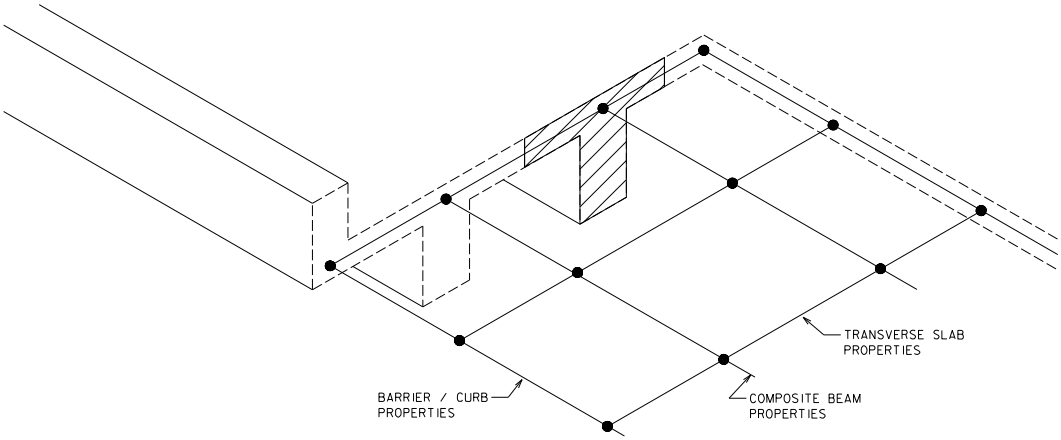


**a.) Plane Grillage**

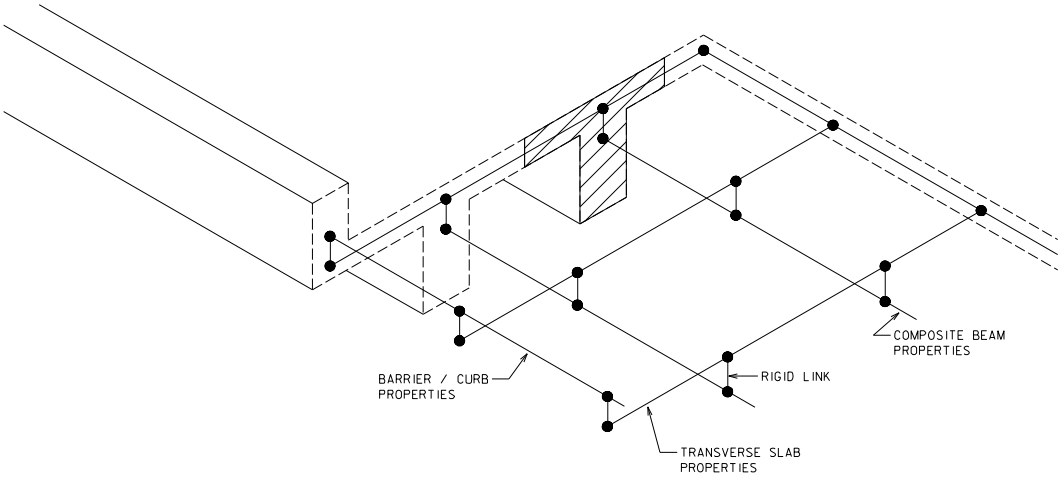


**b.) Downstand Grillage**

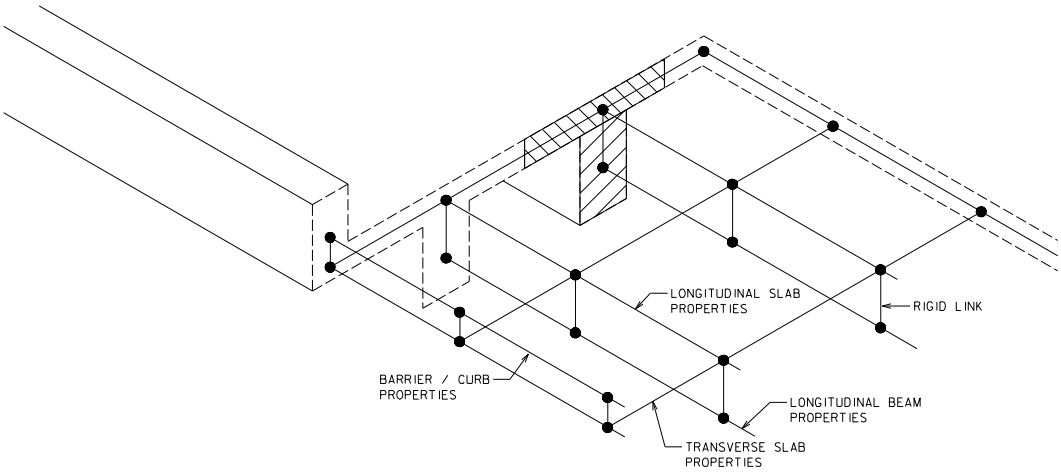


**c.) Space Frame**

**Figure 6.4. Grillage Idealizations of a Typical Beam and Slab Bridge.**

The longitudinal member grillage properties should be calculated about the centroid of the member the grillage element is intended to represent. The change in element centroid from interior to exterior beam due to variations in effective slab width is not recognized in this method of analysis. Hambly comments that if the beam spacing exceeds 1/6th of the effective span or the slab cantilever exceeds 1/12th of the span then shear lag should be considered in the computation of effective width. It is presumed that otherwise the full width of slab from beam to beam including cantilever slabs can be used in computing the cross-sectional properties of the beams. For computation of the torsional constant, the sum of the torsional stiffness of the bare beam is added to that of the tributary slab width.

Transverse members should be located at 1/4th to 1/8th of the effective span apart though Hambly states that this is somewhat arbitrary. The transverse member flexural and torsional properties are as follows:

$$I = \frac{bd^3}{12}$$
$$C = \frac{bd^3}{6} \qquad (6.3)$$

These equations represent the flexural stiffness of a slab element intended to represent a tributary longitudinal length of "b" and a slab thickness of "d". Note that the torsional constant for a wide and thin rectangle is $bd^3/3$ but since the slab is expected to participate in the transverse and longitudinal directions in torsion this halving of the torsional constant is advocated. An allowance for transverse diaphragms is also made assuming the diaphragm is composite with the slab with an assumption that the effective portion of the slab acting as a composite slab with the diaphragms is 0.3 times the spacing of the longitudinal beams.

Hambly comments on the difficulties in "properly" computing material stiffnesses since a slab for instance may be considered uncracked for longitudinal positive moments but cracked in the transverse direction or over a continuous support. Although it is recommended that these issues at least be considered, no guidelines are given to specifically address the situation.

One of the problems with a typical plane grillage is the loss of geometric consistency in the model. The relative distance between longitudinal and transverse elements is lost in the sense that the longitudinal beams whose composite centroids are generally within the beam cross-section and the transverse slab elements whose centroids are at mid-plane of the slab are assumed to be concurrent. In so doing, the membrane forces in the slab are somewhat underestimated and the inter-beam shear (shear lag) phenomenon is not properly modeled. A grillage which does not account for relative vertical separation of structural elements is not as efficient in distributing load nor can it depict the movement of the neutral axis across the width of the bridge. Upward movement of the neutral axis occurs in the beams carrying a majority of the load since the membrane action of the structure causes significant axial tension forces in the heavily loaded beams. Conversely, beams remote from the load are subjected to axial compressive forces which tend to lower the neutral axis. This varying neutral axis location causes a series of internal couples to

arise in the bridge which reduces the amount of load carried by the most heavily loaded elements and results in a more efficient distribution of live load across the width of the bridge.

As an alternate to the plane grillage, Hambly discusses a model known as a downstand grillage. A downstand grillage does not coalesce the longitudinal and transverse elements into the same plane rather it treats them as independent elements separated by a rigid link that enforces compatibility conditions on the displacements of the structure. The structure is transformed from a plane to a space frame but still uses the general beam type elements in the creation of the model. For instance, it is no longer necessary to assume that the interior and exterior beams have the same centroid nor to disregard the vertical separation of the beams and slab. A downstand (upstand) grillage also allows for simple consideration of barrier rails/parapets whose centroids lie above the deck. It is important to include these edge stiffening effects since they significantly influence the distribution of loads placed in exterior lanes.

Johnson and Buckby (1979) discuss various aspects of the behavior of composite steel beam and concrete deck bridges. Their discussion of the grillage analysis of structures is of particular relevance. Johnson and Buckby conclude the following about the suitability of the grillage method of analysis.

- Grillage analysis is best for beam and slab deck bridges.
- Each longitudinal member should be represented by a grillage beam with a minimum of five and preferably nine such elements. This may include the addition of nominal longitudinal elements between beams which have the stiffness characteristics of a small portion of the slab.
- Each transverse diaphragm should be represented by a transverse beam along with a minimum of five transverse beams to represent the slab. It is recommended that when computing the properties for diaphragm members, a composite portion of slab be included in the analysis.
- Transverse elements should extend to the physical edge of slab and be connected to longitudinal elements even if there is no edge stiffening.
- For skewed decks, transverse beams should be orthogonal to the main members.

Johnson and Buckby caution that when an edge beam element is included to account for the edge stiffening due to a curb or parapet, the analytical results in the vicinity of the edge beam may be misleading and should be checked using a method that considers this effect. One such method is that of Bakht and Jaeger (1985). Johnson and Buckby's conclusion regarding lack of accuracy near edge beams (barrier rails) is troubling in that the use of the grillage method was initially advocated in this project as a potential higher order analysis of load distribution in damaged bridges where damage was to the exterior beams.

Johnson and Buckby present a complete design of a bridge in which the grillage method is used for the determination of live load distribution. Shear lag (the use of an effective width) was neglected; each beam's composite properties were computed assuming a participatory slab half way to the nearest beam or in the case of exterior beams, equal to the overhang. The moment of inertia specified for the beams was with respect to the neutral axis of this composite section and variation of neutral axis location from interior to exterior beams is neglected. Bach's method was employed to compute the torsional constant but the

contribution due to the slab is purposely halved, i.e., $bt^3/6$ instead of $bt^3/3$ since the slab will participate in carrying torsional stresses in orthogonal directions. This grillage analysis concluded that statical distribution of loads to the exterior stringer (assumes the slab is discontinuous at the first interior stringer) was very conservative. The analysis did not include an edge beam element representative of a continuous traffic barrier.

Jaeger and Bakht have written extensively on the behavior of bridge structures, particularly with respect to live load distribution. In Jaeger and Bakht (1982), the authors present a series of recommendations associated with the idealization of various structures using the grillage analogy. The authors contend that the grillage method is suitable even when effects such as edge stiffening, non-prismatic stiffness, and large skew are present. The inherent "feel" a designer acquires for the behavior of a bridge using the grillage method is also cited as an advantage. One principal advantage of grillage methods over a more complicated finite element analysis is that the grillage method uses beam elements and thus the results are output in the form of shears, moments, torsions, and axial loads. In contrast to this method, finite element analysis results are output as stresses and strains that must then be integrated over the beam cross-section to obtain force resultants. Jaeger and Bakht present the following rules regarding idealization of bridge structures using the grillage method.

Longitudinal members should be located to coincide with the centroid of the composite beam and slab section. These beam elements are assigned the properties of the composite beam. No attempt is made to distinguish between the differences in neutral axis location for interior and exterior beams. The flexural inertia is simply that of a transformed composite beam with the exception that the effects of shear lag, i.e. the reduction in effective flange width, are not considered. The portion of slab assumed to act compositely with the beam is the beam spacing for interior beams and half the beam spacing plus overhang for exterior beams. This is both convenient and reasonable since small changes in longitudinal stiffness of the composite beam have negligible effects on the overall load distribution characteristics of the bridge. If a beam has non-prismatic properties, i.e., a haunched beam, or in this research, isolated damage, the beam properties may be accurately represented by a series of stepped segments or alternately using the equivalent moment of inertia procedure described in Bakht and Jaeger (1988) and Jaeger and Bakht (1989). The torsional inertia of the longitudinal elements is the summation of the torsional inertia of the beam plus that of the slab reduced by a factor of 1/2. This is expressed as

$$K_T = K_g + \frac{St^3}{6} \tag{6.4}$$

where $K_g$ is the torsional constant of the beam and S represents the beam spacing. Transverse members, primarily representing portions of the slab spanning between beams, are assigned the flexural inertia of the tributary width of slab represented plus a torsional constant, $J_y$, defined as

$$GJ_y = EI_y$$

$$\therefore J_y = \left(\frac{E_c}{G_c}\right)\left(\frac{L_x t^3}{12}\right) \tag{6.5}$$

where $E_c$ and $G_c$ represent the Modulus of Elasticity and shear modulus of the deck concrete and $L_x$ is the tributary width of slab represented. If Poisson's ratio is taken to be zero, the equation for $J_y$ reduces to that presented by other researchers, $L_x t^3/6$ for a thin rectangle. Jaeger and Bakht, advise that transverse elements be extended to the physical edge of the slab and connected with longitudinal element at that location. If the edge beam is not present or explicitly modeled, a notional stiffness should be assigned to the edge elements.

Loads must also be idealized; there are several approaches for load idealization. These include assuming the slab to act as a simple span between beams and simply assigning to each longitudinal member its portion of the vertical load. The alternate approach is the common fixed end forces approach commonly used in structural analysis where the beams are assumed to receive vertical and bending forces from placement of the vertical loads. In the case of transverse apportionment of the vertical loads, one must recognize that the fixed end actions which develop in the transverse member constitute flexural bending but are input as loads on the longitudinal elements as torsional forces. Neglecting these bending components in the input of structural loads leads to large errors for wide beam spacings and for loads on cantilevered slabs. As an alternate to apportioning the vertical loads to the longitudinal beam elements, additional longitudinal elements midway between the beams may be added and assigned the properties of a central region of the slab. This idealization has been shown to slightly improve the accuracy of the results.

Kirkpatrick et al. (1985) discuss the load testing of four inverted-tee bridges in Northern Ireland and compares the experimental results to those obtained from a grillage analysis. The pretensioned beams in the bridge are used side-by-side with only a nominal gap between the 1 m wide bottom flanges. The top flange is only slightly wider than the web and supports a cast-in-place formwork system. The beams have a nominal 28-day compressive strength of 42 MPa and the slab, 30 MPa.

Strains were monitored at midspan with vibrating wire strain gages. Two loaded trucks each weighing 294 kN were positioned at various locations along the bridge. In order to determine the effect of the upstand barrier rail system on load distribution, load tests were conducted both before and after the rail was cast. Strains were converted to stresses using a nominal elastic modulus and these stresses converted to individual beam moments via a calculated section modulus. The load per beam was compared to the total measured moment across the width of the bridge and from this, the fraction of live load per beam was determined.

Because there are a large number of beams in a bridge of this type, for instance 20 beams in one of the test bridges, a simplification in the grillage model was made in that each analytical longitudinal member represented two physical beams. This produced reasonable results on the global scale but underestimated the results locally under the loaded beams. A second mesh with one analytical element per beam line was

created and found to be in closer agreement with the experimental results. The effect of the upstand rail was to decrease the bottom flange tensile stress in several beams near the edge of the bridge under exterior lane loading. The exterior lane position was critical for this bridge. The grillage model with an upstand rail underestimated the experimental stresses while the grillage model with no rail provided a reasonable correlation to experimental tests in which the rail stiffness was participatory. The authors concluded that the grillage model based on the beam properties alone be used to model bridges of the type tested since such a model provided a conservative estimate of the moments in the most heavily loaded beams and eliminated the complexity of trying to assign the longitudinal stiffness contribution from the upstand rail system.

Kostem (1986) presents the results of a comparative study of load distribution and bridge behavior comparing a three-dimensional finite element analysis of two bridges with a grillage analysis of the same. The finite element analysis was conducted using the SAP IV program while the grillage analysis used the STAAD-III program. The bridges were Pennsylvania Department of Transportation standard bridges composed of simply-supported prestressed concrete stringers at right angles to the supporting substructure. The bridges contain eight beam lines on 6 ft centers with a 7.5 in. deck. Bridge 1 had a length of 50 ft while Bridge 2 was 78 ft long. Three vehicle configurations were used to load the bridge, the standard AASHTO HS20 loading, a six axle vehicle representing a concrete mixing truck, and a third load with eight axles used as a permit load in the State of Pennsylvania. The vehicles were positioned to cause the maximum midspan moment in each model and were positioned in an extreme edge lane of the bridge and centered transversely on the bridge. The moment gradient across the transverse width of the bridge due to the edge lane load pattern was anticipated to represent a worst case scenario for the grillage model.

The grillage analysis divided the longitudinal elements into ten equal spaces and connected these longitudinal nodes with transverse elements representing the tributary slab. This discretization results in 80 longitudinal elements and an additional 77 transverse elements. The composite properties of the slab were based on full-width participation of the slab in computing the flexural and torsional stiffness constants. This forms an upper bound on structural stiffness. One of the inherent limitations of the grillage analysis is that the longitudinal beam and transverse slab, whose centroids are naturally at different vertical locations, are assumed to be coplanar. The membrane forces that develop in a real structure in the beam and slab are lost in this type of analysis. When interpreting the results of a grillage analysis, the biaxial stresses in the slab must be carefully determined.

Results are presented for interior and exterior beam moments, reactions, and deflections for load in interior and exterior lanes from both the finite element and grillage analyses. For the longer bridge, Bridge 2, the grid analysis overestimated the deflections and moments in the “loaded” beam (i.e. exterior beam moment when exterior lane is loaded, etc.) by 5-20%; the best comparison to the finite element model results occurred when examining the moment response of interior beams with interior lanes loaded. The widest disparity was for exterior beam moments with exterior lanes loaded. Examining the results for

Bridge 1, the shorter bridge, one notices a general trend towards overestimation of moment and deflection once again from the grillage analysis with the exception of Truck 2, the concrete mixer, where the grillage model underestimates the response of an exterior beam by as much as 25%. Reactions are generally underestimated by the grillage method. Kostem concludes that a crude assessment of the results indicates that as span length increases, accuracy of the grillage analysis increases. The data do not support this conclusion but to the contrary, the prediction of deflection is markedly better in the short bridge than in the long. Exterior beam moment predictions were off by roughly the same percentage. The only case where the longer bridge demonstrated better convergence was in interior beam moment with interior lanes loaded.

The effectiveness of lateral load distribution was studied by examining the response of an interior beam when exterior lanes are loaded and vice versa. The correlation was very poor. In some cases, the grillage analysis predicted a response of the opposite sign of the finite element analysis, for instance, upward instead of downward deflection. The exterior beam moment when interior lanes are loaded is only 15-30% of that predicted using finite element analysis. The interior beam moment due to exterior lane loading was roughly 70-90% of the finite element results. The grillage consistently underestimates the moment response by a significant amount. This is an indication that the live load distribution characteristics of Kostem's grillage model is poor compared to the response predicted using finite element techniques. The results indicate a worst case scenario whereby when exterior beams are loaded, they do not shed load nearly as efficiently to interior beams in a grillage model as in a finite element model. Conversely, interior lane loads are not well dispersed to the edge beams but stay tightly concentrated over the central beams in the loaded area.

Kostem concludes that the grillage analysis is accurate for the assessment of exterior beams with exterior beams loaded and interior beams with interior beams loaded but is poor in predicting global load distribution characteristics. He contends that there is little proven information on the computation of torsional properties for the longitudinal members, and on the computation of properties of the transverse members in general. It is stated that with the emergence of finite element techniques, little time has been spent on refining/proving the grillage method of analysis.

In 1994, AASHTO released the first edition of the LRFD Bridge Design Specifications. In these specifications, new live load distribution formulas consistent with the NCHRP 12-26 recommendations and the 1994 Guide Specification (AASHTO, 1994) are employed. As an alternate to the empirical equations presented by AASHTO, refined methods of analysis are also advocated. These methods are detailed in Articles 4.4, 4.5 and 4.6 of the LRFD Specifications. A brief description of the AASHTO modeling guidelines of Article 4.6.3 is presented below.

For the inclusion of a reinforced concrete deck in mathematical models, it is recommended that they be analyzed as isotropic elements fully effective along the entire bridge length. Wheel loads should be modeled as patch loads applied to the deck.

In modeling the main longitudinal elements of beam and slab bridges, the following recommendations are given:

- Preferably nine nodes per beam span should be used
- When employing plate and beam elements, it is preferable to maintain the relative vertical distance between the elements (rigid offset, master/slave specification). If this is not possible, the longitudinal and transverse elements can be located at mid-thickness of the plate as long as consideration of eccentricity is made in member property specification.
- For grid analysis, an effective width should be considered.
- Notional transverse elements should be used to model the deck.
- St. Venant torsional inertia should be considered and computed in accordance with C4.6.2.2.1 of the LRFD Specifications. Torsional stiffness of the slab should be based on one-half the width of the effective slab used for flexural stiffness computations.

Zokaie, Imbsen and Osterkamp (1991) present a summary paper of the work conducted for the NCHRP 12-26 study on improved live load distribution factors which were eventually included in the AASHTO LRFD Specification with minor modification. In their paper, recommendations are presented dealing with the appropriate level of rigor required for accurate assessment of bridge behavior under live load. A three-level approach is described in which a level one analysis encompasses generalized equations for live load distribution, level two includes grillage analysis as well as influence surface approaches, and a level three analysis is a full three-dimensional finite element analysis. The authors contend that with some care, the grillage method will give results close to those of the more sophisticated finite element analysis methods. The authors also describe the accuracy of the empirical live load distribution factors to be within five percent of a detailed (level-three) analysis.

Barker and Puckett (1997) present a series of analytical models of varying degrees of complexity which they used to examine live load distribution in a single-span steel bridge with composite concrete deck. Both grillage and combined beam and plate models are used.

Barker and Puckett use a plane grillage model in their analysis. Computation of beam and slab properties generally follows the AASHTO recommended procedure previously presented. Because of the loss of geometric consistency in the plane grillage model, the beam eccentricity from the center of deck is considered by computing a moment of inertia with respect to mid-plane of the deck. The transformation is of the form $I = I_g + A_g e_g^2$ where $I_g$ and $A_g$ are the moment of inertia and area of the basic beam and $e_g$ is the eccentricity of the centroid of the basic beam from the mid-height of the slab. This inertia is further modified by transforming the girder to equivalent slab material using the modular ratio and adding the moment of inertia of the effective width of slab calculated about its own centroidal axis. A grillage model as so described was found to produce distribution factors somewhat less than those computed using the AASHTO LRFD empirical equations.

Barker and Puckett also generated a more detailed finite element analysis but once again assuming the beam and slab to be in the same plane. The beam eccentricity was considered in a fashion similar to that employed in the grillage analysis with the only modification being no provision of an effective slab width. The slab was modeled by shell elements with in-plane effects neglected but the plate bending components retained. Results of the finite element analysis indicated more effective distribution of live loads bending moments than did the grillage but still in general conformance with the LRFD distribution factors.

Aswad and Chen (1994) discuss the impact that the AASHTO LRFD distribution factors have on the design of prestressed concrete I-beams and spread box beams. In their work, the empirical equations for live load distribution originally introduced as a guide specification and henceforth incorporated into the AASHTO LRFD specifications are compared to computer model predictions. Computer models were developed using the ADINA and STAAD general-purpose computer programs. The objective of their work was to illustrate that refined computer models produce a lower estimated live load per beam. Ten bridges were analyzed in their study. The derivation of distribution factors from finite element results is explained.

Only the ADINA program analyses are presented in the aforementioned paper. In the ADINA analysis, the stiffened plate model such as shown in Figure 6.5 is used whereby the deck is modeled by a series of orthotropic shell elements and the beams by an isoparametric eccentric beam element acting as a stiffener. Composite action was attained by specifying rigid links between the beam and slab. Material properties were assumed to be linear with different material constants specified for the cast-in-place and precast portions of the structure. The torsional constant for the precast beam elements was based on the method of Eby (1973). An orthotropy correction was made for the stiffness of the slab based on the square of the ratio of the beam spacing to the clear slab span. This factor is used to adjust the Modulus of Elasticity of the plates in the transverse direction. Beams were assumed to be pinned at their ends for transverse axis rotation but were torsionally restrained.

Because a beam element is used to model the eccentric beam and it is rigidly linked to the slab, output from the analysis will consist of axial tension in addition to bending in the beam elements. This axial and bending force can be used in the common P/A+M/S equation to obtain the bottom flange stress in the beams where A and S are based on the basic (non-composite) beam. The total moment resisted by the composite section requires integration of the slab stresses over the effective flange width and superposition of the local moment resisted by the beam element as represented in the following equation:

$$M_c = M_b' + \int_0^b M_{slab}\,dl \tag{6.6}$$

where:

$M_c$ = Total moment reisted by the composite section

$M_b'$ = Moment resisted by the beam element

$M_{slab}$ = Moment per unit width resisted by the slab element

b = Effective width of the slab

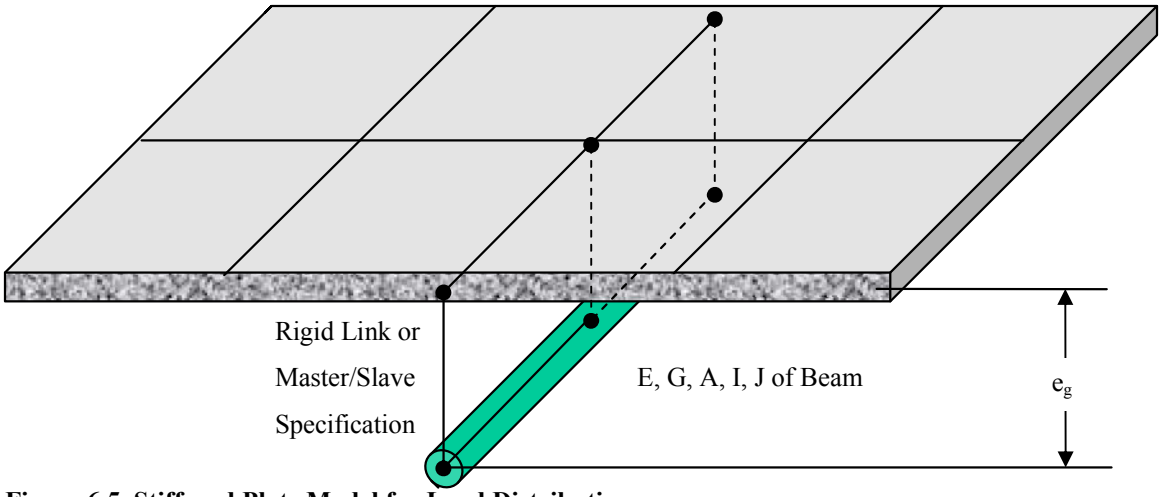


**Figure 6.5. Stiffened Plate Model for Load Distribution.**

The term $M_b'$ is the beam moment referenced to a plane within the slab. If the reference plane in the slab is taken as the location of the compression resultant due to the trapezoidal stress distribution in the slab, the integral term vanishes. A uniform stress distribution in the slab places the resultant a mid-thickness while a reasonable upper bound for the resultant would be at 2/3 of the depth of the slab measured from the beam top. Aswad and Chen assume an average location of 60% of the slab thickness from the top of the beam for the compression resultant. In so doing the moment resisted by the composite section can be computed as $M_c = M_b' = M_b + P(y_t + 0.6t_s)$ where $y_t$ is the distance from the centroid of the bare beam to the top fiber of the beam. An alternate procedure is to compute the moment resisted by using simple beam theory, $M_c = S_{bc} f_b$ where $S_{bc}$ is a computed composite section modulus taking into account the effects of shear lag if deemed necessary and $f_b$ is the bottom fiber stress in the beam element. Aswad and Chen comment that for the test bridges studied, both of these approaches gave essentially the same results with the second approach yielding only slightly higher (1-2%) values of distribution factors.

To validate the numerical models developed, the authors compared their ADINA analysis with published results from others' field tests and found excellent correlation. Confident in the models, they then analyzed eight AASHTO I-beam bridges and two spread box bridges. Span to depth ratios were varied as were material properties. For the I-beam bridges, the midspan diaphragm was modeled as non-composite with the slab and the barrier rail stiffening effect was ignored.

Distribution factors from the computer analysis were between 4-11% less than predicted by LRFD for interior beams and when multiple lane reduction factors were considered, the distribution factors were on the order of 20% less than predicted by code for an interior beam. This is a greater savings than postulated by Zokaie et al. (1991). Aswad and Chen determined that the code underestimates the distribution to exterior beams by 7-15% without the inclusion of barrier rail stiffness which may skew the results even further. There is no commentary on how the distribution factor for the exterior beams was

calculated though the AASHTO LRFD Specification prescribes several methods with the most severe governing the design.

## 6.3. Validation of Modeling Techniques

The first task in this portion of the research program was to collect information regarding analytical modeling of bridge structures using a variety of techniques. This was presented in the previous section. Following the literature review which concerned two main methods of analysis, the stiffened plate and grillage method, models of both types were created for the analysis of the center span of the I-680 bridges.

It was decided at the outset of this project that any analysis conducted for purposes of understanding/validating the field behavior should be of a fairly simple nature using software commonly available in design offices. This was a deliberate decision since it was envisioned that if a suitable idealization could be made for the undamaged and damaged bridges that accurately reflected the experimental behavior, the analysis method would have practical application in the analysis of future damaged P/C bridges. It was decided that the STAAD-III program would be used as the analysis tool since it can be used to model frame structures such as a plane or space frame grillage and also to model structures using a combination of solid, plate and beam elements. An additional reason for the use of the STAAD-III software was that it is already an analysis tool used by the Iowa DOT.

In order to test the program's ability to accurately model structures using both the stiffened plate and grillage method of analysis, it was decided to first test the STAAD program against published results from other programs. This is an important validation since many analysis programs have different element formulations and allow for different variations in inputting of material properties, boundary conditions, load idealizations, etc. The results of this validation study are presented below.

### 6.3.1. Grillage Model Validation

For purposes of validating the STAAD program to model plane grillage structures, a published solution was selected for comparison. The published solution comes from the text by Barker and Puckett (1997), example problem 6.4. The example presents the plane grillage analysis of a six-beam bridge composed of simply-supported steel stringers and a concrete deck. One of their load cases was selected as the basis for comparison, Load Case 1, a load placement that causes maximum moment in the bridge due to load in a single lane against the barrier rail. After discussion with the text authors, it was concluded that the equivalent nodal moments in the text have incorrect signs. However, since the comparison is to the published solution, the moments have also been incorrectly modeled in STAAD.

Barker and Puckett use the formula $I = I_g + A_g e_g^2$ where $I_g$ and $A_g$ are the moment of inertia and area of the basic beam and $e_g$ is the eccentricity of the centroid of the basic beam from mid-height of the

slab to compute the moment of inertia of the composite beam. This is analogous to assuming that the neutral axis of the structural system is at the mid-height of the slab. Following the transformation of the beam to the centerline of the slab, the steel stringer was transformed into equivalent concrete using the modular ratio, n = 8. The longitudinal stiffness of the composite slab, $St_s^3/12$, was added to form the total composite stiffness. Using a beam area, $A_g$=31.7 in.$^2$, beam inertia, $I_g$=4,470 in.$^4$, eccentricity of beam and slab centroids, $e_g$=18.92 in., slab thickness $t_s$=8 in. and a beam spacing, S=8 ft, results in a combined longitudinal stiffness following transformation of 130,576 in.$^4$. Similarly, the torsional stiffness of the composite girder of the transformed torsional constant of the beam and the $St_s^3/6$ torsional contribution of the slab is 8,232 in.$^4$. For the transverse members spaced on 7 ft centers, the flexural inertia is $bt_s^3/12$ and the torsional constant $bt_s^3/6$ with b = 84 in.; these values are 3,584 in.$^4$ and 7,168 in.$^4$, respectively.

Figure 6.6 presents the simply supported bridge model used to test the STAAD program against the previously published solution. The longitudinal beams are numbered 1 to 6 from left to right. Beams 1 and 2 are loaded in this model. A comparison of the maximum moments in each beam from Barker and Puckett's solution vs. the STAAD solution is presented in Table 6.2; the agreement is excellent. The closeness of the results indicates that STAAD can accurately simulate the distribution of bending forces. The reader is referred to Section A.1 of Appendix A for the STAAD input file used to create the grillage model presented in Figure 6.6.

The method of analysis proposed by Barker and Puckett differs from most others in the computation of longitudinal stiffness. In Section 6.2, various recommendations were given for the computation of section properties for grillage members. In the presentation of the work of Hambly (1976), Johnson and Buckby (1979), and Jaeger and Bakht (1982), the authors all concur that the computation of the longitudinal stiffness of the main members should be made about the centroid of the composite beam and slab section not about the mid-plane of the slab as done by Barker and Puckett. For an interior beam in Barker and Puckett's model, the composite moment of inertia about the centroid of the composite beam is 108,065 in$^4$ and for an exterior beam the moment of inertia is 105,973 in$^4$. This represents a decrease in flexural stiffness of 17% and 19% for the interior and exterior beams, respectively. The results from a grillage analysis with these member properties, the properties for the transverse members being the same, are also presented in Table 6.2 under the heading and STAAD (b). There is no meaningful difference in the results for main member bending regardless of which approach is used for computation of the longitudinal beam flexural inertia. It can be concluded that the results of the STAAD model agree with a published solution. It can also be concluded that for the particular bridge studied, substantial changes in longitudinal flexural inertia have a negligible effect on the longitudinal bending moment distribution in the bridge. This confirms that live load distribution is rather insensitive to substantial changes in longitudinal stiffness and is predominantly related to the transverse stiffness characteristics of the structure.

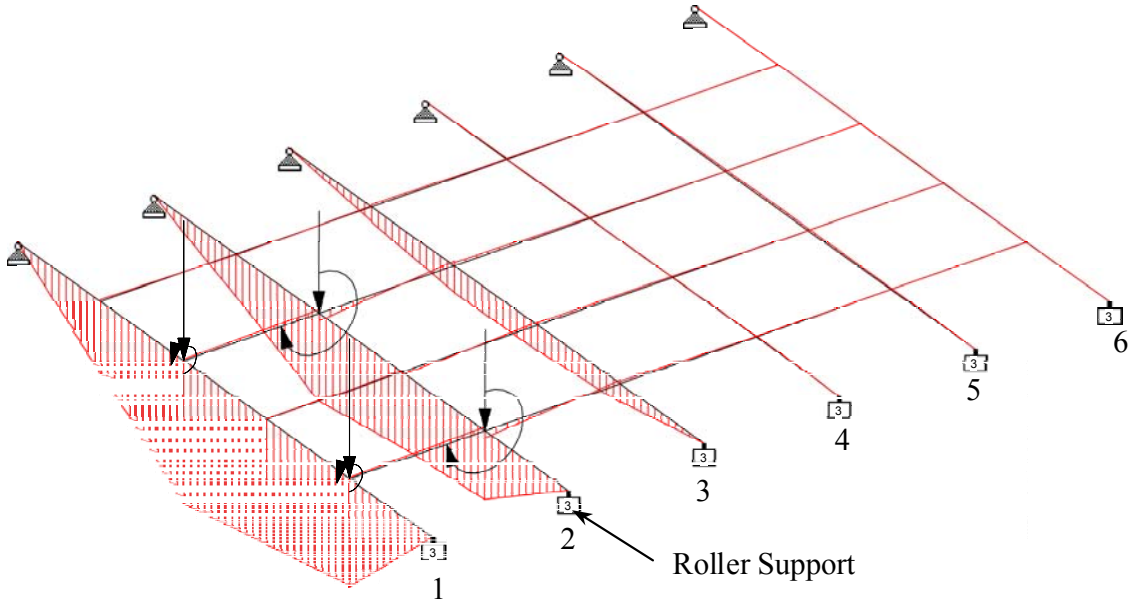


**Figure 6.6. Applied Loads and Resulting Bending Moment Diagrams, Grillage Model.**

**Table 6.2. Comparison of STAAD Solution to Published Grillage Results.**

| | Live Load Moment in Each Beam, ft-kips | | | | | |
|---|---|---|---|---|---|---|
| | Beam 1 | Beam 2 | Beam 3 | Beam 4 | Beam 5 | Beam 6 |
| Barker & Puckett | 203 | 123 | 37 | 0 | -4 | -1 |
| STAAD | 201 | 124 | 37 | -1 | -3 | 0 |
| STAAD (b) | 200 | 124 | 39 | 0 | -3 | -1 |

The observation that for significant changes in main member flexural inertia the longitudinal moment in the most heavily loaded beam decreases by less than 1% is important. It may be similarly concluded that localized changes in flexural inertia have little effect on the overall distribution of forces. This was studied by arbitrarily reducing the composite flexural inertia of the center 20% of Beam 1 by 50%. The maximum moment in the exterior beam decreased from 200 ft-kips to 187 ft-kips, a 6.5% reduction while the moment in Beam 2 increased from 124 ft-kips to 139 ft-kips, an increase of 12.1%. Moments in Beams 3 through 6 were essentially unchanged. This isolated study indicates that little change in load distribution should be expected due to damage. This was also shown as there were only subtle differences between the experimental deflected shapes of the damaged WB bridge and the repaired WB / undamaged EB bridge as previously discussed in Chapter 3 of this report. Similar analytical conclusions were presented in Tables 4.6 through 4.8 of Chapter 4.

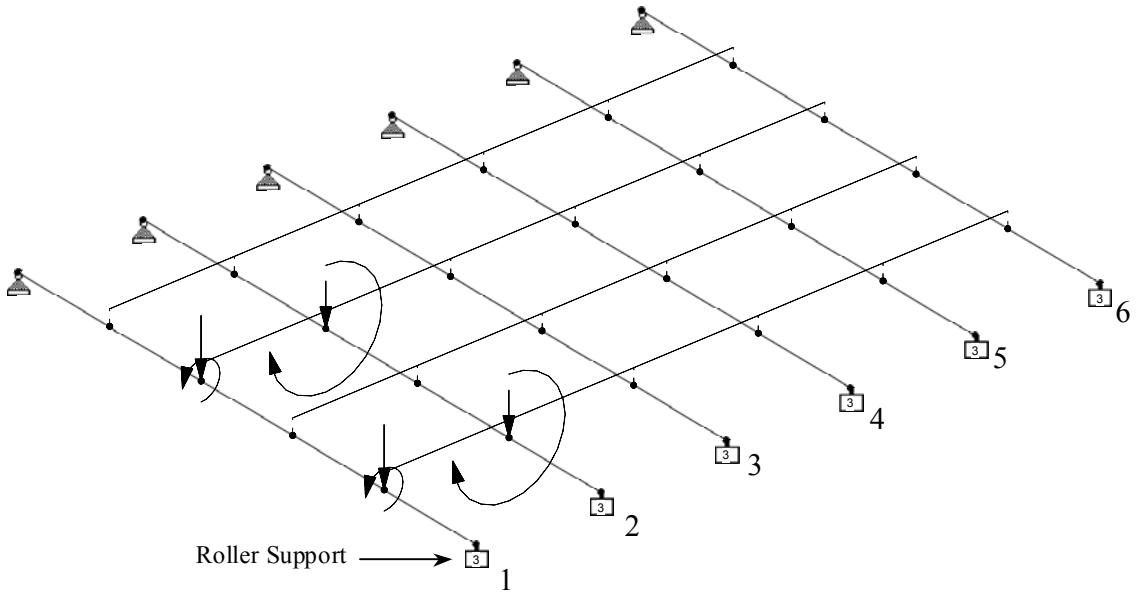


**Figure 6.7. Downstand Grillage Model of Barker and Puckett's Example Bridge.**

For comparison to the co-planar grillage model, STAAD (b), previously presented, a downstand model, shown in Figure 6.7, was created for the same bridge and loading. The STAAD input file for this model is presented in Section A.2 of Appendix A. In the downstand idealization depicted, the longitudinal members are assigned the cross-sectional properties and geometric centroid of the composite beam and slab section. The cross sectional properties of the longitudinal members are as previously described for the planar STAAD (b) model; the interior beams have a moment of inertia of 108,065 $in^4$ and the exterior beams, 105,973 $in^4$. The transverse member properties are the same as in the planar analysis. The only difference between the planar analysis and the downstand grillage is that an eccentric link is provided between the centroid of the composite beam and the mid-plane of the slab. For the bridge in question, the centroid of the composite section is only 4.7 in. below the centroid of the slab so the elements in Figure 6.7 are separated by a very short rigid link.

Results from the original STAAD (b) plane grillage are compared to those from the downstand model in Table 6.3. As can be observed, the results from the plane and downstand analyses are essentially the same though this is likely due to the small offset of the composite beam section from the centerline of the slab. A three-dimensional model is usually somewhat more efficient at distributing load than is the two-dimensional plane grillage. The total internal moments in the plane and downstand grillage are the same and compare well to a total applied moment on the bridge of 358 ft-kips.

**Table 6.3. Comparison of Plane and Downstand Grillage Models.**

| | Live Load Moment in Each Beam, ft-kips | | | | | | |
|---|---|---|---|---|---|---|---|
| | Beam 1 | Beam 2 | Beam 3 | Beam 4 | Beam 5 | Beam 6 | Total Moment |
| STAAD (b) | 200 | 124 | 39 | 0 | -3 | -1 | 359 |
| Downstand Grillage | 199 | 124 | 39 | 2 | -3 | -2 | 359 |

### *6.3.2. Stiffened Plate Model Validation*

Another relatively simple modeling technique for bridge analysis is the use of stiffened plate models. The following discussion on model validation serves two purposes. First, a comparison of a stiffened plate solution published by Aswad and Chen (1994) using the ADINA program will be compared to a STAAD model of the same bridge. Secondly, a stiffened plate model of the Barker and Puckett example bridge will be created to determine if there are significant differences in live load distribution characteristics for bridges modeled using the grillage and stiffened plate methods.

#### *6.3.2.1. Comparison of STAAD and ADINA Models*

As previously described in Section 6.2 of this report, Aswad and Chen (1994) used the ADINA program to assess the correctness of the empirical live load distribution factors in the AASHTO LRFD specification. In an appendix of their paper, the authors present the analysis of a particular test case to illustrate their method of analysis. Details of the model bridge to be analyzed follow.

The model bridge was a 96 ft long simple span composed of five AASHTO Type V precast beams spaced on 10 ft centers. The bridge had a 48 ft total width and a 44 ft roadway. The barrier rail was not integral with the slab, which was 9 in. thick. The beam area and flexural moments of inertia are standard tabulated properties while the torsional constant was computed using the methods proposed by Eby et al. (see Section 6.1 of this report). The authors used a minimum of 12 equal spaces along the length of the beam (actual number of divisions was not specified) for the nodes of the beam and plates. Each plate extended from the centerline of beam to midway between beams, i.e., had a width of S/2. The deck concrete had a Modulus of Elasticity, E, of 4,067 ksi. Because of the difference in clear span of the deck vs. center to center beam spacing, the authors use an orthotropy factor, $D_y = (S/\text{Clear Span})^2$, to modify the E of the plates in the transverse direction. The value for $D_y$=2.37 for the bridge in question, i.e., $E_{transverse}$=9,639 ksi. The E for the beam concrete was specified as 5,250 ksi. The midspan diaphragm was 10 in. wide and 36 in. high. The live load was three full lanes of HS-25 design load without impact and no reduction for multiple presence.

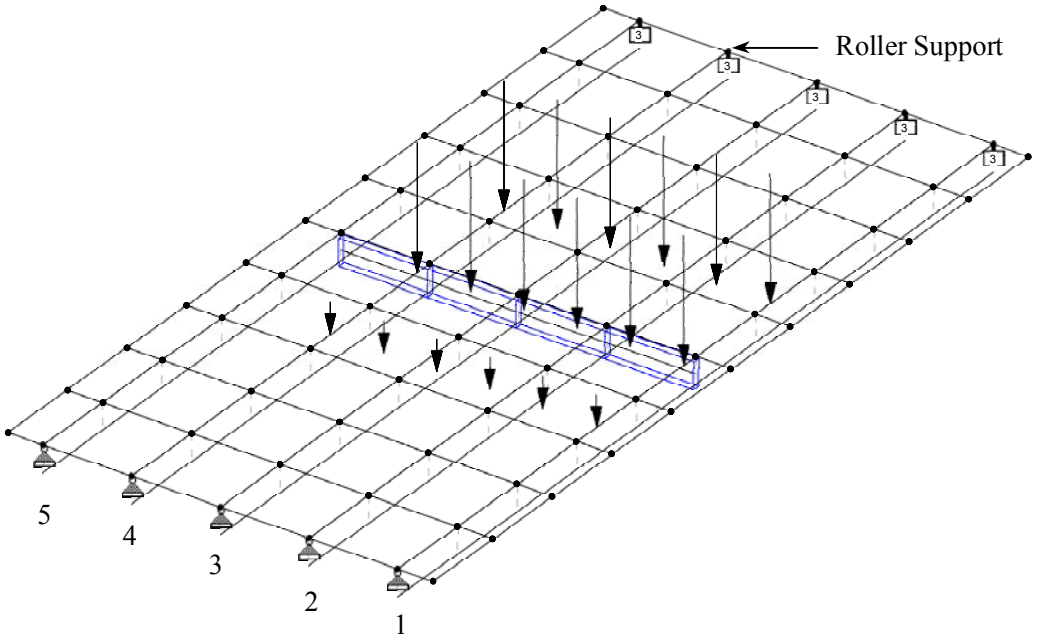


**Figure 6.8. STAAD Stiffened Plate Model of the Aswad and Chen Test Bridge.**

The STAAD model depicted in Figure 6.8 uses a different mesh that that used by Aswad and Chen. A total of ten elements were used along the length of the beam (9.6 ft long elements) and the plates were assumed to extend from the centerline of beam to adjacent beam (10 ft wide) or to the edge of the 4 ft overhang. The aspect ratio of the plates is 1.04 : 1 for the plates between beams and 2.4 : 1 for the overhang plates. In contrast to the ADINA model where orthotropic stiffness can be specified for the plate elements, the STAAD analysis only allows for isotropic material properties. In order to assess the STAAD program's sensitivity to different slab moduli, separate runs were made assuming the slab to have an isotropic E equal to the longitudinal slab stiffness used in the ADINA model, 4,067 ksi, and an isotropic E equal to the transverse modulus used in the ADINA model, 9,639 ksi.

Some modifications are also required for modeling the boundary conditions. In order to model the eccentrically stiffened plate, the beam element is assigned an offset from the centerline of the plate using the STAAD "member offsets" command. From the STAAD manual (Research, 1998), the *"Member offset command can be used for any member whose starting or ending point is not concurrent with the given incident joint. This command enables the user to account for the secondary forces which are induced due to the eccentricity of the member."* Only frame elements can be offset from specified nodal locations. Finite elements must coincide with the nodes. STAAD has an explicit master/slave provision but finite elements can not be connected to the slaved joints. Since only the active (master) degrees of freedom can be supported and the slab can not be a slave to the beams, the supports for the structure were placed on the underside of the slab. The beam was connected to the slab using the "member offsets" command. This support configuration is presented in Figure 6.8. The beam elements in the longitudinal direction are

depicted as lines located below the plates with a dashed line representing a rigid link. The diaphragm, input as a 10 in. x 36 in. rectangular element, is depicted as a solid element at midspan.

The loads applied to the model consist of 3 lanes of HS25 truck loading without impact or multiple lane reduction. The wheel line closest to the barrier, i.e. 2 ft from the rail per AASHTO's provisions, is located directly over Beam 1. Other wheels are spaced transversely across the width of the deck at 6 ft intervals also per the AASHTO load and lane geometry.

Th major differences between the STAAD model and that created by Aswad and Chen using ADINA can be summarized as the isotropic vs. orthotropic nature of the deck, fineness of the finite element mesh, and direct vs. indirect support of the beams. All other parameters were replicated as closely as possible from the original work.

A comparison of the moments per beam from the ADINA and STAAD models is presented in Figure 6.9. The resultant moment resisted per composite beam is found using the method proposed by Aswad and Chen, $M_c = M_b' + P(y_t + 0.6t_s)$ where $M_c$ is the moment resisted by the composite beam, $M_b'$ is the bending moment in the eccentric beam element, P is the axial force in the beam, $y_t$ is the distance from the beam centroid to the top fiber of the basic beam, and $t_s$ is the slab thickness. Two STAAD model results are presented. STAAD (a) is based on assuming that the E of the isotropic slab is the same as the transverse orthotropic stiffness of the ADINA model, 9,639 ksi. The second model, STAAD (b), assumes an isotropic Modulus of Elasticity equal to the longitudinal modulus from the ADINA analysis, 4,067 ksi. In general, the results from both STAAD analyses agree favorably with those from ADINA with the largest difference in moments in the most lightly loaded beam, Beam 5. The results indicate that the STAAD model predicts a less-efficient distribution of moments than does the ADINA model, i.e., higher moments in those beams nearest the loads. The average of the two STAAD analyses is 103, 107, 107, 97, 71% of the results from the ADINA analysis for Beams 1-5, respectively. With the exception of Beam 5, the agreement is very good. The total static moment at midspan is 5,400 ft-kips. The ADINA, STAAD(a) and STAAD(b) total moments at midspan are 5,335, 5,316 and 5,333 ft-kips, respectively. All three models accurately predict the total internal moment to within 1/2%, the slight differences from the static moment being due to the approximate method used for computing the total moment resisted by the composite section.

Examining the results from the three analyses, the authors have concluded that the STAAD models agree with those from a more complicated finite element analysis even in light of differences in mesh density, boundary conditions and slab material properties. The STAAD models accurately and conservatively predict the moments in the most heavily loaded beams. The underestimation of the smallest moment, that in Beam 5, is of no real significance. Significant changes in the isotropic Modulus of Elasticity of the slab had minimal influence on the distribution of forces in this study. Because the ADINA models were previously shown by Aswad and Chen to agree with the experimental results from field tests, the STAAD model is also indirectly calibrated/in agreement with, experimental data.

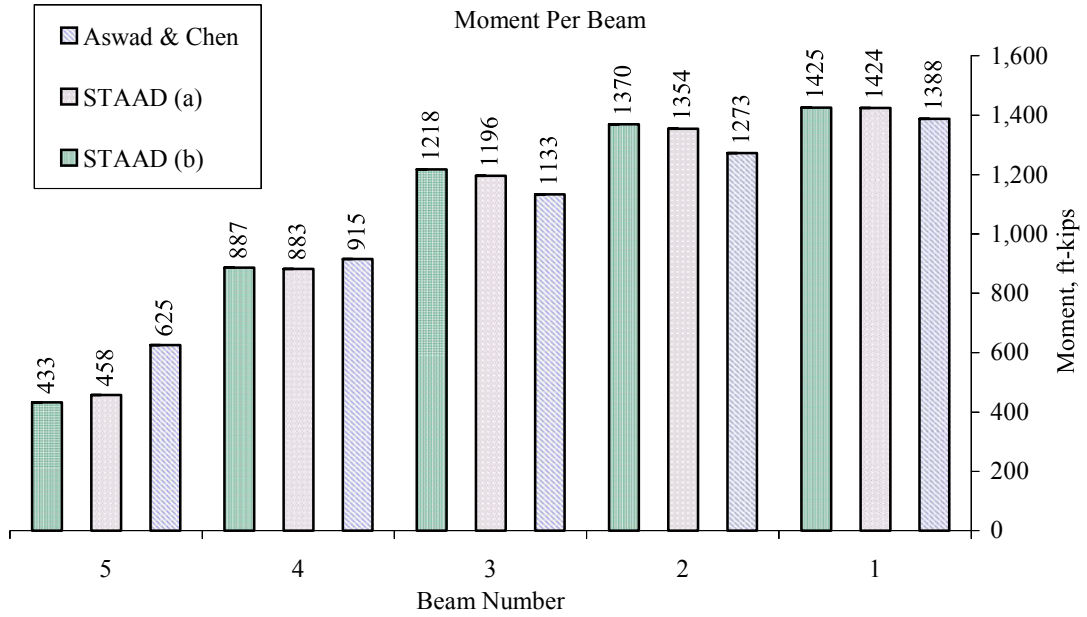


**Figure 6.9. Moments Resisted by Each Beam of the Aswad and Chen Test Bridge.**

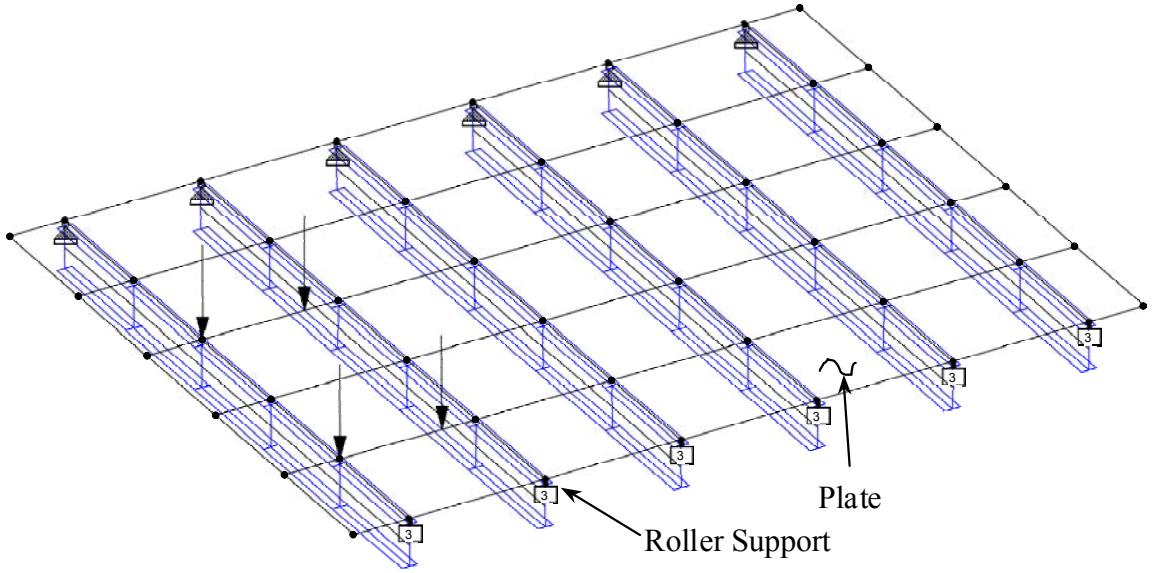


**Figure 6.10. Stiffened Plate Model of the Barker and Puckett Example Bridge.**

As a separate but equally important validation of the stiffened plate method, the results from the downstand grillage of the Barker and Puckett example bridge will be compared to those of a stiffened plate model of the same bridge. The stiffened plate model of the bridge is presented in Figure 6.10. The eccentrically linked W30x108 steel stringers are shown as are the deck plates and concentrated loads.

**Table 6.4. Comparison of STAAD Models Using Different Modeling Techniques.**

| | Live Load Moment in Each Beam, ft-kips | | | | | | |
|---|---|---|---|---|---|---|---|
| | Beam 1 | Beam 2 | Beam 3 | Beam 4 | Beam 5 | Beam 6 | Total Moment |
| Plane Grillage (Corrected) | 212 | 133 | 21 | -5 | -3 | 0 | 358 |
| Downstand Grillage (Corrected) | 209 | 131 | 26 | -3 | -3 | -1 | 359 |
| Stiffened Plate (a) | 202 | 124 | 28 | -2 | -3 | 0 | 349 |
| Stiffened Plate (b) | 214 | 113 | 30 | 0 | -3 | 0 | 354 |
| Damaged Plate (a) | 186 | 137 | 28 | -3 | -3 | 0 | 345 |
| Damaged Plate (b) | 198 | 126 | 29 | -2 | -3 | 0 | 348 |

The stiffened plate model was loaded two ways. The first load case involved application of the equivalent nodal loads used to analyze the grillage model though the direction of equivalent nodal moments was corrected. In the second load case, depicted in Figure 6.10, wheel loads were applied directly to the surface of the plates. The results of both analyses are presented in Table 6.4 as Stiffened Plate (a) and (b), respectively. Using the same equations for composite beam moments previously presented, the total moment per beam was computed for both load idealizations and compared to the corrected plane and downstand grillage models with the nodal moments acting in the proper direction.

The stiffened plate models are in general agreement with the corrected grillage models. The distribution of forces to the six beams is similar in all four of the grillage/stiffened plate models. If one considers the downstand model to be the higher order grillage analysis, the maximum deviation of the stiffened plate models from the downstand results is 5 ft-kips in Beam 1 (2.4%) with the stiffened plate predicting the higher value. For practical purposes, one should not determine equivalent nodal loads by hand since the software algorithms convert loads applied anywhere on the plate to equivalent nodal loads. One can observe though that the difference between the solution with equivalent loads input by hand compares favorably with the solution where the software determined the equivalent forces.

Similar to the damage sensitivity analysis conducted on the grillage models, a simulated amount of damage was inflicted on the middle 20% of Beam 1 of the bridge. The beam area as well as flexural and torsional inertia were reduced by 50%. In the stiffened plate analysis, the damage can be directly applied to

the beam element as opposed to the grillage models where the damage must be computed as an effect on the composite section. The damage model results are also presented in Table 6.4 as Damaged Plate (a) and (b). The effect of the damage is the same as that observed in the grillage model; the decrease in exterior beam moment due to the presence of isolated damage results in a redistribution of moment into the first interior beam.

### *6.3.3. Model Validation Summary*

From the discussions in the previous section regarding model testing, it can be concluded that the STAAD program is accurate in analyzing the example bridge using both methods of analysis. The grillage model was found to correlate very well with the published results from Barker and Puckett using their assumptions for longitudinal member stiffness as well as the stiffness assumptions promoted by other authors. Both approaches yielded essentially the same results. The grillage model was intentionally subjected to main member damage with the damage being a 50% reduction in the exterior beam longitudinal stiffness. Redistribution of load to the adjacent interior beam was noticeable.

The stiffened plate model in STAAD was compared to a more complex orthotropic model created by Aswad and Chen using the ADINA program. The results from the STAAD and ADINA model correlate well with the maximum error in the most heavily loaded beam being approximately 2.7%, the STAAD model producing the larger moments. A stiffened plate model of Barker and Puckett's bridge, previously analyzed using a grillage model, was also created. Two types of load idealization were employed, specification of equivalent nodal loads and direct loading of the plates. Results from both idealizations are acceptable as compared to those from the grillage model. A sensitivity analysis of the stiffened plate model was conducted with damage to the main longitudinal element consisting of a 50% reduction in all geometric properties. The results are consistent with the grillage models of the damaged bridge.

From this analysis, one can conclude that either the grillage model in the plane or downstand form, or the stiffened plate model, are acceptable idealizations for bridges, damaged or undamaged. Results from the models compare well with the results from other researchers using different software, boundary conditions and element types. Due to the excellent performance of the STAAD models, they will be used throughout the remainder of this investigation.

## ***6.4. Analytical Results for the Beebeetown Bridges***

### *6.4.1. Undamaged and Repaired Bridge Results*

This section discusses the results obtained from analytical models of the undamaged EB and repaired WB bridges. The intent was to develop a model that replicates the measured bridge response so that the load distribution characteristics of the baseline structure could be evaluated.

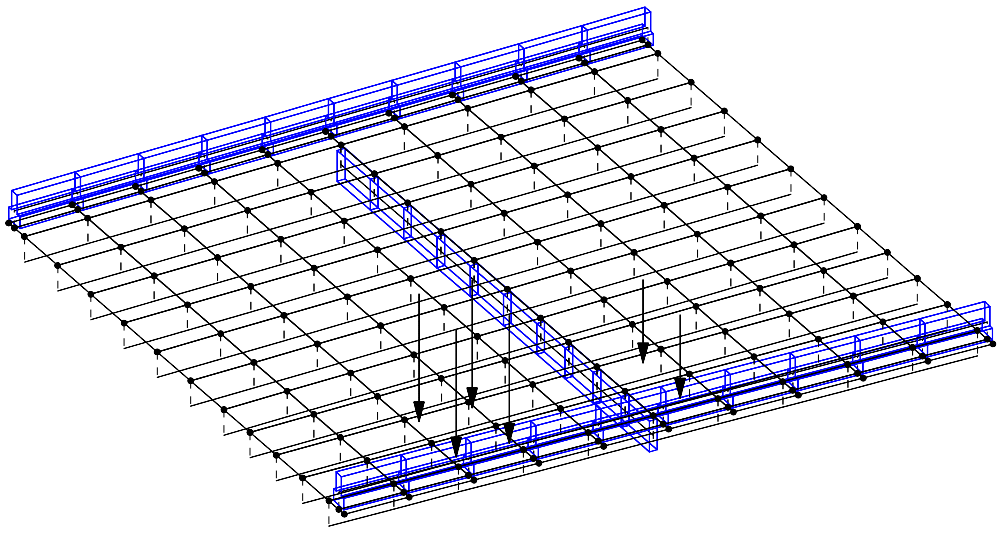

**Figure 6.11. Isometric View, Center Span with Load at L1-P4.**

### *6.4.1.1. Stiffened Plate Model of the Undamaged/Repaired Bridges.*

An overall view of the model of the center span of the Beebeetown bridges is presented in Figure 6.11. The load shown is with the rear tandem center at the quarter point of the span (L1E/W-P4). Due to the fact that the experimental data recorded on both the EB and WB bridges tend to indicate that the bridge behaves as three simple spans under the action of live load (see Chapter 3), the center span was modeled as an isolated span. However, there is some continuity in the bridge since the slab, curb and rail are continuous though the beams are not. Details of the modeling procedure for the center span follow. The input file for this model is presented in Section A.3 of Appendix A.

The beam elements have the properties of an Iowa DOT B55 beam, an area, A = 382.5 $in^2$, torsional constant, $K_T$ = 7980 $in^4$, weak axis moment of inertia, $I_y$ = 5980 $in^4$, and major axis moment of inertia, $I_z$ = 62,000 $in^4$. The beam is eccentrically linked to the mid-plane of the cast-in-place concrete slab by a 26.44 in. rigid offset. The slab is represented by a shell element having a thickness of 9 in. This is the average thickness of the slab and overlay as determined by cores taken from the WB bridge. The cast-in-place diaphragm is 8 in. wide and 32 in. high, composite with the slab but with no moment capacity at the intersection of the diaphragm and beam web. The diaphragm centroid is also rigidly offset from the slab by a distance of 20.5 in., the distance from the centroid of the diaphragm to mid-plane of the slab. The curb and rail section were modeled as eccentric T-beams linked by rigid offsets to the slab. The curb is 20 in. wide and 12 in. high with the rail being 10 in. wide and 20 in. high. These are the standard dimensions of an Iowa DOT retrofit curb and rail section. The loads were idealized as being point loads applied to the deck. The rear tandem, consisting of four pairs of two tires, was idealized as a total of four point loads, 6 ft apart in the transverse direction, each exerting a force of 11.38 kips. The front axles consist of two point loads, 7.41 kips each. This loading corresponds to Truck 1 previously described in Figure 3.6 of Chapter 3.

**Table 6.5. Variable Parameters in Center Span Stiffened Plate Models.**

| Model # | Diaphragm Active? | | Rail Active? | | Modulus of Elasticity | | Support Fixity | |
|---|---|---|---|---|---|---|---|---|
| | Y | N | Y | N | 4,600 ksi | 7,000 ksi | Simple | Fixed |
| SP-1 | ■ | | ■ | | ■ | | ■ | |
| SP-2 | ■ | | ■ | | ■ | | | ■ |
| SP-3 | ■ | | ■ | | | ■ | ■ | |
| SP-4 | ■ | | ■ | | | ■ | | ■ |
| SP-5 | ■ | | | ■ | ■ | | ■ | |
| SP-6 | ■ | | | ■ | ■ | | | ■ |
| SP-7 | ■ | | | ■ | | ■ | ■ | |
| SP-8 | ■ | | | ■ | | ■ | | ■ |
| SP-9 | | ■ | ■ | | ■ | | ■ | |
| SP-10 | | ■ | ■ | | ■ | | | ■ |
| SP-11 | | ■ | ■ | | | ■ | ■ | |
| SP-12 | | ■ | ■ | | | ■ | | ■ |
| SP-13 | | ■ | | ■ | ■ | | ■ | |
| SP-14 | | ■ | | ■ | ■ | | | ■ |
| SP-15 | | ■ | | ■ | | ■ | ■ | |
| SP-16 | | ■ | | ■ | | ■ | | ■ |

The boundary conditions for the actual bridge are somewhat complicated. The slab, curb and rail are continuous for all three spans while the beams are three individual single-span elements. The beam ends are not encased in a common pier diaphragm. Pintles have purposely been omitted from the bearings of Beams 1, 2, 10 and 11. As an envelope of the actual response, the beam ends were considered to be either pinned or fully fixed. In addition to the boundary condition variability, there is also the possibility of variations in the degree of diaphragm participation, degree of composite action of the curb and rail section and potential variations in the actual Modulus of Elasticity, E, from the theoretical value. It is already known from the field tests that the diaphragm strains are low, an indication that the diaphragms could be omitted from the bridge model. The isolated beam tests also indicated a large variation in E from the theoretical value. The theoretical E value was 4,600 ksi while that derived from the M/EI data recorded during the isolated beam tests suggest an E of approximately 7,000 ksi. In order to parametrically study these possible variations, the 16 test cases presented in Table 6.5 were established. The intent was to vary the parameters one at a time to study the sensitivity of the model to the individual modifications. The deflected shape results at midspan of the center span for all 16 models and for three different load positions are presented.

Figures 6.12 through 6.15 present the experimental vs. analytical response of the midspan region of the center span of the undamaged EB bridge and the repaired WB bridge. Internal moments from the analysis in Beams 1-3 and 5 for the cases presented in Table 6.5 are presented in Table 6.6. Representative load cases from the numerous load positions along the bridge were evaluated using the models. The three load cases selected represent a single truck in Lane 1 (L1E/W(R)-P5), two trucks end-to-end as close to the barrier rail as possible, (L1E/W(R)-P4&P6), and two trucks in adjacent lanes positioned at midspan, (L1&L2E/W(R)-P5). These test positions were previously described in Chapter 3 of this report.

The results from the load cases will be used in several ways. The effects of end fixity will be studied as it relates to the deflected shape of the bridge and henceforth the moment carried in particular beam lines. The odd numbered models have simply supported ends while the even number models have fixed supports. The participation of the diaphragms will be studied by comparing the results from Models SP-1 through SP-8 to those of Models SP-9 through SP-16. Edge stiffening effects will be determined using models in which the barrier rail and curb are included or purposely excluded from the model. Finally, the effect of varying the E for all elements will be examined.

The effect of the variation in E is to decrease the deflections in the bridge when comparing the results of the 7,000 ksi models to those using 4,200 ksi as the E value. However, examining the moments in the beams, there is no change since the E value was increased uniformly for all members (see Table 6.6). The net result is no change in forces just a decrease in deflections.

The effect of the removal of the diaphragms was studied. In the models in which the diaphragm was included, the diaphragms were pinned at their ends thus eliminating any moment transfer. The axial capacity of the eccentric diaphragm was maintained. The net result is that the diaphragm acts as an eccentric tension/compression only member located below the deck. In models where the diaphragm is indicated as not being active, the axial capacity of the diaphragm was discounted.

Examining the deflected shapes for models SP-1 to SP-8 , models with a diaphragm, and comparing the results to models SP-9 to SP-16, those without a diaphragm, along with the table of computed moments, one finds that for the load cases with loads placed in Lane 1, there is essentially no change in the moment in the exterior beam, Beam 1. Refer to parts (a) and (b) of Figure 6.12 through Figure 6.15 and Table 6.6 for the computed moments. Models SP-1 and SP-9 are used for comparison. The overall effect appears to be that for the extreme load cases placed as close to the edge beam as possible, there is no change in moment in the exterior beam due to the presence or absence of the diaphragm. For loads in Lane 1, the presence of the diaphragm decreases the moments in Beams 2 and 3 by 10% while increasing those in Beam 5. For the multi-lane loading, the moment in Beam 1 is higher in model SP-1 than in model SP-9. The moments in all other beams are lower in model SP-1 than they are in SP-9. In general for Lane 1 loading the diaphragm moderately helps to distribute load to the interior of the bridge but the load in the exterior beam is slightly higher in multi-lane loading when the diaphragm is included.

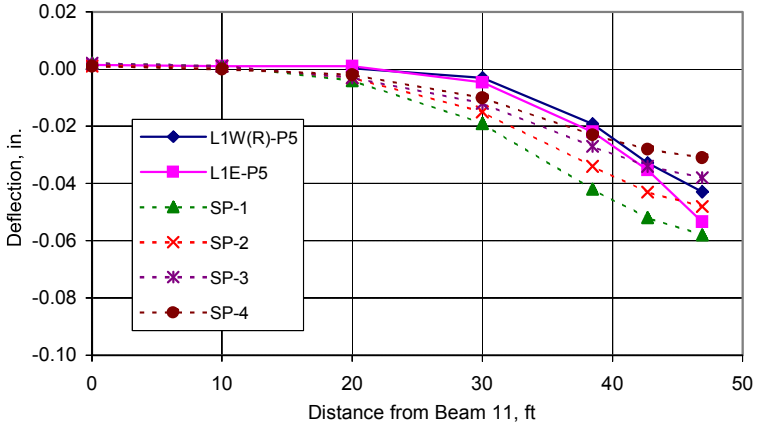


**a.) Load Position L1E/W(R)-P5**

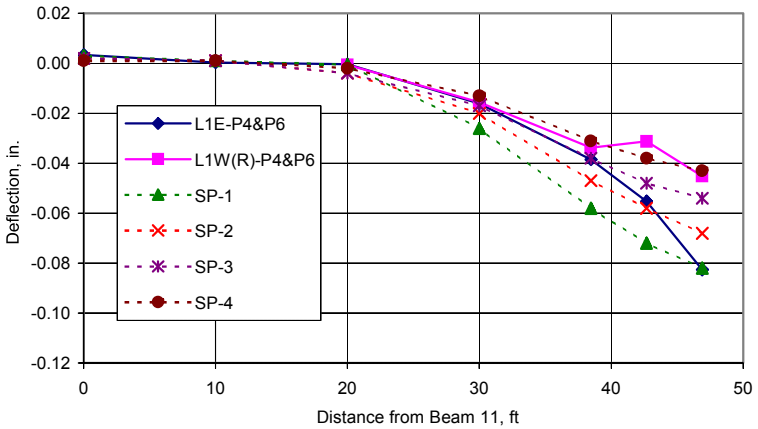


**b.) Load Position L1E/W(R)-P4&P6**

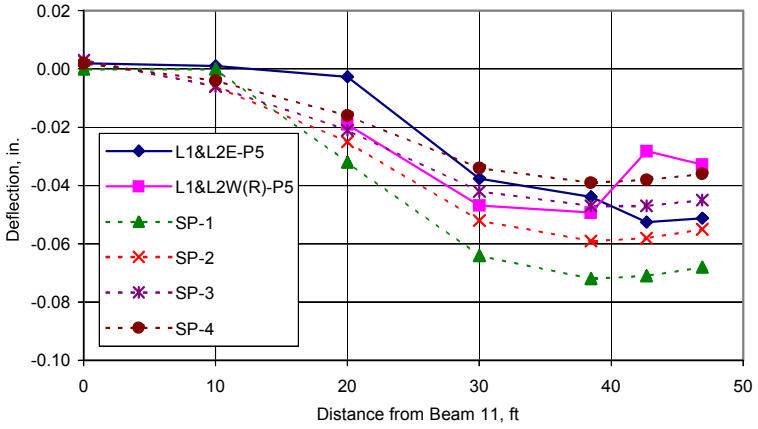


**c.) Load Position L1&L2E/W(R)-P5**

**Figure 6.12. Analytical vs. Experimental Deflection, Stiffened Plate Models SP-1 to SP-4.**

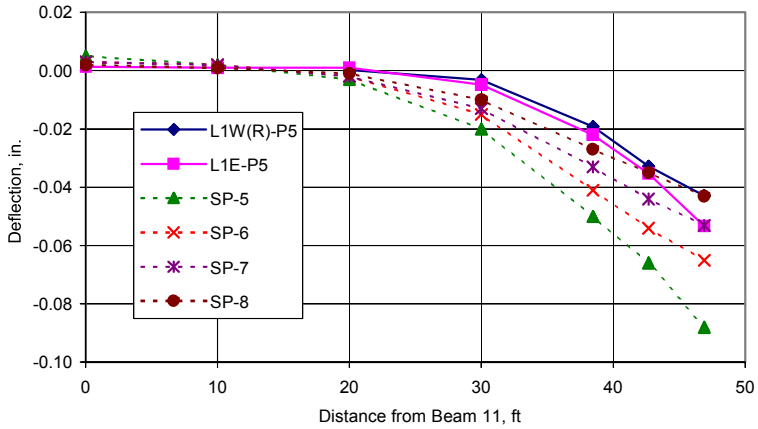


**a.) Load Position L1E/W(R)-P5**

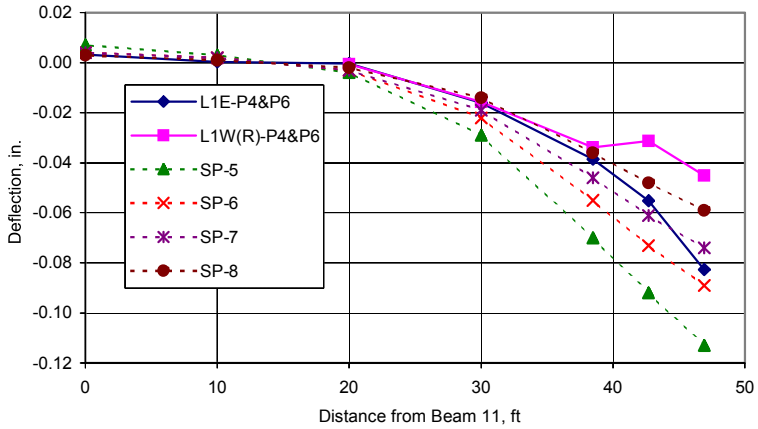


**b.) Load Position L1E/W(R)-P4&P6**

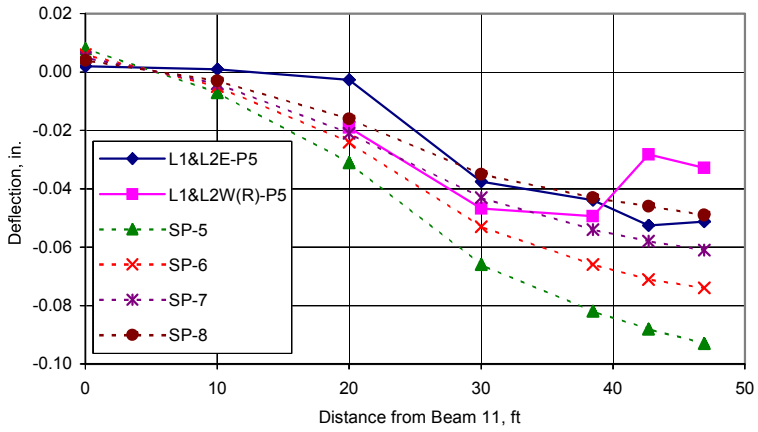


**c.) Load Position L1&L2E/W(R)-P5**

**Figure 6.13. Analytical vs. Experimental Deflection, Stiffened Plate Models SP-5 to SP-8.**

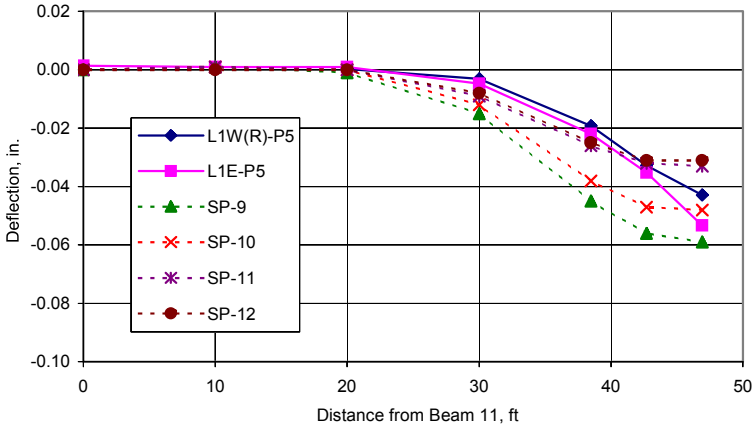


**a.) Load Position L1E/W(R)-P5**

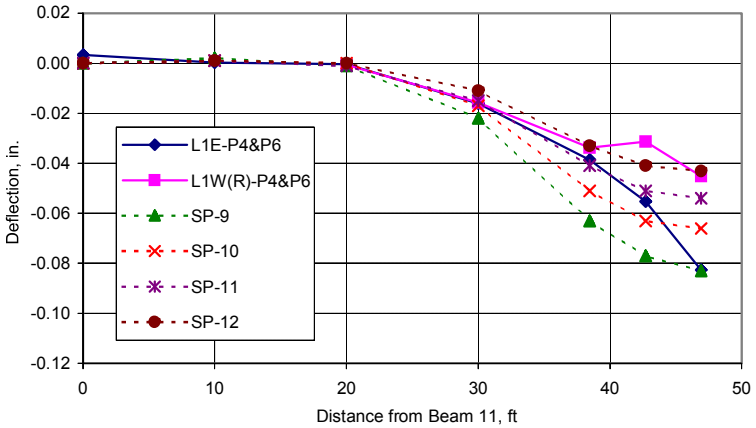


**b.) Load Position L1E/W(R)-P4&P6**

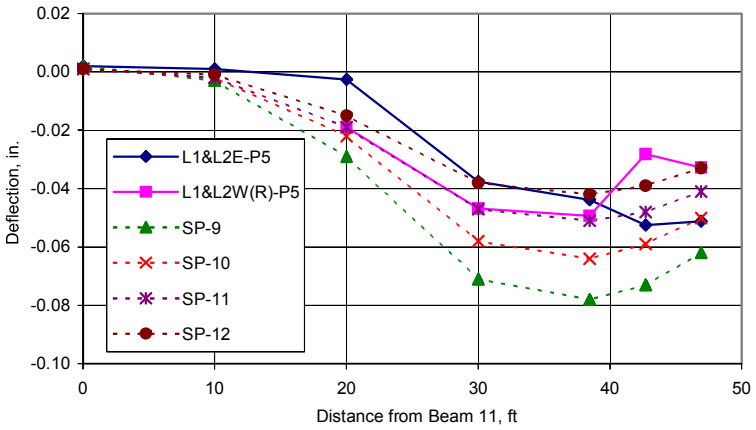


**c.) Load Position L1&L2E/W(R)-P5**

**Figure 6.14. Analytical vs. Experimental Deflection, Stiffened Plate Models SP-9 to SP-12.**

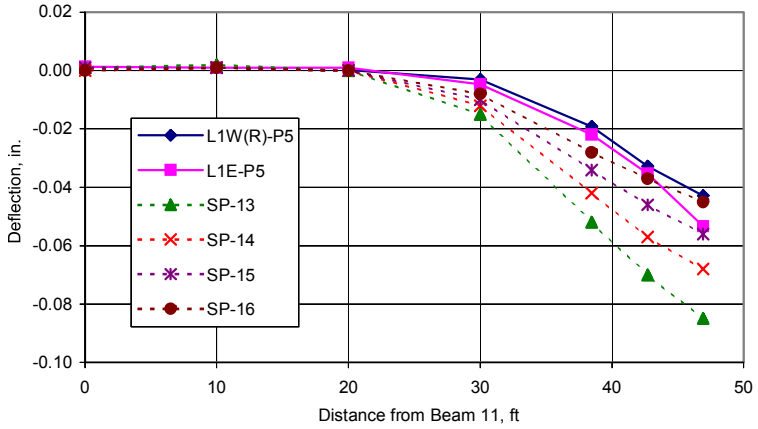


**a.) Load Position L1E/W(R)-P5**

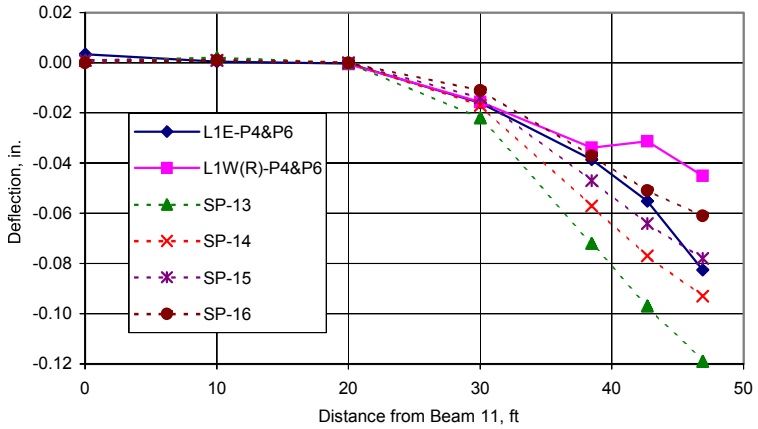


**b.) Load Position L1E/W(R)-P4&P6**

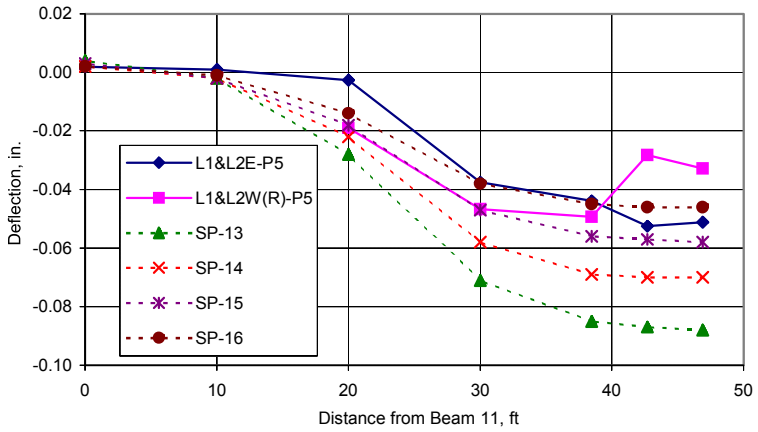


**c.) Load Position L1&L2E/W(R)-P5**

**Figure 6.15. Analytical vs. Experimental Deflection, Stiffened Plate Models SP-13 to SP-16.**

**Table 6.6. Computed Moments in Beams 1-3, 5 Due to Variations in Load Placement and Model Parameters.**

| Model # | Beam 1 Live Load Moment, ft-kips | | | Beam 2 Live Load Moment, ft-kips | | | Beam 3 Live Load Moment, ft-kips | | | Beam 5 Live Load Moment, ft-kips | | |
|---|---|---|---|---|---|---|---|---|---|---|---|---|
| | L1-P5 | L1-P4&P6 | L1&L2-P5 | L1-P5 | L1-P4&P6 | L1&L2-P5 | L1-P5 | L1-P4&P6 | L1&L2-P5 | L1-P5 | L1-P4&P6 | L1&L2-P5 |
| SP-1 | 159 | 195 | 183 | 142 | 157 | 191 | 112 | 122 | 188 | 47 | 67 | 170 |
| SP-2 | 140 | 166 | 158 | 126 | 132 | 167 | 99 | 103 | 166 | 39 | 54 | 150 |
| SP-3 | 159 | 195 | 183 | 142 | 157 | 191 | 112 | 122 | 188 | 47 | 67 | 170 |
| SP-4 | 140 | 166 | 158 | 126 | 132 | 167 | 99 | 103 | 166 | 39 | 54 | 150 |
| SP-5 | 207 | 250 | 236 | 172 | 198 | 226 | 131 | 148 | 211 | 51 | 72 | 175 |
| SP-6 | 181 | 210 | 202 | 151 | 165 | 195 | 114 | 122 | 182 | 41 | 57 | 153 |
| SP-7 | 207 | 250 | 236 | 172 | 198 | 226 | 131 | 148 | 211 | 51 | 72 | 175 |
| SP-8 | 181 | 210 | 202 | 151 | 165 | 195 | 114 | 122 | 182 | 41 | 57 | 153 |
| SP-9 | 159 | 196 | 166 | 157 | 175 | 194 | 124 | 137 | 205 | 36 | 53 | 192 |
| SP-10 | 140 | 166 | 145 | 140 | 149 | 170 | 111 | 117 | 179 | 29 | 42 | 168 |
| SP-11 | 159 | 196 | 166 | 157 | 175 | 194 | 124 | 137 | 205 | 36 | 53 | 192 |
| SP-12 | 140 | 166 | 145 | 140 | 149 | 170 | 111 | 117 | 179 | 29 | 42 | 168 |
| SP-13 | 216 | 264 | 221 | 185 | 214 | 224 | 137 | 155 | 219 | 35 | 51 | 191 |
| SP-14 | 187 | 219 | 189 | 162 | 178 | 194 | 120 | 129 | 189 | 28 | 40 | 168 |
| SP-15 | 216 | 264 | 221 | 185 | 214 | 224 | 137 | 155 | 219 | 35 | 51 | 191 |
| SP-16 | 187 | 219 | 189 | 162 | 178 | 194 | 120 | 129 | 189 | 28 | 40 | 168 |

The support conditions were varied, either pinned (rotation permitted and translation restrained in x, y, and z axes) or fully fixed. Recall that due to STAAD's modeling constraints, the supports are on the underside of the slab. The effect of end fixity obviously reduces the midspan moments in the beam. In an analysis of a bridge whose capacity is questionable, it is not recommended to use fixed end models since the actual rotational restraint at the bearings is unknown and it is conservative to neglect the restraint. Additionally, for the models created for the Beebeetown bridges, results from the fully fixed models typically deflect less than the experimental results, while several of the pinned models are closer to the measured results. For this reason, the only models that will be discussed further are those with pinned ends.

Finally, the issue of barrier rail stiffness is discussed. Models SP-1 – SP-4 and SP-5 – SP-8 are the same with the exception that in models SP-5 – SP-8 the barrier rail has been disabled in the model. The reader is referred to Figures 6.12 and 6.13 for a comparison of models SP-1 – SP-4 to models SP-5 – SP-8 for the same load positions. All eight of the models exhibit the proper trend in the transverse deflected shapes and in estimating deflection magnitudes though models SP-1 in Figure 6.12 and models SP-5 and SP-6 in Figure 6.13 diverge the greatest from the experimental data. There are still five remaining bridge models whose results are closest to the experimental data, but removing from further consideration models SP-2, SP-4 and SP-8 based on fixed end conditions, there are only two remaining models, SP-3 and SP-7. These two models both presume an active diaphragm, E = 7,000 ksi, and simple support conditions, the only difference being that model SP-3 includes the rail and curb while model SP-7 discounts them. From examination of the two models, their accuracy can be judged to be about the same in terms of their ability to predict the experimentally recorded deflected shapes though model SP-3, that including the rail, appears slightly more accurate. The distribution of moments in the two different models is very different however as evidenced by the computed moments presented in Table 6.6. Based on the extensive body of information that exists concerning field testing of bridges, some of which was presented in Chapter 2 of this report, it is the opinion of the authors that for this bridge, in which the rail is continuous and composite with the deck, the most accurate model is SP-3.

In model SP-3, the total internal moment across the 11 beam lines plus the two composite barrier rails was computed to be 1,294 ft-kips for load case L1&L2-P5, this is comparable to the external moment of 1,310 ft-kips (655 ft-kips per lane). The moment in Beam 1 due to the two test trucks in adjacent lanes was computed to be 183 ft-kips, a lane load distribution factor of 183/655 = 0.28 or a wheel line distribution factor of 0.56. The predicted distribution factor using the AASHTO Standard Specifications is S/5.5 for exterior beams less than 6 ft on center where S=4.25 ft at midspan of the center span. The AASHTO distribution factor is 0.77 wheel lines, 38% higher than that measured. The maximum moment was in Beam 2, 191 ft-kips, also much less than predicted by AASHTO. As a measure of the safety of the beams, Beam 1W, previously discussed in Chapter 5, failed at a total applied moment of 2,467 ft-kips.

### *6.4.1.2. Grillage Model of the Undamaged and Repaired Bridges.*

Having established what the authors believe to be the most representative model of the undamaged behavior of the center span of the Beebeetown bridges, the results of the stiffened plate model SP-3 will be compared to a grillage analysis of the same bridge. Recall that model SP-3 presumes a participatory diaphragm, edge stiffening due to the curb and rail, simple support conditions and an E of 7,000 ksi. These values will be used in the grillage. A downstand grillage model will be the basis for comparison since the downstand grillage can more accurately capture the participation of the eccentrically located (with respect to the mid-plane of the slab) beam and rail sections. However, as previously discussed in Section 6.3.1, the differences between the downstand and plane grillage models are not significant.

A plan and isometric view of the grillage idealization of the center span of the I-680 Beebeetown bridges is presented in Figure 6.16. The idealization is similar to that created for the stiffened plate models previously presented. Nodes are located at the tenth points along the 11 main beam lines. The nodes are assumed to be coincident with the centroid of the composite section of the beam and tributary slab. For the span in question, the beam spacing is variable. The typical interior beams, Beams 6 through 10, have a constant spacing of 5 ft, 2.5 ft on each side of the beam. Beams 1 and 11 have slightly asymmetric slabs due to the overhang and Beams 2 through 5 have spacing's on either or both sides less than 2.5 ft. However, the differences in beam spacing makes little difference in the overall properties of the composite section. A summary of the composite section properties of the longitudinal and transverse beams is presented in Table 6.7. The slight difference in centroidal axis location for beams having less than a 5 ft wide tributary slab is ignored. All beam nodes are located at an elevation consistent with the centroid of a typical interior beam, i.e., centroid of beam is 15.5 in. from top fiber of P/C beam, 20 in. from the center of the slab. The differences in section properties are accounted for, however, in the grillage input. The only nodes not coincident with the beam centroids are those under the barrier rail; these nodes are at the mid-plane of the deck. Typically, the slab is "slaved" to the beam element using the "member offsets" command, however, since no beam line lies under the rail, an additional line of nodes was needed under the rail location. The barrier rail is offset to these nodes which are in turn connected to a slab element offset from the beam centroid. The rail properties are computed internally by STAAD as an inverted T-section.

In order to compute the element properties for the grillage model, the following assumptions were made. The E value was assumed to be 7,000 ksi for all elements, Poisson's ratio, 0.2, and the Shear Modulus, G, equal to 4,200 ksi. The full 9 in. slab plus overlay was used for section property calculations and the effective width was the center to center beam spacing or half the beam spacing plus overhang for the exterior beams. For the flared beams, the longitudinal element properties are constant along the span and represent the properties at midspan. The torsional constants for the longitudinal and transverse slab were computed to be $bt^3/6$ in accordance with the recommendations presented in Section 6.2 of this report.

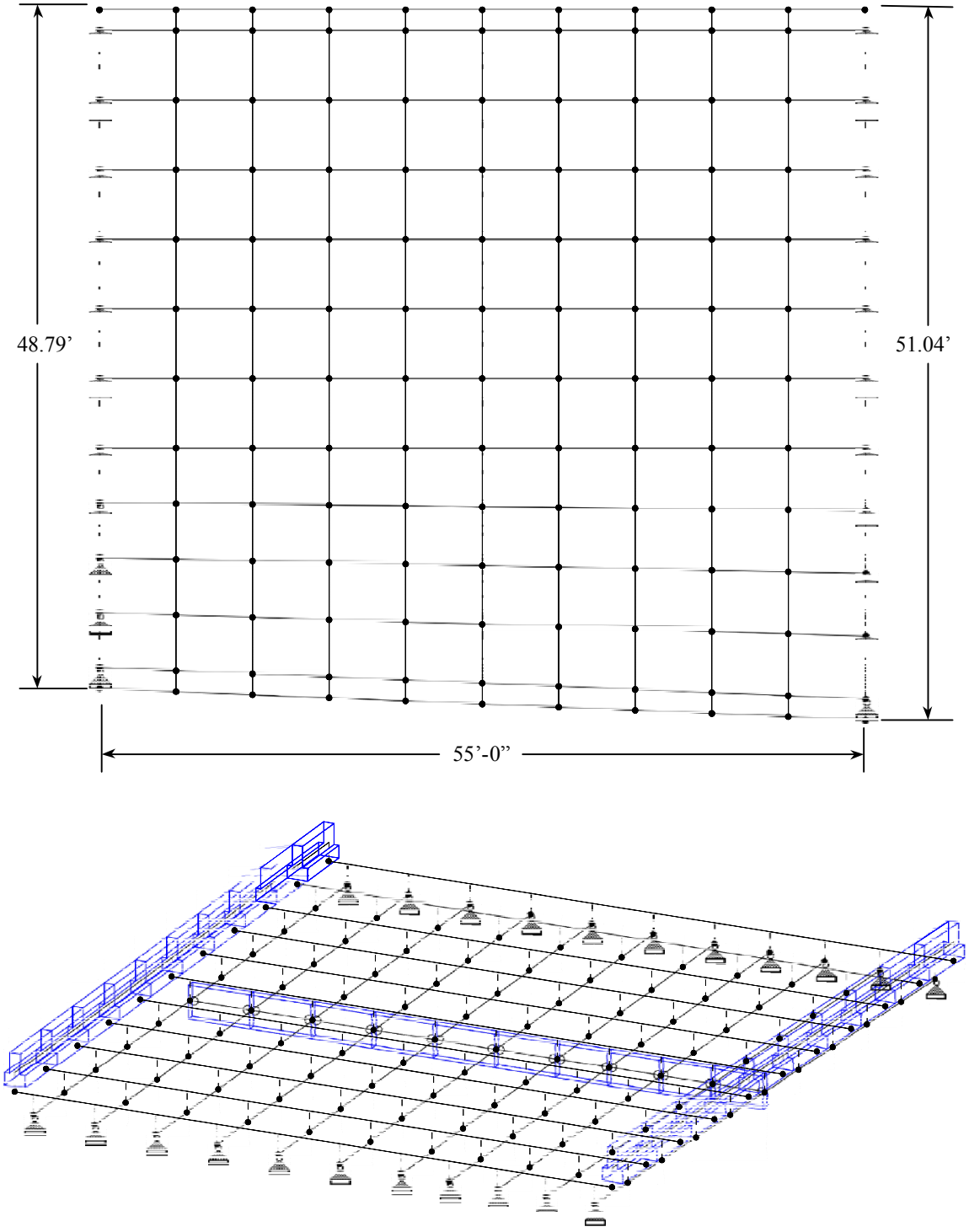


**Figure 6.16. Plan and Isometric View of Downstand Grillage of the I-680 WB Center Span.**

**Table 6.7. Grillage Properties for Longitudinal and Transverse Members, Undamaged Center Span.**

| Member | Area, $in^2$ | $I_x$ ($K_T$), $in^4$ | $I_y$, $in^4$ | $I_z$, $in^4$ | $Y_{top}$, in. |
|---|---|---|---|---|---|
| Beam 1 | 855 | 14,360 | 113,690 | 212,960 | 16.3 |
| Beams 2-4 | 842 | 14,180 | 104,650 | 210,950 | 16.5 |
| Beams 5 | 882 | 14,720 | 133,380 | 216,800 | 16.0 |
| Beams 6-10 | 923 | 15,270 | 167,160 | 222,170 | 15.5 |
| Beam 11 | 896 | 14,906 | 144,060 | 218,640 | 15.8 |
| Transverse Slab, 5.5 ft x 9 in. | 594 | 8,020 | 162,000 | 4,010 | N/A |

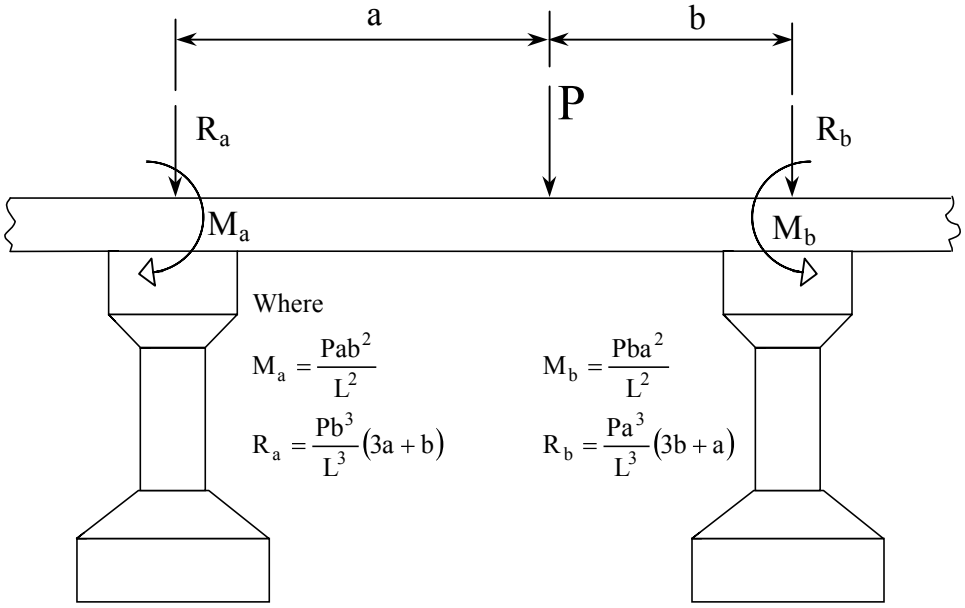


**Figure 6.17. Idealization of Equivalent Member Loads for Wheel Loads Between Beam Elements.**

For purposes of loading the model, the equivalent member/nodal force approach is used (see Figure 6.17). Distribution of forces applied to the slab spanning between beams is presumed to be one way, directly to the longitudinal members. The force applied to the longitudinal member is a combination of the vertical reaction as well as a torque. This is analogous to the approach taken in Section 6.3.1 of this report except that in the aforementioned analysis, loads coincided with longitudinal node/transverse member locations. The load cases investigated were the same as those used in the stiffened plate models to determine if a reasonably similar distribution of internal moments exists in the grillage model and the stiffened plate model.

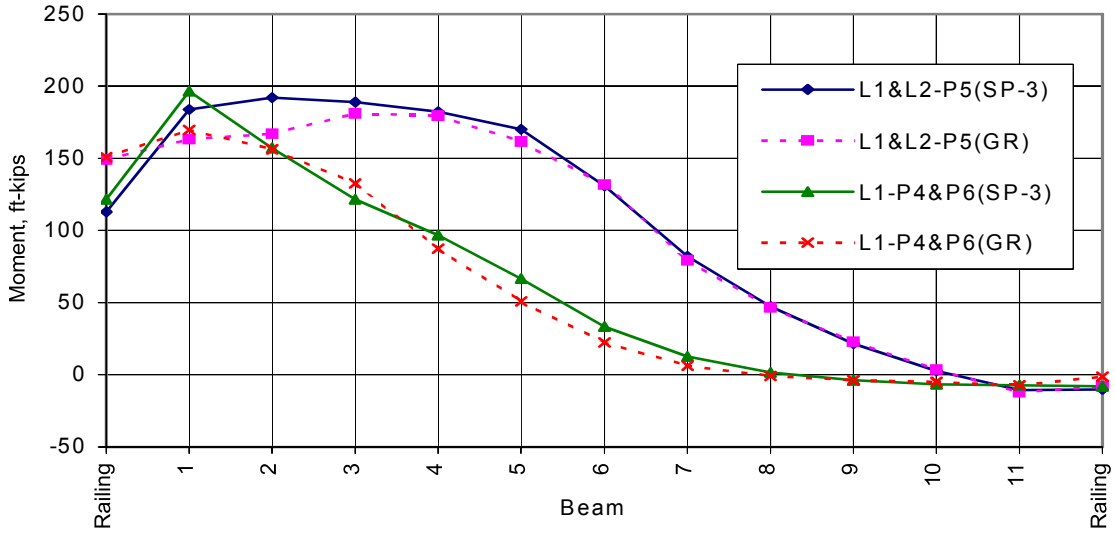


**Figure 6.18. Moments in Longitudinal Beams as Predicted by the Stiffend Plate and Grillage Models.**

Figure 6.18 presents a comparison of the internal moments per beam, including that portion carried by the curb and rail section for both the stiffened plate model believed to be most representative of the bridge behavior, SP-3, and a similar grillage model, GR. The results are plotted for load cases L1&L2-P5 (Trucks 1 and 2 in adjacent lanes) as well as L1-P4&P6 (Trucks 1 and 2 centered in the middle span). There is generally very good agreement between the two models except in the immediate vicinity of Beams 1 and 2. In the area of Beams 1 and 2 and the adjacent rail, the grillage model distributes more load to the rail and correspondingly less to the adjacent beams. This is a localized effect however and the grillage and stiffened plate models agree very well from Beam 3 to the opposite side of the bridge model. From the grillage model, the maximum moment was predicted to be 170 ft-kips in Beam 1 for load case L1-P4&P6 while the stiffened plate predicts a moment of 197 ft-kips in the same beam, 16% more. Similarly, for load case L1&L2-P5, the grillage model predicts the maximum moment of 181 ft-kips to be in Beam 3 while the stiffened plate predicts a maximum moment of 192 ft-kips in Beam 2; the corresponding moment in Beam 3 is 189 ft-kips. A review of the grillage and stiffened plate models indicates that in general they agree very well, certainly to within the precision reasonably attainable in load distribution calculations. The stiffened plate is somewhat more conservative in that a greater portion of the edge moment is resisted by several longitudinal beams and less by the curb and rail section. This may be the result of several effects such as loads being applied at the deck level in the stiffened plate analysis and directly to the beams in the grillage, or the assumption of unidirectional load transfer in the grillage load idealization. Regardless of the source of the difference, both models are considered to be reasonable predictions of the general load distribution characteristics of the undamaged structure. Both models predict load distribution factors significantly less than those stipulated in the AASHTO Standard Specifications.

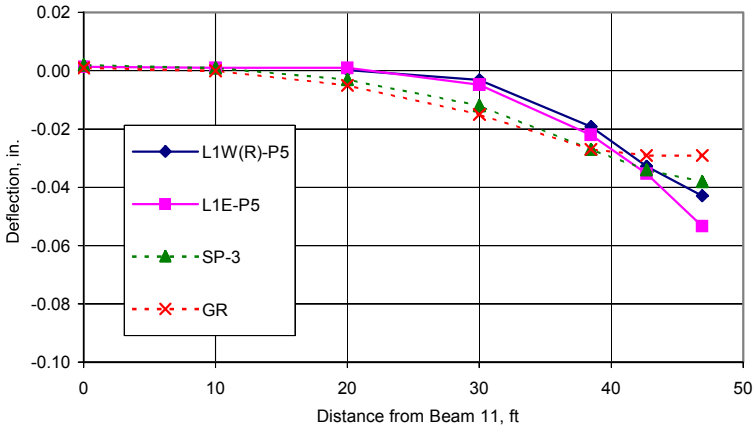


**a.) Load Position L1E/W(R)-P5**

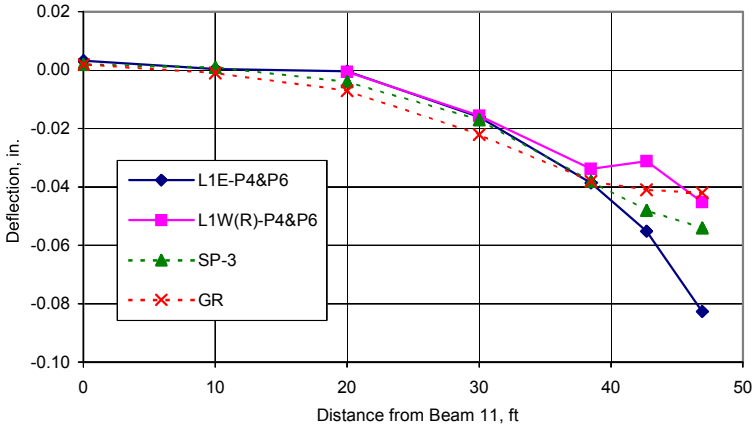


**b.) Load Position L1E/W(R)-P4&P6**

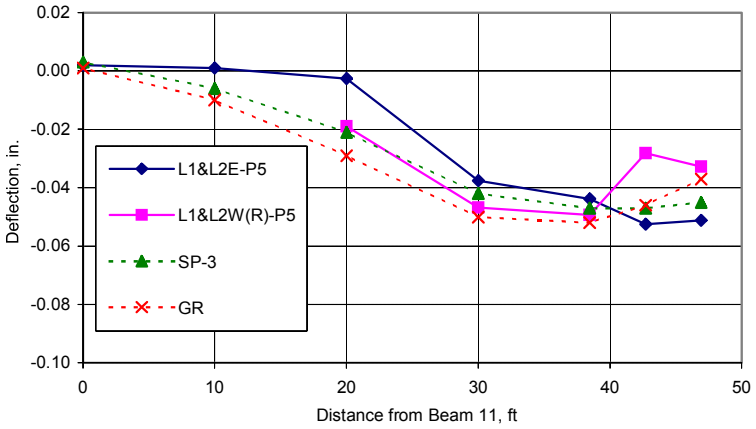


**c.) Load Position L1&L2E/W(R)-P5**

**Figure 6.19. Comparison of Experimental, Stiffened Plate and Grillage Model Deflected Shapes.**

As an additional comparison of the grillage and stiffened plate models, the predicted live load deflections at midspan of the center span (transverse Section 3) are presented in Figure 6.19. Similar to the trend observed for the moments in the two models, the deflections in the models are reasonably close throughout the entire width of the bridge, the greatest differences being in Beams 1 and 2; the grillage model is stiffer in this region. Once again, however, both models are reasonably accurate in predicting deflections as they also were at predicting internal moments in the various longitudinal members. The stiffened plate is however, in the opinion of the authors, a slightly better model for prediction of deflections in the bridges tested. Because of the slightly better deflection performance of the stiffened plate model, key because the primary means for calibrating the models to the experimental behavior is the centerline deflection, only the stiffened plate will be used to study member damage effects on deflections and load distribution.

### *6.4.2. Analysis of the Damaged Center Span*

In this section, the analytical modeling of the damaged center span of the WB bridge is presented. For additional details regarding the location and extent of damage, refer to Chapter 3. As previously noted, the damage consisted of main member damage to Beams 1W and 2W of the WB bridge with damage consisting primarily of the complete loss or extensive fracturing of much of the bottom flange of Beam 1W with lesser damage to Beam 2W. Web cracking spread throughout much of the damaged region. All other beams are undamaged.

The most difficult aspect of modeling accidental damage is quantifying the loss of section in terms of its extent and effect on member stiffness characteristics. Throughout the remaining discussion, assumptions are based on the beam inspection reports, inspection photos, and first-hand assessment of the damage. Using this information, it is assumed that the entire bottom flange up to the bottom of the web, i.e., the bottom 13 in. of the beam (see Figure 3.3), is missing over a finite length. The length selected is 20% of the beam length (11 ft) for Beam 1W and 10% (5.5 ft) for Beam 2W. This is a longer length than physically missing from the beams but is representative of the region of the beam in which rather extensive flange cracking was evident. It is an attempt to consider the cracked zone of the damaged beams in a simple fashion. The damage is asymmetric, located entirely west of midspan. The somewhat arbitrary nature of the extent of the damage was to represent the scenario that a practicing engineer might face. If one is faced with attempting to model a damaged member, assumptions must be made regarding the extent of damage. Without experimental data for calibrating a theoretical model, an assumed amount and length of damage is required.

Having assumed that the entire lower 13 in. of the beam (1/3 of the total beam height) is missing from the member, new member properties are required. The undamaged and damaged beam properties are presented in Table 6.8. The effect of the bottom flange removal is to substantially reduce the area, flexural and torsional inertia of the damaged beam and to cause an upward shift of the centroidal axis.

**Table 6.8. Member Properties of the Undamaged and Damaged Iowa DOT 55 ft Long P/C B Beams.**

| Member | Area, $in^2$ | $I_x$ ($K_T$), $in^4$ | $I_y$, $in^4$ | $I_z$, $in^4$ | $Y_{top}$, in. |
|---|---|---|---|---|---|
| Undamaged | 382.5 | 7,980 | 5,156 | 62,000 | 21.94 |
| Damaged | 194.5 | 1,760 | 1,356 | 10,930 | 10.79 |

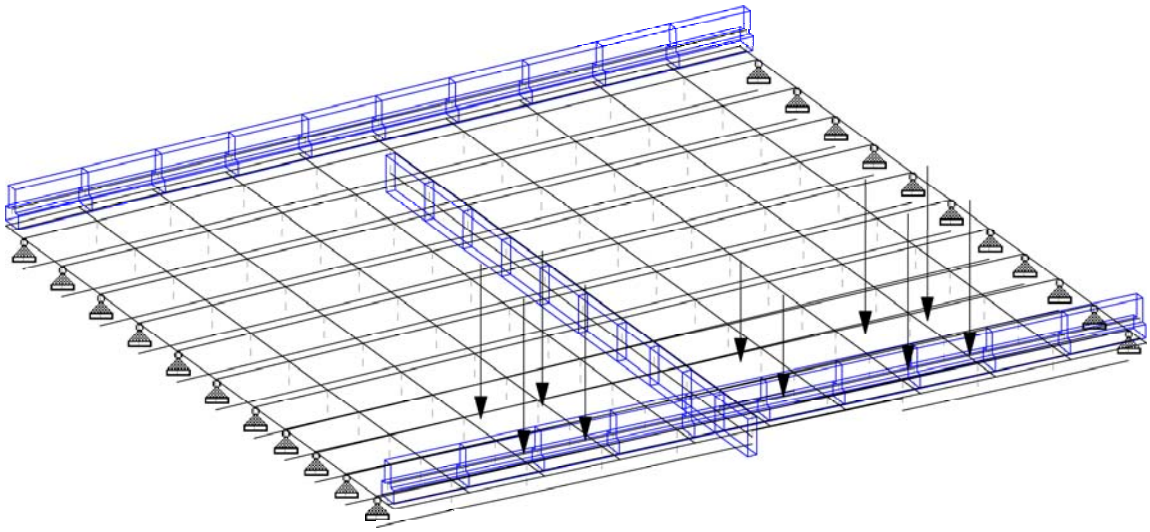

**Figure 6.20. Stiffened Plate Model of Damaged WB Center Span, Load at L1-P4&P6 Shown.**

For computation of the torsional constant of the damaged beam, the equations of Figure 6.3 were used in lieu of the equations of Eby et al. used to compute the torsional constant for the undamaged beam. When the bottom flange is removed or made smaller, several of the terms in Eby's equations become unstable/undefined and inaccurate results are produced. This is the reason for the alternate approach of Figure 6.3. The beam was modeled as a rectangular flange and web in accordance with the idealization presented in Figure 6.2.

An isometric view of the stiffened plate model with the damaged elements is presented in Figure 6.20. The damaged members along Beam 1W are noticeable in the figure to the right of the midspan diaphragm location. Because of the way the beam elements are linked to the bottom of the slab, the relative vertical distance between the centroid of the undamaged and damaged beams is noticeable. With the exception of the damaged regions of Beam 1W and 2W, all other parameters are the same as for the previously tested undamaged model, SP-3.

A series of transverse sections at midspan are presented in Figure 6.21 for the previously described damage scenario. The figures are similar to those previously presented in that they depict the deflections at midspan for various beams due to the three load cases used for model evaluation. In parts (a) and (b) of this figure, the agreement between the experimental and analytical model is excellent while for part (c) there are slight discrepancies but the agreement is still good when one considers the magnitude of the deflections.

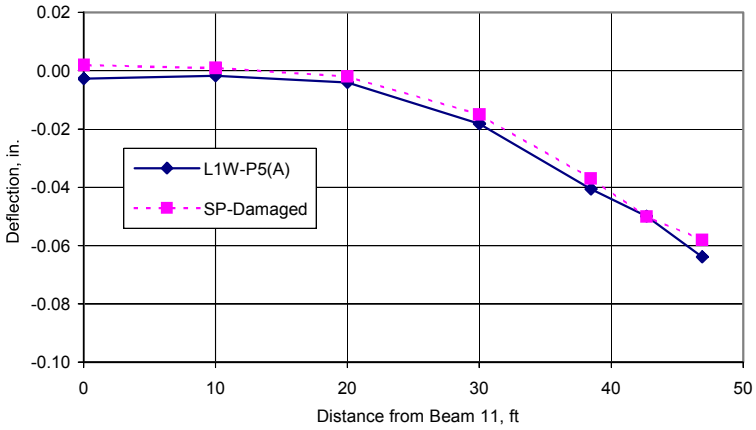


**a.) Load Position L1E/W(R)-P5**

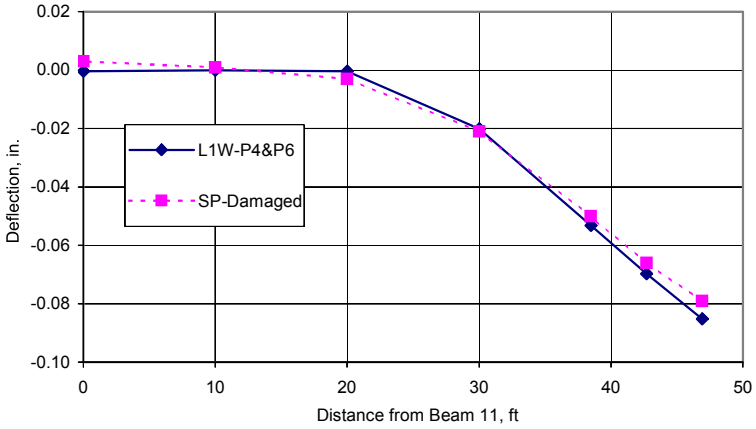


**b.) Load Position L1E/W(R)-P4&P6**

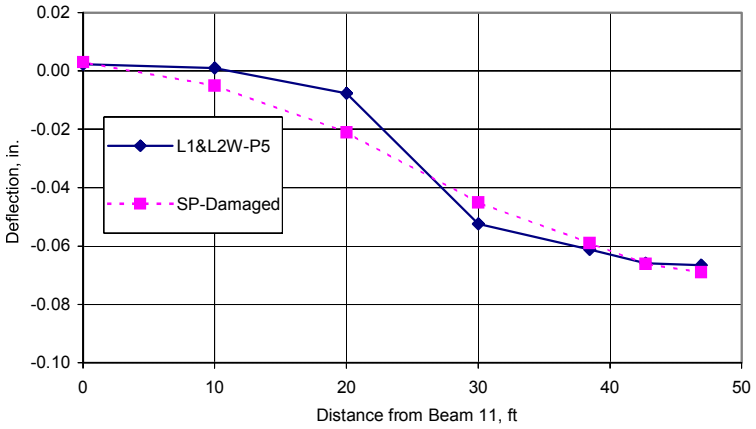


**c.) Load Position L1&L2E/W(R)-P5**

**Figure 6.21. Comparison of Experimental and Analytical Deflections for the Damaged WB Bridge.**

From the results presented in these three transverse sections at midspan of the damaged center span, it can be concluded that the arbitrary amount and extent of damage inflicted to Beams 1W and 2W was reasonable. Recall that the assessment of damage was subjective and based strictly on visual observation of the damage to the bottom flange and web of the beams in question. An alternate approach would have been to "back into" the results by modifying the model numerous times until the analytical and experimental deflections were in agreement. However, such an approach is of little practical value since a practitioner in most cases will not have access to measured deflections for the calibration process.

Following the deflection graphs, the internal moments calculated at midspan are presented for all three load cases in Figure 6.22. The results from the original SP-3 undamaged model are presented as solid lines and those from the damaged model analysis as dashed lines. The figure indicates a rather significant redistribution of moments due to the loss of section previously described. The moments in damaged Beams 1W and 2W are decreased by approximately 1/3 to 1/2 with the majority of the redistributed moment being taken up by the barrier curb and rail as well as by Beams 3W and 4W. Note that although there is a slight increase in Beams 5W and beyond, the differences are insignificant. The majority of the redistributed load is absorbed by the adjacent members in close proximity to the damaged elements indicating that for this bridge (and likely for bridges in general), redistribution of load is a highly localized effect. For the case of Trucks 1 and 2 in adjacent lanes, L1&L2-P5, the moment resisted by Beam 3W increases from 189 ft-kips to 261 ft-kips (38% increase). The predicted moment for this beam based on the applied vehicle configuration and the S/5.5 distribution suggested by AASHTO is 253 ft-kips indicating that even in the presence of redistributed live loads due to exterior beam damage, the analytically predicted moment is only 8 ft-kips higher than predicted by AASHTO for an undamaged structure. For this analysis and this bridge, the AASHTO distribution factors in the Standard Specification are safe estimates of the live load in the undamaged beams even following live load redistribution.

The load is being redistributed through the flexural/torsional stiffness of the slab with localized stress increases in the slab near the damage. Stress contours for transverse bending of the slab are presented in Figure 6.23 for load case L1-P4&P6 where the units for the contours are ft-kips/ft of width of plate. The transverse bending moment for the undamaged case never exceeds 0.68 ft-kips/ft while for the damaged case, the moments are as high as 1.2 ft-kips/ft in the vicinity of the load. Also note that the higher transverse moments are obviously located over the damaged region and that the moments per foot are not symmetric about midspan as they are for the undamaged bridge.

### *6.4.3. Center Span Analytical Modeling Summary*

Section 6.4 has concentrated on developing analytical models of both an undamaged and a damaged span representative of the center span of the I-680 WB bridge in Beebeetown, IA. The first task was to develop undamaged models that replicated the behavior of the undamaged EB and repaired WB bridges; two types of models were developed.

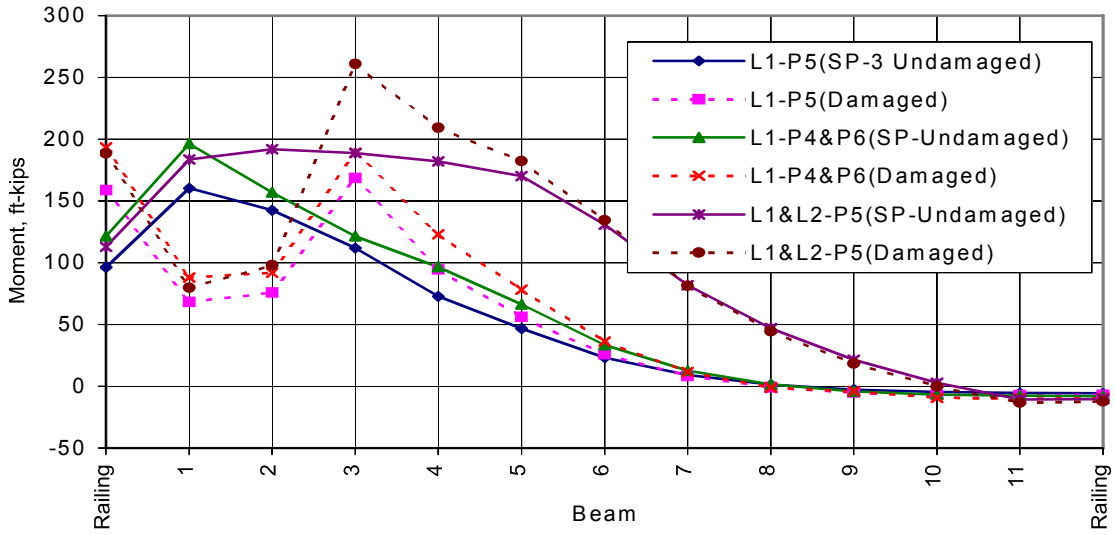


**Figure 6.22. Load Distribution Comparisons, WB Bridge, Undamaged and Damaged Models.**

The first model generated was a stiffened plate type of which 16 model variations were created. Variables studied included the boundary conditions, Modulus of Elasticity of the beam and deck material, and the participation of the diaphragm and barrier rails in load distribution. From examination of the 16 different models, it was concluded that a stiffened plate model in which the beams were simply supported and in which the diaphragm and rail were active in distributing load most closely represented the experimental results. The stiffened plate model results indicate that the AASHTO Standard Specification formulas for exterior and interior beam live load distribution are highly conservative for this bridge. The predicted moments according to AASHTO are 38% higher than predicted by the model for the exterior beam indicating the significant benefits of a refined analysis for live load distribution.

Next, a grillage model with the same boundary conditions, material properties, and participatory elements was created. The results for the grillage model agreed fairly well with those from the stiffened plate for both deflection and internal bending moment. There were slight differences in the models in the vicinity of the most heavily loaded beams with the grillage model tending to predict moments in the barrier curb and rail somewhat higher than the moments from the stiffened plate model and the moments in the most heavily loaded beams several percent less than those found using the stiffened plate model. However, considering the many assumptions that go into creating even the simplest models of either type, both models are considered acceptable for practical applications.

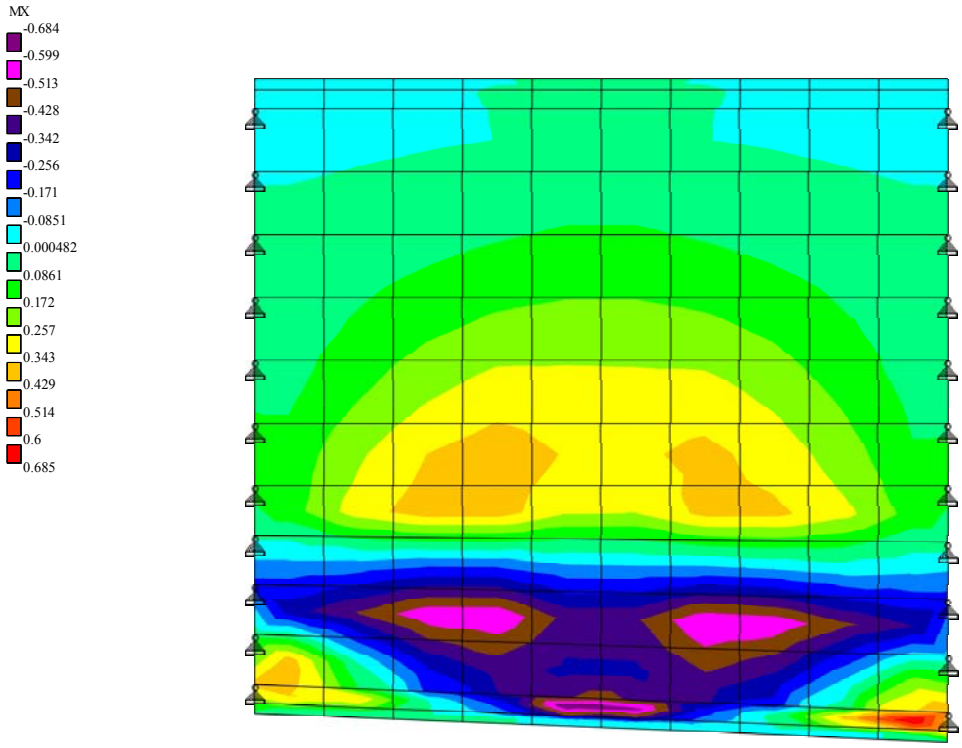


**a.) Bending Moment, MX (Transverse Slab Bending), Undamaged Model.**

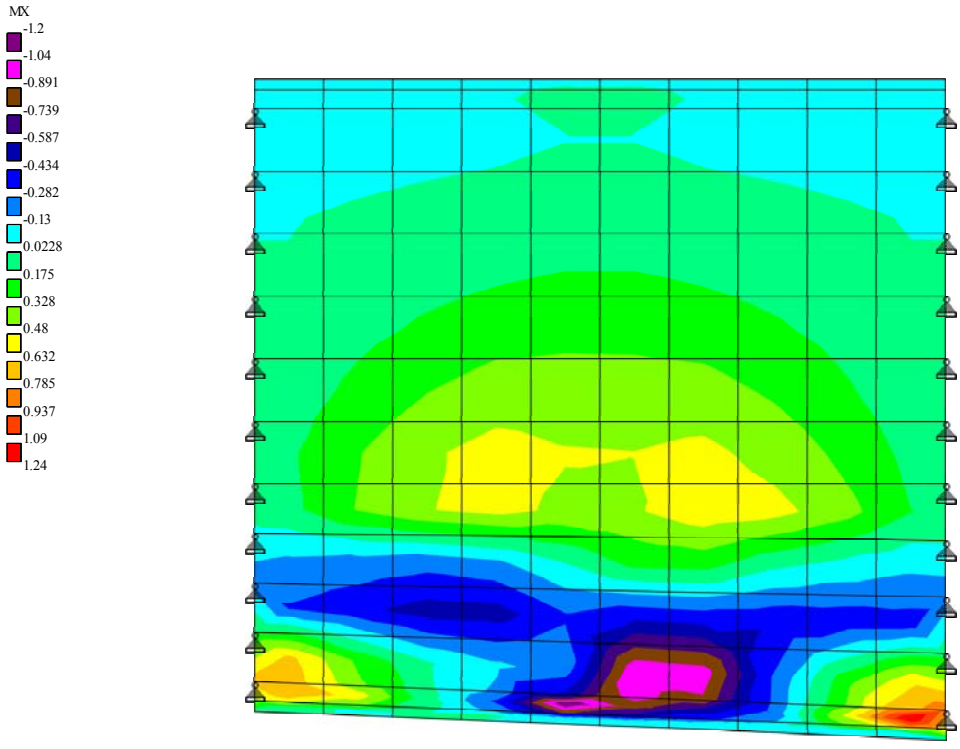


**b.) Bending Moment, MX (Transverse Slab Bending), Damaged Model.**

**Figure 6.23. Transverse Slab Bending, WB Bridge, Load Case L1-P4&P6.**

Finally, a damaged model was created in which the area, flexural and torsional properties of the eccentric beam elements were locally modified to account for damage. It was determined that a subjective amount of damage, the limits of which were established from visual examination of the beams, resulted in models which very accurately simulated the experimental behavior. The damaged models indicated a very significant decrease (1/3 to 1/2) in resisted moment in the damaged beams with the load being redistributed to the adjacent rail and beams. Redistribution was determined to be a localized effect with only the nearest beams participating in resisting the redistributed load. Even under the action of the "normal" plus redistributed moments, the most heavily loaded interior beam had an internal moment in general agreement with what AASHTO would predict as a live load distribution factor for an undamaged structure. This indicates that that empirical live load distribution factors, found highly conservative for this bridge, are reasonable estimates of total live load in undamaged beams near the damaged region even following live load redistribution.

# *CHAPTER 7*
# *SUMMARY, CONCLUSIONS AND RECOMMENDATIONS*

## *7.1. Summary*

This report has documented the research results from several major tasks, all of which address a particular aspect of the performance of damaged P/C bridges. A brief summary of the individual tasks follows.

In Chapter 3, the results of the field tests conducted on the I-680 bridge were presented. The original tests were conducted on the damaged WB structure and the complementary EB structure; subsequent tests were conducted on the WB bridge following the replacement of the damaged beams.

For the damaged WB bridge vs. undamaged EB bridge, it was generally noted that the end span behavior was similar; the main differences were observed in the center spans. The maximum deflection in the center span of the damaged WB bridge was 0.064 in. under a single truck placed as close as possible to the damaged beams (L1W-P5). Under the action of two trucks, both placed near midspan over the damaged beams (L1-P4&P6), the maximum deflection was recorded to be 0.085 in., or approximately L/7900. For the EB bridge, the maximum deflection was 0.083 in., L/8100. For both bridges, the deflections are very small. Very little load was transferred by flexure in the intermediate diaphragms. There was experimental evidence, later confirmed by analytical modeling, of the redistribution of load from the damaged beam lines to undamaged beams of the WB bridge. The stress range in the exposed strands of the damaged WB bridge beams was small due in large part to the redistribution of moments away from the damaged beams. Some end restraint was present in the bridges, likely due to the corroded bearings and also to the continuity of the slab, curb and rail along the entire length of the bridge. The general conclusion regarding restraint is that the beams behave essentially as simply-supported specimens. This was determined through examination of the longitudinal deflected shapes of the beams under various loading conditions.

For subsequent tests performed on the repaired WB bridge following beam replacement, the general conclusion is that the replacement of damaged Beams 1W and 2W results in the WB and EB bridges behaving essentially the same. There is strong evidence to conclude that the differences in the prior year tests of the damaged WB bridge and undamaged EB bridge are attributable to the influence of isolated main member damage. Replacement of the damaged beams does not result in perfect agreement between the WB and EB bridges but the agreement is much better than between the damaged WB and undamaged EB structures.

A portion of the experimental test results for the model bridge are discussed in Chapter 4. A more extensive presentation of the data can be found in Paradis (1998). Throughout the comparisons for the P/C beams, the R/C deck and the prestressing steel strands, bridge behavior was not significantly affected until

strands were removed from the damaged beam. Concrete damage alone was not sufficient to cause relative changes in behavior. Even then, bridge behavior in general is not significantly affected until critical levels of damage are reached (Damage Level 10 or higher, which corresponds to a 33% loss of prestress force in the tensile zone). When load is placed a distance away from the damaged region, bridge behavior remains relatively unchanged. The beam on the opposite side of the bridge model is not adversely affected by the load placed at any location even at the highest levels of damage. In addition, loading of the beam adjacent to the damaged member (i.e. the interior beam) produced no changes in observed bridge behavior in nearly all cases. This indicates that undamaged regions of the bridge are not affected when loads are applied away from the damaged member. Even with a large loss of prestress force (over 80%), significant strength remains in the damaged beam indicating that changes in load paths and/or lateral load distribution have occurred. The investigation of transverse load distribution by moment fractions reveals that the moment in Beam 2 (an undamaged beam) approximately doubles between the initial and final damage conditions. At the same time, stress levels in the damaged beam remain well below the ultimate strength of the section. This indicates that a significant degree of redundancy is present in this bridge model. The amount of transverse load distribution in this bridge model is most likely at the minimum expected level for the type of testing performed in this investigation. Increases in deck thickness and span length would significantly increase the degree of lateral load distribution at the levels of damage tested.

Isolated beam testing was performed and documented in Chapter 5 of the report. Results were presented for two beams removed from service and two beams originally part of a large-scale laboratory model.

For the beams removed from the I-680 bridge, Beams 1W and 2W, the test results indicate that both the damaged and repaired beams have strengths in excess of that expected even when measured material strengths are used in the computation. Beam 1W, the damaged specimen tested in the “as-removed” condition, behaved elastically during the service load tests. During the ultimate load test, Beam 1W exhibited a ductile response. At a maximum moment of 2,467 ft-kips, the beam failed in shear through the damaged web region; the midspan deflection was approximately 10 in. at failure. Beam 2W was strengthened with CFRP longitudinal plates and external fabric stirrups. The retrofit was intended to replace the capacity of two severed strands. In tests conducted prior to the retrofit, Beam 2W behaved elastically during multiple tests. The stiffness of the beam was determined through use of the known applied moments and measured curvature. The stiffness was fairly constant along the beam except in the damaged region where the measured elastic stiffness was 1/8th to 1/9th of the stiffness at other locations. After strengthening, the beam was tested again with the effect of the repair on beam stiffness being most significant in the damaged region of the beam. The repaired beam failed at a moment of 2,760 ft-kips. Even when this moment is corrected for a slightly smaller dead load moment in Beam 2W as compared to Beam 1W, the repaired beam was still substantially stronger (12%) than the unstrengthened specimen. Failure was sudden with the complete collapse of the specimen occurring at a midspan deflection in excess of 5 in.

The CFRP plates were efficiently used; at failure the stress in the plates was 85% of the ultimate tensile strength of the material. For both Beams 1W and 2W, the strains and deflections measured as isolated specimens are many times greater than those measured in-situ. This is a reflection once again of the live load distribution characteristics of the I-680 bridges.

Two beams removed from the ISU model bridge were also tested to failure. The first beam, Beam 1, was a control specimen tested in order to obtain the baseline behavior and strength of an undamaged specimen. The second beam, Beam 2, was intentionally damaged with damage consisting of partial removal of the bottom flange and the severing of three prestressing strands. Following this damage, the beam was repaired using CFRP plates and GFRP external fabric transverse confinement. The results from the Beam 1 tests indicate that the beam is ductile and strong. At ultimate load, the total moment of 1,487 ft-kips was approximately 11% higher than the predicted strength and the beam deflected in excess of 5 in. at midspan. The effective prestress was measured for this beam using the crack reopening load method; the measured crack reopening load corresponds to a prestress loss of 31.5 ksi, only 80% of that predicted. At failure, the beam was heavily cracked with primarily vertical flexural cracks in the constant moment region, diagonal tension cracks outside of the constant moment region and web shear cracks near the supports. Beam 2W, the strengthened specimen, behaved similar to Beam 1until progressive failure of the CFRP strengthening system commenced at a total moment of 1,384 ft-kips. Failure was a combination of plate debonding from the substrate and failure of the substrate. Following debonding of the plates, the resulting beam capacity returned to that of an unstrengthened specimen and testing ceased following a long yield plateau. It should be noted that although the CFRP strengthening eventually debonded from the beam, this was not until the beam had a total applied moment in excess of the theoretical capacity of an undamaged specimen, i.e., the repair performed its intended function.

Analytical modeling of the I-680 bridges as well as other test bridges is discussed in Chapter 6. A comprehensive review of live load distribution and computer modeling techniques was provided so that practicing engineers would confidently be able to create reasonable models for determination of live load distribution. Prior to analyzing the I-680 undamaged, repaired, and damaged bridges, the analysis software, STAAD-III, was first validated by comparing the published results of other authors and other software to those obtained using STAAD for the analysis.

In the first test case, a plane grillage model of a six-beam cross section was created. Comparisons of the results from the STAAD analysis to the published solution are excellent. A second, more refined grillage, a downstand grillage, was created for comparison to the plane grillage; the live load distribution characteristics of the downstand model are similar to those of the plane grillage model. A stiffened plate model was also created of the same bridge with the consensus that all three modeling techniques yield results that can be considered acceptably accurate considering the number of variables in the analysis. A second test case, that of a P/C bridge modeled using the stiffened plate method, was also described. In the published solution, orthotropic slab properties are specified and a finer mesh was used than in the analysis

conducted in this report. Nevertheless, the analysis conducted as part of this research indicates that the STAAD stiffened plate model is accurate compared to a more refined model created using the ADINA program.

Having established the suitability of the software and modeling techniques, a stiffened plate and grillage model of the undamaged/repaired center span of the I-680 bridge was created. Sixteen different stiffened plate models were created to conduct a sensitivity analysis on the effect of changes in boundary conditions, rail and diaphragm participation, and Modulus of Elasticity. The most reasonable model, in the opinion of the authors, includes the diaphragm and rail in the model and treats the beams as simply supported. Uniform changes in E to all members have no effect on internal force distribution, only an effect on the deflection of the model. The agreement of both models with the deflections measured in the field is excellent and the predicted moments from the analysis are substantially lower than predicted using the empirical live load distribution factors in the AASHTO Standard Specifications. The grillage model slightly under-predicts the moments in the most heavily loaded beams and overestimates the moment carried by the curb and rail as compared to the stiffened plate. However, the maximum difference between the two models is approximately 16% with the stiffened plate being the more conservative estimate of the longitudinal beam moments.

The undamaged model was then modified with an estimated amount of damage where the estimated damage was subjectively determined based on assessment of the inspection report, photographs, and personal viewing of the damaged structure. The amount of damage imposed on the model resulted in a reduction in the moment of inertia of the P/C beam of approximately 80% with lesser but still significant decreases in torsional stiffness and area. The subjective amount of damage resulted in deflections in the analytical model in excellent agreement with those determined in the field. The damaged stiffened plate model indicates that substantial redistribution of moment occurs. The moments in the damaged beams are significantly reduced while the moment in the barrier rail and several adjacent interior beams increases substantially. Even with the redistributed moments being added to the “normal” amount of live load carried by the most heavily loaded intact interior beam, the maximum live load moment is still only approximately that predicted if one used the empirical S/5.5 distribution factor found in AASHTO. This indicates that for this bridge, the live loads in the damaged member are significantly reduced and that the AASHTO live load distribution factor is so conservative that even in the presence of redistributed moments, the interior beams are not overloaded.

## ***7.2. Conclusions and Recommendations***

The results of this research are promising in that they answer some of the previously unanswered questions regarding the strength and overall performance of damaged P/C bridges. The research also contributes to the limited amount of literature on the CFRP strengthening of damaged P/C beams. Some general recommendations for treating similarly damaged structures are presented below.

The I-680 bridges are atypical structures with very small beam spacing and a thick slab and overlay. The damaged beams are also located very near a large curb and rail section. These factors certainly positively influenced the performance of the bridge. The numerous tests conducted in this investigation along with the supporting analyses indicate that the I-680 beams did not need to be removed for strength purposes. This was demonstrated by both determining the strength of the damaged beams and by analyzing numerous analytical models of the bridge to determine the live load effects in the damaged structure. Though used on an atypical bridge, the modeling techniques demonstrated in this report are routinely used in bridge analysis and can be confidently used in the analysis of future damaged P/C beam bridges with more typical beam spacings and slab thicknesses. Both the grillage and stiffened plate modeling techniques can be used, the level of analysis should be left to the discretion of the engineer although the modeling guidelines presented in Section 6.2 of the report should be consulted during the creation of the model.

Testing of the ISU bridge model is important in that it demonstrates that for a relatively significant loss of section, the influence of damage on adjacent beams is minimal. Only after a significant portion of the beam is removed, and more importantly some of the prestressing strands, does the behavior begin to change significantly.

In future damaged P/C bridges, if an analysis indicates that the damaged beam(s) does not possess the strength to resist the applied loads, strengthening techniques that were easily installed were demonstrated to substantially increase the capacity of the damaged beams. The retrofits used only required minimal restoration of the original beam cross-section. In both retrofitted beams, the strength of the repaired specimen exceeded that of a theoretically undamaged specimen and the beams demonstrated a ductile response. From the limited experience gained during this research project, the use of well-distributed confinement wraps appears to be beneficial in maintaining bond between the CFRP and the concrete. Although only two beams were tested during this research project, there is a large amount of literature to support the conclusion that CFRP strengthening can be effectively employed for flexural strengthening of reinforced concrete beams. Additional experimental information on the CFRP strengthening of damaged P/C beams will be obtained as part of a companion project currently underway at Iowa State University.

It should be noted that one of the conclusions of this research is not to say that all damaged beams should be saved to the exclusion of other important considerations. Long term durability of the patch material and strengthening system was not examined though others have conducted such investigations. Fatigue performance of the pre-cracked beams was not investigated. Because cracked P/C beams experience much higher stress ranges in the strands exposed during the collision, remaining fatigue life needs to be considered. However, with beam damage typically occurring in exterior beams where the number of load cycles is low and the stress range lower due to the stiffening effect of the curb and rail plus the better load distribution predictions of refined analysis, the predicted fatigue life may still be sufficient. If the bridge owner can obtain new beams as compensation following an accident investigation, this is the

best long-term solution. However, the current research is most useful when it is the owner's responsibility to fund the repair or when making decisions relative to traffic restrictions on damaged bridges.

# *CHAPTER 8*
# *NEEDS FOR FURTHER INVESTIGATION*

During the course of this investigation, a number of issues were studied including live load distribution in damaged and undamaged bridges as well as in a large-scale bridge model. Additionally, tests were conducted on four isolated P/C beams, two strengthened and two without strengthening. Several important conclusions were drawn about the load distribution and remaining strength characteristic of damaged P/C bridges yet questions remain. A synopsis of the issues requiring further investigation is presented below.

- Although the bridge tests conducted herein demonstrated a significant load redistribution away from the damaged exterior and first interior beams to the undamaged interior beams and curb/rail system, this is partly due to the relatively thick slab and overlay and the narrow beam spacing. A broader sample of damaged bridges should be tested in order to better understand the behavior of damaged bridges with more typical beam and slab geometries.
- Work should continue on validating the analytical methods presented herein. The most important determination is a rational method for determining the effect of local damage on member properties required of an analytical model. The analysis conducted herein, though seemingly very accurate, was based on a subjective assessment of the amount of damage.
- Additional analysis should be performed concerning the design of CFRP retrofits. The work in the area of design methodology development for strengthening R/C beams has received significant attention, i.e., (Malek and Saadatmanesh, 1998), yet a comparable effort concerning the retrofit of P/C beams is not evident in the literature.
- The durability of CFRP retrofit beams needs to be demonstrated to the satisfaction of the bridge owners. This research has not addressed issues such as durability of the patch concrete, long-term durability of the epoxy, and finally long-term performance of the beam and its future susceptibility to other modes of failure, i.e., fatigue of the prestressing strands. There is a significant body of information concerning these issues though it was not within the scope of this project to review and comment on these issues. An expanded literature review would sufficiently summarize the state-of-the-art relative to these concerns.
- An investigation of methods to predict the shear strength of damaged beams should be undertaken. Tests on the Beebeetown beams demonstrated appreciable shear strength in the region of significant web damage. The code-based methods for shear strength prediction are inadequate.
- No method was proposed herein for modeling the effect of concrete and strand damage on the effective prestress in the intact strands. A tool for analyzing this effect would be beneficial and thus should be developed.

# *CHAPTER 9*
# *ACKNOWLEDGEMENTS*

The investigation presented in this report was conducted by the Bridge Engineering Center under the auspices of the Engineering Research Institute of Iowa State University. The research was sponsored by the Iowa Department of Transportation and the Iowa Highway Research Board under Research Project HR-397.

The authors of this report would like to extend their sincere thanks to the many individuals without whose help this project could not have been completed. Specifically, the authors would like to acknowledge the following for their support and cooperation.

- The authors would like to thank Mr. William A. Lundquist, formerly the Bridge Engineer for the State of Iowa, for his support of the project. Additionally, the authors would like to thank the many DOT personnel whose assistance was required to test the I-680 bridges.
- Sincere appreciation is expressed to the ISU staff whose assisted in the many phases of this project, specifically Douglas Wood, Structures Laboratory Supervisor, without whose help the work could not have been performed. Additionally, the assistance of the many undergraduate and graduate students who worked in the laboratory and field-testing portions of this project is greatly appreciated.
- The generosity of those who donated both material and construction time to this project was a significant benefit. In particular, the assistance of Joe Mockapetris and Greg Reisz of Sika, and the staff of Specialty Construction of Madrid, Iowa was required for the retrofit of Beam 2 removed from the bridge model. Additionally, Fiber Reinforced Systems of Columbus, OH and Lithko Construction, also from Ohio were responsible for the retrofit of Beam 2W removed form the Beebeetown Bridge. A sincere thanks is also extended to Steve Morton of the Ohio DOT for his assistance in coordinating the retrofit of the Beebeetown beams.
- The assistance of the staff of Wilson Concrete, LaPlatte, NE, and the University of Nebraska, Omaha, is sincerely appreciated for providing the facilities used in the testing of the Beebeetown beams.

# *APPENDIX A*
# *SAMPLE COMPUTER MODELS*

This Appendix presents the STAAD input files for three different computer models whose results were presented in Chapter 6 of this report. The first model, presented in Section A.1, is a plane grillage model of a six-beam bridge used to test the STAAD program's ability to model such a structure. The results from this model are presented in Section 6.3.1. The second model, from which the downstand grillage results of Section 6.3.1 are obtained, is presented in Section A.2. Finally, the input file for a stiffened plate model of the undamaged center span of the WB I-680 bridge in Beebeetown, IA is presented in Section A.3.

## *A.1. Barker and Puckett Example Grillage (Section 6.3.1 and Figure 6.6)*

```
STAAD FLOOR PUCKETT 6.4
START JOB INFORMATION
ENGINEER DATE 01-OCT-98
END JOB INFORMATION
INPUT WIDTH 79
UNIT FEET KIP
JOINT COORDINATES
1 0 0 0 6 40 0 0
REPEAT 5 0 0 7
MEMBER INCIDENCES
1 1 7
REPEAT 5 1 1
REPEAT ALL 4 6 6
31 7 8 35
REPEAT 3 5 6
UNIT INCHES KIP
MEMBER PROPERTY AMERICAN
1 TO 30 PRIS AX 1022 IX 8231 IY 589824 IZ 130576
31 TO 50 PRIS AX 672 IX 7168 IY 395136 IZ 3584
CONSTANTS
E 3600 ALL
POISSON 0.15 ALL
SUPPORTS
1 TO 6 31 TO 36 PINNED
UNIT FEET KIP
LOAD 1 1 TRUCK LOADED NEAR MIDSPAN
JOINT LOAD
13 25 FY -18.5 MZ 6
14 26 FY -13.5 MZ -18
PERFORM ANALYSIS
PRINT ANALYSIS RESULTS
FINISH
```

## *A.2. Barker and Puckett Downstand Grillage (Section 6.3.1 and Figure 6.7)*

```
STAAD SPACE PUCKETT 6.4 MODELED AS A DOWNSTAND GRILLAGE
START JOB INFORMATION
ENGINEER DATE 01-OCT-98
END JOB INFORMATION
INPUT WIDTH 79
UNIT FEET KIP
JOINT COORDINATES
1 0 0 0 6 40 0 0
REPEAT 5 0 0 7
MEMBER INCIDENCES
* GENERATING MAIN MEMBERS
1 1 7
REPEAT 5 1 1
REPEAT ALL 4 6 6
*GENERATING TRANSVERSE MEMBERS
31 7 8 35
REPEAT 3 5 6
UNIT INCHES KIP
MEMBER PROPERTY AMERICAN
1 TO 30 PRIS AX 1022 IX 8231 IY 589824 IZ 108065
31 TO 50 PRIS AX 672 IX 7168 IY 395136 IZ 3584
CONSTANTS
E 3600 ALL
POISSON 0.15 ALL
MEMBER OFFSET
* CG OF COMPOSITE SEC'N = 29.13", THEREFORE E=29.83+4-29.13=4.7"
31 TO 50 START 0 4.7 0
31 TO 50 END 0 4.7 0
SUPPORTS
1 TO 6 31 TO 36 PINNED
UNIT FEET KIP
LOAD 1 1 TRUCK LOADED NEAR MIDSPAN
JOINT LOAD
13 25 FY -18.5 MZ 6
14 26 FY -13.5 MZ -18
PERFORM ANALYSIS
PRINT ANALYSIS RESULTS
FINISH
```

## *A.3. I-680 Stiffened Plate Model SP-3 (Section 6.4.1 and Figure 6.11)*

```
STAAD SPACE BEEBEETOWN UNDAMAGED CENTER SPAN
START JOB INFORMATION
ENGINEER DATE 06-OCT-99
END JOB INFORMATION
INPUT WIDTH 72
* DIAPHRAGM ACTIVE, RAIL ACTIVE, E=7000, PINNED SUPPORT
UNIT FEET KIP
JOINT COORDINATES
*NODES AT EDGE OF PLATE AND CENTERLINE OF RAILING
1 0 0 -2.3333 11 55 0 -2.3333
12 0 0 -1.5 22 55 0 -1.5
23 0 0 47.29 33 55 0 49.54
34 0 0 48.123 44 55 0 50.373
*NODES FOR EACH BEAM LINE
100 0 0 45.79 110 55 0 48.04
200 0 0 41.842 210 55 0 43.53
300 0 0 37.895 310 55 0 39.02
400 0 0 33.947 410 55 0 34.51
500 0 0 30 510 55 0 30
600 0 0 25 610 55 0 25
700 0 0 20 710 55 0 20
800 0 0 15 810 55 0 15
900 0 0 10 910 55 0 10
1000 0 0 5 1010 55 0 5
1100 0 0 0 1110 55 0 0
MEMBER INCIDENCES
*DIAPHRAGM MEMBERS
1 105 205
REPEAT 9 1 100
*RAILING MEMBERS
12 12 13 21
23 23 24 32
*MAIN MEMBERS
101 100 101 110
201 200 201 210
301 300 301 310
401 400 401 410
501 500 501 510
601 600 601 610
701 700 701 710
801 800 801 810
901 900 901 910
1001 1000 1001 1010
1101 1100 1101 1110
ELEMENT INCIDENCES SHELL
10001 1 12 13 2 TO 10010
10011 12 1100 1101 13 TO 10020
10021 100 23 24 101 TO 10030
10031 23 34 35 24 TO 10040
10101 200 100 101 201 TO 10110
```

10201 300 200 201 301 TO 10210
10301 400 300 301 401 TO 10310
10401 500 400 401 501 TO 10410
10501 600 500 501 601 TO 10510
10601 700 600 601 701 TO 10610
10701 800 700 701 801 TO 10710
10801 900 800 801 901 TO 10810
10901 1000 900 901 1001 TO 10910
11001 1100 1000 1001 1101 TO 11010
UNIT INCHES KIP
**MEMBER PROPERTY AMERICAN**
***RAILING PROPERTIES (RETROFIT CURB AND RAIL)**
12 TO 21 23 TO 32 PRIS YD 32 ZD 10 YB 12 ZB 20
***BEAM PROPERTIES**
101 TO 110 201 TO 210 301 TO 310 401 TO 410 501 TO 510 601 TO 610 -
701 TO 710 801 TO 810 901 TO 910 1001 TO 1010 1101 TO 1110 -
PRIS AX 382.5 IX 7980 IY 5980 IZ 62000
1 TO 10 PRIS YD 32 ZD 8
**ELEMENT PROPERTY**
10001 TO 10040 10101 TO 10110 10201 TO 10210 10301 TO 10310 -
10401 TO 10410 10501 TO 10510 10601 TO 10610 10701 TO 10710 -
10801 TO 10810 10901 TO 10910 11001 TO 11010 THICKNESS 9
**MEMBER OFFSET**
1 TO 10 START 0 -20.5 0
1 TO 10 END 0 -20.5 0
12 TO 21 23 TO 32 START 0 17.77 0
12 TO 21 23 TO 32 END 0 17.77 0
101 TO 110 201 TO 210 301 TO 310 401 TO 410 501 TO 510 601 TO 610 -
701 TO 710 801 TO 810 901 TO 910 1001 TO 1010 1101 TO 1110 -
START 0 -26.44 0
101 TO 110 201 TO 210 301 TO 310 401 TO 410 501 TO 510 601 TO 610 -
701 TO 710 801 TO 810 901 TO 910 1001 TO 1010 1101 TO 1110 -
END 0 -26.44 0
**CONSTANTS**
E 7000 ALL
POISSON 0.2 ALL
**SUPPORTS**
300 310 400 410 500 510 600 610 700 710 800 810 900 910 PINNED
100 110 200 210 1000 1010 1100 1110 PINNED
**MEMBER RELEASE**
***RELEASE AXIAL AND MOMENT AT EACH END OF P/C BEAMS (EXPOSED BEAM FACES)**
101 201 301 401 501 601 701 801 901 1001 1101 START FX MZ
110 210 310 410 510 610 710 810 910 1010 1110 END FX MZ
***DIAPHRAGM MOMENT RELEASE**
1 TO 10 START MZ
1 TO 10 END MZ
UNIT FEET KIP
**LOAD 1 L1W-P4**
ELEMENT LOAD
10203 PR -11.38 -1.31 -1.94
10103 PR -11.38 0.59 -2.19
10203 PR -11.38 -1.13 2.56
10103 PR -11.38 0.78 2.31
10206 PR -7.41 -0.95 0.56

10106 PR -7.41 0.78 0.31
**LOAD 2 L1W-P5**
ELEMENT LOAD
10205 PR -11.38 -1.03 1.13
10105 PR -11.38 0.76 0.88
10206 PR -11.38 -0.98 0.13
10106 PR -11.38 0.76 -0.12
10209 PR -7.41 -0.81 -1.87
10109 PR -7.41 0.76 -2.12
**LOAD 3 L1W-P6**
ELEMENT LOAD
10208 PR -11.38 -0.9 -1.3
10108 PR -11.38 0.8 -1.6
10209 PR -11.38 -0.8 -2.3
10109 PR -11.38 0.8 -2.6
**LOAD 4 L2W-P4**
ELEMENT LOAD
10503 PR -11.38 -0.6 -1.9
10403 PR -11.38 0.9 -2.2
10503 PR -11.38 -0.4 2.56
10403 PR -11.38 1 2.31
10506 PR -7.41 0.19 0.56
10406 PR -7.41 1.55 0.31
**LOAD 5 L2W-P5**
ELEMENT LOAD
10505 PR -11.38 0 1.13
10405 PR -11.38 1.4 0.88
10506 PR -11.38 0.16 0.13
10406 PR -11.38 1.5 -0.1
10509 PR -7.41 0.76 -1.87
10409 PR -7.41 2.04 -2.12
**LOAD 6 L2W-P6**
ELEMENT LOAD
10508 PR -11.38 0.56 -1.3
10408 PR -11.38 1.9 -1.6
10509 PR -11.38 0.74 -2.3
10409 PR -11.38 2 -2.6
**LOAD COMB 7 L1W-P4+P6**
1 1.0 3 1.0
**LOAD COMB 8 L2W-P4+P6**
4 1.0 6 1.0
**LOAD COMB 9 L1&L2-P5**
2 1.0 5 1.0
PERFORM ANALYSIS
PRINT ANALYSIS RESULTS
FINISH

# *REFERENCES*


Abdel-Halim, Mohamed, Richard M. McClure, and Harry H. West. 1987. Overload Behavior of an Experimental Precast Prestressed Concrete Segmental Bridge. PCI Journal v. 32 no. 6 (November-December): 102-123.

Abendroth, R.E., F. W. Klaiber, and M. W. Shafer. 1991. Lateral Load Resistance of Diaphragms in Prestressed Concrete Girder Bridges, Final Report for HR-319. Ames, IA: Iowa Department of Transportation.

Aboutaha, Riyad, Roberto Leon, and Abdul-Hamid Zureick. 1997. Rehabilitation of Damaged AASHTO Type II Prestressed Girder Using CFRP. In Proceedings of the Second Symposium on Practical Solutions for Bridge Strengthening and Rehabilitation, Kansas City, MO, March 24-25, 1997, by Iowa State University. Ames, IA: Department of Civil and Construction Engineering, Iowa State University, 293-301.

American Association of State Highway and Transportation Officials. 1994. AASHTO LRFD Bridge Design Specifications. Washington, DC: American Association of State Highway and Transportation Officials.

American Association of State Highway and Transportation Officials. 1996. Standard Specifications for Highway Bridges – 16th ed., 1996. Washington, DC: American Association of State Highway and Transportation Officials.

Aswad, Alex and Yohchia Chen. 1994. Impact of LRFD Specification on Load Distribution of Prestressed Concrete Bridges. PCI Journal (September-October): 78-89.

Bakht, Baidar, and Leslie G. Jaeger. 1985. Bridge Analysis Simplified. New York: McGraw-Hill Book Company.

Bakht, Baidar, and Leslie G. Jaeger. 1988. Dealing with Varying Moments of Inertia of Girders in Bridge Analysis. Canadian Journal of Civil Engineering v. 15: 232-239.

Barker, Richard M., and Jay A. Puckett. 1997. Design of Highway Bridges Based on AASHTO LRFD Bridge Design Specifications. New York: John Wiley & Sons.

Buckle, I. G., A. R. Dickson, and M. H. Phillips. 1985. Ultimate Strength of Three Reinforced Concrete Highway Bridges. Canadian Journal of Civil Engineering v. 12: 63-72.

Burdette, Edwin G., and David W. Goodpasture. 1974. Test to Failure of a Prestressed Concrete Bridge. PCI Journal (May-June): 92-103.

Burdette, E. G., and D. W. Goodpasture. 1988. Correlation of Bridge Load Capacity Estimates with Test Data. Washington, D.C.: Transportation Research Board. NCHRP Report 306.

Civjan, S. A, J. O. Jirsa, R. L. Carrasquillo, and D. W. Fowler. 1995. Method to Evaluate Remaining Prestress in Damaged Prestressed Bridge Girders. Austin, TX: Center for Transportation Research, University of Texas at Austin. CTR 1370-2.

Civjan, S. A, J. O. Jirsa, R. L. Carrasquillo, and D. W. Fowler. 1998. Instrument to Evaluate Remaining Prestress in Damaged Prestressed Concrete Bridge Girders. PCI Journal (March-April): 62.71.

Collins, Michael P. and Denis Mitchell. 1991. Prestressed Concrete Structures. Englewood Cliffs, NJ: Prentice Hall.

Daniels, J. H., W. Kim, and J. L. Wilson. 1989. Recommended Guidelines for Redundancy Design and Rating of Two-Girder Steel Bridges. Washington, D.C.: Transportation Research Board. NCHRP Report 319.

Deatherage, James Harold. 1987. Investigation of Variables Affecting Beam-Slab Bridge Load Capacity. Ph.D. dissertation, University of Tennessee, Knoxville.

Eby, Clifford C., John M. Kulicki, Celal N. Kostem, and Martin A. Zellin. 1973. The Evaluation of St. Venant Torsional Constants for Prestressed Concrete I-Beams. Bethlehem, PA: Fritz Engineering Laboratory, Department of Civil Engineering, Lehigh University.

Feldman, Lisa R., James O Jirsa, David W. Fowler, and Ramon L. Carrasquillo. 1996. Current Practice in the Repair of Prestressed Bridge Girders. Austin, TX: Center for Transportation Research, University of Texas at Austin. CTR 0-1370-1.

Feldman, Lisa R., James O. Jirsa, and Edward S. Kowal. 1988. Repair of Bridge Impact Damage. Concrete International. (February): 61-66.

Gosbell, K. B. and L. K. Stevens, 1968. Test Loading of a Full-Scale Bridge. In Proceedings of the Fourth Conference of the Australian Road Research Board, v. 4, part 2, 2018-2041.

Halsey, J. Todd, and Richard Miller. 1996. Destructive Testing of Two Forty-Year-Old Prestressed Concrete Bridge Beams. PCI Journal v. 41 no. 5 (September-October): 84-93.

Hambly, Edmund C. 1976. Bridge Deck Behaviour. London: Chapman Hall

Heins, Conrad P., and John T. C. Kuo. 1975. Ultimate Live Load Distribution Factor for Bridges. Proceedings of the American Society of Civil Engineers v. 101, no. ST7 (July): 1481-1496.

Heins, Conrad P., and Alan D. Kurzweil. 1976. Load Factor Design of Continuous-Span Bridges. Proceedings of the American Society of Civil Engineers v. 102 no. ST6 (June): 1213-1228.

Hsu, Thomas T. C. 1984. Torsion of Reinforced Concrete. New York: Van Nostrand Reinhold Company

Idriss, Rola L., and Kenneth R. White. 1991. Secondary Load Paths in Bridge Systems. In Third Bridge Engineering Conference, Papers Presented at the Third Bridge Engineering Conference, March 10-13, 1991, Denver, CO. Washington, D.C.: Transportation Research Board, 194-201. Transportation Research Record 1290.

Jaeger, Leslie G., and Baidar Bakht. 1982. The Grillage Analogy in Bridge Analysis. Canadian Journal of Civil Engineering. v. 9: 224-235.

Jaeger, Leslie G., and Baidar Bakht. 1989. Bridge Analysis by Microcomputer. New York: McGraw-Hill Book Company.

Johnson, R .P., and R. J. Buckby. 1979. Composite Structures of Steel and Concrete - Volume 2 Bridges. London: Granada.

Jones, Kathleen, ed. 1996. Repairing Damaged Prestressed Girders. Texas Department of Transportation Technical Quarterly. TQ10-3/10-4 (August): 1-7.

Kirkpatrick, J., A. E. Long, W. M. C. Stevenson and A. Thompson. 1985. Load Tests on Prestressed Concrete Multi-Girder Bridge Decks. In Strength Evaluation of Existing Concrete Bridges, SP-88, by the American Concrete Institute. Detroit: American Concrete Institute, 23-38.

Khaleel, Mohammad Ahmad. 1992. Reliability-Based Analysis, Sensitivity and Design of Partially Prestressed Concrete Systems. Ph.D. dissertation, Washington State University.

Kostem, Celal N. 1986. Approximations and Errors in the Grillage Analysis of Multibeam Bridges. In Official Proceedings of the 3rd International Bridge Conference. Pittsburgh: Engineers Society of Western Pennsylvania, 214-218.

Kostem, Celal N., and Ernesto S. deCastro. 1977. Effects of Diaphragms on Lateral Load Distribution in Beam-Slab Bridges. In Transportation Research Record 903. Washington, D.C.: Transportation Research Board, 6-9.

Kreger, Michael, Patrick M. Bachman and John E. Breen. 1989. An Exploratory Study of Shear Fatigue Behavior of Prestressed Concrete Girders. PCI Journal v. 34 no. 4 (July-August): 104-125.

Labia, Yolanda, M. Saiid Saiidi, and Bruce Douglas. 1996. Evaluation and Repair of Full-Scale Prestressed Concrete Box Girders. Reno, NV: University of Nevada, Reno. CCEER-96-2.

Labia, Yolanda, M. Saiid Saiidi, and Bruce Douglas. 1997. Full-Scale Testing and Analysis of 20-year-Old Pretensioned Concrete Box Girders. ACI Structural Journal v. 94 no. 5 (September-October): 471-482.

Lane, John S., Dr. P. Samuel Fasholé-Luke, and Michael B. Leeming,. 1997. The Role of 3-Dimensional Finite Element Analysis in Plate Bonding Using Advanced Composite Materials. In Structural Faults & Repair – 97, Proceedings of the Seventh International Conference on Structural Faults and Repair, 10th July, 1997, edited by Professor M. C. Forde, v. 1, 271-275. Edinburgh, Scotland: Engineering Technics Press.

Lane, John S., Michael B. Leeming, John J. Darby, and Dr. P. Samuel Fasholé-Luke. 1997. Field Testing of 18m Post-Tensioned Concrete Beams Strengthened with CFRP Plates. In Structural Faults & Repair – 97, Proceedings of the Seventh International Conference on Structural Faults and Repair, 10th July, 1997, edited by Professor M. C. Forde, v. 1, 209-214. Edinburgh, Scotland: Engineering Technics Press.

Leon, R. T., S. A. Olson, and C. W. French. 1990. Twenty-Year-Old Prestressed Bridge Girders: Assessment of Current Condition and Evaluation of Impact Damage Repair. In Proceedings – Second Workshop on Bridge Engineering in Progress, October 29-30, 1990, Reno, Nevada, by the National Science Foundation. Washington, D.C.: National Science Foundation, 151-154.

Lichtenstein, A. G. and Associates, Inc. 1993. Bridge Rating Through Nondestructive Load Testing. Washington, D.C.: Transportation Research Board. NCHRP 12-28(13)A.

Malek, A. M., and H. Saadatmanesh. 1998. Design Equations and Guidelines for Reinforced Concrete Beams Strengthened with FRP Plates. In Fiber Composites in Infrastructure, Proceedings of the Second International Conference on Composites in Infrastructure, ICCI 98. Tuscon, AZ, 5-7 January, 1998. Tuscon, AZ: Department of Civil Engineering, University of Arizona, 603-617.

Marianos, Ward Nihcolas Jr. 1992. Fatigue Life of Partially Prestressed Concrete Bridge Girders. Ph.D. Dissertation, Tulane University.

Mast, Robert F. 1998. Analysis of Cracked Prestressed Concrete Sections: A Practical Approach. PCI Journal (July-August): 80-91.

Mateega, Robert Eugene. 1997. Analytical Investigation of Damaged Prestressed Concrete Bridges. M.S. Thesis, Iowa State University.

Nanni, Antonio, Marco Arduini, and Thomas E. Boothby. 1997. Behavior of Simply-Supported and Continuous RC Beams Strengthened with Carbon FRP Sheets. In Proceedings of the Second Symposium on Practical Solutions for Bridge Strengthening and Rehabilitation, Kansas City, MO,

March 24-25, 1997, by Iowa State University. Ames, IA: Department of Civil and Construction Engineering, Iowa State University, 261-270.

National Cooperative Highway Research Program. 1998. Manual for Bridge Rating Through Load Testing. Washington, DC: Transportation Research Board. NCHRP Research Results Digest 234.

Olson, S. A., C. W. French, and R. T. Leon. Reusability and Impact Damage Repair of Twenty-Year-Old AASHTO Type III Girders, Final Report. Minneapolis: Department of Civil and Mineral Engineering, University of Minnesota, May 1992.

Paradis, Ryan. 1998. Experimental Investigation of a Prestressed Concrete Girder Bridge Model. . M.S. Thesis, Iowa State University.

Pessiki, Stephen, Mark Kaczinski, and Herbert H. Wescott. 1996. Evaluation of Effective Prestress Force in 28-Year-Old Prestressed Concrete Bridge Beams. PCI Journal v. 41 no. 6 (November-December): 78-89.

Phillips, LeRoy, LeRoy Ornberg, George Kotlers, and Dean Bierwagen. 1995. Committee Report on Overheight Collision Damage on Bridges, March 24, 1995. Report to William A. Lundquist, Bridge Engineer, Iowa Department of Transportation. Iowa Department of Transportation, Office of Bridges and Structures.

Research Engineers. 1998. STAAD / Pro v. 2.0. Research Engineers, Inc., Yorba Linda, CA.

Saiidi, M., Y. Labia, and B. Douglas. 1997. Repair of a Full-Scale Prestressed Concrete Box Girder and Fatigue Performance of the Repaired Girder. In Proceedings of the Second Symposium on Practical Solutions for Bridge Strengthening and Rehabilitation, Kansas City, MO, March 24-25, 1997, by Iowa State University. Ames, IA: Department of Civil and Construction Engineering, Iowa State University, 305-314.

Shahawy, Mohsen A. 1995. Nondestructive Strength Evaluation of Florida Bridges. In Nondestructive Evaluation of Aging Bridges and Highways, Proceedings of the International Society for Optical Engineering, 6-7 June 1995, Oakland CA. Bellingham, WA: International Society for Optical Engineering, 101-123.

Shanafelt, George O., and Willis B. Horn. 1980. Damage Evaluation and Repair Methods for Prestressed Bridge Members. Washington, D.C.: Transportation Research Board. NCHRP Report 226.

Shanafelt, George O., and Willis B. Horn. 1985. Guidelines for Evaluation and Repair of Prestressed Concrete Bridge Members. Washington, D.C.: Transportation Research Board. NCHRP Report 280.

Sika Corporation. 1997. Sika® Carbodur® – Engineering Guidelines for the use of CarboDur® (CFRP) laminates for structural strengthening. Lyndhurst, NJ: Sika Corporation.

Tamberg, K. G. 1968. Aspects of Torsion in Concrete Structure Design. In Torsion of Structural Concrete, ACI Publication SP-18, by the American Concrete Institute. Detroit: American Concrete Institute, 7-67.

Zobel, Robert S., R. L. Carrasquillo, and D. W. Fowler. 1997. Repair of Impact Damaged Prestressed Bridge Girder Using a Variety of Materials and Placement Methods. Construction and Building Materials, v. 11 nos. 5-6: 319-326.

Zobel, R. S. and J. O. Jirsa. 1998. Performance of Strand Splice Repairs in Prestressed Bridge Girders. PCI Journal (November-December): 72-84.

Zobel, R. S., J. O. Jirsa, D. W. Fowler, and R. L. Carrasquillo. 1997. Evaluation and Repair of Impact-Damaged Prestressed Concrete Bridge Girders. Austin, TX: Center for Transportation Research, University of Texas at Austin. CTR 1370-3F.

Zokaie, Toorak, Roy A. Imbsen, and Timothy A. Osterkamp. 1991. Distribution of Wheel Loads on Highway Bridges. In Third Bridge Engineering Conference – Papers Presented at the Third Bridge Engineering Conference, March 10-13, 1991, Denver CO. Washington, D.C.: Transportation Research Board, 119-123. Transportation Research Record 1290.